

**The spatial and temporal characterization of hepatic macrophages during acute liver  
injury**

by

Manuel Flores Molina

Department of Microbiology, Infectious Diseases, and Immunology

Faculty of Medicine

Université de Montréal

A thesis

submitted to Université de Montréal

in partial fulfillment of the requirements for the degree of

Doctor of Philosophy (Ph.D.) in Virology and Immunology

August 2022

© Manuel Flores, 2022

This thesis is titled:

The spatial and temporal characterization of hepatic macrophages during acute liver injury

Presented by:

Manuel Flores Molina

Was evaluated by:

Dr. Heather Melichar, Président-rapporteur

Dr. Naglaa Shoukry, Directrice de recherche

Dr. Hugo Soudeyns, Membre du jury

Dr. Sonya MacParland, Examineur Externe

Dr. Sylvain Meloche, Représentant de la Doyenne

## Abstract

The immune response is spatially and temporally regulated. Immune cells are part of a larger community of interconnected immune and non-immune cell populations that coordinate their actions mostly through cell-cell intercellular signaling. In the liver, the distribution pattern, and the composition of the immune compartment evolve during an immune response to injury influencing disease pathology, progression, and response to treatment. Hence, information on the location and interacting partners of immune cells in the hepatic tissue is critical for the proper understanding of their functions in health and disease. However, the spatial organization of hepatic resident and infiltrating immune cells in response to acute injury, and the functional consequences of their specific topographical distribution, remain poorly defined.

Hepatic macrophages are key effector cells during homeostasis and in response to injury and are involved in the pathogenesis of several liver diseases. The heterogeneity and plasticity of the macrophage compartment in the liver have only recently started to be appreciated with the emergence of RNA sequencing, flow cytometry, and mass cytometry. Detailed transcriptomic and phenotypic profiling have deeply expanded our understanding of macrophage biology. However, these technologies involve tissue disruption with loss of spatial information and tissue context. Therefore, the spatial and temporal profiling of liver macrophages in tissue samples during the steady state, and in response to injury, provide novel information on how the macrophages relate to neighboring cells and their behavior during immune responses.

In the first part of this study, we designed a strategy for the spatial phenotyping of hepatic immune cells in tissue samples. This strategy combined serial and sequential labeling, and digital tissue alignment to overcome current limitations in the number of markers that can be simultaneously visualized. In addition, we generated protocols for automated quantification of cells of interest in whole tissue sections which removed the subjectivity associated with quantification by visual inspection and greatly increased the area and the speed of the analysis. As a result, a larger number of immune cell populations were visualized, quantified, and mapped, and their spatial relations were determined in an unbiased manner.

In the second part of this study, we monitored the kinetics, and spatial dynamics of resident Kupffer cells (KCs) and infiltrating monocyte-derived macrophages (MoMFs) in response to acute liver

injury with CCl<sub>4</sub>, to gain insight into their functional roles, and the distribution of labor between them. KCs and MoMFs exhibited different tissue distribution patterns and cell morphology, different kinetics, and occupied neighboring but unique microanatomical tissue locations. KCs and MoMFs displayed a different capacity to replenish the macrophage pool upon acute injury, and were differentially related to hepatic stellate cells. Different kinetics and spatial profiles revealed that KCs and MoMFs have distinct spatial signatures and suggest that they perform distinct functions during the wound-healing response to acute liver injury.

In summary, we optimized techniques and put together a strategy for the spatial profiling of hepatic immune cells. Then, we used this methodology to profile resident and infiltrating macrophage subpopulations to gain insight into their biology and distinct contribution to healing in response to acute liver injury. Overall, the observations made in this study suggest that the spatial and temporal behavior of a given subpopulation of immune cells underlie its ability to perform its specific functions during the immune response.

**Keywords: Tumor microenvironment, multiplex immunofluorescence, FFPE, image analysis, tissue alignment, tissue heatmap, VIS software, Kupffer cells, monocyte-derived macrophages, hepatic stellate cells, CCl<sub>4</sub>-induced acute liver injury, spatial phenotyping, wound healing response.**

## **Résumé**

La réponse immunitaire est régulée spatialement et temporellement. Les cellules immunitaires font partie d'une plus grande communauté de populations cellulaires interconnectées qui coordonnent leurs actions par la signalisation intercellulaire. Suivant une blessure hépatique, la distribution et la composition du compartiment immunitaire évoluent rapidement au fil du temps. Par conséquent, l'information sur la position des cellules immunitaires dans le tissu hépatique est essentielle à la bonne compréhension de leurs fonctions dans la santé et la maladie. Cependant, l'organisation spatiale des cellules immunitaires en réponse à une atteinte hépatique aiguë, ainsi que les conséquences fonctionnelles de leur distribution topographique spécifique, restent mal comprises.

Les macrophages hépatiques sont des cellules effectrices clés pendant l'homéostasie et en réponse à des blessures, et sont impliqués dans la pathogenèse de plusieurs maladies du foie. L'hétérogénéité et plasticité des macrophages dans le foie a été exposée avec l'émergence du séquençage de l'ARN, la cytométrie en flux et la cytométrie de masse. Ces techniques ont sensiblement contribué à la compréhension de l'origine, et fonctions des macrophages dans le foie. Cependant, ces technologies impliquent la destruction du tissu pour la préparation de suspension cellulaires ce qui entraîne une perte d'information spatiale et de contexte tissulaire. Par conséquent, la caractérisation spatiale et temporelle des macrophages dans le tissu hépatique pendant l'homéostasie tissulaire, et en réponse à une blessure, fournit une nouvelle information sur la façon dont les macrophages se rapportent aux cellules voisines et leur comportement pendant les réponses immunitaires.

Dans la première partie de cette étude, nous avons conçu une stratégie pour le phénotypage spatial des cellules immunitaires hépatiques dans des échantillons de tissus. Cette stratégie combine techniques d'imagerie et l'alignement numérique des images pour surmonter les limitations actuelles du nombre de marqueurs pouvant être visualisés simultanément. En outre, nous avons généré des protocoles pour la quantification automatisée des cellules d'intérêt dans des sections de tissus pour réduire la subjectivité associée à la quantification par inspection visuelle, et pour augmenter la surface et la vitesse de l'analyse. Par conséquent, un plus grand nombre de populations de cellules immunitaires ont été visualisées, quantifiées et cartographiées, et leurs relations spatiales ont été déterminées.

Dans la deuxième partie de l'étude, nous avons déterminé la cinétique et la dynamique spatiale des cellules de Kupffer (KCs) et des macrophages dérivés de monocytes (MoMFs) en réponse à une atteinte hépatique aiguë au CCl<sub>4</sub>, afin de mieux comprendre leurs rôles fonctionnels, et la répartition du travail entre eux. Nous avons constaté que les KC et les MoMFs présentent des différences au niveau de la distribution tissulaire, la morphologie, et la cinétique. En plus, seulement les KCs ont proliféré pour repeupler la population de macrophages résidents pendant la réparation tissulaire. Finalement, nous avons montré que le degré de colocalisation de KCs et des MoMFs avec les cellules stellaires est différent. En plus, cette colocalisation varie avec la progression de la réponse immunitaire. Dans l'ensemble, nous avons montré que les KCs et les MoMFs ont des profils spatiaux et temporels différents en réponse à une atteinte hépatique aiguë.

Dans l'ensemble, les observations faites dans cette étude suggèrent que le comportement spatial et temporel d'une sous-population donnée de cellules immunitaires est distinct et sous-tend sa capacité à remplir ses fonctions spécifiques pendant la réponse immunitaire.

**Mots-clés : Microenvironnement tumoral, immunofluorescence multiparamétrique, FFPE, analyse d'images, alignement tissulaire, carte de chaleur tissulaire, logiciel VIS, cellules de Kupffer, macrophages dérivés de monocytes, cellules stellaires, lésion hépatique aiguë induite par CCl<sub>4</sub>, phénotypage spatial, réponse de cicatrisation.**

## Contents

<b>Abstract</b>	<b>3</b>
<b>Résumé</b>	<b>4</b>
<b>Abbreviations and Acronyms:</b>	<b>9</b>
<b>List of figures</b>	<b>21</b>
<b>Acknowledgments</b>	<b>24</b>
<b>1.a. The spatial organization of the hepatic immune system as a determinant of tissue physiology and pathology</b>	<b>1</b>
<b>1.b. Microanatomy of the liver</b>	<b>2</b>
<b>1.c. Parenchymal cells of the liver</b>	<b>5</b>
<b>1.c.2. Cholangiocytes</b>	<b>8</b>
<b>1.d. Non-parenchymal cells of the liver</b>	<b>9</b>
<b>1.d.1. Liver Sinusoidal Endothelial Cells (LSECs)</b>	<b>9</b>
<b>1.d.2. Hepatic Stellate Cells (HSCs)</b>	<b>15</b>
<b>1.d.3. Portal Fibroblasts</b>	<b>19</b>
<b>1.e. Liver Resident Immune Cells</b>	<b>22</b>
<b>1.e.1.b. Liver Capsular Macrophages (LCMs)</b>	<b>31</b>
<b>1.e.2. Hepatic Dendritic Cells</b>	<b>37</b>
<b>1.e.3. Hepatic Resident Lymphocytes</b>	<b>40</b>
<b>1.e.3.a Hepatic Innate Lymphoid Cells</b>	<b>41</b>
<b>1.e.3.b Hepatic NK Cells</b>	<b>47</b>
<b>1.e.3.c Hepatic NKT Cells</b>	<b>52</b>
<b>1.e.3.d Hepatic MAIT Cells</b>	<b>57</b>
<b>1.e.3.e Hepatic <math>\gamma\delta</math> T Cells</b>	<b>61</b>
<b>1.e.3.f Hepatic tissue-resident memory T cells</b>	<b>68</b>
<b>1.f. The emerging atlas of the hepatic tissue</b>	<b>71</b>
<b>2.a.1. Rationale</b>	<b>72</b>
<b>2.a.2. Hypothesis</b>	<b>73</b>
<b>2.a.3. Objectives</b>	<b>74</b>
<b>Chapter 3: Manuscript 1</b>	<b>75</b>
<b>Visualization, Quantification, and Mapping of Immune Cell Populations in the Tumor Microenvironment</b>	<b>75</b>

<b>Chapter 4: Manuscript 2</b>	<b>111</b>
<b>Distinct spatial distribution and roles of Kupffer cells and monocyte-derived macrophages in mouse acute liver injury</b>	<b>111</b>
<b>5.a. Summary of the thesis</b>	<b>165</b>
<b>5.b. Development of a methodology for increased multiplexing capability and spatial phenotyping in the hepatic tissue</b>	<b>166</b>
<b>5.c. Spatio-temporal characterization of the hepatic macrophage compartment in response to acute liver injury</b>	<b>168</b>
<b>5.c.1. Wound healing response to CCl<sub>4</sub>-induced acute liver injury</b>	<b>170</b>
<b>5.c.1.a. Necroinflammation in response to CCl<sub>4</sub>-induced acute liver injury</b>	<b>171</b>
<b>5.c.1.b Tissue repair in response to CCl<sub>4</sub>-induced acute liver injury</b>	<b>173</b>
<b>5.c.1.c. Parenchymal and non-parenchymal cell proliferation during early tissue repair in response to CCl<sub>4</sub>-induced acute liver injury</b>	<b>175</b>
<b>5.c.1.d. Kinetics of the major innate and adaptive immune cell populations in response to CCl<sub>4</sub>-induced acute liver injury</b>	<b>175</b>
<b>5.c.1.e. Profile of myeloid cells during the wound healing response to CCl<sub>4</sub>-induced acute liver injury</b>	<b>180</b>
<b>5.c.1.f. Neutrophils in response to acute liver injury</b>	<b>182</b>
<b>5.c.1.g. Inflammatory monocytes and MoMFs in response to acute liver injury</b>	<b>192</b>
<b>5.c.1.h. Kupffer cells in acute liver injury:</b>	<b>194</b>
<b>5.d. Conclusions</b>	<b>198</b>
<b>5.e. Limitations and Future Directions</b>	<b>199</b>
<b>5.f. Graphical Abstract</b>	<b>202</b>
<b>5.g. Phenotype of main myeloid and lymphoid liver resident populations included in this thesis</b>	<b>203</b>
<b>Chapter 6: References</b>	<b>205</b>
<b>Annexe 1 : Manuel Flores Curriculum Vitae</b>	<b>258</b>



## **Abbreviations and Acronyms:**

### **A**

AAMs: Alternatively activated macrophages

ACLF: Acute-on-chronic liver failure

ACTB: Actin beta

Adamstl2: A disintegrin and metalloproteinase with thrombospondin motifs 2

ADCC: Antibody-dependent cellular cytotoxicity

AEBP1: AE binding protein 1

AHR: Aryl hydrocarbon receptor

AIC: Autoimmune cholangitis

AIH: Autoimmune hepatitis

AILI: Acute-induced liver injury

ALA: amebic liver abscesses

ALD: Alcoholic liver disease

ALT: Alanine aminotransferase

APAP: N-acetyl-p-aminophenol

APC: Antigen-presenting cell

APP: Analysis protocol package

AQP1: Aquaporin

Arg-1: Arginase 1

AST: Aspartate aminotransferase

ATP: Adenosine triphosphate

AXL: AXL receptor tyrosine kinase

A2ALDH1A2: Aldehyde dehydrogenase 1 family member

## **B**

BCL-2: B-cell lymphoma 2

BCR: B cells receptor

BDL: Bile duct ligation

BEC: Biliary epithelial cell

BFA: Brefeldin A

BM-KCs: Bone marrow-derived Kupffer cells

Blimp-1: B-lymphocyte-induced maturation protein-1

## **C**

CaHSCs: Central vein-associated HSCs

CCL2: C-C motif chemokine ligand 2

CCL3: C-C motif chemokine ligand 3

CCL4: C-C motif chemokine ligand 4

CCL5: C-C motif chemokine ligand 5

CCl<sub>4</sub>: Carbon tetrachloride

CCL7: C-C motif 7 chemokine ligand 7

CCR2: C-C motif chemokine receptor 2

CD: Cluster of differentiation

cDCs: Classical DCs

CDH1: Cadherin 1

CFTR: Cystic fibrosis transmembrane regulator

CHB: Chronic hepatitis B

CITE-Seq: cellular indexing of transcriptomes and epitopes by sequencing

CLEC3B: C-type lectin domain family 3-member B

CLEC4F: C-type lectin domain family 4-member F

CLIP1: CAP-Gly domain-containing linker protein 1

CMV: Cytomegalovirus

CODEX: CO-Detection by indexing

COIs: Cells of interest

Col1a1: Collagen type I alpha 1 chain

Col15a1: collagen type XV alpha 1 chain

Con A: Concanavalin A

CSF: Colony stimulating factor

CSF-1R: Colony-stimulating factor receptor 1

CTGF: Connective tissue growth factor

CXCL1: Chemokine (C-X-C motif) ligand 1

CXCL2: Chemokine (C-X-C motif) ligand 2

CXCL5 : Chemokine (C-X-C motif) ligand 5

CV: Central vein

CX3CL1: CX3C chemokine ligand 1

CX3CR1: CX3C chemokine receptor 1

CYP3A4: Cytochrome P450 3A4

CYR61: Cysteine-rich angiogenic inducer 61

NASH: Mass cytometry or cytometry by time of flight

C1qa/b/c: Complement C1q subcomponents a, b, and c

## **D**

DAMP: Damage-associated molecular pattern

DAPI: 4',6-diamidino-2-phenylindole

DC: Dendritic cell

DEFB1: Beta-defensin 1

DN: Double negative

DPT: Dermatotoponin

## **E**

ECM: Extracellular matrix

EGF: Epidermal growth factor

Entpd2: Ectonucleoside triphosphate diphosphohydrolase 2

Eomes: Eomesodermin

EPCAM: Epithelial cell adhesion molecule

ER: Endoplasmic reticulum

ESAM: Endothelial cell-selective adhesion molecule

## **F**

FAS: Fas cell surface death receptor

Fbln2: Fibulin 2

FFPE: Formalin-fixed paraffin-embedded

FGF: Fibroblast growth factor

FGFR2: Fibroblast growth factor receptor 2

FlowSOM: Flow with self-organizing maps

Fn1: Fibronectin-1

FOV: Fields of view

FoxP3: Forkhead box P3

FXRD2: FXRD domain-containing ion transport regulator 2

F4/80: EGF-like module-containing mucin-like hormone receptor-like 1

## **G**

Gas6: growth arrest-specific 6

GATA: GATA binding protein

G-CSF: Granulocyte colony-stimulating factor

GSEA: Gene-set enrichment analysis

GF: Germ-free

GFP: Green fluorescent protein

GM-CSF: Granulocyte macrophage colony-stimulating factor

Gsn: Gelsolin

GZM B: Granzyme B

$\alpha$ -GalCer:  $\alpha$ -galactosylceramide

## **H**

HA: Hepatic artery

HAI: Histological activity index

HBV: Hepatitis B virus

HBsAg: Hepatitis B surface antigen

HCC: Hepatocellular carcinoma

HCV: Hepatitis C virus

HDN: High-density neutrophils

HES1: Hairy and enhancer of split-1

HFD: High-fat diet

HGF: Hepatocyte growth factor

HIV: Human immunodeficiency virus

HLA-DR: Human leukocyte antigen – DR isotype

HMOX1: Heme oxygenase 1

Hobit: Homolog of Blimp-1 in T cells

HSCs: Hepatic stellate cells

H&E: Hematoxylin and eosin

## I

Iba1: Ionized calcium-binding adaptor molecule 1

IBEX: Iterative bleaching extends multiplexity

IDO: Indoleamine 2,3-dioxygenase

IFN- $\gamma$ : Interferon  $\gamma$

IFNLR1: Interferon lambda receptor 1

IGF: Insulin-like growth factor

IHC: Immunohistochemistry

IHL : Intrahepatic leukocyte

IL: Interleukin

ILC: Innate lymphoid cell

iNKT: Invariant natural killer T cells

IRI: Ischemia reperfusion injury

Itgam 1: Integrin alpha M chain

Itgb3: Integrin beta chain beta 3

## **J**

JAG1: Jagged 1

## **K**

KCs: Kupffer cells

KLH: Keyhole limpet haemocyanin

KO: Knock out

KRT: Keratin

## **L**

LBP: Lipopolysaccharide binding protein

LCMs: Liver capsular macrophages

LCMV: Lymphocytic choriomeningitis virus

LCN2: Lipocalin 2

LDNs: Low-density neutrophils

LN: Lymph nodes

LPS: Lipopolysaccharide

lr-NK: liver resident NK cells

LSECs: Liver sinusoidal endothelial cells

LTi: Lymphoid tissue inducer cells

Ly6C: Lymphocyte antigen 6 complex

Ly6G: Lymphocyte antigen 6 complex locus G6D

LRAT: Lecithin retinol acyltransferase

## **M**

MAIT: Mucosal-associated invariant T cells

MARCO: Macrophage receptor with collagenous structure

MCD: methionine-choline-deficient diet

MCMV: Murine cytomegalovirus

M-CSF: Macrophage colony-stimulating factor

MDR2: Multidrug resistance-2 gene

MDSC: Myeloid-derived suppressor cell

MFI: Mean fluorescent intensity

MERTK: Proto-oncogene tyrosine-protein kinase MER

MFAP4: Microfibril-associated protein 4

Mfge8: Milk fat globule-EGF factor 8 gene

MHC: Major histocompatibility complex

MHV: Murine hepatitis virus

MICA: MHC class I chain-related protein A

MICB: MHC class I chain-related protein B

mIF: Multiplex immunofluorescence

MIP-1 $\alpha$ : Macrophage inflammatory protein-1 $\alpha$

MMPs: metalloproteinase

MoKCs: Monocyte-derived Kupffer cells

MoMFs: Monocyte-derived macrophages

MPO: Myeloperoxidase

MR1: MHC-related 1 molecule



## **N**

NAFLD: Non-alcoholic fatty liver disease

NAS: NAFLD activity score

NASH: Non-alcoholic steatohepatitis

NCMs: Non-classical monocytes

NETs: Neutrophil extracellular traps

NF- $\kappa$ B: Nuclear factor kappa B

NK: Natural killer cells

NKRs: Natural killer receptors

NKT: Natural killer T cells

NO: Nitric Oxide

NOTCH2: Neurogenic locus notch homolog protein 2

NPCs: Non-parenchymal cells

NRP1: Neuropilin 1

## **P**

PaHSCs: Portal vein-associated HSCs

PAMP: Pathogen-associated molecular pattern

PBC: Primary biliary cholangitis

PBMCs: Peripheral blood mononuclear cells

PBS: Phosphate buffered saline

pcSeq: Paired cell sequencing

PDGF: Platelet-derived growth factor

pDCs: Plasmacytoid dendritic cells

PD-1: Programmed cell death protein 1

PD-L1: Programmed death-ligand 1

PF: Portal fibroblast

PGE2: Prostaglandin E2

PLBD1: Phospholipase B domain containing 1

PRR: Pattern recognition receptor

PLZF: Promyelocytic leukemia zinc-finger

PSC: Primary sclerosing cholangitis

PSR: Picrosirius red

PT: Portal tract

PTH1R: Parathyroid hormone 1 receptor

PV: Portal vein

## **R**

RBP1: Retinol binding protein 1

RELN: Reelin

RFP: Red fluorescent protein

RNA: Ribonucleic acid

ROI: Region of interest

ROR $\gamma$ t: RAR-related orphan receptor

ROS: Reactive oxygen species

RT: Room temperature

## **S**

SD-IVM: Spinning-disk confocal intravital microscopy

SEM: Scanning electron microscopy

SCID: Severe combined immunodeficiency disease

SCF: Stem cell factor

scRNA-seq: Single cell RNA sequencing

SD: Space of Disse

SD-IVM: Spinning-disk confocal intravital microscopy

SLOs: Secondary lymphoid organs

snRNA-seq: Single-nucleus RNA sequencing

SOX9: SRY (sex determining region Y)-box 9

SPF: Specific pathogen-free

SPP1: Secreted phosphoprotein 1

Stab2: Stabilin 2

$\alpha$ SMA:  $\alpha$ -smooth muscle actin

S1PR1: Sphingosine-1-phosphate receptor 1

## **T**

TAA: Thioacetamide

TAPs: Tissue-associated pixels

T-bet : T-box-transcription factor TBX21

TC: Tissue compartment

T<sub>CM</sub>: Central memory T cells

T<sub>conv</sub>: Conventional T cells

T<sub>EM</sub>: Effector memory T cells

TCR: T cell receptor

TFF2: Trefoil factor 2

TGF $\beta$ : Transforming growth factor  $\beta$

Timd4: T cell immunoglobulin and mucin domain containing 4

Tim-3: T cell immunoglobulin and mucin-domain containing-3

TLR: Toll-like receptor

TME: Tumor microenvironment

TNF- $\alpha$ : Tumor necrosis factor  $\alpha$

TRAIL: TNF-related apoptosis-inducing ligand

T<sub>RM</sub>: Resident memory T cells

t-SNE: t-distributed stochastic neighbor embedding analysis

## **V**

VEGF: Vascular endothelial growth factor

VIPR1: Vasoactive intestinal peptide receptor 1

VLDL: Very low-density lipoprotein

VSIG4: V-set and immunoglobulin domain containing 4

## **W**

WT: Wild type

## **Y**

YS-KCs: Yolk sac-derived Kupffer cells

## List of figures

### Chapter 1:

Figure 1: The histological and functional unit of the liver.

Figure 2: Schematic representation of the hepatic sinusoid.

Figure 3: Cell composition of the healthy adult liver.

Figure 4: Schematic representation of the metabolic zonation of the liver.

Figure 5: High resolution image of a hepatic sinusoid.

Figure 6: CD8<sup>+</sup> T cells contact hepatocytes through discontinuation points in the sinusoidal walls.

Figure 7: KCs project processes through the fenestrae of LSECs.

Figure 8: Immunomodulation by liver LSECs.

Figure 9: HSCs and KCs establish direct contact in the healthy liver.

Figure 10. HSC zonation across the healthy liver lobule.

Figure 11: PFs secrete collagens in response to biliary injury.

Figure 12: KCs exhibit zoned distribution in the healthy liver.

Figure 13: High resolution images of LCMs.

Figure 14: MoMFs are recruited to the injury site during acetaminophen-induced liver injury.

Figure 15: CCR2<sup>+</sup>CX3CR1<sup>+</sup> monocyte-derived macrophages surround and enter the site of hepatic sterile injury.

Figure 16: NKT cells (CXCR6-GFP in green) are enriched around CD1d positive periportal areas.

Figure 17: The phenotype of human MAIT cells and their mechanisms of activation.

### Chapter 3:

Figure 1: Schematic representation of the strategy for visualizing, quantifying, and mapping immune cells in the TME.

Figure 2: Staining of serial tissue sections and image alignment.

Figure 3: Automated tissue detection/segmentation and generation of respective ROIs.

Figure 4: Identification and quantification of COIs in the TCs stroma and parenchyma.

Figure 5: Tissue heatmaps of COIs in the TME.

Supplementary Figure S1: Validation of tissue alignment.

Supplementary Figure S2: Zoomed view of tissue heatmaps.

Supplementary Figure S3: Colocalization Analysis.

#### **Chapter 4:**

Figure 1: CCl<sub>4</sub>-induced acute liver injury is characterized by a necroinflammatory phase followed, at 48 h post-injury, by an early tissue repair phase and then a late one from 72 hours onward.

Figure 2: Hepatic resident lymphocytes are partially depleted during the necroinflammatory phase and recover during the tissue repair phase of CCl<sub>4</sub>-mediated acute liver injury, while intrahepatic myeloid cells respond by inflammatory mediators' release.

Figure 3: The wound healing response to acute liver injury is associated with an influx of circulating myeloid cells.

Figure 4: KCs and MoMFs exhibit different distribution patterns and kinetics during acute liver injury whereby early transient depletion of CLEC4F<sup>+</sup> KCs is followed by recruitment of IBA1<sup>+</sup>CLEC4F<sup>-</sup> macrophages then return to baseline conditions during repair.

Figure 5: CLEC4F<sup>+</sup> KCs and IBA1<sup>+</sup>CLEC4F<sup>-</sup> macrophages are in close contact in the necrotic area but exhibit different kinetics, microanatomical location, and morphology.

Figure 6: IBA1<sup>+</sup>CLEC4F<sup>-</sup> macrophages exhibit phenotypic markers of MoMFs.

Figure 7: CLEC4F<sup>+</sup> KCs of yolk sac origin replenish the hepatic macrophage pool during tissue repair.

Figure 8: IBA1<sup>+</sup> CLEC4F<sup>-</sup> macrophages interact with aHSCs to a greater extent than CLEC4F<sup>+</sup> KCs.

Figure S1: Ki67 levels are highest at 48 h post CCl<sub>4</sub>.

Figure S2: Circulating phagocytes are recruited to the liver in response to CCl<sub>4</sub>-induced acute injury during the necroinflammatory and tissue repair phases.

Figure S3: Recovered CD11b<sup>+</sup> MHCII<sup>+</sup> CD64<sup>+</sup> F4/80<sup>+</sup> cells express CX3CR1, and therefore are not KCs.

Figure S4: IBA1<sup>+</sup> CLEC4F<sup>-</sup> macrophages, and CLEC4F<sup>+</sup> KCs exhibit different microanatomical locations in response to CCl<sub>4</sub>-induced acute liver injury.

Figure S5: Globular-shaped IBA1<sup>+</sup> cells infiltrate the necrotic tissue at 24 h and replace hepatocytes in the area surrounding CVs by 48 h post CCl<sub>4</sub>.

Figure S6: IBA1<sup>+</sup> CLEC4F<sup>-</sup> macrophages and IBA1<sup>+</sup> CLEC4F<sup>+</sup> KCs are present in murine fibrotic liver.

Video: Activated hepatic stellate cells, IBA1<sup>+</sup>CLEC4F<sup>-</sup> macrophages, and CLEC4F<sup>+</sup> KCs establish direct contact around injured central veins at 48 h post CCl<sub>4</sub>.

## Chapter 5:

Figure 18: Myeloid cells and particularly MoMFs increase Arg-1 expression during tissue repair.

Figure 19: CCl<sub>4</sub> injury induces two temporarily separated waves of neutrophil infiltration.

Figure 20: Neutrophils accumulate in the capsule of CCl<sub>4</sub>-injured mice during necroinflammation and seem to access the parenchyma through discontinuation points in the network of IBA1<sup>+</sup> capsular macrophages.

Figure 21: The neutrophils that infiltrate the liver during necroinflammation exhibit different cellular density than neutrophils infiltrating the liver during repair.

Figure 22: Neutrophil depletion before CCl<sub>4</sub> injury has no impact on tissue damage but decreases the expression of fibrogenic cytokines and activation markers of HSCs during early repair.

Figure 23: Neutrophils, Macrophages, and aHSCs spatially and temporally overlap in the centrilobular necrotic area at 48h post CCl<sub>4</sub> treatment.

Figure 24: Neutrophils colocalize with IBA1<sup>+</sup> CLEC4F<sup>-</sup> MoMFs and IBA1<sup>+</sup> CLEC4F<sup>+</sup> KCs during tissue repair.

## Acknowledgments

To my better half, my wife Ivonne Alvarez Moreno. Thank you for your love and support along this long journey! For all the happiness you bring to my life every day. For your never-ending belief in me. For sharing with me all the ups and downs of creating a new life for us in a new country. For our beautiful family. Te adoro! To my daughters, Alejandra, and Isabel. Papá is about to have more time for you, I can't wait. Mis niñas lindas! To my mother, Mercedes Molina Rivas, for nurturing in me the love for life, nature, truth, and science. For all the sacrifices you have made. Te quiero mucho! To my sisters, Vivian Flores, and Silvia Durán, my aunt Matilde Molina, my parents-in-law Luis Alvarez y Mariela Moreno, always there for me and my girls.

I am deeply grateful to the Canadians and Quebecers, who have welcomed me and my family, and funded my training, projects, and dreams. I am enormously thankful to the funding agencies that supported me during my studies (bourse de recrutement de la faculté de médecine, bourse d'excellence Gabriel-Marquis, and doctoral fellowship from the fonds de recherche du Québec).

I thank Dr. Naglaa Shoukry, my supervisor, for her guidance, advice, and help to become a scientist. Thank you for the weekly meetings that forced me to articulate my ideas and to better communicate my results! Thank you for the internal journal clubs that shaped my critical judgment, and for allowing me to explore unexpected observations that were the origin of new projects.

I have a great appreciation for the colleagues I had the opportunity to work with. Thank you, Mohamed Abdelnabi, for sharing with me your passion for immunology, and for the hard and excellent work. Thank you, Sabrina Mazouz, you are a scientist and an artist. My project owes a lot to your unique skills and generosity. I hope we will keep working together in the future. I am also very grateful to Dr. Ghada Hassan for the scientific input into my manuscript and thesis corrections. I always appreciated the rigor, quality, and commitment of your work. Thank you, Deborah Villafranca-Baughman, for your friendship, your contagious joy, and your insatiable scientific curiosity that worked so well for my project! I was also blessed to have Dr. Petronela Ancuta as my professor and committee member. You are an inspiration for me, Dr. Petronela, as a scientist, a professor, and a deeply human and decent person. Thank you Nicolás Belforte for the



artwork you did with our images and figures, your revisions and suggestions, and all the great imaging tips.

I have enormous gratitude towards Liliane Meunier, Véronique Barrès, and Gabriela Fragoso. You taught me to process tissue and gave me tips for imaging, and even antibodies. You are amazing professionals and generous people. I owe you each one of my nice and clean images. Thank you, Aurélie Cleret-Buhot, for training me in image analysis, and directing me to the optimal technical solutions, what a huge and positive influence on my work. I would also like to thank Nathalie Bédard for excellent flow cytometry training, and continuous help to identify and get the resources my project required.

Finally, I want to thank my friends and Colombian family in Montreal that give me the joy that makes life worth living. Michael Dahabieh, mon ami, it has been an inspiration to see you growing as the scientist you have become. Papi Chulo loves you. Néstor y Holman, mis hermanos y compadres, you really know how to support science. Thank you for letting me recharge batteries every weekend with you and your families. Se les quiere!

## **Chapter 1: Introduction**

### **1.a. The spatial organization of the hepatic immune system as a determinant of tissue physiology and pathology**

The immune response is a spatially and temporally regulated process. Cells implicated herein are part of a larger community of interconnected immune as well as non-immune cell populations that coordinate their actions partly in a contact-dependent manner and through cell-cell intercellular signaling. In any given tissue, the distribution pattern, and the composition of its immune compartment evolve during an immune response influencing disease pathology, progression, and response to treatment (1-6). Hence, information on the location and interacting partners of immune cells in the tissue is critical for the proper understanding of their functions in health and disease (1, 4, 6). Concerning the hepatic tissue, the focus of this thesis, the spatial organization of its resident and infiltrating immune cells, and the functional consequences of their specific topographical distribution, is gaining growing attention but remains insufficiently characterized (7, 8).

The liver is the largest internal organ of the body and is home to vital and complex biosynthetic and biodegradative metabolic pathways. In addition, the liver acts as a filter for gut-derived blood, enriched in both, harmless dietary antigens, and potentially harmful microbiota and pathogen-derived antigens. This unique property led to the evolution of distinctive immunological mechanisms that ensure an active state of tolerance towards innocuous antigens while retaining the capability of responding to pathogens (1). To support the complexity of its physiological needs, the hepatic tissue harbors a unique array of tissue-adapted immune cells that fulfill varied immunological functions in health and disease (1). The composition and spatial organization of this network underlie its ability to sense and respond to tissue-damaging agents, and to restore tissue homeostasis upon injury. Consequently, a hallmark of tissue pathology is the alteration of the spatial organization and composition of hepatic immune cells.

Confirming the importance of the spatial distribution of hepatic cells is the metabolic zonation in the liver. Indeed, the spatial separation of different metabolic pathways along the hepatic sinusoidal axis creates location-dependent gene expression patterns in hepatocytes, liver sinusoidal endothelial cells (LSECs), and hepatic stellate cells (HSCs), all of them proven interacting partners of immune cells (9-14). Since hepatic immune cells occupy specific niches, are positioned at

strategic locations, and entertain stable and dynamic interactions with surrounding tissue cells, it follows that metabolic spatial zonation may influence their phenotype and function.

While newly emerging multiomic single-cell and bulk technologies have provided a wealth of knowledge on the genome, epigenome, transcriptome, and proteome of hepatic immune cells, these procedures involve tissue disruption and the consequent loss of information about location and cell-cell interactions (15-22). Therefore, the development of *in situ* multiplex imaging systems with spatial resolution at the single-cell level is required for characterizing the tissue context and the interacting partners of immune cells and better understanding their contribution to tissue physiology and pathology.

The introductory chapter of this thesis first provides an overview of the microanatomy of the liver as the foundation for a proper understanding of the positioning of immune cells in the tissue. We will next introduce the main parenchymal and non-parenchymal cells of the liver that constitute the interacting partners of resident and infiltrating immune cells in health and disease. Next, we will review the current knowledge on the composition, function, and spatial distribution of the hepatic immune system, and highlight present gaps in our understanding of the spatio-temporal properties of the immune response to liver injury. Then, in the first manuscript of this study (chapter 3), we will introduce the strategy that we developed for increased multiplexing and spatial phenotyping of immune cells in the liver. In the second manuscript (chapter 4), we will present the results of applying some of the techniques and principles of this strategy to dissect the macrophage compartment in response to acute liver injury. Finally, in chapter 5 we will discuss the main findings, the overall significance, and limitations of this study, and the suggested future directions.

### **1.b. Microanatomy of the liver**

The structural organization of the liver has profound implications for its immune function

The definition of the fundamental structural and functional unit of the liver has been the subject of multiple reformulations and heated controversy since first described by Kiernan et al. in 1833 (23). However, to understand the organization of the immune system in the hepatic tissue, three structural concepts have been instrumental: the classical lobule, the hepatic acinus, and the hepatic sinusoid.

The classical lobule is considered the histological unit of the liver. The hepatic lobule can be described as a hexagon composed of a central vein in the center point and portal triads located at every vertex. Portal triads are arrangements of a portal venule, a hepatic artery, and a bile duct (Figure 1A). In the classical lobule, cords of connected hepatocytes radiate outward from the central vein to the portal triads with the basolateral membrane of hepatocytes facing capillary vessels called sinusoids. Sinusoids are lined with a fenestrated endothelium composed of LSECs. The blood from the portal vein mixes with the arterial blood and flows through the sinusoids toward the central vein. A narrow space known as the space of Disse separates hepatocytes from the endothelial lining (24).

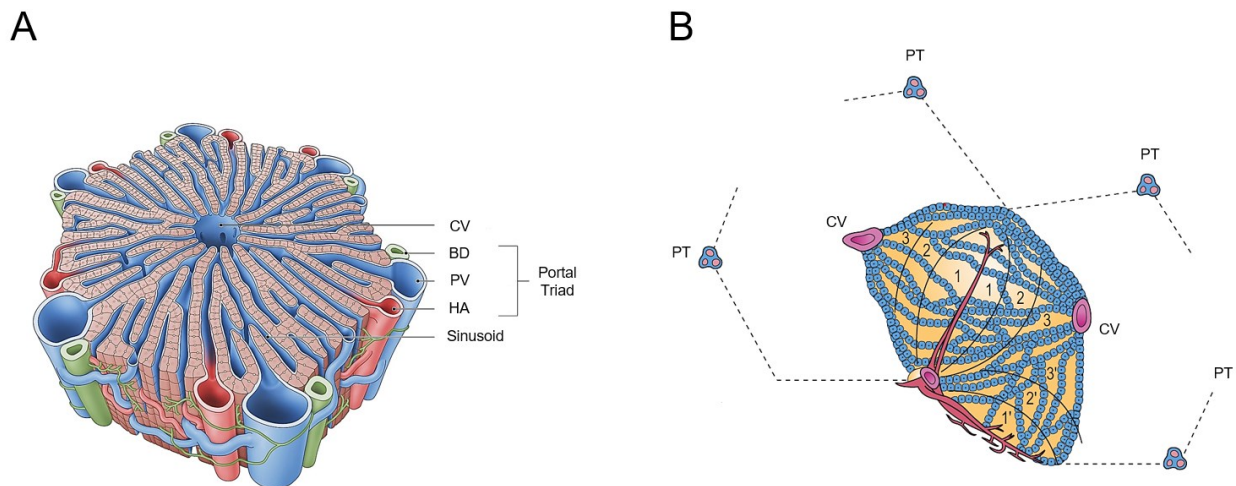


**Figure 1: The histological and functional unit of the liver.** A) Schematic representation of the classical lobule as a hexagon composed of plates of hepatocytes radiating outward from the central vein to the portal triads. B) Diagrammatic representation of the simple acinus and the zonal arrangement of hepatocytes. Two neighboring classic lobules are outlined by the discontinuous lines, and the acinus occupies adjacent sectors of these. The acinus is arranged around the terminal branches of the portal vein, hepatic artery, and bile ductule. Zones 1, 2, and 3 represent areas that receive blood progressively poorer in nutrients and oxygen. Central vein (CV), portal tract (PT), portal vein (PV), hepatic artery (HA). Caption and image adapted from reference (25).

On the other side, the liver acinus as conceptualized by Rappaport in 1954, is the functional unit of the liver and comprises the portion of liver parenchyma perfused by a terminal branch of the

portal vein and hepatic artery that drains into two adjacent central veins (Figure 1B) (26). The hepatic acinus is divided into zones perfused with blood with different levels of oxygen and nutrients. Zone 1 is assigned to the hepatocytes closest to the hepatic artery and therefore perfused with highly oxygenated and nutrient-rich blood, while zones 2 and 3 refer to hepatocytes closer to the central veins that are perfused with blood with lower levels of oxygen and nutrients.

Hepatic sinusoids are arguably the structural feature most frequently referred to by immunologists. Sinusoids are the microvascular units of the liver. Sinusoids are low-pressure vascular channels lined by LSECs (Figure 2). LSECs regulate the exchange of molecules and plasma between the intra-sinusoidal compartment and the perisinusoidal space of Disse (27). This space contains a low-density basal membrane–like matrix that facilitates this bidirectional exchange. The lumen of the sinusoids harbors several phagocyte and lymphoid populations that in a concerted action detect and clear pathogens, toxins, aged cells, and waste products coming from the portal or the systemic circulation (28).

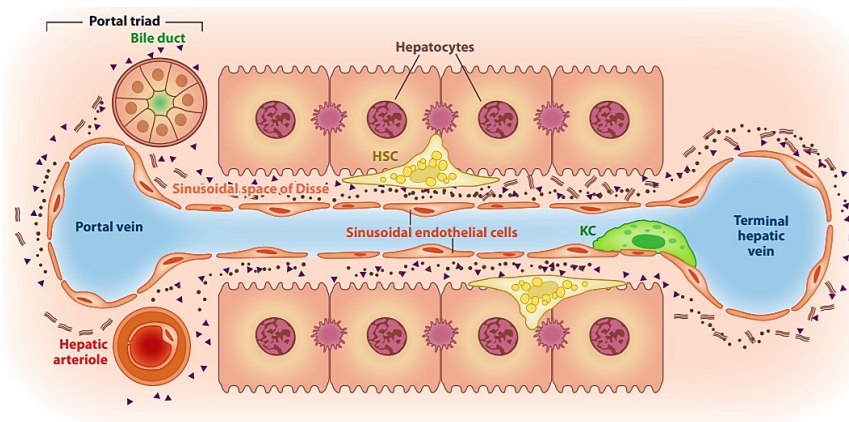


**Figure 2: Schematic representation of the hepatic sinusoid.** Sinusoids are capillary vessels that carry oxygenated and nutrient-rich blood from the portal area to the central vein. The sinusoids are lined by a fenestrated endothelium formed by LSECs and house several immune populations like KCs and other non-depicted immune populations. The perisinusoidal space of Disse separates the endothelium from the hepatocytes and is occupied by HSCs. Caption and image adapted from reference (28)

### 1.c. Parenchymal cells of the liver

The liver is a vital organ composed of parenchymal and non-parenchymal cells (NPCs) (Figure 3). Parenchymal cells in the hepatic tissue are the hepatocytes and cholangiocytes which carry out the essential metabolic, synthetic, and detoxifying functions of the liver and make up more than two-thirds of the total hepatic cells.

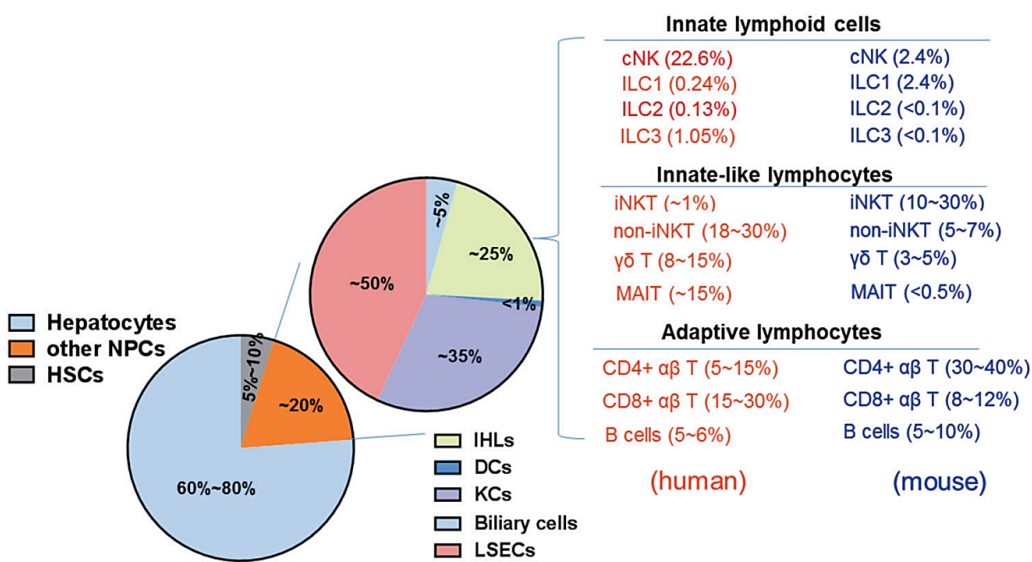


**Figure 3: Cell composition of the healthy adult liver.** The liver is composed of parenchymal hepatocytes and nonparenchymal cells (NPCs), including hepatic stellate cells (HSCs) and other NPCs (KCs, LSECs, DCs, biliary cells, and IHLs). According to the features of immune responses, IHLs are divided into three groups: innate lymphoid cells, innate-like lymphocytes, and adaptive lymphocytes. The numbers indicate the estimated proportion of each population relative to the total number of IHLs, NPCs, or total liver cells. Lymphocyte subsets within human and murine IHLs are shown in red and blue, respectively. KCs Kupffer cells, LSECs liver sinusoidal endothelial cells, DCs dendritic cells, IHLs intrahepatic lymphocytes, ILC innate lymphoid cell, NK natural killer, LTI lymphoid tissue-inducer, iNKT invariant natural killer T, non-iNKT non-

*invariant natural killer T, MAIT mucosal-associated invariant T cells. Caption and image adapted from reference (29).*

### **1.c.1. Hepatocytes**

The major hepatic parenchymal population is the hepatocytes. Hepatocytes constitute up to two-thirds of the total number of liver cells (30). As with all epithelial cells, hepatocytes have apical and basolateral membranes. The apical membranes harbor the bile canaliculus, while the basolateral membranes face the perisinusoidal space of Disse. Hepatocytes are powerful biosynthetic factories. Consequently, they possess enlarged endoplasmic reticulum (ER) and Golgi apparatus devoted to the synthesis and transport of secretory products including albumin, clotting and complement factors, acute-phase proteins, and bile components among others. In addition, hepatocytes endocytose dietary lipids, biotransform, and store them as lipid droplets, and subsequently release them in circulation as very low-density lipoprotein (VLDL) particles. Finally, hepatocytes express the largest detoxifying machinery of the body, counting with about 50 different cytochrome P450 enzymes embedded in the ER membrane (31, 32). These enzymes metabolize dietary-derived fat-soluble toxins into water-soluble excretory products that are subsequently secreted via the bile, urine, or sweat.

Hepatocytes in the murine and human liver are histologically, biochemically, and functionally heterogeneous. A major determinant of such heterogeneity is the metabolic zonation established along the sinusoids by gradients of oxygen, nutrients, metabolites, hormones, and cytokines (Figure 4). Thus, the hepatocyte function varies according to its specific location along the porto-central sinusoidal axis. Examples of zoned expression of metabolic pathways by pericentral hepatocytes include *de novo* lipogenesis, glycolysis, drug metabolism, and bile acid and heme synthesis. On the contrary, oxidative phosphorylation, gluconeogenesis, albumin, and urea secretion are more active processes in periportal hepatocytes (10, 33). Not surprisingly, zoned expression of metabolic pathways explains the spatial pattern of injuries observed in several liver pathologies including centrilobular necrosis in acetaminophen-induced toxicity and accumulation of lipid droplets around central veins in non-alcoholic fatty liver disease (NAFLD) (34-36).

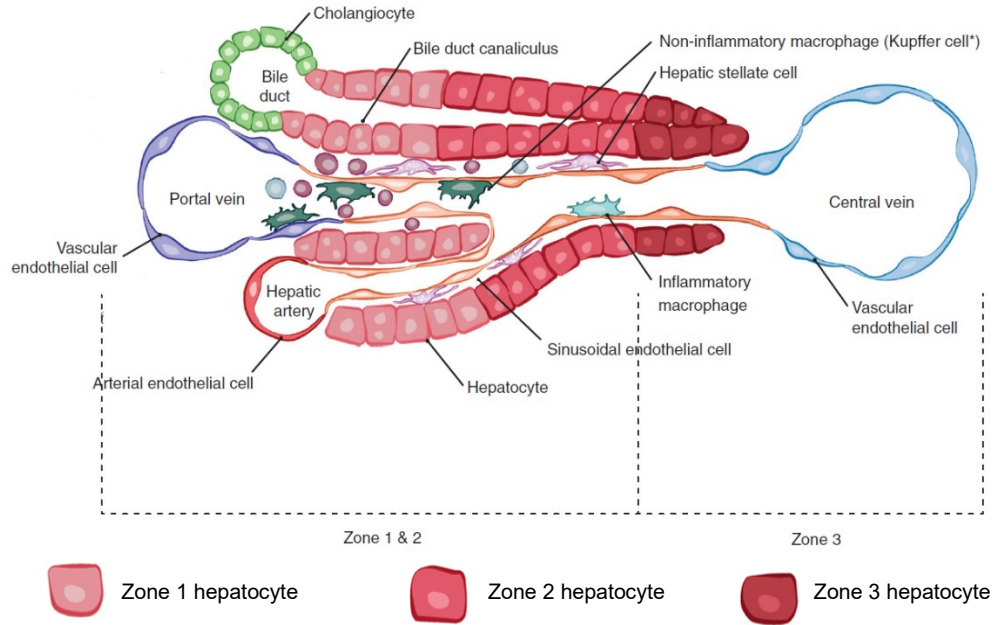


**Figure 4: Schematic representation of the metabolic zonation of the liver.** Highly oxygenated and nutrient-rich blood enters the sinusoids at the level of the portal tracts (zone 1) and slowly flows towards the central vein (zone 3). Zone 1 hepatocytes (periportal) perform tasks that require more energy and nutrients. Zone 3 hepatocytes (pericentral), with access to less oxygenated blood, carry out tasks with lower energy demands. Caption and image adapted from reference (13).

In the last few years, single-cell RNA sequencing (scRNA-seq) has become a powerful technique for mapping the transcriptomic landscape of hepatic cells. scRNA-seq on liver parenchymal cells from mice and humans has further confirmed the existence of different subpopulations of hepatocytes that cluster according to the expression of zonation markers, thereby validating the tight association between transcriptional signatures of hepatocytes and spatial location (12, 13). These studies have revealed that up to 50 % of hepatocyte genes exhibit zoned expression patterns (12, 13, 37-40). One major principle of metabolic hepatic zonation revealed in this matter is that energetically demanding processes are enriched in periportal hepatocytes that are bathed in oxygen and nutrient-rich blood. Conversely, tasks with lower energy demands are performed by pericentral hepatocytes with access to less oxygenated blood (39, 41). Interestingly, while in the murine liver, hepatic progenitor cells are selectively located in the canal of Herring (oval cells), in humans, hepatocytes with stem-like properties were heterogeneous regarding zonation markers suggesting a more dispersed spatial distribution of these cells in the human liver parenchyma (13, 42). To summarize, the spatial organization of hepatocytes influences their gene-expression and



functional profiles and allows for the simultaneous execution of varied and divergent tasks within the same tissue environment.

### **1.c.2. Cholangiocytes**

The second parenchymal population is cholangiocytes. Cholangiocytes are the epithelial cells lining the bile ducts and represent about 3 to 5% of all liver cells. Cholangiocytes are organized in a system of vessels known as the biliary tree. They participate in the production and transport of bile and therefore they are key actors in the excretion of waste products and the digestive function of the bile. Cholangiocytes exhibit morphological and functional heterogeneity according to their position in the biliary tree. Small and large cholangiocytes exhibit different secretory functions (43). Immature, poorly differentiated cholangiocytes are present in the Canals of Hering. These cholangiocytes are progenitor cells exhibiting stemness and the capability to differentiate into hepatocytes especially in situations of extensive hepatocellular death frequently seen in several liver pathologies. On the other hand, cholangiocytes in larger and more oxygenated bile ducts are more differentiated. In general, along the biliary tree, differential access to oxygen and metabolites determines the metabolic, secretory, and absorptive properties of cholangiocytes and therefore their phenotype (44).

The transcriptional profile of cholangiocytes has been recently established by scRNA-seq in mice, and the combination of scRNA-seq/single-nucleus RNA sequencing (snRNA-seq) in humans (13, 20, 45). Compared to hepatocytes, murine cholangiocytes displayed upregulated expression of epithelial cell adhesion molecule (*Epcam*), cadherin 1 (*Cdh1*), SRY-box transcription factor 9 (*Sox9*), secreted phosphoprotein 1 (*Spp1*), keratin 7 (*Krt7*), keratin 19 (*Krt19*), jagged 1 (*Jag1*), neurogenic locus notch homolog protein 2 (*Notch2*), and hairy and enhancer of split-1 (*Hes1*) (20). Similarly, human cholangiocytes were found to express the highest levels of *KRT7*, *KRT19*, *SOX9*, and *EPCAM* compared to all other hepatic cell populations, and exhibited a secretory (e.g., cystic fibrosis transmembrane regulator (*CFTR*), FXFD domain-containing ion transport regulator 2 (*FXFD2*), and trefoil factor 2 (*TFF2*)), and pro-inflammatory signature (e.g., lipocalin (*LCN2*), *CXCL1*, and *CXCL6*) (13). Regarding human cholangiocytes, their profiling using snRNA-seq and scRNA-seq resulted in the identification of two transcriptionally distinct subpopulations (45). One subset was classified as mature large cholangiocytes expressing differentiated cholangiocyte-

associated markers consistent with bile duct cholangiocytes, and a second subset of small and less differentiated B-cell lymphoma 2 (*BCL2*) positive cholangiocytes. Mature cholangiocytes expressed high levels of *SPP1*, *SOX9*, aquaporin (*AQP1*), cysteine-rich angiogenic inducer 61 (*CYR61*), *KRT8*, *KRT7*, *KRT18*, beta-defensin 1 (*DEFB1*), *CXCL1*, and *CD24*. Small cholangiocytes expressed high levels of progenitor-associated markers including fibroblast growth factor receptor 2 (*FGFR2*), and *SOX6* (45).

Cholangiocytes can be affected by insults of various origins including genetic, infectious, immune-mediated, malignant, vascular, and idiopathic. If these insults persist, the resultant chronic inflammation leads to fibrosis, cholangiocarcinoma, and liver failure (46). The most important immune-mediated cholangiopathies are primary biliary cholangitis (PBC), primary sclerosing cholangitis (PSC), and autoimmune cholangitis (AIC) (47). In the subsequent sections of this introduction, we will revise the current knowledge on the involvement of hepatic immune cells in these pathologies.

#### **1.d. Non-parenchymal cells of the liver**

The NPCs of the liver include non-immune and immune cellular populations (Figure 3). Since immune NPCs will be the subject of a separated section, we will focus herein on the main non-immune NPCs including LSECs, HSCs, and portal fibroblasts (PF).

##### **1.d.1. Liver Sinusoidal Endothelial Cells (LSECs)**

Endothelial cells are the building blocks of hepatic vessels. The liver is a highly vascularized organ with different subsets of endothelial cells lining the big, medium size, and capillary vessels. Several types of hepatic endothelial cells have been described. scRNA-seq on the murine liver has defined four transcriptionally distinct endothelial populations: LSECs, central venous R-Spondin 3 (*Rspo3*) positive endothelial cells, carboxypeptidase E (*Cpe*) positive CD320<sup>+</sup> portal vein endothelial cells, arterial allograft inflammatory factor 1 like (*Aif1l*) positive endothelial cells, and lymphatic podoplanin (*Pdpn*) positive endothelial cells (19, 48). Since immune cells mainly interact with LSECs during homeostasis and in response to injury, in this introduction we will focus on this specialized subset of endothelial cells that line the sinusoids.

LSECs line the hepatic sinusoids forming a barrier between the bloodstream and the parenchyma (49). These specialized endothelial cells are histologically, functionally, and phenotypically unique. Their most conspicuous features compared to other capillary endothelial cells is the absence of a basement membrane and the presence of fenestrations clustered in sieve plates (Figure 5) (50). Fenestrations are dynamic pores with diameters of ~50–150 nm along the membranes of LSECs that allow the selective and dynamic exchange of macromolecules and plasma between the intrasinusoidal blood and the perisinusoidal interstitial fluid (27, 51). Advanced microscopy techniques have shown that CD8<sup>+</sup> T cells and Kupffer cells can directly contact hepatocytes through discontinuation points in the endothelial layer or directly through the fenestrations in LSECs (Figures 6 and 7) (52-55). Whether other intrasinusoidal immune populations use this mechanism for accessing the perisinusoidal compartment is still unknown.

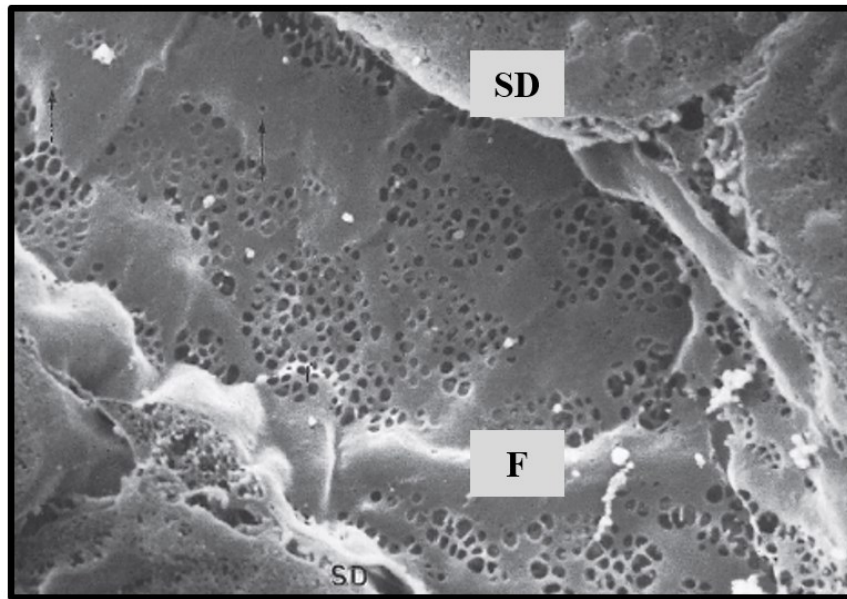


**Figure 5: High resolution image of a hepatic sinusoid.** Scanning electron microscopy (SEM) illustrating normal hepatic sinusoid in rat liver. Endothelial fenestrations (F) of about 0.1  $\mu\text{m}$  are grouped in sieve plates. SD, space of Disse. Caption and image adapted from reference (24).

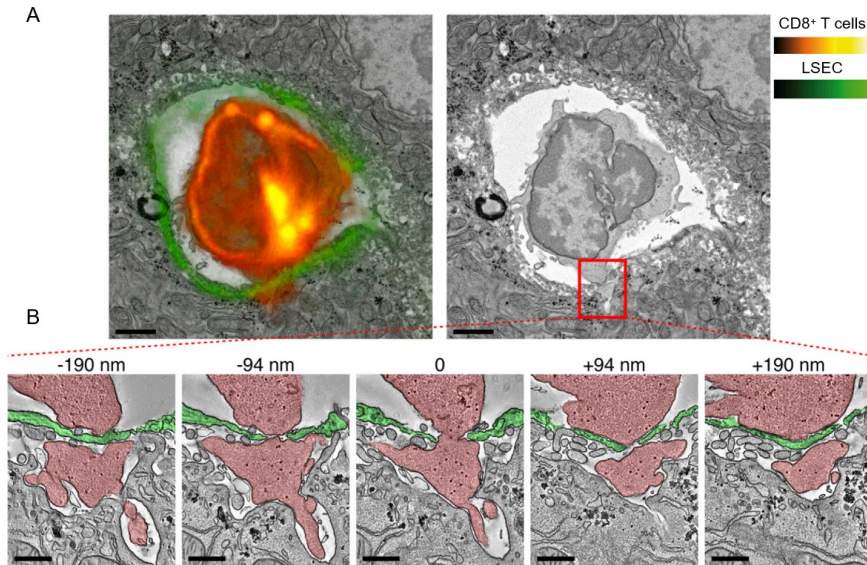


**Figure 6:  $CD8^+$  T cells contact hepatocytes through discontinuation points in the sinusoidal walls.** (A) Correlative confocal and transmission electron microscopy of the liver of a hepatitis B c antigen (HBcAg) transgenic mouse whose LSEC express membrane-targeted tdTomato that was injected 30 min earlier with antigen-specific  $CD8^+$  T cells. Left: overlay of the Ag-specific  $CD8^+$  T cells and LSEC fluorescence (red and green, respectively). Right: electron micrograph alone. Scale bars represent 2 mm. (B) Transmission electron tomograms of five selected serial slices from the area delineated by the red inset in (A). The numbers indicate the z-distance from the middle section.  $CD8^+$  T cells and LSEC are indicated by the red and green overlay, respectively. Scale bars represent 500 nm. Caption and image adapted from reference (52).

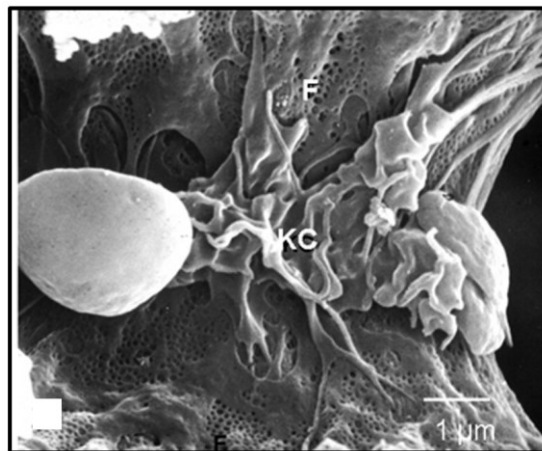


**Figure 7: KCs project processes through the fenestrae of LSECs.** Scanning electron micrograph of Kupffer cell (KC) attached to the luminal surface of sinusoidal endothelium by processes that penetrate fenestrae (F). The scale bar represents 1  $\mu\text{m}$ . Caption and image adapted from reference (54).

LSECs are strategically positioned to act as a filter of blood coming from the systemic circulation and from the gut. Functionally, LSECs are powerful scavengers due to their elevated endocytic activity and high expression of scavenger receptors which account for the remarkable waste removal capacity of these cells (56, 57). Among the waste products cleared by LSECs are immune complexes, advanced glycation end products, and microbial antigens (49, 58). The scavenger activity of LSECs has also been linked to the clearing of blood-borne viruses. It has been estimated that about 90 % of viral particles during infection are removed by LSECs (59). However, viruses like hepatitis B virus (HBV) and hepatitis C virus (HCV) have evolved mechanisms to subvert this function and use LSEC's fenestrate to access the subendothelial compartment and further spread (60, 61). In addition to the removal of waste and microbial-derived products, LSECs contribute to homeostasis by maintaining HSC in the quiescent state in a vascular endothelial growth factor (VEGF) and nitric oxide-dependent manner and thereby preventing undesirable fibrogenic responses (62, 63).

LSECs perform several immune-related functions and are important players in balancing tolerance to harmless gut-derived antigens versus immunity against invading pathogens (Figure 8). LSECs express a variety of pathogen recognition receptors (PRRs) allowing them the rapid sensing of microbial products and pathogens. This includes but is not limited to toll-like receptors (TLRs) 1 to 9, and intracellular nucleotide-binding oligomerization domain (NOD-like) receptors (64-66). Signaling through these PRRs can lead to both tolerance and immune activation depending on the nature of the stimuli, the dose, and the cytokine environment. A well-studied example is the response to chronic exposure to lipopolysaccharide (LPS) during homeostasis. LSECs remove about 75% of the gut-derived LPS (67). While LPS sensing through TLR4 leads to activation of nuclear factor- $\kappa$ B (NF- $\kappa$ B) in most cell types, in LSECs, LPS signal during homeostasis is associated with reduced nuclear translocation of NF- $\kappa$ B and consequently reduced leukocyte adhesion and recruitment. In addition, TLR4 signaling in LSECs leads to IL-10 production and

downregulation of the antigen-presenting machinery further enforcing tolerance in the hepatic tissue (68, 69).

### Immune Tolerance by LSECs

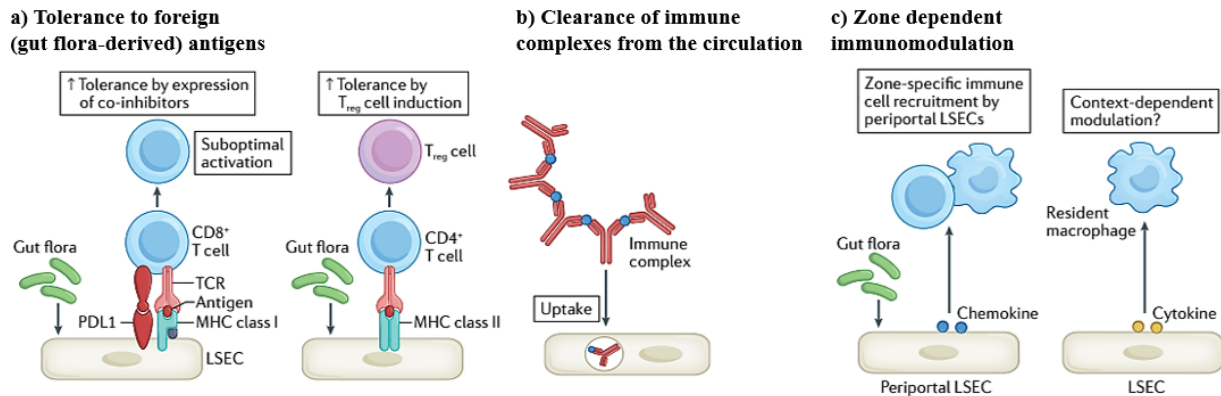


**Figure 8: Immunomodulation by liver LSECs.** A) LSECs with immunomodulatory properties facilitate tolerance to harmless gut flora-derived antigens through co-inhibition of CD8<sup>+</sup> T cells via the checkpoint ligand PDL1 upon cross-presentation of gut flora-derived antigens or through the induction of regulatory Treg cells. B) LSECs clear immune complexes from circulation via uptake and degradation. C) Periportal LSECs sense gut bacteria and recruit resident macrophages and lymphocytes through chemokine gradients. Caption and image adapted from reference (70).

Under physiological conditions, LSEC scavenger receptors mediate antigen capture, processing, and presentation which is key for the induction of T-cell tolerance to harmless food-derived antigens (71, 72). Moreover, LSECs express MHC class I and class II, and costimulatory ligands like CD40, CD80, and CD86, and therefore, can modulate adaptive immune responses through antigen presentation to T cells (1, 73). Interestingly, antigen presentation by LSECs has been linked to tolerogenic activity and maintenance of hepatic immune homeostasis (66, 74). Programmed death-ligand 1 positive (PD-L1<sup>+</sup>) LSECs cross-present antigens to CD8<sup>+</sup> T cells resulting in tolerization of the responding CD8<sup>+</sup> T cells. This mechanism is responsible for oral tolerance to food-derived antigens and is hijacked by tumor cells to escape immunity (75, 76). In addition, LSECs can also present antigens to naïve CD4<sup>+</sup> T cells in the context of MHC class II molecules leading to the development of regulatory T cells (71, 72, 75-77). Despite the tolerogenic nature of antigen presentation by LSECs, the presence of harmful pathogens can rapidly shift the

balance toward immune activation. This shift is dependent on antigen load and the presence of inflammatory mediators (e.g., IL-2 and IL-6), and leads to the recruitment and activation of monocytes, macrophages, and neutrophils (68, 73, 78-80).

LSECs significantly change their phenotype and behavior during chronic pathological conditions. The most prominent change is the loss of LSEC fenestrations in a process called capillarization that also involves the development of an organized basement membrane (81-83). LSEC capillarization facilitates HSC activation and is therefore a major player in the pathogenesis of liver fibrosis. scRNA-seq analysis in human cirrhotic versus normal liver has revealed the presence in the necrotic niche of LSECs that are absent in healthy liver (19). The origin of these LSECs is a subject of current debate.

LSECs are spatially and functionally heterogeneous despite sharing the same origin. So far, this heterogeneity has only been linked to metabolic hepatic zonation. Recently developed paired-cell sequencing (pcRNAseq) technology applied to pairs of hepatocytes and LSECs allowed reconstructing the spatial zonation of murine LSECs using the spatial information of paired hepatocytes (11). This analysis revealed significant zonation in more than 35 % of the genes of murine LSECs (e.g., Wnt ligands and *Rspo3*). Zonation was also found in human LSECs with about 67% of genes displaying zonated expression patterns along the porto-central sinusoidal axis (13, 37). The different transcriptional profiles of Zone 1 vs. Zone 2 and 3 LSECs suggest a division of labor along the porto-central sinusoidal axis. Zone 1 or periportal LSECs were enriched in transcripts associated with vessel development, pathways of translation, targeting ER, and TNF activation. By contrast, Zone 2 and 3 (pericentral) LSECs were enriched for transcripts associated with innate immunity, phagocytosis, leukocyte activation, and antibacterial defense (13). The most interesting finding of these studies is the shared expression of zonated genes across cell types (e.g., expression of *Notch* target *Hes1* and *Ctsl* in hepatocytes and colocalized LSECs), suggesting that the activity of genes can be spatially regulated (11, 12).

In summary, LSECs contribute to the tolerogenic environment of the liver through several mechanisms including the removal of dietary antigens, toxins, and other pathogen-derived products, tolerization of CD4<sup>+</sup> and CD8<sup>+</sup> T cells, and induction of regulatory T cells. However, early detection of tissue damage or pathogen invasion by LSECs can overcome these tolerogenic

pathways and induce rapid activation of the endothelium, recruitment of leukocytes, and promotion of adaptive immune responses.

### 1.d.2. Hepatic Stellate Cells (HSCs)

HSCs were first described by Karl Wilhelm von Kupffer in the 19<sup>th</sup> century (84). They are in the space of Disse in contact with the basolateral membrane of hepatocytes and the anti-luminal side of LSECs (Figure 2). HSCs have prominent dendritic-like processes that they use to make contact and sample hepatocytes. Recent studies have revealed that quiescent HSCs are also in direct contact with sinusoidal KCs that reach them through processes they project across the endothelial barrier (Figure 9) (85). scRNA-seq on hepatic mesenchymal cells identified a signature for HSCs in the mouse healthy liver characterized by the increased expression of lecithin retinol acyltransferase (*Lrat*), reelin (*Reln*), extracellular matrix protein 1 (*Ecm1*), vasoactive intestinal peptide receptor 1 (*Vipr1*), collectin kidney 1 (*Colec11*), parathyroid hormone 1 receptor (*Pth1r*), *Hgf*, regulator of G protein signaling 5 (*Rgs5*), and nerve growth factor receptor (*Ngfr*). Gene ontology enrichment analysis showed that over-represented GO terms included retinoic metabolic process, regulation of lipid metabolism, antigen processing and presentation, and vitamin A metabolic process (9).

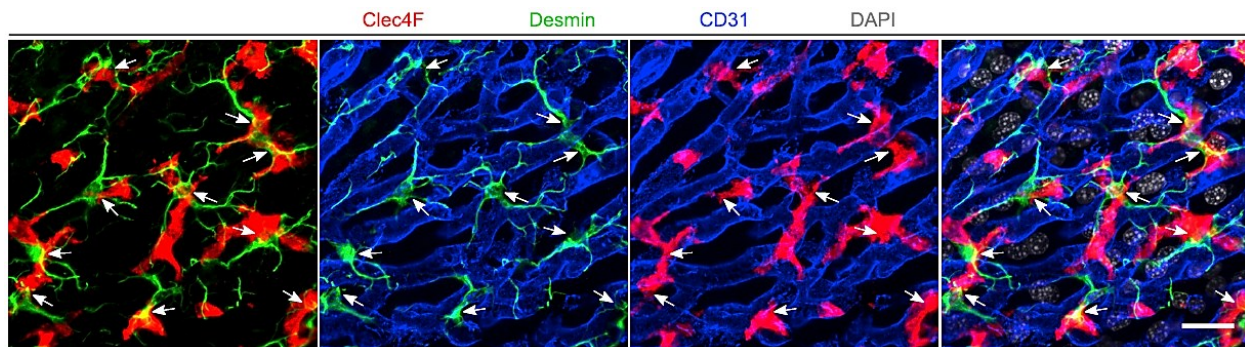


**Figure 9: HSCs and KCs establish direct contact in the healthy liver.** Mouse liver sections stained for CLEC4F (red, KCs), Desmin (green, HSCs), CD31 (blue, LSECs), and DAPI (gray). Arrows pointing at colocalization between Desmin<sup>+</sup> HSCs and CLEC4F<sup>+</sup> KCs. Scale bar, 20  $\mu$ m. Caption and image adapted from reference (85).

At steady state, quiescent HSCs are the main store of vitamin A in the body. Notably, the vitamin A droplets in HSCs display a heterogeneous pattern that is dependent on their spatial position along



the porto-central sinusoidal axis with periportal HSCs exhibiting bigger droplets (86). Interestingly, the activation of HSCs upon injury is accompanied by the loss of vitamin A droplets. Whether this loss of droplets is required for activation or is one of its consequences remains unanswered (87).

Upon injury, HSCs can sense damage from neighboring hepatocytes, LSECs, or KCs through several PRRs that recognize damage and pathogen-associated molecular patterns (DAMPs and PAMPs). This initiates a sequence of events that induces the conversion of quiescent vitamin-A-rich HSCs into proliferative, fibrogenic, and contractile activated HSCs (aHSCs). The net effect of HSC activation is the increase in the deposition of fibrillar collagens in the surrounding extracellular matrix (ECM). While other hepatic populations can contribute to fibrillar collagen production upon injury, it is now clear that aHSCs are the main cellular source of fibers irrespective of the underlying liver etiology (88, 89).

The activation process of HSCs has been conceptualized as a two-step process that consists of initiation, and perpetuation. During initiation, HSCs sense the damage via paracrine signaling and become more responsive to cytokines and other stimuli. Multiple early activating signals have been proposed, including lipid peroxides and apoptotic bodies from injured/dead hepatocytes, TGF $\beta$  released from the ECM, fibronectin secreted by activated LSECs, growth factors from platelets (PDGF, EGF, and TGF $\beta$ ), and reactive oxygen species (ROS) from activated KCs. HSCs are cellular nodes that integrate these multiple signals of damage and become activated in response to them. The process of maintenance and amplification of the activated phenotype is called perpetuation and is dependent on autocrine and paracrine signaling (e.g., TGF $\beta$  signaling). During perpetuation, HSCs differentiate into myofibroblast-like cells and become proliferative, and motile, starting secreting fibrillar collagens, and releasing chemokines and cytokines that influence the behavior of infiltrating immune cells (87, 90-93).

There is accumulating evidence pointing to the potential immunomodulatory activity of HSCs. Since aHSCs become motile and can respond to chemokines gradients (e.g., CCL2), they migrate and colocalize with other immune cells that respond to the same chemoattractants. In addition, aHSCs themselves produce chemokines for monocyte/macrophages like CCL2, CCL5, CCL21, and CX3CL1, and neutrophils like CXCL1 (81, 94-96). This may explain the frequent observation of HSCs colocalized with both macrophages and neutrophils in the injury site (Figure 18). In

addition, aHSCs have been shown to release IL-6 and IL-10 which can modulate the behavior of immune cells (87, 97-99). Moreover, HSCs are unconventional antigen-presenting cells (APCs). Upon activation, HSCs upregulate the expression of antigen-presenting molecules MHC class I and II, non-classical MHC-like molecules CD1c and CD1d, and costimulatory molecules CD40, CD80, and CD86 (100-102). Winau et al. demonstrated that aHSCs presented microbial lipids and activated NKT cells *in vivo* in a CD1d-dependent manner. Furthermore, aHSCs processed the entire ovalbumin protein and presented/cross-presented peptides to CD4<sup>+</sup> and CD8<sup>+</sup> T cells respectively, in co-culture systems inducing expansion of antigen-specific T cell clones (101).

Beyond their capacity to remodel the ECM through the deposition of fibers, aHSCs are critical players in the wound healing response to hepatocellular injury through the production and secretion of a large repertoire of growth factors that influence tissue cell proliferation and consequently, repair. aHSCs have been shown to secrete TGF $\alpha/\beta$ , epidermal growth factor (EGF), stem cell factor (SCF), insulin-like growth factor (IGF), connective tissue growth factor (CTGF), fibroblast growth factor (FGF), and macrophage colony-stimulating factor (M-CSF). All these factors are upregulated during the wound healing response to hepatic injury and have powerful mitogenic activity on specific hepatic resident populations leading to the effective replacement of dead and damaged tissue cells and restoration of tissue homeostasis (103-109).

scRNA-seq combined with *in situ* RNA hybridization (RNAscope) and immunofluorescence staining on hepatic mesenchymal cells from mice, uncovered that HSCs are spatially and functionally zoned (Figure 10). Two topographically distinct subpopulations of HSCs were delineated: portal vein-associated HSCs (PaHSCs) and central vein-associated HSCs (CaHSCs). These subpopulations exhibited two opposed signatures with PaHSCs expressing genes including and associated with *Ngfr* and integrin beta chain beta 3 (*Itgb3*), and CaHSCs expressing genes including and associated with a disintegrin and metalloproteinase with thrombospondin motifs 2 (*Adamts12*) and *Rspo3* (9). Based on the sequencing data, the best markers selected for imaging were NGFR and Adamts12 (RNAscope) for PaHSCs and CaHSCs respectively. Imaging the healthy liver with these markers revealed the enrichment of NGFR<sup>+</sup> cells around portal tracts and the enrichment of Adamts12<sup>+</sup> cells around central veins (Figure 10). The healthy human liver showed similar zoned distribution of NGFR and Adamts12 in HSCs (9). Interestingly, certain zoned markers expressed by HSCs are also genes with zoned expression within the LSECs

(e.g., high expression of *Itgb3*) in peri-portal LSECs versus high expression of *Rspo3* in peri-central LSECs) suggesting spatial modulation of transcriptional programs (9).

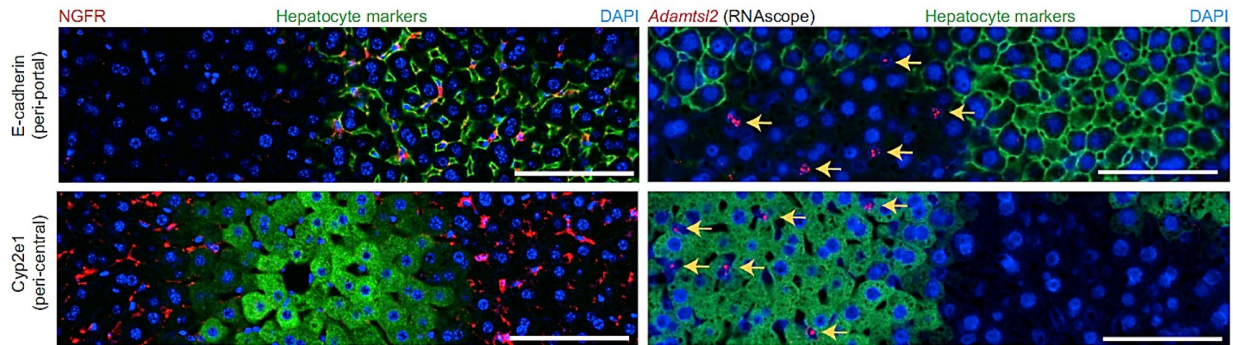


**Figure 10. HSC zonation across the healthy liver lobule.** Representative immunofluorescence and RNAscope images of healthy murine livers: NGFR/Adamtsl2 (RNAscope) (red), E-cadherin/Cyp2e1 (immunofluorescence) (green), DAPI (blue). Scale bar, 100  $\mu$ m. The yellow arrows indicate Adamtsl2<sup>+</sup> cells. Caption and image adapted from reference (9).

Interestingly, CaHSCs were identified as the dominant pathogenic collagen-producing subset that is expanded upon chronic central vein injury with CCl<sub>4</sub> (9). Whether this pathogenic role of CaHSCs is intrinsic to this subset or is simply the consequence of the location of the CCl<sub>4</sub> injury (central vein injury) remains to be elucidated (9).

HSCs from healthy human livers were recently profiled using scRNA-seq and snRNA-seq (45). Two clusters were identified. The first cluster expressed high levels of markers of quiescent HSCs including hepatocyte growth factor (*HGF*), parathyroid hormone 1 receptor (*PTH1R*), reelin (*RELN*), vasoactive intestinal peptide receptor 1 (*VIPR1*), and retinol-binding protein 1 (*RBPI*). The second cluster was enriched for pathways of inflammation (e.g., interferon lambda receptor 1 (*IFNLR1*), lipopolysaccharide-binding protein (*LBP*), *IL4R*, *IL6R*, *CXCL2*, and *CXCL12*), pathways of antigen presentation (e.g., *HLA DMB*, *HLA DMA*, *CD74*, and *CAP-Gly domain-containing linker protein 1 (CLIP1)*), pathways of retinol metabolism (e.g., cytochrome P450 family 2 subfamily C member 9 (*CYP2C9*), and aldehyde dehydrogenase 1 family member (*A2ALDH1A2*)), and pathways associated with angiogenesis (e.g., *VEGFA* and *VEGFB*). Thus, this subset was classified as activated HSCs (45). In this study, spatial transcriptomics showed that the transcriptional signatures of these two HSC clusters were dispersed throughout the healthy liver tissue, and no HSC zonation was reported (45). However, this result does not necessarily

contradict the previously reported zonation of human HSCs based on the topographically separated expression of *Ngfr* and *Adamtsl2* along the porto-central sinusoidal axis (9). The apparent conflict could be the consequence of the different profiling techniques used. While the first study used spatial transcriptomic, which relies on a combination of microscopy and RNA sequencing, the second study profiled HSCs by RNA *in situ* hybridization (RNAscope) and immunofluorescence that rely on binding of probes and antibodies to RNA or antigens respectively, and subsequent signal amplification (9, 45).

In summary, HSCs are the main hepatic population involved in the synthesis, secretion, and organization of ECM components both in health and disease. HSCs exhibit spatial zonation and are important partners of immune cells due to their capacity to sense damage, produce cytokines, chemokines, and growth factors, and act as unconventional APCs. How the spatial zonation of HSCs may impact the activation and effector functions of resident and infiltrating immune cells remains to be established.

### **1.d.3. Portal Fibroblasts**

Portal fibroblasts (PFs) are the resident fibroblasts of the portal tract (110). They are located underneath the epithelial layer around the portal vein and are proposed to form a support system that maintains the structural integrity of portal tracts (111). PFs were first distinguished from HSC as an alternate source of myofibroblasts in the bile duct ligation (BDL) model of biliary fibrosis. Activated PFs were identified as  $\alpha\text{SMA}^+$   $\text{Desmin}^-$  cells proliferating around injured portal tracts. Interestingly, these PFs were associated with collagen bundles, suggesting their potential involvement in matrix deposition (112).

Difficulties in labeling and isolating PFs have determined that their role in health and disease remains poorly defined and controversial. There is no single marker of PFs. They are rather defined by a combination of several markers including elastin, Thy1, Fibulin 2, and ectonucleotidase NTPDase 2, and the lack of HSC markers (e.g., Desmin) (110, 113).

PFs have been shown to give rise to myofibroblasts and proliferate in response to biliary injury (111, 114-117). However, their relative contribution to the deposition of fibrillar collagens is still controversial. Early immunofluorescence studies found that a periportal population of myofibroblasts lacking markers of HSCs, expanded very early upon BDL. This population was

assumed to be PFs and exhibited different kinetics relative to HSCs (117). In a similar study, Desmoulière et al. showed that the deposition of ECM components (e.g., laminin, fibronectin EIIIA, collagen I and IV, procollagen III, elastin, tenascin) in the portal area post-BDL preceded myofibroblastic differentiation and therefore could not be attributed to HSCs (118). Furthermore, *in vitro* experiments with freshly isolated PFs showed that they secrete type I and III fibrillar collagens (119-121). Collectively, these studies strongly pointed at PFs as early contributors to matrix deposition in models of cholestatic disease, but definitive confirmation could not be reached due to the lack of specific markers. What these studies did prove though was the existence of a non-stellate cell population of portal myofibroblasts that expanded during biliary injury (122).

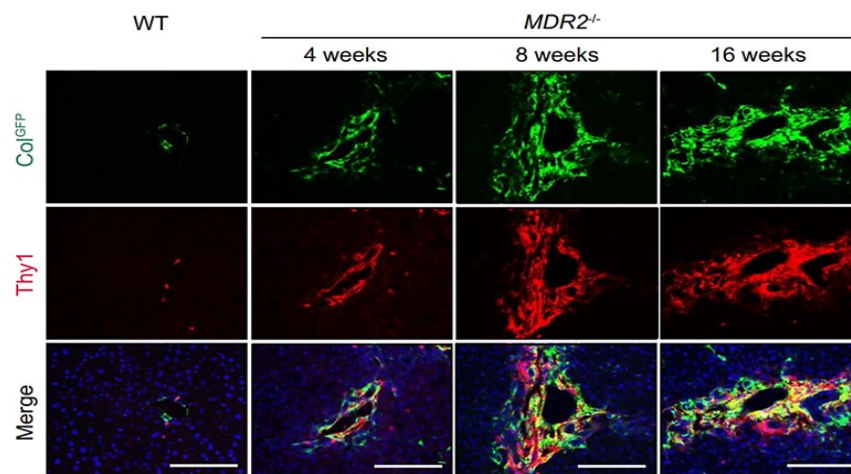


**Figure 11: PFs secrete collagens in response to biliary injury.** Immunofluorescence showing colocalization of collagen 1a1 (green), and the specific PF marker Thy1 (red) in liver sections from WT (left column), and fibrotic MDR2 KO mice (3 right columns). DAPI is blue. Scale bar, 100  $\mu\text{m}$ . \* indicates portal tracts. Caption and image adapted from reference (123).

Conversely, cell fate mapping studies by Mederacke et al. using the LRAT YFP mice found that HSCs are the main source of ECM fibers in biliary injury models. According to this study, only a small population of myofibroblasts, representing about 10 % of the total, could be potentially derived from PFs (88). Since this study investigated relatively late time points upon BDL, it was suggested that the possibility of PFs contributing to fiber deposition at earlier time points could not be ruled out (122). This hypothesis was tested in two recent studies using different models of cholestatic disease (123, 124). In the first study, the authors used BDL on Col1a1 GFP mice and reported that PFs expressed Col1a1 (GFP<sup>+</sup>) in the uninjured liver and proliferate upon BDL but with a limited number of PFs becoming  $\alpha\text{SMA}^+$  myofibroblasts (124). However, the second study

using the MDR2 KO mice showed similar contributions from PFs and HSCs to the pool of myofibroblasts in response to biliary injury. Colocalization of *Coll1a1* and the PF marker *Thy1* around fibrotic portal tracts in the livers of MDR2 KO strongly suggested a major role of PFs in collagen deposition during biliary injury (Figure 11) (123). Taken together, these studies have confirmed that PFs are expanded during biliary injury. However, different injury models and mouse strains have provided conflicting results and there is still no consensus on the role of PFs as major contributors to fibrosis in human disease. Further studies are warranted to settle this important question.

Single-cell technologies have been recently used to profile murine and human PFs (9, 13, 45). The marker genes identified for murine PFs were *Cd34*, C-type lectin domain family 3-member B (*Clec3b*), gelsolin (*Gsn*), dermatopontin (*Dpt*), microfibril-associated protein 4 (*Mfap4*), ectonucleoside triphosphate diphosphohydrolase 2 (*Entpd2*), collagen type XV alpha 1 chain (*Coll15a1*), and fibulin 2 (*Fbln2*). Gene Ontology enrichment terms associated with murine PFs included ECM organization and connective tissue development in line with their postulated role as cells in charge of the maintenance of the structural integrity of portal tracts. Imaging showed that *CD34*<sup>+</sup> PFs were mostly located in the portal niche, adjacent to biliary epithelial cells but absent in the sinusoidal areas. In addition, a few PFs were also found in the second layer of central veins (9). Concerning human PFs, two clusters were annotated by scRNA-seq and snRNA-seq. The most abundant cluster exhibited high expression of markers of lipid metabolism (aldehyde oxidase 1 (*AOX1*) and phosphodiesterase 3b (*PDE3b*)), inflammatory mediators (e.g., *IL18R1* and *IL15RA*). The second subset of human PFs, presented enriched expression of collagen-associated genes (e.g., *COL1A1*, *COL3A1*, *COL1A2*, and actin beta (*ACTB*)), matrix remodeling genes (e.g., matrix metalloproteinases 23b (*MMP23b*), *MMP14*, tissue inhibitor of metalloproteinases 1 (*TIMP1*) and *TIMP2*), inflammatory mediators (e.g., *CSF1*, *IL32*, and *CCL2*), and fibrosis-associated genes (e.g., AE Binding Protein 1 (*AEBP1*), *IL33*, and *TGFBR2*) (45).

In summary, PFs are a heterogeneous population that protects and provides mechanical support to bile ducts. Activated PFs play important roles in cholestatic liver disease and are early contributors to fibrosis. However, their contribution during advanced fibrosis is still controversial and dependent on the injury model and the mouse strain. Single-cell technologies are better at defining

the phenotype of this elusive hepatic population and will assist the development of better methods for their isolation and study.

### **1.e. Liver Resident Immune Cells**

The liver is an immunological barrier that protects the organism by removing gut-derived microbial products, pathogens, food antigens, and waste products from the blood. Several unique immunomodulatory mechanisms function in the liver to prevent unwanted immune activation in response to innocuous antigens, and yet deliver immunity to infection. This delicate balance between tolerance and immunity is the product of the coordinated action of a large network of resident immune cells adapted to the hepatic tissue (125, 126). The liver harbors the largest macrophage population of the body, the KCs, and unusually large populations of other innate cells and innate-like lymphocytes including DCs, NK and NKT cells, mucosal-associated invariant T cells (MAIT), and  $\gamma\delta$  T cells. These hepatic resident immune cells occupy specific niches and cooperate with other non-hematopoietic neighboring cells in a spatially regulated manner to fulfill the protective function of the liver (1).

Immune profiling of intrahepatic leukocytes in mice versus humans has revealed considerable differences in the composition of the immune compartment (Figure 3) (29). The divergence between mice and humans in terms of the type and frequency of intrahepatic immune cells is the result of the interaction of genetic differences with environmental variables (e.g., diet, pathogens) throughout their evolutionary history. Despite the phylogenetic relatedness between mice and humans, mice often respond to injuries and therapeutic interventions in ways that differ from humans (127). Therefore, it is not possible to directly extrapolate to humans the observations made in mouse models.

#### **1.e.1. Liver Macrophages**

Hepatic macrophages are myeloid cells that constitute the largest macrophage population in the body. Liver macrophages perform metabolic and immune tasks that are crucial for organ and systemic homeostasis. Not surprisingly, dysregulation of macrophage numbers and effector functions is linked to the pathogenesis of multiple liver diseases (128).

Recent data obtained by newly developed multiomic techniques have revealed that the hepatic macrophage compartment is more heterogeneous than previously thought. At least three subpopulations of macrophages have been identified in the healthy liver of mice: KCs, liver capsular macrophages (LCMs), and monocyte-derived macrophages (MoMFs). This diversity can be expanded during inflammation as demonstrated in acute injury models where GATA6<sup>+</sup> peritoneal macrophages, non-classical monocyte/macrophages, and a spectrum of MoMFs temporarily infiltrate the liver (13, 128-132). The few studies that have compared the transcriptional profiles of KCs, LCMs, and MoMFs demonstrated that these are distinct subpopulations but have also shown a great degree of transcriptional convergence between MoMFs and KCs in certain but not all experimental conditions (85, 129, 131, 133). Compared to mice, the composition of the macrophage compartment in the healthy human liver is less known but at least two subpopulations or resident macrophages have been identified: CD68<sup>+</sup> MARCO<sup>+</sup> (macrophage receptor with collagenous structure) and CD68<sup>+</sup> MARCO<sup>-</sup> macrophages (13).

In recent years, multiple reports on macrophages co-expressing markers of M1 and M2 phenotypes, and in varied degrees and combinations, have exposed the limitations of the classical paradigm of M1 versus M2 polarization states when applied to the liver (134). Unbiased techniques such as scRNA-seq have revealed that rather than purely pro-inflammatory or anti-inflammatory phenotypes, hepatic macrophages can adopt a spectrum of functional states in response to the varied and changing environmental cues present in the tissue (135). Although the subpopulations of hepatic macrophages display great plasticity and share multiple phenotypic markers and functions, they exhibit distinctive ontogenic markers and spatial location, and sometimes non-overlapping roles during homeostasis and in response to injury (128).

In the subsequent sections, we will discuss the unique characteristics and functions of the different hepatic macrophage subsets as well as their plasticity and phenotypic overlap. In addition, we will review the information available on the spatial and temporal behavior of liver macrophages during homeostasis and in response to injury, and we will precise the gaps of knowledge that still exist in our understanding of how hepatic macrophage are organized in the tissue, how they relate to neighboring cells, and how this interaction impacts tissue physiology and pathology.



### **1.e.1.a. Kupffer Cells**

The most studied hepatic macrophage subpopulation is the KCs. KCs were first described by Karl Wilhelm von Kupffer in 1876 who assimilated them to the hepatic endothelium (136). Subsequently, Tadeusz Browicz correctly identified them as macrophages (137). With more than a century of research, a wealth of knowledge has accumulated on KCs, but the lack of awareness of macrophage heterogeneity in the liver, and the absence of specific KC markers in most of these studies recommend being cautious while considering these data.

KCs are the largest population of tissue-resident macrophages. Fate-mapping studies have shown that KCs originate from yolk-sac progenitors during embryonic development and are self-renewing (138-141). KCs are in the sinusoids frequently at bifurcation points, but they project processes across the endothelium and reach the perisinusoidal space of Disse where they can directly contact hepatocytes and HSCs (Figure 9) (85, 142).

Traditionally, KCs have been considered sessile cells that lack motility. Pioneering work using intravital imaging revealed that steady-state KCs did not change their shape or position in the sinusoids during several hours of direct observation (143). However, this view was challenged by early observations arguing that cells fitting the location and profile of KCs can migrate along sinusoidal walls (144). Interestingly, the attribution of the term sessile to KCs derived from early experiments using a bone marrow chimera infectious model where the observation was made that KCs did not migrate to the influenza-induced inflammatory foci composed of CD8<sup>+</sup> T cells (130). These early observations made in specific tissue contexts cemented the notion of KCs as stationary cells. However, studies monitoring the spatial behavior of KCs in response to different types of injury are lacking (130). Hence, the potential motility of KCs during immune responses cannot be dismissed with the current evidence (143, 145-147).

Functionally, KCs exhibit an M2-like anti-inflammatory phenotype in the healthy liver. The analysis of KCs by scanning electron microscopy has shown that they have a stellar morphology and possess multiple microvilli. Bonnardel et al., using conditional depletion of KCs, RNA sequencing, and intravital imaging recently showed that LSECs, HSCs, and hepatocytes are the major interacting partners of KCs, compose the KC niche, and provide signals determining the KC identity (85).

KCs are enriched in the periportal and in mid-central zones (7, 148, 149). The morphological and functional properties of KCs are zoned along the porto-central sinusoidal axis. KCs are larger, more phagocytic, less responsive to inflammatory triggers, and more abundant in the periportal than in the centrilobular regions (Figure 12) (149-151). However, a recent study that performed spatial transcriptomics found that while KC location was zoned in the murine liver, there was no zonation pattern in the gene expression profiles of KCs (152).

Interestingly, the spatial polarization of KCs is established in mice at the time of weaning and is dependent on the commensal microbiota as demonstrated using specific pathogen-free (SPF) versus germ-free (GF) mice. Antibiotic treatment of SPF mice abolished KC zonation while cohousing of GF mice with SPF induced it demonstrating that spatial polarization of KCs is a dynamic process dependent on the gut microbiota (7). Moreover, zoned gradients of CXCL9 along the porto-central axis expressed by LSECs in response to microbial products were shown to be responsible for the asymmetric distribution of KCs. Thus, LSECs have a role in shaping the positioning of KCs (7). Furthermore, disruption of TLR signaling in LSECs eliminated the zonation of KCs in SPF mice, while LPS treatment induced it in GF mice (7). These results suggested that sensing microbial products by LSECs through their TLRs, leads to asymmetric expression of chemokines. Since alterations in the composition of the gut microbiota can result in differences in the type and quantity of TLR ligands that reach the liver, the microbiota diversity may influence the distribution of KCs in the hepatic sinusoids.

The functional benefit of KC zonation was brilliantly demonstrated in a model of *Listeria monocytogenes* (Lm) infection where KC zonation was replaced by a homogeneous distribution of KCs along the porto-central sinusoidal axis, leading to more bacteria passing to the general circulation and reaching the spleen (7). Therefore, the specific localization of immune cells in the liver is linked to host protection. Further research is warranted to unveil the role of KC zonation in other liver pathologies.

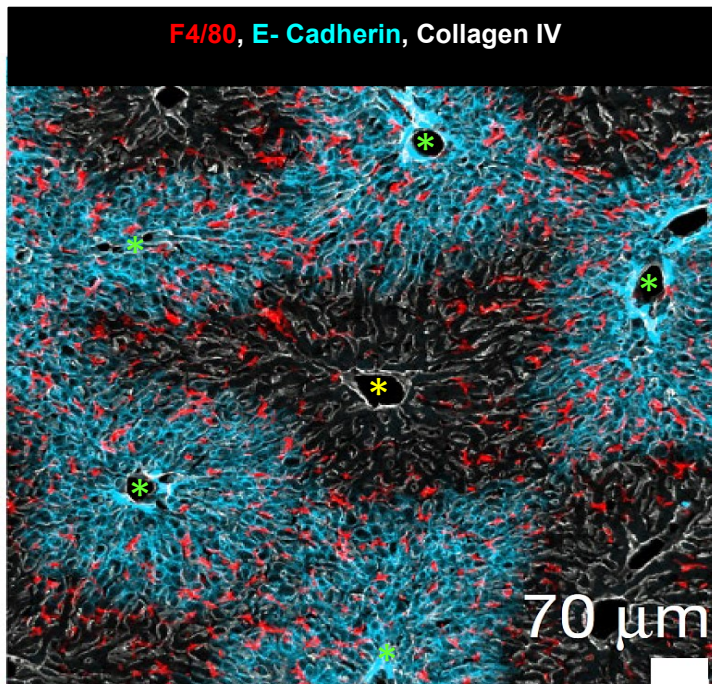


**Figure 12: KCs exhibit zoned distribution in the healthy liver.** Representative immunofluorescence staining showing the polarized distribution of KCs in the murine healthy liver. KCs (F4/80, red) are enriched around portal tracts (\*, green) compared to central veins (\*, yellow). Caption and image adapted from reference (7).

Traditionally, murine KCs have been identified as  $CD45^+ CD11b^{int} F4/80^+ CX3CR1^-$  cells by flow cytometry, and as  $F4/80^+$  cells by imaging, but none of these markers is KC-specific. More recently, the C-type lectin domain family 4-member f (CLEC4F), also known as the Kupffer cell receptor, has been identified as a unique marker of murine KCs (152-155). CLEC4F is a galactose- and fucose-binding receptor that is involved in glycolipid presentation to NKT cells and phagocytosis of desialylated platelets in mice upon bacterial infection (155-157). CLEC4F is co-expressed with F4/80 on KCs in the liver but is absent in macrophages in the lung, kidney, brain, thymus, spleen, bone marrow, and blood monocytes (155, 158). Therefore, CLEC4F is sufficient to identify KCs in tissue-based studies, and the combination of  $CD45^+ CD11b^{int} F4/80^+ CLEC4F^+$  can reliably identify murine KCs by flow cytometry (85). Thus, future research using the CLEC4F marker will allow a more precise delineation of the KC's role in health and disease. Since the human ortholog gene for murine CLEC4f does not encode a full-length protein and is not expressed in the liver, CLEC4F cannot be used as a marker for human KCs (159).

In addition, RNA-seq studies have revealed markers that can be used to distinguish yolk sac-derived murine KCs (YS-KCs) from monocyte-derived macrophages including *MARCO*, T cell immunoglobulin and mucin domain containing 4 (*Timd4*), and stabilin 2 (*Stab2*) (129, 133, 148).

Recently, a study combining unbiased single-cell transcriptomic, translomic, and proteomic approaches revealed that embryonically-derived  $\text{Timd4}^+\text{CLEC4F}^+$  KCs can be further subdivided into two subsets in the murine healthy liver:  $\text{CD206}^{\text{low}}\text{CD107b}^-\text{ESAM}^-$  or KC1, and  $\text{CD206}^{\text{hi}}\text{CD107b}^+\text{ESAM}^+$  or KC2 (160, 161). KC1s constitute 70 to 80 % of all KCs and KC2s represent 20 to 30%. KC1s and KC2s shared the same morphology by cyospin protocol and had overlapping distribution patterns *in situ* as shown by measuring the average distance of KC1s and KC2s to the closest portal triad. On the other hand, pathway analysis revealed a stronger immune signature in KC1s compared to KC2s. In addition, KC2s exhibited increased expression of genes and proteins involved in metabolic functions. High-fat diet expanded the KC2 subpopulation and depletion of KC2 cells led to reduced weight gain, reduced steatosis, and improved glucose tolerance suggesting the involvement of KC2s in the pathogenesis of the non-alcoholic fatty liver disease (NAFLD) (160). It is worth noting that the existence of the KC2 subset has been recently disputed by a study that profiled KCs in the liver of healthy mice using a combination of scRNA-seq, snRNA-seq, spatial transcriptomics, and cellular indexing of transcriptomes and epitopes by sequencing (CITE-Seq) (152). This study demonstrated that cells fitting the profile of KC2s are artifacts generated by the profiling of LSEC-KC doublets.

Regarding human KCs, there is agreement on CD68 as a reliable marker of tissue macrophages (162). scRNA-seq studies using healthy livers from neurologically deceased donors revealed two populations of  $\text{CD68}^+$  KCs at steady state that were classified as tolerogenic  $\text{MARCO}^+$  KCs and inflammatory  $\text{MARCO}^-$  KCs (13). Pathway analysis revealed that  $\text{CD68}^+$   $\text{MARCO}^-$  KCs were enriched for pathways involved in inflammation with the expression of lysozyme (*LYZ*), cystatin A (*CSTA*), and *CD74*. On the other side,  $\text{CD68}^+$   $\text{MARCO}^+$  KCs exhibited higher expression of markers associated with tolerogenic and immunosuppressive functions (e.g., V-set and immunoglobulin domain containing 4 (*VSIG4*), heme oxygenase 1 (*HMOX1*), and *CD163*). The spatial mapping of  $\text{MARCO}^+$  KCs revealed that they are concentrated in the periportal area and comparison analysis showed that they are transcriptionally similar to long-lived, embryonically derived, and tolerogenic murine KCs (13, 45, 133, 154). On the other hand, human  $\text{CD68}^+$

MARCO<sup>-</sup> KCs have a transcriptional profile like murine MoMFs with low expression of CD163 and high expression of phospholipase B domain containing 1 (*PLBD1*) (13, 154). Unlike tolerogenic MARCO<sup>+</sup> KCs, spatial transcriptomics revealed the enrichment of inflammatory MARCO<sup>-</sup> KCs in the pericentral region indicating that the two major subpopulations of macrophages in the human liver exhibit different spatial profiles (45).

During homeostasis, KCs perform multiple tasks, including phagocytosis of particulate material, engulfment of opsonized pathogens, aged cells, and platelets (163-165). In addition, they are involved in iron and lipid metabolism and the removal of toxins (e.g., LPS) (166-168). Interestingly, *in vitro* stimulation of human KCs with LPS leads to the production and release of anti-inflammatory IL-10, a phenomenon that has been called endotoxin tolerance and proposed as an adaptive mechanism to persistent and physiological exposure to gut-derived LPS (169). Moreover, KCs are active enforcers of T cell tolerance at the steady state, which may play a role in oral tolerance to food-derived and commensal bacteria-derived antigens. Notably, KCs express MHC class II, costimulatory molecules, and PD-L1, and present antigens to circulating naïve CD4<sup>+</sup> T and CD8<sup>+</sup> T cells. Priming of naïve CD4<sup>+</sup> T cells by KCs during homeostasis results in the generation of regulatory T cells. On the other hand, antigen presentation to CD8<sup>+</sup> T cells by KCs at the steady state leads to deletional tolerance (170-173). KCs have also been shown to reduce inflammation in several injury models. For instance, KCs reduced ConA-induced tissue damage through a mechanism involving IL-10 (174). In addition, PD-L1<sup>+</sup> CD80<sup>-</sup> KCs captured, processed, and presented antigens to T cells *in vivo* leading to the development of IL-10-producing FoxP3<sup>+</sup> Tregs (171). VSIG4 expression by KCs was also linked to tolerance induction in T and NKT cells in the model of ConA-induced hepatitis (175). Moreover, expression of indoleamine 2,3-dioxygenase (IDO) and Fas ligand by KCs have been shown to mediate immunosuppression of T cells in the context of allograft acceptance in liver transplantation (172, 176, 177).

Even though KCs have a rather immunosuppressive profile at the steady state, they are strategically positioned to detect incoming threats from the portal and general circulation and rapidly and vigorously respond to them (128). In the inflammatory context, KCs switch from a tolerogenic to a pro-inflammatory phenotype. Not surprisingly, KCs express a large repertoire of PRRs including TLRs, NOD-like receptors, and RIG-I-like receptors. PRR signaling mediates the release of inflammatory chemokines and cytokines that promotes the recruitment and activation of other

immune cells leading to the removal of invading pathogens (164, 178, 179). For instance, activated KCs coordinate the influx of monocytes and neutrophils to the injury site through the secretion of CCL2, CXCL1, and CXCL2. Accordingly, the depletion of KCs reduces neutrophil infiltration in a model of sterile injury (180, 181). Multiple signals can induce KC activation including reactive oxygen species (ROS), DAMPs released by dying hepatocytes, opsonized pathogens, and PAMPs like LPS (182). For instance, LPS-mediated activation of KCs leads to the synthesis and release of TNF- $\alpha$ , IL-1 $\beta$ , IL-6, IL-12, IL-18, and IFN- $\gamma$ . Notably, *in vitro* work showed that the shift from endotoxin tolerance to activation of KCs was dependent on the dose of LPS (183). Similarly, during inflammation due to toxic injury with CCl<sub>4</sub> or methionine- and choline-deficient diet, KCs induced IFN $\gamma$ -producing CD4<sup>+</sup> T cells (171).

The functional role of KCs during the wound-healing response to acute liver injury has been determined using clodronate-loaded liposomes that selectively induce apoptosis in KCs (184). Consistent with the notion of KCs as tissue-resident sentinels, the depletion of KCs reduced neutrophil recruitment in the model of sterile injury with a thermal probe (181). In addition, KC depletion in models of acute toxic injury leads to delayed repair (184-187). For instance, studies using the toxins N-acetyl-p-aminophenol (APAP) and thioacetamide (TAA) have found that ablation of KCs rather than exacerbating liver injury seems to extend the period where tissue damage markers like ALT and percent of the necrotic area remain elevated, suggesting deficits in pro-repair functions (185, 186). However, KC depletion before CCl<sub>4</sub> injury led to aggravated inflammation and increased tissue damage. In one study, the lack of KCs caused increased myeloid cell infiltration and higher levels of pro-inflammatory TNF $\alpha$  in response to CCl<sub>4</sub>-induced acute liver injury. Pre-treatment of mice with a neutralizing anti-TNF $\alpha$  Ab significantly decreased the serum ALT levels after CCl<sub>4</sub> administration suggesting that KCs may play a protective role by preventing TNF $\alpha$ -induced tissue damage (187). In addition, the depletion of KCs significantly reduced hepatic expression of the major monocyte chemokine CCL2 upon CCl<sub>4</sub> injury. Further characterization of KCs isolated from CCl<sub>4</sub>-treated mice revealed that they produced large amounts of CCL2 *ex vivo* compared to hepatic non-KC myeloid cells. Since CCL2 and its receptor CCR2 are required for monocyte infiltration upon acute liver injury, depletion of CCL2-producing KCs may reduce the accumulation of inflammatory monocytes and their pro-repair MoMF descendants in the injury site and thereby delay the healing process (133, 186).

KCs are also involved in vessel protection and repair. In the APAP model, an overdose of N-acetyl-p-aminophenol leads to centrilobular necrosis, inflammation, and repair (188). In this model, KC depletion resulted in increased hepatic vascular permeability, red blood cell accumulation, and activation of LSECs (186). Furthermore, isolated KCs upregulated the expression of angiogenic genes in response to APAP. Therefore, KCs play a hepatoprotective role through the prevention of excessive activation of the sinusoidal endothelium in response to toxic injury, and the promotion of re-vascularization (189). Finally, the pro-repair functions of KCs also involve the restoration of the ECM upon toxic injury. In the APAP model, KCs phagocytose fibrin which is a major component of the provisional ECM generated during the repair. This is a necessary step for the regeneration of the normal ECM (185, 190).

KCs are key contributors to host defense against bloodborne bacteria. A study using intravital imaging revealed that KCs cooperate with platelets for the capture and elimination of gut-derived intracellular bacteria *Bacillus cereus* and *Staphylococcus aureus* (191). In addition, periportal KCs have been shown to capture gut-derived intracellular bacteria reaching the sinusoids and preventing their passage to the general circulation via the central vein (7). Other than bacteria capture, necroptotic death of KCs protects against intracellular bacteria. A recent study showed that in mice infected with *Listeria monocytogenes*, necroptotic-infected KCs orchestrated type 1 immune response through the recruitment of IFN- $\gamma$ -producing inflammatory monocytes and MoMFs with a microbicidal activity that was crucial for pathogen control and host protection at early stages of the response. Concomitantly, IL-1 $\beta$  from dying KCs induced IL-33 release by hepatocytes that, in cooperation with basophil-derived IL-4, directed the phenotypic switch from inflammatory monocytes into MoMFs. These observations were replicated in *Salmonella enterica* suggesting that necroptotic death of KCs may have evolved as a mechanism to indirectly provide immunity against intracellular bacteria and simultaneously promote repair upon infection resolution (192).

In summary, KCs are key effector cells for the maintenance of tissue homeostasis through the removal of dietary and microbial-derived products, and the induction of T-cell tolerance. However, in the presence of pathogens or sterile injury, KCs sense the damage and trigger an immune response tailored to the type of threat. KCs are spatially zoned and their spatial distribution

influences their capacity to phagocytose bacteria. How the location of KCs along the porto-central sinusoidal axis impacts other KC effector functions has not been established yet.

### **1.e.1.b. Liver Capsular Macrophages (LCMs)**

Besides the KCs that occupy the sinusoidal compartment, a population of LCMs forms a network in the hepatic capsule that prevents the spreading of pathogens from the peritoneal cavity into the liver (Figure 13). Unlike KCs that are embryonically derived, LCMs originated from circulating monocytes. Even though LCMs exhibit dendritic morphology, mass cytometry or cytometry by time of flight (CyTOF) revealed that they express very low levels of CD11c and do not express CD103. Instead, LCMs express macrophage markers like F4/80, CD64, CSF-1R, and CD14, (131). LCMs do not express the canonical KC markers CLEC4F and Timd4, nor the monocytic marker Ly6C, indicating they are a phenotypically different subpopulation of hepatic macrophages. LCMs did not express the peritoneal macrophage markers integrin alpha M chain (Itgam 1) and fibronectin-1 (Fn1). In addition, profiling of blood mononuclear cells showed that LCMs are not present in the periphery (133). Further emphasizing the unique profile of LCMs compared to KCs, transcriptomic data identified a distinctive macrophage program enriched for cytokine-cytokine receptor interactions, hematopoietic cell lineage, G-coupled protein receptor signaling pathway, and signal transduction (131).

Interestingly, the LCM network develops postnatally and is temporarily associated with the weaning of the mice and the establishment of the microbiota. *In vivo* blockade of CSF-1R signaling resulted in the depletion of LCMs suggesting their dependence on colony-stimulating factors (CSFs).

Functionally, LCM sense invading bacteria and produce neutrophil chemokines. LCM depletion reduced neutrophil recruitment and increased the dissemination of the pathogens *Mycobacterium bovis bacillus* and *Listeria monocytogenes* from the peritoneal cavity into the liver (131).



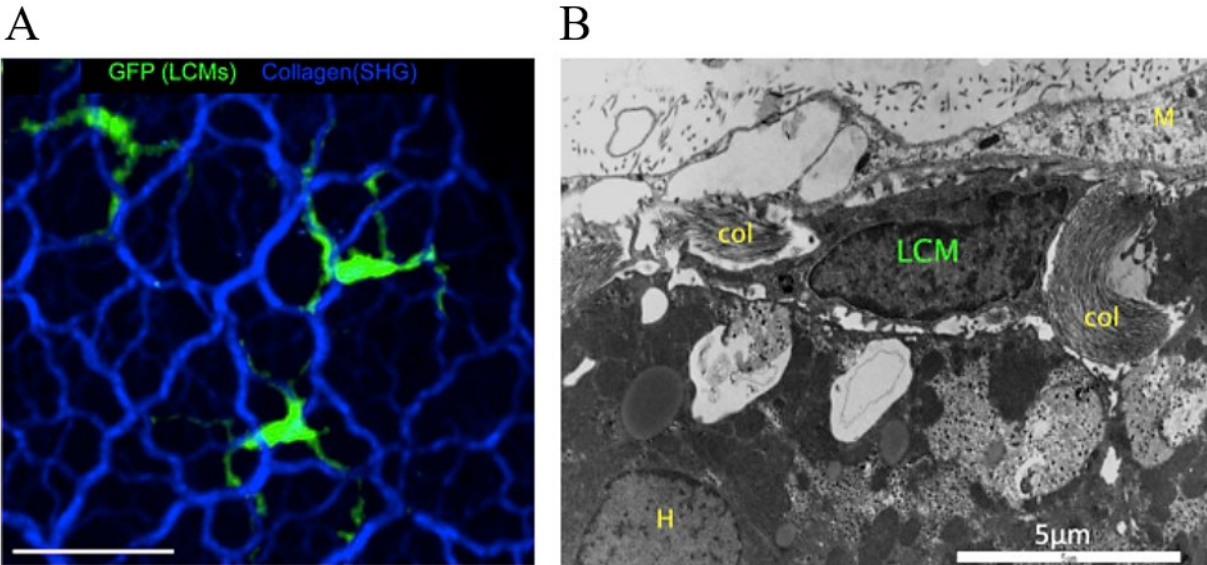


**Figure 13: High resolution images of LCMs.** (A) LCMs (GFP<sup>+</sup> cells) in the liver capsule of a CD207-EGFP (enhanced green fluorescent protein) mouse. LCMs are green and collagen is blue. Bar, 50  $\mu$ m. (B) Electron microscopy image of WT mouse liver capsule, depicting an LCM interacting with collagen fibers (col). Abbreviations: M, mesothelial cells; H, hepatocytes. Bar, 5  $\mu$ m. Caption and image adapted from reference (131).

In summary, LCMs occupy a separate niche compared to KCs and MoMFs, exhibit a distinctive morphology, and perform complementary sentinel and protective functions during the steady state and in response to bacterial invasion. Further investigation is required to define the role of LCMs in other acute and chronic liver pathologies.

### 1.e.1.c. Monocyte-Derived Macrophages (MoMFs)

A third population of liver macrophages is the MoMFs. MoMFs have been described as the “emergency response team” that is recruited to the liver upon injury. However, several reports have documented the existence of a small population of MoMFs in the livers of uninjured mice (133, 152, 193). In contrast, in the healthy human liver, MoMFs are present in high numbers as determined by scRNA-seq (13). Indeed, a study showed that 4 out of 5 donors had larger populations of CD68<sup>+</sup> MARCO<sup>-</sup> MoMF than CD68<sup>+</sup> MARCO<sup>+</sup> KC. However, CD68<sup>+</sup> MARCO<sup>-</sup> MoMFs may be overrepresented in the scRNA-seq data set probably due to inefficient isolation of

CD68<sup>+</sup> MARCO<sup>+</sup> KCs as suggested by MARCO IHC staining in the same study showing high density of MARCO<sup>+</sup> macrophages around portal tracts (13).

During inflammation due to pathogen invasion or toxic injury, MoMFs are massively recruited to the injured liver and significantly contribute to the expansion of the myeloid compartment during inflammation and repair (133, 193-196). MoMFs have been linked to self-resolving and chronic hepatic inflammation with both protective and pathogenic roles assigned to them depending on the specific experimental model or human liver disease (128, 135).

In mice, hepatic MoMFs originate from bone marrow-derived circulating Ly6C<sup>hi</sup> CCR2<sup>+</sup> CX3CR1<sup>low</sup> inflammatory monocytes (133, 134, 193). Upon injury or infection, activated KCs, HSCs, and LSECs release monocyte/macrophage chemokines that induce the recruitment of inflammatory monocytes to the injury site via CCR2 and CCR8 (182, 197-200). Recruited inflammatory monocytes differentiate into MoMFs at the injury site in a process that involves the downregulation of Ly6C and upregulation of CX3CR1 (133, 134).

Remarkable plasticity and heterogeneity characterize the population of infiltrating monocytes and their descendants during hepatic inflammation. In sterile and toxic models of hepatic injury, recently infiltrated MoMFs exhibit a pro-inflammatory and pro-fibrogenic profile characterized by elevated expression of TNF $\alpha$ , IL-1 $\beta$ , and TGF $\beta$ , and reduced expression of anti-inflammatory IL-10. However, with the progression of the wound healing response, and under the influence of environmental cues and cytokine signaling, MoMFs gradually adopt a pro-restorative phenotype. This phenotypic switch takes place at the injury site and is dependent on IL-4, IL-10, CX3CL1, neutrophil-derived ROS, and phagocytosis (94, 134, 193, 201, 202). The plasticity of MoMFs is especially illustrated by their ability to infiltrate the liver upon ablation of KCs and differentiate into long-lived self-renewing, fully differentiated KCs in the KC-DTR mice (mouse in which KCs expressed the human diphtheria toxin receptor) (154). These repopulating cells have been called monocyte-derived KCs (MoKCs) due to their transcriptional similarities to the original embryonic KCs they replaced (154).

In the uninjured murine liver, the embryonic, yolk sac-derived KC pool self-maintain by *in situ* proliferation with no contribution from monocytes (141). However, in several pathological conditions and experimental models that lead to KC death, the resident macrophage pool can be replenished by either proliferation of remaining KCs or by MoKCs, also called bone marrow-

derived KCs (BM-KCs) (133, 154, 192, 203). Currently, conditions that promote either one of these replenishment pathways are incompletely understood (85, 203). For example, toxic liver injury with acetaminophen (APAP) leads to partial depletion of KCs that recover exclusively through the proliferation of remaining KCs when damage subsides (133). In this model, transcriptome microarray analysis comparing KCs to infiltrating MoMFs revealed more than 800 differentially expressed genes between these two subpopulations of hepatic macrophages (133). Among these were included multiple genes associated with the wound healing response (e.g., scavenger receptors, C-type lectins, complement receptors, and ECM-remodeling enzymes) strongly suggesting a division of labor between KCs and MoMFs (133). By contrast, KCs depletion due to radiation-induced injury or selective KC depletion using diphtheria toxin led to the engraftment of monocytes that differentiated into MoKCs or BM-KCs (129, 154). BM-KCs expressed KC-associated transcription factors and KC core genes (e.g., CLEC4F), adopted fixed positions in the sinusoids, morphologically changed to resemble the original embryonic KCs with stellar shape and long processes, and acquired the capacity to self-maintain just as their embryonic counterparts (85, 129, 154). Interestingly, BM-KCs and the original embryonic KCs exhibited overlapping and distinct functional properties. For instance, BM-KCs and embryonic KCs had comparable clearance levels of affected red blood cells and similar responses to *Leishmania* infection in terms of uptake and killing of these parasites. However, BM-KCs were more efficient at phagocytosing bacteria (*Listeria monocytogenes* and *Neisseria meningitidis*) than embryonic KCs (129). Moreover, BM-KCs exhibited a more pro-inflammatory phenotype and promoted tissue damage compared to the original embryonic KCs in murine non-alcoholic steatohepatitis (NASH) models (204). In summary, depending on the inflammatory context, infiltrating inflammatory monocytes can differentiate into transitory MoMFs that do not integrate into the KC niche, or can give rise to self-renewing BM-KCs which transcriptionally, phenotypically, and functionally resemble but are not identical to embryonic KCs.

The role of MoMFs has been studied in the model of acetaminophen-induced liver injury (AILI) (133, 194). In this model, MoMFs were the most abundant myeloid population during early repair but contracted to almost disappear by the end of the wound healing response (133). Importantly, antibody-mediated depletion of CCR2<sup>+</sup> monocytes and thereby of their MoMF descendants, resulted in increased bridging necrosis and ballooning degeneration during tissue repair demonstrating that pro-repair functions of MoMFs are crucial for proper healing upon AILI (133).

In this regard, microarray-based transcriptional profiling comparing monocytes and their MoMFs descendants during the repair phase of AILI, revealed significant upregulation of bridge molecules and receptors in MoMFs (e.g., proto-oncogene tyrosine-protein kinase MER (*Mertk*), AXL receptor tyrosine kinase (*Axl*), growth arrest-specific 6 (*Gas6*), milk fat globule-EGF factor 8 gene (*Mfge8*), and complement C1q subcomponent a, b and c (*C1qa/b/c*)). These bridge molecules and receptors are involved in the uptake of apoptotic cells strongly suggesting the involvement of MoMFs in the clearance of debris and dead hepatocytes during the repair phase of AILI (132, 187).

Few studies, and in a limited number of models, have addressed the spatial properties and interacting partners of MoMFs during liver injury. In the AILI model, MoMFs accumulated around injured central veins during necroinflammation and early repair in a CCR2-dependent manner (Figure 14) (133, 194). Another study dissected the spatio-temporal trajectory of MoMFs in the model of focal thermal injury (193). In this model, a tiny 0.02 mm<sup>3</sup> sterile necrotic lesion is generated with a thermal probe in the liver. As early as 1 h post-injury, inflammatory monocytes started to accumulate in a CCR2-dependent manner forming a packed ring around the lesion (Figure 15). Subsequently, between 8 and 48 h post-injury, these monocytes transitioned from Ly6C<sup>hi</sup>CX3CR1<sup>low</sup> into Ly6C<sup>int</sup>CX3CR1<sup>+</sup> MoMFs in the perimeter of the lesion before entering to the deepest regions of the necrotic tissue. MoMF differentiation was IL-4- and IL-10-dependent and was crucial for debris clearing and collagen redeposition (193). Subsequent studies showed that iNKT cells are the source of IL-4 that directs phenotypic switching of MoMFs in this model (205). In addition, in a model of fibrosis regression, Ramachandran et al. found that CD11b<sup>hi</sup>F4/80<sup>int</sup> Ly6C<sup>int</sup> macrophages (MoMFs) were expanded at the time of maximal scar resolution and were the main producers of matrix-degrading metalloproteinase enzymes (MMPs), and their selective depletion caused persistent fibrosis (134). Collectively, these studies firmly established that MoMFs are generated at the injury site from recruited inflammatory monocytes where they perform crucial effector functions for the resolution of inflammation and the restoration of tissue homeostasis.

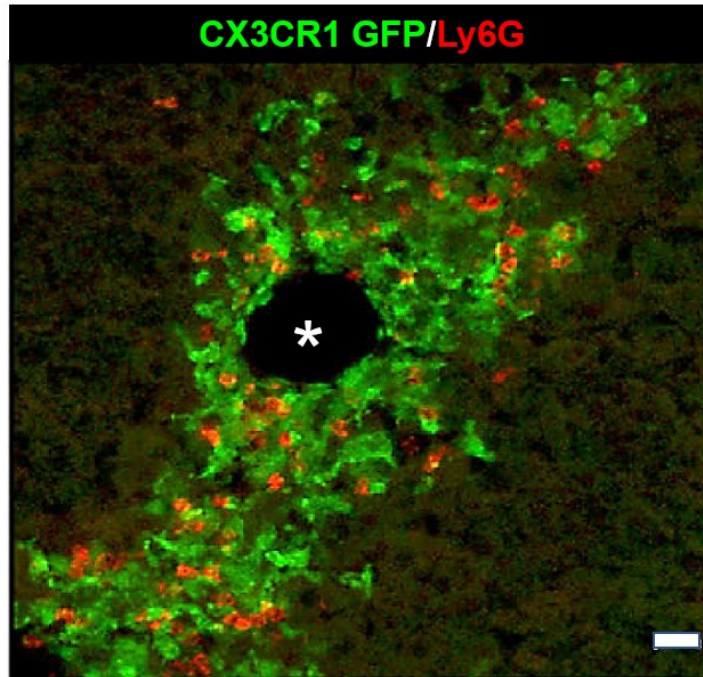


**Figure 14: MoMFs are recruited to the injury site during acetaminophen-induced liver injury.** Immunofluorescence staining on a liver section at 48 h after injury. MoMFs are shown in green in the  $CX3CR1^{GFP/+}$  reporter mice. Neutrophils (Ly6G) are shown in red. Scale bar, 20  $\mu\text{m}$ . \* indicates central vein. Caption and image adapted from reference (194).

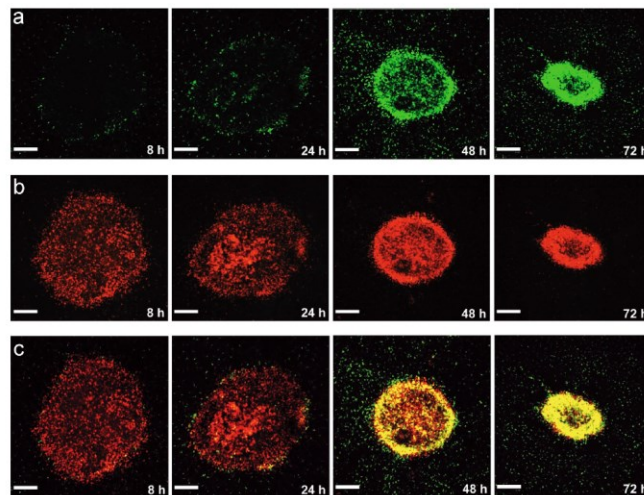


**Figure 15:  $CCR2^+CX3CR1^+$  monocyte-derived macrophages surround and enter the site of hepatic sterile injury.** (a-c) Representative images taken 8 to 72 h after focal injury to the liver of  $CCR2^{RFP/+}/CX3CR1^{GFP/+}$  mice. (a) GFP, (b) RFP, and (c) overlay. Bars, 200  $\mu\text{m}$ . Caption and image adapted from reference (193).

In addition, hepatic MoMFs provide protective immunity against pathogen invasion. During murine and human schistosomiasis, inflammatory monocytes are recruited to the site of egg deposition. The Th2 environment induced by *Schistosoma* eggs is rich in IL-4 and IL-13 that induce alternative activation of monocytes giving rise to alternatively activated macrophages (AAMs). AAMs exert important roles in granuloma formation and limit tissue damage caused by *Schistosoma* eggs (206). AAMs secrete IL-10 and TGF- $\beta$  that prevent Th1-mediated collateral tissue damage, and promote repair, but over-solicitation of these pathways in chronic schistosomiasis leads to fibrosis development (207-209).

Despite the above-mentioned protective properties, several studies have linked MoMFs to the pathogenesis of liver diseases. For instance, in a model of high-fat diet and alcohol feeding, inflammatory MoMFs accumulated in a NOTCH1-dependent manner and were linked to increased hepatocellular death (210). In another study, the human counterparts of murine Ly6C<sup>+</sup> inflammatory MoMFs, defined as CD14<sup>hi</sup> CD16<sup>-</sup> monocytes, were found to be involved in the progression of alcoholic liver disease (ALD) and NASH, primary biliary cholangitis (PBC), and sclerosing cholangitis (PBS) through the secretion of proinflammatory cytokines and chemokines TNF $\alpha$ , IL-1 $\beta$ , CCL1, and CCL2 (182, 211).

Collectively, these reports suggest that MoMFs are diverse, and the outcome of their activity is context-dependent. Since MoMFs constitute one of the most abundant immune populations in the inflamed liver and exhibit great functional plasticity, a deeper understanding of their biology in different disease contexts holds the potential to contribute to the development of new drugs and interventions.

### **1.e.2. Hepatic Dendritic Cells**

Dendritic cells (DCs) are the most potent antigen-presenting cells (APCs) in the body. Their main function is antigen uptake and processing, migration to draining lymph nodes, and presentation of antigenic peptides to T cells to induce T cell-mediated immunity. DCs are tissue-resident hematopoietic cells derived from common bone marrow macrophage/dendritic cell progenitors (212). They comprise a heterogeneous population of sentinel cells linking the innate and adaptive arms of the immune system (213). The signals provided by DCs to T cells depend on their maturation state, the DC subset, the cytokine microenvironment, and importantly, the tissue (214).

During the steady state, DCs are immature and highly endocytic (215). Antigen uptake in the context of inflammatory signals like PAMPs, DAMPs, or cytokines, leads to DC activation and maturation and concomitant migration to draining lymph nodes (LNs) where they encounter and present antigens to T cells. Different inflammatory signals induce specific activation patterns leading to DCs with distinctive cytokine profiles that instruct the differentiation of responding T cells towards the appropriate effector function to eliminate the threat. Conversely, the presentation of self or foreign harmless antigens under steady-state conditions, in the absence of costimulatory signals, activating cytokines, or PAMP/DAMP sensing, leads to the deletion of autoreactive T cell clones and the development of T regs. Therefore, the interactions between DCs and T cells dictate both T cell immunity and tolerance (216-220).

As a tissue in contact with gut-derived blood, enriched in commensal and food antigens, the liver harbors a population of liver-adapted DCs that plays a critical role in preventing undesired adaptive responses against self or innocuous antigens while still being able to prime T cells against invading pathogens (221, 222). In rats and mice, DCs are preferentially located in the periportal and interstitially between hepatocytes (223, 224). In addition, a recent report documented a subpopulation of subcapsular DCs that forms a network below the mesothelial layer that surrounds the murine liver (148).

Functionally, hepatic DCs are rather tolerogenic compared to other DC subpopulations. The tolerogenic microenvironment of the liver has been invoked to explain the slow maturation process of hepatic DCs and their rather immunosuppressive phenotype. IL-10 and TGF $\beta$  produced at steady state by LSECs, KCs and HSCs lead to the development of regulatory hepatic DCs exhibiting reduced expression of MHC II and the costimulatory ligands CD80 and CD86 (225). In addition, HGF may be involved in the induction of tolerogenic DCs in the liver tissue (226). In this regard, *in vitro*-generated DCs, from HGF-treated monocytes, upregulated IL-10 and induced the differentiation of allogeneic T cells into IL10-producing Tregs (226). The fact that HGF can be produced by KCs, HSCs, and LSECs further supports the possibility of this factor playing a role in the induction of tolerogenic DCs (227). In a comparative study, hepatic DCs exhibited a relatively immature phenotype compared to splenic DCs, were more endocytic, and exhibited a reduced capacity for allogeneic T-cell activation suggesting a more tolerogenic phenotype (222).

Mechanistically, hepatic cDCs were shown to induce allogeneic T-cell apoptosis in a FasL-mediated manner (228).

Hepatic DCs can be divided into two major groups: plasmacytoid DCs (pDCs) and conventional DCs (cDCs). Characterization of hepatic DCs by flow cytometry defined a subset of plasmacytoid DCs or pDCs (CD11c<sup>int</sup> B220<sup>+</sup>, CD11b<sup>-</sup>), and two subsets of circulating DCs or cDCs (CD11c<sup>+</sup> CD11b<sup>+</sup> B220<sup>-</sup>). cDCs can either be immature (CD11c<sup>int</sup> CD40<sup>lo</sup> CD80<sup>lo</sup> CD86<sup>lo</sup> MHC class II<sup>lo</sup>) or mature (CD11c<sup>hi</sup> CD40<sup>hi</sup> CD80<sup>hi</sup> CD86<sup>hi</sup> MHC class II<sup>hi</sup>) with the former being more frequent than the latter (229). The functional characterization of these DC subsets showed that B220<sup>+</sup> but not B220<sup>-</sup> DCs produced type I interferon in response to *in vitro* murine cytomegalovirus (MCMV) infection. Similarly, only the B220<sup>+</sup> subset expanded in response to MCMV infection suggesting that this is a subset specialized in fighting viruses (229). In another study, the profiling of extravascular sub-mesothelial CX3CR1<sup>+</sup> DCs revealed that they expressed high levels of antigen-processing and presentation-related genes suggesting a potential role in the priming of T cells against pathogens accessing the liver from the peritoneal cavity (148).

Despite their modulatory profile, in the presence of inflammatory signals, hepatic DCs can induce innate and adaptive immune responses. For instance, upon TLR ligation, hepatic DCs produced more proinflammatory cytokines than splenic DCs (222). Hepatic DCs pulsed *in vitro* with hepatitis B surface antigen (HBsAg) or keyhole limpet haemocyanin (KLH) upregulated MHC II and costimulatory molecules and induced pro-inflammatory IL-12 and IFN- $\gamma$  secretion by allogeneic memory T cells (230). However, the reduced APC and costimulatory activity of hepatic DCs in patients with chronic HBV and HCV, as well as in hepatocellular carcinoma patients, diminished T cell-mediated immunosurveillance and led to disease progression (231-235).

The role of hepatic DCs in the modulation of fibrosis was examined in a model of CCl<sub>4</sub>-induced fibrosis regression. Depletion of hepatic DCs upon cessation of CCl<sub>4</sub>, delayed fibrosis regression, and clearance of activated HSCs. Conversely, adoptive transfer or expansion of DCs accelerated the resolution of fibrosis. Interestingly, this effect was dependent on DC-derived MMP9 suggesting that hepatic DCs are directly involved in the remodeling of the ECM during fibrosis regression (236). Even though hepatic DCs are expanded in NASH and express a more mature and pro-inflammatory phenotype than DCs in the healthy liver, their depletion led to increased



production of inflammatory cytokines (TNF- $\alpha$ , IL-6, and IL-1 $\beta$ ) and chemokines (MIP-1 $\alpha$  and G-CSF) and decreased secretion of modulatory IL-10 by other non-parenchymal cells (237).

In summary, hepatic DCs have been associated with both protective and pathogenic roles in liver diseases. They are enforcers of T cell tolerance under homeostatic conditions but can get rapidly activated in the presence of antigens and inflammatory stimuli. The outcome of DC activation is context-dependent and not fully understood. The spatial profiling of the different hepatic DC populations has not been done. More precise delineation of the specific functions of the different DC subsets in health and disease will be the key to the development of targeted interventions that prevent unwanted DC responses while keeping in place the beneficial ones.

### **1.e.3. Hepatic Resident Lymphocytes**

The liver acts as a filter of gut-derived blood enriched in commensal- and food-derived antigens. In addition, blood from the systemic circulation carrying aged cells, and occasionally cancer cells, pathogens, and toxins enter the liver through the hepatic artery and is filtered in the sinusoids by LSECs, KCs, and DCs (1, 238). Complex and diverse immunological mechanisms have evolved to properly cope with this heavy antigenic influx and to balance tolerance to harmless antigens versus response to harmful ones (238). These diverse immunological functions of the liver are supported by unusually large populations of resident innate, unconventional (innate-like), and conventional (adaptive) lymphocytes (1, 13, 239). These groups of resident lymphocytes exhibit different activation requirements, kinetics, and location, and therefore represent complementary modalities of immune responses (240, 241).

Studies in the last decade have dissected the lymphocyte compartment in non-lymphoid organs revealing great internal phenotypic and functional heterogeneity and non-overlapping characteristics of tissue-resident lymphocytes compared to recirculating subsets (239, 241). In the liver, resident lymphocytes encompass the full spectrum from innate to adaptive. Innate lymphocytes include innate lymphoid cells (ILCs), natural killer cells (NK cells), and tissue-inducer cells (LTi). Hepatic unconventional lymphocytes comprise invariant NKT cells (iNKT), mucosal-associated invariant T cells (MAIT), and  $\gamma\delta$  T cells. Finally, tissue-resident memory T cells (T<sub>RM</sub>) are adaptive lymphocytes that can gradually colonize the liver in response to repeated exposure to hepatotropic pathogens (1, 242-261).

Tissue-resident lymphocytes share multiple features that distinguish them from recirculating lymphocytes. The transcription factors Hobit and Blimp1 are the transcriptional regulators of a universal program of tissue retention present in most tissue-resident lymphocytes (262). For instance, tissue-resident lymphocytes lack expression of lymph node homing molecules (e.g., CCR7 and CD62L) and tissue egressing S1P receptors and rather express high levels of chemokine receptors that mediate migration and establishment in non-lymphoid organs (e.g., CXCR3, CXCR6) (239, 241). Tissue residency is further facilitated by the expression of adhesion molecules like CD103, CD69, CD49a, and CD44. In addition, the expression of cytokine receptors and pre-storage of effector molecules allow tissue-resident lymphocytes to sense and rapidly respond to incoming threats (239, 241). In this section, we will introduce the main populations of liver-resident lymphocytes, and discuss their phenotype, distribution, and functions during health and disease.

### **1.e.3.a Hepatic Innate Lymphoid Cells**

Innate lymphoid cells (ILCs) are a heterogeneous population of Non-B Non-T lymphocytes that do not express rearranged antigen-specific receptors. ILCs are largely tissue-resident and are enriched in barrier tissues including the liver (263). All ILCs develop in the bone marrow but can acquire tissue-specific transcriptional signatures (264). ILCs integrate signals from alarmins, and cytokines released during pathogen invasion or tissue damage and orchestrate antimicrobial responses and tissue repair (265). ILCs are also involved in non-immune tasks that are important for the maintenance of tissue homeostasis like thermal regulation, circadian rhythms, and tissue remodeling (265).

ILCs are classified into five groups according to the expression of phenotypic markers, signature cytokines, and transcription factors. These groups are NK cells, LT<sub>i</sub> cells, ILC1s, ILC2s, and ILC3s (264). All these ILC subsets are present in the murine and human liver (266-269). Except for NK cells, all other ILCs are non-cytotoxic. Functionally, ILC1s, tissue-resident NK cells, ILC2s and ILC3s are the innate counterparts of adaptive T helper 1 (Th1), T<sub>RM</sub> cells, T helper 2 (Th2), and T helper 17 (Th17) cells respectively. Each group of ILCs and its respective equivalent T cell subset share the type of pathogens they target, the signature cytokines they produce, and the transcription factors they depend on for their differentiation and lineage commitment (264, 270-

272). ILC1s and Th1 cells respond to intracellular pathogens, produce the signature cytokine IFN $\gamma$ , and depend for their differentiation on the expression of T-box transcription factor TBX21 (T-bet). For instance, ILC1s protect the intracellular protozoan parasite *Toxoplasma gondii* and the intracellular bacteria *Salmonella enterica* (273, 274). Tissue-resident NK cells (tr-NK) and T<sub>RM</sub> cells are both cytotoxic, depend on T-bet and Eomes for development, and both target tumor and virally infected cells which they kill using perforin and granzymes (241). ILC2s and Th2 cells express GATA Binding Protein 3 (GATA3) and the type 2 signature cytokines IL-4, IL-5, and IL-13 and specialize in the protection against helminths and venoms. In this regard, it has been shown that ILC2s mediate the expulsion of the worms *Nippostrongylus brasiliensis* and *Heligmosomoides polygyrus* (275, 276). Both ILC2s and Th2 cells produce amphiregulin to promote epithelial cell proliferation required for the repair of the massive tissue damage caused by large parasites (239, 277, 278). Finally, ILC3s and Th17 cells express RAR-related orphan receptor gamma-t (ROR $\gamma$ t), produce IL-17 and IL-22, and protect against extracellular bacteria and fungi mainly in barrier tissues (279). For example, mice lacking IL-22-producing ILC3s exhibited more bacteria translocation and were more susceptible to intestinal infection with *Citrobacter rodentium* (280). Similarly, the role of ILC3s in protecting against fungi is well illustrated in humans with certain mutations in RORC leading to reduced ILC3s and repeated *Candida albicans* infections (281).

Despite their apparent functional redundancy, ILCs and adaptive T cells perform complementary and non-redundant functions due to differences in the location and kinetics of the response. While naive Th cells are in secondary lymphoid organs and take several days to mature and mount a response in peripheral tissues, ILCs are tissue residents and respond almost immediately to pathogen invasion and/or tissue damage. Upon injury or pathogen invasion, ILCs are activated by neighboring resident myeloid and stromal cells, leading to the rapid release of pre-stored cytokines (264). Therefore, by rapidly responding to pathogens or damage and selectively producing specific and polarizing cytokines and chemokines, ILCs limit pathogen spreading and influence the specific type of adaptive response that is triggered (282).

A challenging aspect of ILC research is the lack of specific markers. Instead, ILCs are defined by the absence of adaptive lymphocyte lineage markers and the expression of several NK receptors. In addition, the expression of ILC-associated markers can be tissue-dependent and can change upon activation (264).

Except for NK cells, the study of hepatic ILCs is relatively recent and few reports are available (239, 265-267, 283-286). Since NK cells are the most studied ILC population in the liver, we will dedicate a separate section to them. In the murine healthy liver, ILCs represent 2% of total leukocytes. Within the hepatic ILCs, NK cells represent more than 80% followed by ILC1s, and the ILC2 and ILC3 subpopulations are relatively rarer (287, 288). The fact that the majority of hepatic ILCs are antiviral NK cells suggests that murine hepatic ILCs may primarily protect the host by fighting hepatotropic viruses and probably virally infected cancer cells. Similarly, the profiling of human ILCs showed that all ILC subsets are present in the human liver, with ILC1s as the most abundant subpopulation according to one study and NKp44<sup>-</sup> ILC3s according to another (266, 289). A comparative study found that the human liver has a different ILC subset composition compared to the gut and tonsil, suggesting specialized roles for hepatic ILCs. While ILC1s and ILC2s were more frequent in the adult liver than in the gut, hepatic NKp44<sup>+</sup> ILC3s were almost absent. However, NKp44<sup>-</sup> ILC3s were very frequent. In addition, human hepatic ILCs expressed tissue-retention markers like CD69 and lacked lymph node homing receptor CD62L, but lacked other molecules expressed by T<sub>RM</sub> cells like CD49a and CD103, indicating that these receptors are not important for tissue residency in the human liver (266).

The spatial organization of hepatic ILCs is still unknown. The fact that ILCs are phenotypically defined by the simultaneous lack of expression of adaptive lymphocyte lineage markers plus the expression of several ILC markers has made the visualization and mapping of ILCs difficult. However, imaging of ILC1s defined as NKp46<sup>+</sup>CD49a<sup>+</sup> by immunofluorescence showed that they are present in the periportal areas of the healthy liver. This observation is based on the visualization of a single field of view with one portal track showing five NKp46<sup>+</sup>CD49a<sup>+</sup> cells and therefore has limited value (290). Therefore, the distribution of ILCs in the liver and how it relates to their sentinel function is still to be determined. Since ILCs are defined by the simultaneous expression of multiple markers, the new high-parameter imaging technologies like the CO-Detection by indEXing (CODEX) would be the tool of choice for ILC spatial profiling in the liver and other organs (291).

The study of hepatic ILCs has linked this heterogeneous population to both protective and pathogenic roles (267). Phenotypically, hepatic murine ILC1s are CD45<sup>+</sup> Lin<sup>-</sup> CD62L<sup>-</sup> Eomes<sup>-</sup> Tbet<sup>+</sup> Hobit<sup>+</sup> CD49b<sup>-</sup> CD49a<sup>+</sup> TRAIL<sup>+</sup> CD69<sup>+</sup> NK1.1<sup>+</sup> NKp46<sup>+</sup> CD127<sup>+</sup> IL1Rβ<sup>+</sup> Sca-1<sup>+</sup> CD90<sup>+</sup>

CD200R1<sup>+</sup> and CXCR6<sup>+</sup>. ILC1's main effector molecules are TRAIL, IFN- $\gamma$ , TNF- $\alpha$ , GM-CSF, and GZM B (29, 264). ILC1s in the liver have also been called liver-resident NK cells (lr-NK) (253, 256). In an infectious model with MCMV, IL-12 released by cDC1s induced early activation of ILC1s and subsequent release of IFN- $\gamma$  before activation of NK cells (292). Thus, ILC1 protected the mice early during viral infection and limited viral replication and spreading. One study found that ILC1s in the murine liver is derived from a resident population of fetal progenitor Lin<sup>-</sup>Sca-1<sup>+</sup>Mac-1<sup>+</sup> hematopoietic stem cells that give rise to hepatic ILC1s in response to IFN- $\gamma$ . Thus, type 1 response characterized by IFN- $\gamma$  secretion can expand the population of hepatic ILC1s (293). However, in a recent report, hepatic ILC1s were shown to be heterogeneous regarding origin and function and were distinguished according to the expression of Ly49E. Fate mapping experiments showed that Ly49E<sup>+</sup> ILC1s are embryonically derived and cytotoxic, but Ly49E<sup>-</sup> ILC1s are bone marrow-derived and exhibit immunological memory (294). Another study found that hepatic ILC1s proliferated in an IL-12- and IL-18-dependent manner following infection with MCMV. MCMV-experienced ILC1s upregulated expression of the IL-18R, a marker of CD8<sup>+</sup> T memory cells (295). Furthermore, IL-18R<sup>+</sup> ILC1s exhibited enhanced responses to pathogen rechallenge *in vivo*, suggesting the development of immunological memory in this subset. In addition, hepatic ILC1s were shown to protect mice during acute liver injury with CCl<sub>4</sub>. In this model, ILC1s upregulated the T cell activation markers CD25 and CD69 and produced IFN- $\gamma$  which promoted hepatocyte survival through upregulation of the inhibitor of apoptosis Bel-xL (296). Accordingly, CCl<sub>4</sub> treatment in Hobbit-deficient mice, which have reduced hepatic ILC1s, led to exacerbated injury compared to their wild-type counterparts. Interestingly, the upregulation of the activation of the markers CD25 and CD69 on ILC1s was dependent on signaling through the IL-7R, suggesting the role of cytokines in ILC1 activation (296). However, it has been proposed that ILC1s play a pathogenic role during chronic hepatitis B (CHB). In this regard, the number of ILC1s was increased in CHB and correlated with tissue damage and IFN- $\gamma$  secretion. However, this study found no causal link between ILC1s and CHB progression (297).

Hepatic murine ILC2s are CD45<sup>+</sup> Lin<sup>-</sup> CD62L<sup>-</sup> KLRG1<sup>+</sup> ST2<sup>+</sup> Sca-1<sup>+</sup> CD49b<sup>-</sup> CD49a<sup>+</sup> TRAIL<sup>+</sup> IL-25R<sup>+</sup> CD69<sup>+</sup> NK1.1<sup>-</sup> GATA-3<sup>+</sup> CD127<sup>+</sup> c-Kit<sup>+</sup> Sca-1<sup>+</sup> ICOS<sup>+</sup> MHC II<sup>+</sup> and IL-33R<sup>+</sup>. The main ILC2-effector molecules are IL-4, IL-5, IL-9, IL-13 and amphiregulin. In the liver, ILC2s exacerbated concanavalin A-induced (ConA) immune-related hepatitis (288, 298). Treatment of mice with Con A increased the secretion of the alarmin IL-33 that mediated activation and

expansion of hepatic ILC2s (288, 298). Activated ILC2s exhibited increased expression of GATA-3 and the type 2 cytokines IL-5, IL-9, and IL-13 in response to epithelial stress markers like the alarmins IL-25 and IL-33. In addition, eosinophils that are important mediators of tissue injury in this model were decreased upon ILC2 depletion, leading to reduced tissue damage (298, 299). Furthermore, IL-33-activated ILC2s upregulated MHC II and co-stimulatory molecules CD80 and CD86 and mediated the activation, expansion, and differentiation of naïve antigen-specific CD4<sup>+</sup> T cells demonstrating that ILC2s can act as APCs *in vitro*. CD4<sup>+</sup> T cells activated by ILC2s secreted IL-13 but not IFN- $\gamma$ , indicating that ILCs can induce the differentiation of CD4<sup>+</sup> T cells into Th2 cells (288). In turn, the coculture of ILC2s with activated CD4<sup>+</sup> T cells led to increased expression of the activation marker CD25 and the type 2 cytokines IL-4, IL-5, and IL-13 by ILC2s, suggesting that CD4<sup>+</sup> T cells may mediate the *in vivo* activation of ILC2s. Blockade of T cell-derived IL-2 in the co-cultures significantly reduced the activation of ILC2s and their expression of type 2 cytokines (288). These results suggest direct interaction and functional interdependence between ILC2s and CD4<sup>+</sup> T cells in response to Con A injury but studies in the tissue validating this hypothesis are lacking. ILC2s were also implicated in the pathogenesis of liver fibrosis induced by the hepatotoxin CCl<sub>4</sub> (269). In this model IL-33 produced during hepatic injury induced the activation and expansion of ILC2s that in turn secreted the pro-fibrogenic cytokine IL-13, resulting in enhanced HSC activation and collagen deposition (269). In agreement with these observations, the frequency of hepatic ILC2s was found to correlate with the severity of disease in a cohort including PBC, PSC, ALD, NASH, and autoimmune hepatitis (AIH) (289). Another study found an increased frequency of ILC2s in severe vs. mild fibrosis (266). In addition, the expression of IL-33, a potent ILC2 activator, is upregulated during liver cirrhosis in humans (269). Altogether, these results suggest that chronic IL-33-mediated activation and expansion of ILC2s aggravates type 2 inflammation, tissue damage, and fibrosis. The role of ILC2s in protozoan infection was studied in an infection model with *Entamoeba histolytica* (Eh) that spreads to the liver and induces amebic liver abscesses (ALA) (300). Hepatic ILC2s exacerbated the pathogenesis of ALA increasing the number of abscesses and inducing eosinophilia and neutrophilia. Mechanistically, ILC2s expanded in response to Eh-induced IL-33 and produced IL-5. ALA formation was dependent on ILC2s as demonstrated by a reduced number of ALA upon ILC2 depletion in Eh-infected mice (300).

ILC3s are specialized effector cells in the protection of epithelial surfaces. Hepatic ILC3s are CD45<sup>+</sup> Lin<sup>-</sup> RORγt<sup>+</sup> CD4<sup>-</sup> CD127<sup>+</sup> NK1.1<sup>+</sup> and NKp46<sup>+/-</sup> and their main effector cytokines are IL-17 A/F, IL-22, GM-CSF and IFN-γ. There are two subsets of hepatic ILC3s according to the expression of the natural cytotoxicity receptor (NCR) (285). Despite the important roles ILC3 exhibits in gut homeostasis, there is a paucity of studies on the liver (264).

A study found that ILC3s in the human liver were either NKp44<sup>+</sup> or NKp44<sup>-</sup> with an increased prevalence of NKp44<sup>-</sup> ILC3s (266). Human intrahepatic ILC3s were Helios<sup>+</sup> and AHR<sup>-</sup> but still produced significant amounts of IL-22 when stimulated *ex vivo* (266). The physiological role of hepatic ILC3s may be the containment of bacterial dissemination coming from the portal circulation. In this regard, a study where ILCs were depleted using antibodies in RAG1<sup>-/-</sup> mice lacking adaptive lymphocytes, showed the spreading of lymphoid tissue-resident *Alcaligenes spp.* to the liver at the steady state. Infection of the hepatic tissue resulted in inflammation, increased neutrophil infiltration, and elevated levels of LPS and pro-inflammatory cytokines. Blocking of IL-22 without ILC depletion mirrored this phenotype, and IL-22 supplementation in the context of ILC depletion prevented it, indicating that ILC3-derived IL-22 is critical for keeping the commensals in their place and protecting the sterile environment of the liver (301). Interestingly, a report showed that ILC3s are expanded in the early stages of hepatic infection with adenovirus and with lymphocytic choriomeningitis virus (LCMV). ILC3s were a major source of IL-17A/F during early adenoviral infection that mediated the activation of APCs, priming, and effector functions of T cells (283, 284). Furthermore, mice lacking IL-17F but not IL-17A, exhibited reduced numbers of infiltrating T cells, reduced IFN-γ production, and degranulation, and developed a reduced injury. However, the lack of IL-17 A or IL-17F signaling did not impact viral clearance (284). These results are intriguing and demonstrate that hepatic ILC3s get activated in the context of viral infections, but rather than contributing to viral clearance, enhance inflammation and injury (284). In the same line of evidence, the frequency of IL-17A- and IL-22-producing ILC3s is increased in CHB, and in HBV-related liver cirrhosis (286). The role of hepatic ILC3s was also studied in hepatocellular carcinoma (HCC). In a syngeneic mouse model of HCC, NKp46<sup>-</sup> ILC3s proliferated in response to intrahepatic IL-23 and promoted HCC development through secretion of IL-17 and inhibition of CD8<sup>+</sup> T cell-mediated anti-tumor immunity (302). In summary, ILC3s may be bad actors during chronic liver diseases through the secretion of the signature type 3 cytokine IL-17.

Finally, LT<sub>i</sub> cells in the murine liver are CD45<sup>+</sup> Lin<sup>-</sup> ROR $\gamma$ t<sup>+</sup> CD4<sup>+</sup> IL-23R<sup>+</sup> CCR6<sup>+</sup> and AhR<sup>+</sup> and their main effector molecules are lymphotoxin and IL-22 (29). LT<sub>i</sub> cells are essential for the formation of lymph nodes (303). The location and role of the hepatic LT<sub>i</sub> population are still unknown. However, one study found significant enrichment of neuropilin 1-expressing ILCs (NRP1) in fetal versus adult human liver, suggesting that these are the equivalent of murine NRP1<sup>+</sup> LT<sub>i</sub> cells and are involved in the significant lymphoid organogenesis during fetal development (266).

In summary, the study of hepatic ILCs has revealed that they are involved in the early stages of response to pathogens, they are activated by alarmins released by sentinel cells and can rapidly secrete pre-stored cytokines that polarize the adaptive response that is triggered. However, dysregulation of ILC responses can exacerbate tissue damage, increase inflammation, and promote fibrosis and HCC development.

### **1.e.3.b Hepatic NK Cells**

NK cells were discovered in the 1960s. Early studies defined NK cells as large granular lymphocytes possessing cytotoxic activity that was not dependent on prior antigen exposure (304-306). NK cells are derived from hematopoietic progenitors and develop mostly in the bone marrow, but also secondary lymphoid tissue like the spleen, tonsils, and lymph nodes (307). These innate lymphocytes play a key role in immune responses to viral infections and malignancies. NK cell activation depends on a wide array of germline-encoded inhibitory and activating receptors that do not require gene segment rearrangement (308). Varied expression patterns of inhibitory and activating receptors on NK cells define functionally diverse subsets (308). While activating receptors, like NKG2D, recognize ligands expressed by stressed, infected, or malignant cells, the inhibitory receptors recognize constitutively expressed self-molecules (e.g., MHC I and MHC I-like molecules). Missing self or lack of inhibitory signals allows activating signals to prevail. Therefore, the balance between antagonistic inhibitory and activating signals ultimately determines the NK cell activation status (309-311).

NK cells deliver protective immunity against viruses and neoplastic cells through the direct lysis of target cells and indirectly through the release of inflammatory cytokines and chemokines. Mechanistically, the binding of death receptors TRAIL-R and FAS on target cells by their ligands



on NK cells deliver signals that induce apoptosis in target cells. NK cells release cytotoxic granules containing pore-forming molecules like perforin, apoptosis-inducing granzyme B (GZM B), and granulysin that reach and kill target cells (304, 312). In addition, NK cells release anti-inflammatory (e.g., IL-10), and pro-inflammatory cytokines (e.g., TNF $\alpha$  and IFN- $\gamma$ ), and chemokines (e.g., CCL2, CCL4, CCL5) that promote the recruitment, activation, and effector functions of other effector cells (313, 314). Furthermore, subsets of NK cells express the Fc receptor CD16, enabling them to bind antibody-coated target cells and kill them through antibody-dependent cell cytotoxicity (ADCC) (315).

Immunological memory is a recently discovered property of subsets of NK cells, especially those bearing the activating receptor Ly49H that recognizes the MCMV protein m157 (316, 317). Although traditionally seen as innate lymphocytes, NK cells are more and more recognized as effector cells that can respond to certain viruses and haptens in an antigen-specific manner, can expand preserving antigen specificity, and generate memory-like cells able to rapidly respond upon reactivation (256, 316-318). Moreover, memory NK cells can be adoptively transferred, proliferate and mediate protection in recipient mice (316-320). Whether NK cell memory is a phenomenon restricted to a few subsets of NK cells recognizing a limited number of viral proteins, remains to be elucidated.

To optimally perform its function, the liver requires a tolerogenic immune environment that prevents unwanted activation in response to foreign but harmless antigens and still can provide immunity to pathogens. Not surprisingly, hepatotropic viruses like HBV and HCV have evolved mechanisms to take advantage of hepatic tolerance to persist and establish a chronic infection. This evolutionary constraint may explain why the liver harbors the largest tissue-resident NK cell population of the body with unique immunomodulatory properties (1, 253). At present, we know that the murine liver houses at least two subpopulations of NK cells: circulating conventional NK cells (cNK) and liver-resident NK cells (lr-NK). By flow cytometry murine hepatic cNK and lr-NK cells are identified as CD49a<sup>-</sup> DX5<sup>+</sup> and CD49a<sup>+</sup> DX5<sup>-</sup> respectively (253, 256). lr-NK cells reside in the sinusoids, possess memory potential, and seem to originate from hepatic hematopoietic progenitor/stem cells (274). Conversely, hepatic cNK cells are bone marrow-derived, and since they don't express the chemokine receptors involved in sinusoidal retention, they can freely flow in and out of the liver (256). Murine lr-NK and cNK cells also rely on different

transcription factors for their development. While lr-NK cell development depends on T-bet, Hobit, and AhR, cNK cells are T-bet-dependent and require Eomes for their maintenance (244, 253, 260, 262).

lr-NK cells exhibited a distinctive transcriptional profile compared to cNK cells. Gene expression microarray analysis revealed that lr-NK cells differentially expressed inhibitory and activating receptors, cytokines, chemokines, adhesion molecules, cytokine receptors, cytotoxic effectors, and transcription factors. lr-NK cells had increased expression of the chemokine receptors CXCR3 and CXCR6, as well as the activation and tissue-retention marker CD69. Regulatory genes such as *Lag-3*, *Helios*, and *Egr-2* were also upregulated in lr-NK cells while inflammatory transcription factors and cytokines were decreased (e.g., *Eomes*, *Il-1 $\beta$* , *Il-6*, and *Ifn- $\gamma$* ). Functional assays revealed a decreased degranulation potential compared to cNK cells. Overall, the transcriptional profile of lr-NK cells was more tolerogenic compared to hepatic recirculating cNKs (253, 256). While transcriptional and functional profiling of hepatic NK cells has provided great insight into their involvement in tissue homeostasis and immunopathology, studies determining their spatial distribution during the steady state and in response to injury are lagging.

Recent studies have dissected the human hepatic NK cell compartment (243, 252, 257, 321). Two subsets of NK cells were identified in the healthy human liver: liver-resident NK cells (lr-NK) and bone marrow-derived conventional NK cells (cNK) (257, 321). lr-NK cells are highly enriched in the liver and virtually absent in the periphery, reside in the sinusoids, and are CD56<sup>bright</sup> CD69<sup>+</sup> CXCR6<sup>+</sup> CCR5<sup>+</sup> CCR7<sup>-</sup>. lr-NK cells express low levels of CD16, CD57, and perforin suggesting that they are immature, poorly cytotoxic, and cannot perform ADCC (253, 257, 321). Unlike their murine counterpart, human lr-NK cells express high levels of Eomes and low levels of T-bet. Just as murine lr-NK cells, human lr-NK cells retained their phenotype after expansion suggesting potential involvement in memory responses (252). While the tissue residency of specific immune cell subsets is directly tested using parabiosis and adoptive transfer in mouse models, in humans it can only be indirectly inferred. Tissue residency of human lr-NK cells was proposed due to the high expression of CD69, their enrichment in the liver, and their absence in the periphery, and that they are transcriptional and phenotypically similar to murine lr-NK cells (253, 257, 321). In addition, the hepatic sinusoids harbor cell populations that express ligands for CXCR6 and CCR5 and may mediate retention of lr-NK cells (e.g., CCL3, CCL5, and CXCL16) (321, 322). By

contrast, cNK cells found in the human healthy liver are similar to circulating NK cells (321). They are CD56<sup>dim</sup> and lack expression of CD69, CCR5, and CXCR6 and highly express the secondary lymphoid organ homing receptors CCR7 and L-selectin (321).

NK cells play a major role in antiviral immunity. In acute models of viral infection with murine hepatitis virus (MHV), MCMV, and vaccinia virus, depletion of NK cells led to increased hepatic viral titers (up to 500-fold) and exacerbated hepatitis leading to more and larger inflammatory foci than controls. In addition, NK cells induced HBV-specific CD8<sup>+</sup> T cell-mediated immunity in a mouse model mimicking acute HBV infection by hydrodynamic injection of an HBV plasmid. In this model, NK cell depletion led to increased HBV persistence along with the reduced frequency of HBV-specific CD8<sup>+</sup> T cells. By contrast, the adoptive transfer of NK cells restored donor CD8<sup>+</sup> T cell-mediated HBV clearance (323). However, NK cell depletion had no impact on the response to acute nor to chronic infection with LCMV, indicating that NK cell-mediated protection against viral infection is dependent on the type of virus (324). In addition, while NK cells promoted HBV particle clearance in mouse models, the study of acute HBV infection in humans revealed that IFN- $\gamma$  production by circulating NK cells was reduced at peak viremia. Furthermore, peak viremia coincided with peak IL-10 serum levels, suggesting that increased immunosuppressive cytokines during the early stages of HBV infection may prevent full activation and antiviral effector functions of hepatic NK cells (325).

Unlike in the acute setting, most studies have found that NK cell antiviral activity is compromised during chronic viral infection. NK cells are enriched in the liver of patients with CHB and exhibit altered expression of inhibitory and activating receptors which has been linked to functional impairment of NK cells (326). Several studies reported increased expression of the inhibitory receptor NKG2A in circulating NK cells from active versus inactive CHB patients (327, 328). This phenotype was replicated *in vivo* in an HBV-carrier mouse model. In the mice, NKG2A was induced by Treg-derived IL-10 during HBV “infection”. Serum levels of HBV antigen (HBsAg) and viral titers were significantly decreased in anti-NKG2A-treated mice compared to controls (327). Conversely, the downregulation of the activating receptors NKG2D and 2B4 on circulating NK cells from chronic HBV patients contributed to HBV persistence. Reduced NKG2D and 2B4 expression was linked to diminished NK cell-mediated cytotoxicity and IFN- $\gamma$  expression *in vitro* assays (329).

Altered expression of inhibitory and activating receptors on NK cells has also been linked to functional changes during chronic HCV infection. However herein, studies have reported increased expression of activating receptors on NK cells from chronic HCV patients including NKp44, NKp46, NKG2D, and NKp30, which may enhance NK cell cytotoxicity (330-332). Other groups have found no modulation or even decreased expression of activating NK receptors during chronic HCV (333-335). Differences in cohort composition and sampling may partially explain these divergent results. In addition, the frequency of peripheral NK cells was reduced during acute HCV compared to controls. However, peripheral NK cells from acute HCV patients were more cytotoxic and produced higher levels of IFN- $\gamma$  (331, 335). Comparative studies found that NK cells were more activated in the liver than in the blood of chronic HCV patients (330).

Despite their protective effects in antiviral immunity in the acute setting, activated NK cells may cause immune-mediated pathology through cytotoxicity and the production of pro-inflammatory cytokines. This is the case of mild hepatitis induced by the administration of polyinosinic/polycytidylic acid that activates NK cells (336). Activation of hepatic NK cells has also been shown to contribute to fulminant hepatic failure (FHF). In a model of FHF induced by murine hepatitis virus strain 3 (MHV-3), hepatic NK cells upregulated CD69 produced more TNF $\alpha$  and IFN- $\gamma$ , and killed MHV-3-infected hepatocytes in a FasL- and NKG2D-dependent manner. Consistent with the pathogenic role of NK cells in this model, NK cell depletion increased survival by 20% (337). Similarly, severe necroinflammatory damage was caused by NK cell-mediated Fas/Fas ligand interactions in a humanized mouse model of HBV infection demonstrating the pathogenic potential of NK cells during acute severe/fulminant hepatitis B (338).

As in acute injury models, NK cells have also been associated with collateral tissue damage during CHB and chronic HCV infection. The profiling of NK cells in blood samples and liver biopsies from chronic HBV patients showed that activated NK cells were associated with accelerated liver damage as assessed by serum ALT levels and the liver histological activity index (HAI). Interestingly, an increased frequency of hepatic NK cells was associated with a reduced frequency of NK cells in the blood, suggesting active recruitment from the periphery and/or hepatic retention of circulating NK cells in the liver tissue (339). In addition, the degranulation activity of blood NK cells during chronic HCV correlated with ALT levels, and hepatic NK cells were localized within the necrotic area suggesting NK cell-mediated tissue damage (331, 340).

NK cell genetic deficiency has been associated with an increased incidence of various types of cancers in patients and animal models (341-345). In addition, numerous studies reported impaired function of NK cells in cancer patients. NK cells are enriched in the healthy liver and reduced in both the circulation and inside the tumor in HCC (346-349). NK cells gradually become dysfunctional with HCC progression, displaying a reduced expression of TNF $\alpha$ , IFN- $\gamma$ , and a diminished cytolytic potential (346, 349). Cell-cell interactions in the tumor microenvironment have been proposed to explain NK cell dysfunction in HCC. *In vitro* assays showed that pre-incubation of NK cells with autologous Tregs reduced IFN- $\gamma$  secretion and lysis of target cells (346). In addition, the incubation of NK cells with tumor-associated monocytes triggered the transient activation of NK cells and their subsequent exhaustion and death (349). Similarly, myeloid-derived suppressor cells (MDSCs) from HCC patients inhibited autologous NK cell cytotoxicity and cytokine secretion in co-culture systems (350). Finally, PGE2 and IDO derived from HCC-associated fibroblasts suppressed the activation and cytotoxic activity of NK cells (351). Altogether, these studies revealed the negative effect that non-parenchymal cells enriched in HCC potentially have on NK cell function.

In summary, hepatic NK cells can exert potent antiviral and anti-tumoral functions but hold the potential for involvement in the pathogenesis of liver injury when they become dysfunctional or get activated in the wrong setting. The recent dissection and characterization of the different subpopulations of hepatic NK cells open a new era of targeted interventions where specific effector functions can be modulated in individual NK cell subsets, enhancing their protective activity while preventing their pathogenic potential.

### **1.e.3.c Hepatic NKT Cells**

Natural killer T cells (NKT) are large granular innate-like lymphocytes that coexpress the T cell receptor (TCR) and natural killer receptors (352, 353). NKT cells are critical effector cells against viral, bacterial, and parasitic infections. The TCR of NKT cells recognizes endogenous and microbial glycolipid antigens presented by the MHC I-like molecule CD1d (354). The identification of specific glycolipids recognized by NKT cells has been challenging and is still ongoing. However, glycolipids derived from some Gram-negative bacteria (e.g., *Sphingomonas sp.*) and the spirochete *Borrelia burgdorferi* have been identified (355, 356). Two subsets of NKT

cells have been defined based on different usage of TCR gene segments: type I NKT cells also known as iNKT cells that express a semi-invariant TCR ( $V\alpha 14$ - $J\alpha 18$  paired with  $V\beta 8.2$ ,  $V\beta 7$  or  $V\beta 2$  in mice, and  $V\alpha 24$ - $J\alpha 18$  paired with  $V\beta 11$  in human), and type II NKT cells, which are less abundant, and express a more diverse repertoire of TCRs (357).

Tissue-resident NKT cells exhibit an effector memory phenotype. Thus, upon activation, they can rapidly release large amounts of cytokines (261). NKT cells can be activated in a TCR-dependent and a cytokine-driven (TCR-independent) manner. Therefore, in addition to microbial glycolipid antigens, inflammatory mediators can also activate NKT cells in the absence of cognate antigen recognition. The fact that NKT cells can get rapidly activated and express type 1 (IL-12 and IFN- $\gamma$ ), type 2 (IL-4, IL-5, and IL-13) and type 3 (IL-17) cytokines, at early times upon pathogen invasion, make NKT cells very effective actors in the initiation and polarization of the immune response (358-362). The specific cytokine profile of activated NKT cells depends on the type of antigen presented (short vs. long chain glycolipids), the type of APC involved (e.g., DCs vs. hepatocytes), and the type of injury (205, 363, 364).

NKT cells possess a varied repertoire of effector mechanisms they can use to directly eliminate target cells. NKT mostly kills targets through cell-mediated cytotoxicity including secretion of the pore-forming protein perforin and GZM B, and through contact-dependent FAS ligand-induced apoptosis (365).

Given the barrier function of the liver against pathogens and microbial products present in the portal blood, it is not surprising that in both mice and humans, particularly large populations of NKT cells take residency in hepatic tissue. The frequency of NKT cells in the liver is 20 to 100 folds higher than that in any other organ (261). The hepatic tissue houses several cell types that constitutively express CD1d and can present glycolipid antigens to NKT cells. This includes LSECs, KCs, HSCs, and hepatocytes (242, 366-368). Using flow cytometry, murine NKT cells are identified as  $CD3^{int} NK1.1^{+}$  but a more specific identification requires the use of tetramers of CD1d loaded with  $\alpha$ -GalCer. In humans, NKT cells are defined as  $CD3^{+} CD161^{+} CD56^{+} CD69^{+} CD16^{+}$  cells (369).

NKT cells are in the sinusoids but are enriched in the periportal region that expresses high levels of CD1d (Figure 16). Since portal tracts are the site of entry to the liver for most pathogens, strategic positioning of NKT cells in this region may be advantageous (7). In addition, intravital

microscopy has shown that NKT cells randomly move inside the sinusoids at steady state in a patrolling behavior. Activation of NKT cells due to TCR stimulation or exposure to inflammatory cytokines such as IL-12 and IL-18 leads to NKT cell arrest (366, 370). The arrest of NKT cells may be caused by the establishment of stable interactions during antigen presentation between NKT cells and CD1d-expressing sinusoidal and perisinusoidal cells (242).

Hepatic NKT cells protect against bacterial invasion. For instance, in response to *Borrelia burgdorferi* infection, a pathogen that expresses CD1d ligands, iNKT cells formed intimate clusters with CD1d<sup>+</sup> KCs and produced IFN- $\gamma$ . In this model, KCs engulfed *B. burgdorferi* and presented CD1d ligands to iNKT cells, leading to their activation and release of IFN $\gamma$ . Infection of iNKT-deficient mice with *B. burgdorferi* led to pathogen spread in the joints, bladder, heart, and liver, suggesting a role for hepatic iNKT cells in bacterial contention in the sinusoids. Similarly, the depletion of KCs leads to pathogen dissemination (249, 250, 254, 371). Conversely, in Salmonella-induced liver injury, NKT cells exacerbated tissue damage and their removal did not affect bacterial growth. However, the CD1d-mediated presentation of Salmonella-derived glycolipids was not addressed in this study (372).

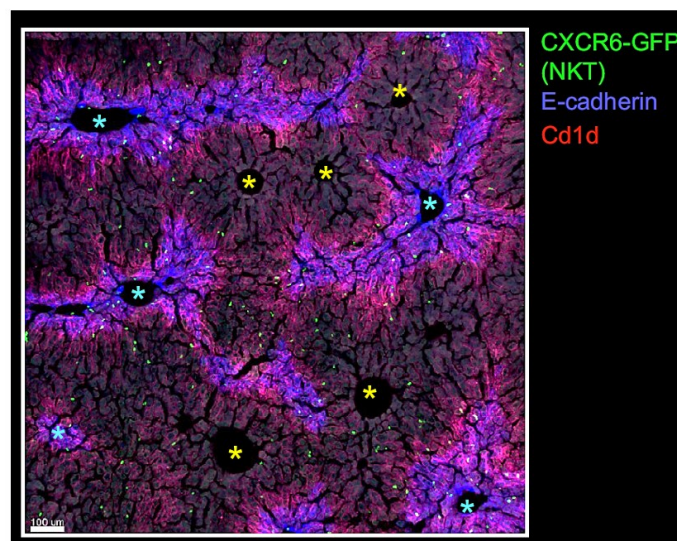


**Figure 16: NKT cells (CXCR6-GFP in green) are enriched around CD1d positive periportal areas.** Multiplex immunofluorescence of healthy murine liver section. E-cadherin (blue) and CD1d (red) are preferentially expressed in periportal hepatocytes. NKT cells are labeled in green (CXCR6-GFP in green). Cyan \* indicates portal tracts. Yellow \* indicates central veins. Caption and image adapted from reference (7).

Similarly, iNKT cells have been shown to protect against hepatotropic virus infection. It is important to keep in mind that, unlike bacteria, the lipids associated with viral particles are all host-derived (356). In one study using HCV-infected human hepatocyte chimeric mice transplanted with human peripheral blood mononuclear cells (PBMCs) and treated with IFN- $\alpha$ , iNKT cells expressed IFN- $\gamma$  and reduced the viral titers (373). Accordingly, the human counterpart of murine iNKT cells exhibited an activated phenotype in the liver of HCV patients (374). In addition, co-culture of CD56<sup>+</sup> T cells with HCV-infected human hepatocytes inhibited HCV replication through IFN- $\gamma$  secretion (375). Moreover, multiple studies have shown that NKT cells are partially depleted during chronic HCV infection (374, 376, 377). Collectively, these observations suggest that hepatic NKT cells may play a role in protection against HCV infection, particularly at early stages, and with disease progression, their gradual depletion may facilitate viral persistence (369).

Regarding the role of NKT cells in HBV infection, a report using primary human and mouse hepatocytes and models of transgenic and adenoviral HBV expression showed that HBV-expressing hepatocytes presented HBV-induced phospholipids in the context of CD1d to NKT cells leading to their activation and subsequent reduction of viral titers (378). In agreement with this, a study showed a reduced frequency of peripheral iNKT cells in CHB patients, which increased to normal levels with viral control (379). However, NKT cells were shown to contribute to hepatic injury during HBV infection in a transgenic mouse model of primary HBV infection. In this case, the immune-induced damage was dependent on the interaction between NKG2D and its ligand (380).

Another important aspect of NKT cell biology is their involvement in tissue repair through the secretion of Th2 cytokines. iNKT cells stimulated healing in a model of sterile focal thermal injury in the liver. *In vivo* imaging showed that iNKT cells arrived early at the injury site, made a turnaround, and a few hours later came back and accumulated at the perimeter of the injury site in a CD1d-dependent manner. The arrest of iNKT cells at the border of the lesion was dependent on IL-12 and IL-18 and their activation led to the secretion of IL-4 associated with the phenotypic switch of inflammatory CCR2<sup>hi</sup> CX3CR1<sup>low</sup> monocytes into reparative CCR2<sup>low</sup> CX3CR1<sup>hi</sup> MoMFs. In addition, CD1d blockade prevented the early accumulation of iNKT cells around the injured area. Moreover, the reduction of the wound size was significantly delayed in the CD1d<sup>-/-</sup>



mice because of reduced IL4-dependent hepatocyte proliferation. Therefore, iNKT cells were essential to promote the resolution of inflammation and tissue repair (193, 205).

Disease progression in models of NAFLD is associated with increased expression of CD1d and accumulation of NKT cells. Furthermore, iNKT cell-deficient mice had less fibrosis and inflammation compared to their WT counterparts (381-383). In the same line, human studies showed that increased frequency of iNKT cells was associated with more advanced cirrhosis and NAFLD (384). Mechanistically, several reports have linked the pro-fibrogenic activity of hepatic iNKT cells to persistent IL-13 secretion in the inflamed and fatty liver (385, 386).

NKT cells play dual roles in models of AIH. A proinflammatory role has been documented in the models of Con A and glycolipid  $\alpha$ -GalCer-induced hepatitis. In both models, hepatocellular injury is mediated by NKT cells through perforin/GZM B secretion, and Fas L-dependent cytotoxicity (387-389). Accordingly, mice lacking NKT cells expressing the invariant V $\alpha$ 14-J $\alpha$ 18 TCR were protected against Con A- and  $\alpha$ -GalCer induced hepatitis (390). By contrast, the anti-inflammatory activity of IL-17-producing NKT cells has also been reported. IL-17 neutralization before  $\alpha$ -GalCer injection significantly exacerbated hepatitis and administration of IL-17 attenuated hepatic inflammation. Unexpectedly, IL-17 neutralization increased hepatic recruitment of neutrophils and proinflammatory monocytes producing IL-12 and TNF- $\alpha$  suggesting an anti-inflammatory effect of NKT cell-derived IL-17 in this model of hepatitis (391). It is important to mention at this point that multiple other reports have documented the pro-inflammatory nature of IL-17 in autoimmune and inflammatory disorders. The presence in the liver of several subsets of IL-17-producing resident T cells (e.g., MAIT cells,  $\gamma\delta$  T cells, Th17 cells) adds another layer of complexity to the definitive understanding of the allegedly anti-inflammatory properties of IL-17 in models of autoimmunity. Therefore, the potential regulatory properties of IL-17 in the liver warrants further investigation.

In summary, the liver harbors a large and heterogeneous population of NKT cells that can rapidly respond to damage or pathogen invasion through the direct killing of infected cells, and secretion of large amounts of either type 1, type 2, or type 3 cytokines. This functional versatility underlies the capacity of hepatic NKT cells to modulate downstream innate and adaptive immune responses and orchestrate the balance between pro- and anti-inflammatory mediators during acute and chronic liver injury. The roles of NKT cells vary in different liver diseases and disease states (261).

A deeper understanding of the multiple factors that determine the protective versus pathogenic effects of NKT cell activation will facilitate the development of interventions harnessing the great therapeutic potential of NKT cells as versatile effectors of immunity in the liver.

#### **1.e.3.d Hepatic MAIT Cells**

Mucosal-associated invariant T (MAIT) cells are unconventional T cells that express semi-invariant  $\alpha\beta$  TCR which recognizes biosynthetic products of the riboflavin synthesis pathway presented in the context of the MHC class I-related molecule MR1 (Figure 17). MAIT cells are highly conserved in mammals suggesting that they perform important immunological functions (392). MAIT cells were first described in 1999 by Tilloy et al., as T cells bearing a canonical TCR  $\alpha$  chain containing V $\alpha$ 7.2–J $\alpha$ 33/12/20 in humans and V $\alpha$ 19–J $\alpha$ 33 in mice, paired with  $\beta$ -chains V $\beta$ 2/V $\beta$ 13 in humans and V $\beta$ 6/V $\beta$ 8 in mice (393). They recognize antigens that are derived from biosynthetic pathways unique to bacteria and yeast and absent in mammals (394, 395).

MAIT cells can be CD4<sup>+</sup>, CD8<sup>+</sup>, or double negative (DN) depending on the tissue and the species. They exhibit an effector memory phenotype (CD45RA<sup>-</sup> CD45RO<sup>+</sup> CD95<sup>hi</sup> CD62L<sup>low</sup> CD44<sup>hi</sup>) which allows them to rapidly respond to antigen encounters with the release of cytokines and chemokines (396, 397). MAIT cells express the transcription factor ROR $\gamma$ t and produce the type 3 signature cytokine IL-17 upon stimulation (398). Unlike conventional T cells (Tconv), MAIT cells sharing the same TCR specificity are abundant in barrier tissues and therefore do not require clonal expansion upon antigen encounter to the same degree Tconv does. This makes MAIT cells important determinants of early response to pathogen invasion (392). Since MAIT cells lack expression of lymph node homing molecules CCR7 and CD62L, they are rarely found in secondary lymphoid organs. However, they are abundant in barrier tissues like the mucosa, the skin, the liver, the lungs, and the urinary tract (399).

MAIT cells are critical effectors of anti-microbial immunity when activated in a TCR-dependent manner. TCR-mediated activation requires both antigen recognition in the context of MR1, and co-stimulatory signals from CD28, TLRs, or cytokines (e.g., IL-1 $\beta$ , IL-7, IL-23, TNF $\alpha$ , and type I IFNs) (259, 398, 400-403). Studies showed that TCR engagement using synthetic antigens alone, in the absence of co-stimulatory signals or PAMPs, did not result in MAIT cell activation (398). Therefore, MAIT cells require, in addition to TCR binding, second and third signals for full

activation, upon which MAIT cells expand and produce inflammatory chemokines and cytokines and eliminate invading pathogens. This activation pathway is important for immunity to pathogens expressing the riboflavin pathway, including some species of bacteria (*Escherichia*, *Lactobacillus*, *Staphylococcus*, *Shigella flexneri*, *Salmonella*, *K. pneumoniae*), mycobacteria (*Mycobacterium bovis*), and fungi (*Saccharomyces*, *Candida*, and *Aspergillus*) (404-410). However, other pathogens that do not produce MR1 ligands can also be the target of MAIT cells through cytokine-driven TCR-independent activation. This is typically the pathway used for MAIT cells to sense and responds to viruses as observed during infection with dengue virus, HCV, and influenza virus (411). TCR-independent activation can be triggered by IL-7, IL-12, IL-15, IL-17, or type I IFN signaling (411-416). Upon activation, MAIT cells can produce large amounts of type 1 (e.g., IFN- $\gamma$  and TNF $\alpha$ ), type 2 (e.g., IL-4, IL-5, and IL-10), and type 3 (e.g., IL-17) cytokines, and can also degranulate and kill infected cells through pore-forming and apoptosis-inducing effector molecules (e.g., perforin and GZM B) (259, 396, 405, 407, 417).

The liver acts as an immunological barrier to gut-derived pathogens when intestinal mucosal defenses are breached due to inflammation and a leaky gut. This way the liver prevents the passage of enteric commensals and pathogens to the general circulation. Hepatic MAIT cells comprise about 50% of all hepatic T cells in humans and play a major role in microbial clearance in this situation (396, 418).

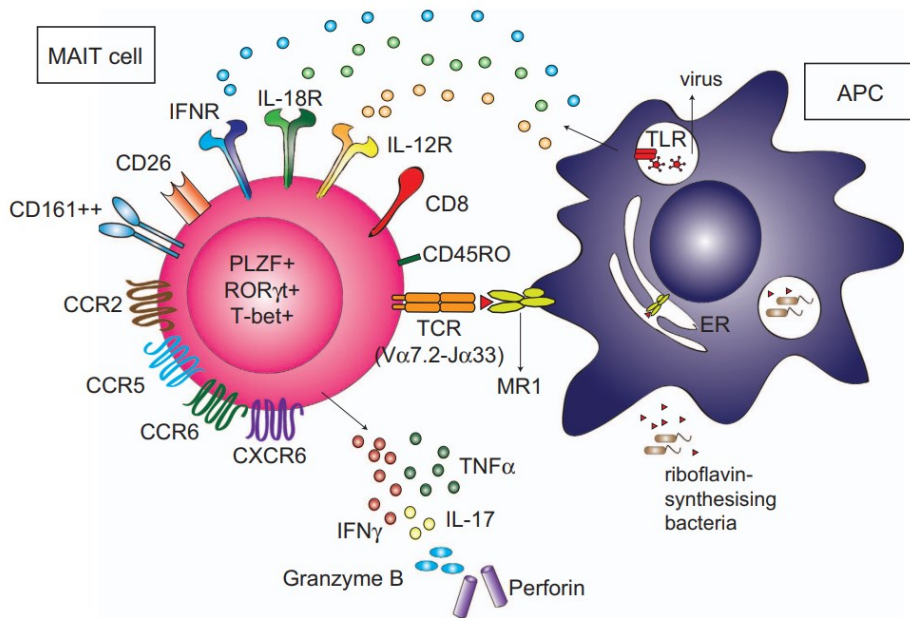


**Figure 17: The phenotype of human MAIT cells and their mechanisms of activation.** Mature MAIT cells in peripheral blood express the chemokine receptors CCR2, CCR5, CCR6, CXCR6, the C-type lectin-like receptor CD161, the dipeptidase CD26, and a CD45RO<sup>+</sup>CCR7<sup>-</sup> effector memory phenotype, with the majority of human MAIT cells expressing the CD8 coreceptor. MAIT cells also express the transcription factors RAR-related orphan receptor  $\gamma$ t (ROR $\gamma$ t), T-bet, and promyelocytic leukemia zinc-finger (PLZF) at rest. During bacterial infection, derivatives of the riboflavin biosynthesis pathway are captured by MR1 and presented on the surface of antigen-presenting cells (APCs). Alternatively, viruses can also rapidly activate MAIT cells in an MR1-independent manner owing to the induction of IL-18, IL-12, and IFN $\alpha$ . Activated MAIT cells express IFN $\gamma$ , TNF $\alpha$ , GZM B, perforin, and IL-17. Caption and image adapted from reference (399).

Few studies have analyzed the role of MAIT cells in the liver during homeostasis and disease. A landmark study by Jeffery et al. revealed the profile of human hepatic and circulating MAIT cells in the healthy liver and a spectrum of autoimmune, toxic, and metabolic diseases, affecting both the biliary epithelium and hepatocytes, including PSC, PBC, ALD, NASH, and acute liver failure (248). Overall, this study showed that MAIT cells are enriched in the liver compared to blood in both healthy and diseased livers with hepatic MAIT cells expressing higher levels of the activation marker CD69. In addition, the frequency of hepatic and circulating MAIT cells is reduced during chronic hepatitis compared to controls.

Human hepatic MAIT cells were shown to preferentially reside in the peri-biliary areas of the portal tracts in both the healthy and the inflamed liver and were associated with immunosurveillance of biliary epithelial cells (BECs) (289). BECs cells express MR1 and were able to activate MAIT cells in *in vitro* assays in a TCR-dependent manner. In agreement with their location, hepatic MAIT cells expressed the homing receptors for the biliary epithelium CXCR6, CCR6, and integrin  $\alpha E\beta 7$  (248, 322, 419, 420).

As mentioned above, human MAIT cells are either CD4<sup>+</sup>, CD8<sup>+</sup>, or DN and these subsets evolve differently during chronic hepatitis. In inflamed livers, the frequency of CD8<sup>+</sup> and DN MAIT cells out of total T cells was reduced, and the frequency of CD4<sup>+</sup> MAIT cells was unaltered. MAIT cells expressed the receptors for IL-12, IL-18, and IL-23 at similar levels in control and chronic hepatitis. *Ex vivo* assessment showed that intrahepatic MAIT cells from chronic hepatitis livers produced mostly TNF $\alpha$  and IFN- $\gamma$ , with a proportion of cells expressing IL-17 and almost undetectable levels of type 2 cytokines. In agreement with the observed cytokine profile, hepatic MAIT cells co-expressed the transcription factors T-bet and ROR $\gamma$ t (248, 259).

A recent study characterized the profile of MAIT cells in NAFLD patients and revealed decreased frequency in the blood compared to healthy controls, and an inverse correlation with the severity of NAFLD. Circulating MAIT cells exhibited a more activated phenotype during NAFLD (higher CD69 and PD-1) and expressed higher levels of the biliary epithelium homing receptor CXCR6 compared to healthy controls. However, a lower percentage of circulating MAIT cells were shown to produce pro-inflammatory TNF $\alpha$  and IFN- $\gamma$  compared to controls while serum levels of IL-4 were increased in NAFLD patients, suggesting a shift from type 1 to type 2 cytokines in MAIT cells in this disease. Multiplex immunofluorescence showed that during NAFLD, MAIT cells could be found in the proximity of degenerated hepatocytes with fat deposits. Moreover, the tissue density of MAIT cells positively correlated with NAFLD activity score (NAS). The simultaneous reduction of MAIT cells in the periphery and their increased tissue density during NAFLD suggest that MAIT cells may be more actively recruited from the circulation or retained in the liver with disease progression. However, the analysis of MAIT cells in a NASH model of methionine-choline-deficient (MCD) diet revealed that MR1 deficient mice, lacking TCR-dependent activation of MAIT cells, had exacerbated disease (ALT, triglyceride, and NAS) compared to wild-type counterparts suggesting a protective role of MAIT cells in NASH (421). Interestingly, livers of

MR1 deficient mice were enriched with classically activated macrophages suggesting that the lack of MAIT cell activation further promotes type 1 inflammation during NASH.

The profile of MAIT cells during ALD was recently addressed by Riva et al. (422). Bacterial infections due to leaky gut are a frequent complication in ALD (423). In this study, authors reported a reduced frequency of circulating MAIT cells in ALD compared to healthy controls (422). In addition, circulating ALD MAIT cells expressed higher levels of the activation markers CD69 and HLA-DR, but expressed similar levels of pro-inflammatory TNF $\alpha$  and IFN- $\gamma$  compared to controls. Moreover, upon *in vitro* challenge with *E. coli*, ALD-derived MAIT cells produced less GZM B. Furthermore, circulating MAIT cells from ALD patients expressed lower levels of IL-17 and ROR $\gamma$ t compared to controls suggesting that the anti-microbial program orchestrated by ROR $\gamma$ t and IL-17 is compromised in these patients. By contrast, ALD livers displayed increased expression of MR1, and ligands for MAIT cell homing receptors, suggesting a potential relocation or selective retention of circulating MAIT cells in ALD livers versus control. However, no differences in the density of hepatic MAIT cells were observed between ALD and controls (422). Altogether, this study demonstrated reduced frequency and increased functional impairments in MAIT cells during ALD.

MAIT cells constitute most of the T cells in the human liver and are likely major players in hepatic immunity. Microbial translocation from the gut is a common occurrence during chronic hepatic disease and hepatic MAIT cells are specialized antimicrobial effector cells in this matter. Studies in the next few years will define how the various subsets of MAIT cells differentially protect the liver during homeostasis and contribute to the pathogenesis of distinct liver diseases. Hopefully, a deeper understanding of MAIT cell biology will lead to harnessing their potent antimicrobial activity for therapeutic purposes.

### **1.e.3.e Hepatic $\gamma\delta$ T Cells**

$\gamma\delta$  T cells are innate-like, non-conventional T cells characterized by the expression of a  $\gamma\delta$  TCR (424).  $\gamma\delta$  T cells occupy different spatial, and functional niches relative to conventional  $\alpha\beta$  T cells.  $\gamma\delta$  T cells are rare in secondary lymphoid organs but abundant in barrier tissues like the skin, the intestine, the lung, the liver, and the uterus. Tissue-resident  $\gamma\delta$  T cells exhibit limited TCR diversity, ensuring that in the same tissue location, multiple  $\gamma\delta$  T cells recognize the same antigen

and efficiently respond to pathogen invasion with no need for extensive prior clonal expansion like  $\alpha\beta$  T cells. This suggests that, unlike the  $\alpha\beta$  TCR repertoire,  $\gamma\delta$  TCRs recognize a limited number of conserved antigens from pathogens or self-molecules. Moreover, unlike  $\alpha\beta$  T cells,  $\gamma\delta$  T cells require neither priming nor recruitment to the site of infection (425). In addition,  $\gamma\delta$  T cells recognize antigens presented not only by MHC but also by MHC-related molecules (e.g., CD1d) (426-430). This includes conserved exogenous and self-lipid antigens like sulfatide, phosphatidylcholine, phosphatidylethanolamine, and phosphatidylglycerol (431-433).  $\gamma\delta$  T cells have different activation requirements and respond earlier than  $\alpha\beta$  T cells to invading pathogens and therefore may be involved in establishing and modulating the early immune response (434, 435).

During development,  $\gamma\delta$  T cells acquire a pre-activated phenotype that allows rapid induction of effector functions upon stimulation (436). Activation of  $\gamma\delta$  T cells is dependent on TCR engagement, signaling through TLRs, and natural killer receptors (NKR). Depending on the subset, the nature of the stimuli, and the inflammatory context, activated  $\gamma\delta$  T cells can produce type 1, type 2, or type 3 cytokines, and display cytotoxic effector functions (437).  $\gamma\delta$  T cells kill target cells through the expression of ligands for death-inducing receptors like Fas L and TRAIL and the release of granules containing perforin and granzymes (438-440). The analysis of  $\gamma\delta$  T cell-deficient mice has revealed a broad array of functions including immunity against extracellular and intracellular pathogens (e.g., bacteria, viruses, parasites), tissue repair, and tumor immunosurveillance (436).

As previously mentioned, the liver is an organ with abundant innate and innate-like immune cells. This is also valid for  $\gamma\delta$  T cells that make up between 15 to 25% of intrahepatic T cells in humans and about 5% in mice suggesting their important role in liver homeostasis and in response to injury (441, 442). In the last decade, the notion of two functionally different subsets of  $\gamma\delta$  T cells, one antigen-experienced and IFN- $\gamma$ -producing, and other antigen-naive and IL-17A-producing, has dominated the view on the heterogeneity of  $\gamma\delta$  T cells (246, 443). However, a recent study using scRNA-seq and t-distributed stochastic neighbor embedding (t-SNE) analysis revealed that murine hepatic  $\gamma\delta$  T cells can be divided into 6 subpopulations in the healthy liver (247). These subsets were more diverse than previously anticipated. Two of these clusters expressed high levels of *Ifng*, *Tbx21*, *CD27*, *Il2rb*, and *NK1.1* suggesting that they are type 1 IFN- $\gamma$ -producing  $\gamma\delta$  T cells and

exhibited cytotoxic potential. Another cluster co-expressed IFN- $\gamma$  and IL-4 suggesting potential involvement in type 2 immunity and tissue repair. There was another cluster enriched in several genes associated with the IL-17 program, such as *Il17a*, *Il17f*, *Il17r*, *Blk*, *Maf*, *Rorc*, and *Ccr6* which may be involved in antimicrobial immunity and neutrophil mobilization. Interestingly, this study identified a cluster of tissue-resident immature  $\gamma\delta$  T cells expressing progenitor genes developmentally linked to the more mature IFN- $\gamma$  producing  $\gamma\delta$  T cell subsets (247).

Neonatal mice have low levels of IL-17-producing hepatic  $\gamma\delta$  T cells, but this population becomes the dominant one after weaning and colonization of the gut by the microbiota. Moreover, hepatic  $\gamma\delta$  T cells were in a more active and mature state (CD44<sup>hi</sup> CD62L<sup>-</sup> CD24<sup>low</sup>) compared to circulating  $\gamma\delta$  T cells and those residents in other tissues. Interestingly, the liver residency of hepatic  $\gamma\delta$  T cells was absent in IL-17A KO mice indicating that IL-17 expression is critical for homing and/or retention of  $\gamma\delta$  T cells in the liver. The establishment of IL-17-producing  $\gamma\delta$  T cells in the liver was dependent on signals derived from the commensal microbes since antibiotic treatment blocked the colonization of the liver by these cells (251).

A study by Kenna et al., profiling human  $\gamma\delta$  T cells, found that they can be divided into three groups according to their  $\delta$  chain expression: V $\delta$ 1<sup>+</sup> chains, V $\delta$ 2<sup>+</sup> chains, and V $\delta$ 3<sup>+</sup> chains. These subsets are unevenly distributed in the blood and the hepatic tissue. Overall,  $\gamma\delta$  T cells were enriched in the liver compared to the blood (6.6% vs. 0.9% of total T cells), and most of them were DN  $\gamma\delta$  T cells (85%). The majority of hepatic  $\gamma\delta$  T cells expressed the V $\delta$ 2 chain (median 56 %), 21% expressed the V $\delta$ 3 chain, and about 10 % expressed the V $\delta$ 1 chain (444). This relative distribution of  $\gamma\delta$  T cell subsets has been recently contested as discussed below (445). Interestingly, different antigens have been associated with these three subsets of  $\gamma\delta$  T cells. For instance, V $\delta$ 1<sup>+</sup>  $\gamma\delta$  T cells recognize stress molecules like MICA and MICB that are upregulated in virally infected and malignant cells (427, 446). By contrast, V $\delta$ 2<sup>+</sup>  $\gamma\delta$  T cells recognize non-peptide antigens (phosphoesters, alkylamines, and nucleotide conjugates) constitutively expressed by intracellular pathogens (447-449). Finally, V $\delta$ 3<sup>+</sup>  $\gamma\delta$  T cells, enriched in the liver and absent in the blood, recognize unknown ligands abundant during viral infections such as cytomegalovirus (CMV) and human immunodeficiency virus (HIV) (440).

A recent study by Hunter et al., uncovered the tissue density, location, and TCR diversity of  $\gamma\delta$  T cells in the human liver (445). Immunohistochemistry with a pan- $\gamma\delta$  TCR antibody revealed that



healthy livers have similar  $\gamma\delta$  T cell density compared to diseased livers including several etiologies like viral hepatitis, NASH, ALD, PSC, and PBC. Hepatic  $\gamma\delta$  T cells were observed in the portal and parenchymal areas, but they were significantly enriched in the parenchyma. The majority of hepatic  $\gamma\delta$  T cells were  $V\delta 2^-$ . The TCR sequencing data showed hepatic enrichment for the  $V\delta 1^+$   $\gamma\delta$  T cell subset over  $V\delta 2^+$  and  $V\delta 3^+$  and confirmed the increased presence of the  $V\delta 3^+$   $\gamma\delta$  T cell subset in the liver compared to the blood in both healthy donors and patients. Overall, the TCR sequencing data was consistent with the notion that the expanded few clonotypes that dominated the repertoire of human intrahepatic  $\gamma\delta$  T cells were the product of infection-directed expansion (445).

The role of hepatic  $\gamma\delta$  T cells in antiviral immunity is dependent on the virus and the disease context (e.g., acute vs. chronic).  $\gamma\delta$  T cells were critical for hepatic protection upon lethal MCMV infection. A protective antiviral effect of  $\gamma\delta$  T cells was uncovered using total T cell-deficient,  $\alpha\beta$  T cell-deficient, and  $\gamma\delta$  T cell-deficient mice, infected with MCMV.  $\gamma\delta$  T cell conferred protection through the secretion of IFN- $\gamma$  and recruitment of NK cells (450). However, in another report,  $\gamma\delta$  T cells exacerbated injury and compromised survival in acute hepatic infection with mouse hepatitis virus strain 3 (MHV-3). In this model, hepatic  $\gamma\delta$  T cells expanded upon infection exhibited a hyperactivated phenotype and released large quantities of TNF $\alpha$ , IFN- $\gamma$ , IL-2, and IL-17. *In vitro* assays showed that  $\gamma\delta$  T cells killed MHV-3 infected hepatocytes in a contact-independent manner, and adoptive transfer of  $\gamma\delta$  T cells into MHV-3 infected mice decreased survival (451). In another study,  $\gamma\delta$  T cell deficiency prevented hepatic NK cell accumulation in a model of Poly I:C administration. This effect was not observed following adenovirus administration in  $\gamma\delta$  T cell-deficient mice suggesting that  $\gamma\delta$  T cell promotion of NK cell infiltration is virus-specific (452). While these studies prove the antiviral potential of  $\gamma\delta$  T cells, they also show that their hyperactivation can lead to immunopathology.

$\gamma\delta$  T cells are reported to be depleted in patients with HBV-associated liver disease, but their role in the pathogenesis of chronic HBV is still insufficiently characterized. In chronic HBV patients during the immune-active phase, the frequency of intrahepatic as well as peripheral  $V\delta 2^+$   $\gamma\delta$  T cells, inversely correlated with disease severity as measured by the liver histological activity index and ALT, suggesting that the  $V\delta 2^+$  subset may play a protective role in decreasing tissue damage. Circulating  $V\delta 2^+$   $\gamma\delta$  T cells exhibited reduced proliferative capacity in immune-active HBV

patients compared to healthy controls but expressed significantly higher levels of activation markers CD69, CD38, and HLA-DR. In addition, V $\delta$ 2<sup>+</sup>  $\gamma\delta$  T cells were enriched in effector memory and reduced in central memory (453, 454). By contrast, in HBV-associated acute-on-chronic liver failure (ACLF), circulating  $\gamma\delta$  T cells expressed higher levels of TNF $\alpha$  and IL-17, and increased expression of GZM B and the degranulation marker CD107a compared to chronic HBV and healthy controls, suggesting a more inflammatory and cytotoxic potential. Furthermore, tissue damage markers positively correlated with TNF $\alpha$ <sup>+</sup> and CD107a<sup>+</sup>  $\gamma\delta$  T cells. Together, these reports suggest that while V $\delta$ 2<sup>+</sup>  $\gamma\delta$  T may contribute to viral control and prevent tissue damage in chronic HBV, they may be pathogenic in more inflammatory contexts like HBV-related ACLF (455).

Unlike chronic HBV infection, levels of circulating  $\gamma\delta$  T cells were reported to be similar in chronic HCV compared to healthy controls. However, circulating V $\delta$ 2<sup>+</sup>  $\gamma\delta$  T cells expressed significantly higher levels of the activation markers CD38 and CD69 in chronic HCV compared to healthy controls, and total numbers correlated with serum ALT levels. Like in chronic HBV, V $\delta$ 2<sup>+</sup>  $\gamma\delta$  T cells from HCV-infected patients were enriched for terminally differentiated effector cells (CD45RA<sup>+</sup> CD27<sup>-</sup>) compared to controls. In addition, while hepatic V $\delta$ 2<sup>+</sup>  $\gamma\delta$  T cells exhibited an impaired capacity to produce IFN- $\gamma$  compared to the circulating counterparts in chronic HCV patients, the markers of cytotoxicity were upregulated demonstrating a bias towards cytotoxicity as the dominant antiviral mechanisms of hepatic V $\delta$ 2<sup>+</sup>  $\gamma\delta$  T cells (456). Another study, in this case on the V $\delta$ 1<sup>+</sup> subset, found that V $\delta$ 1<sup>+</sup>  $\gamma\delta$  T was highly enriched in the liver compared to the blood in chronic HCV patients. In addition, this subset displayed a memory/effector phenotype (CD62L<sup>-</sup> CD45RO<sup>+</sup> CD95<sup>+</sup>) and produced increased amounts of IFN- $\gamma$  with disease progression. Furthermore, the frequency of IFN- $\gamma$  -producing V $\delta$ 1<sup>+</sup>  $\gamma\delta$  T cells was associated with a higher degree of liver necroinflammation suggesting involvement in inflammation-mediated tissue damage (457). Taken together, the available data from patients show that the numbers, phenotype, and function of  $\gamma\delta$  T cells are altered during chronic HCV. However, the lack of satisfactory animal models and the nature of the existing evidence from human samples are insufficient to assign definitive protective or pathological roles to hepatic  $\gamma\delta$  T cells in chronic HCV.

Hepatic  $\gamma\delta$  T cells have been shown to protect against intracellular bacteria through the prevention of immune-mediated tissue damage. In a *Listeria monocytogenes* (Lm) infectious model,  $\gamma\delta$  T cell-

deficient mice ( $\text{TCR}\delta^{-/-}$ ) developed exacerbated disease, characterized by accumulation of inflammatory macrophages, compared to their wild-type counterparts. Co-culture experiments showed that  $\gamma\delta$  T cells killed inflammatory macrophages in a Fas L-dependent manner suggesting that cytotoxic hepatic  $\gamma\delta$  T cells could be protective through the reduction of collateral damage caused by inflammatory macrophages during Lm infection (458). Still, in Lm-infected  $\text{TCR}\delta^{-/-}$  mice,  $\text{TNF}\alpha$ -producing  $\text{CD8}^+$  T cells were shown to accumulate in the livers causing hepatic lesions. Interestingly, the ability of  $\gamma\delta$  T cells to protect against  $\text{TNF}\alpha$ -producing  $\text{CD8}^+$  T cells, was dependent on their capacity to produce IL-10 since the reconstitution of  $\text{TCR}\delta^{-/-}$  infected mice with  $\gamma\delta$  T cells from IL-10-deficient animals failed to prevent liver necrosis. Moreover, *in vitro* cocultures of IL-10-producing  $\gamma\delta$  T cells with  $\text{CD8}^+$  T cells reduced  $\text{TNF}\alpha$  production by  $\text{CD8}^+$  T cells, and this inhibition was abolished with IL-10 neutralizing antibodies (459). Another study found that hepatic  $\gamma\delta$  T cells were the main early producers of IL-17 upon Lm infection.  $\gamma\delta$  T cell-derived IL-17 reduced the bacterial burden in the livers of Lm-infected mice, induced recruitment of neutrophils, and prevented Lm-associated tissue damage demonstrating direct anti-bacterial activity by hepatic  $\gamma\delta$  T cells (460).

In the case of immunity to parasites, hepatic  $\gamma\delta$  T cells have been suggested to play both protective and deleterious roles. In a model of the rodent malaria parasite *Plasmodium yoelii* (Py), hepatic  $\gamma\delta$  T was found to prevent the intrahepatic stages of the Py life cycle indicating that they can mediate protective immunity against parasites (461). Conversely, hepatic  $\gamma\delta$  T cells may induce immunopathology in *Schistosoma japonicum* (Sj) infection. In this model, hepatic  $\gamma\delta$  T cells were the main cellular source of IL-17, the blockage of which reduced hepatic granulomatous inflammation and periportal fibrosis. In addition, IL-17 inhibited the production of soluble egg antigen-specific antibodies. However, this study didn't examine the role of hepatic  $\gamma\delta$  T cells in models of adoptive transfer of  $\gamma\delta$  T cells upon Sj infection, or in a  $\text{TCR}\delta^{-/-}$  infected mice, and consequently, the pathogenic role of these cells could not be definitively established (462). Similarly, hepatic IL-17-producing  $\gamma\delta$  T cells promoted neutrophil recruitment to granulomas induced by Sj infection and aggravated fibrosis (463).

The involvement of hepatic  $\gamma\delta$  T cells in autoimmune liver diseases has been known for more than two decades but remains poorly defined (464). Early studies found that the total numbers of circulating  $\gamma\delta$  T cells were increased in PSC and AIH patients compared to healthy controls and

their livers were highly infiltrated in the periportal areas suggesting a possible role in the pathogenesis of these autoimmune diseases (465). In addition, patients with AIH had an inverted V $\delta$ 1/V $\delta$ 2 ratio in circulating  $\gamma\delta$  T cells and higher IFN- $\gamma$  and GZM B production compared to controls. A positive correlation between GZM B and bilirubin levels suggested the potential contribution of hepatic  $\gamma\delta$  T cells to hepatocellular damage in AIH (466). Moreover, in PBC patients, the V $\delta$ 1<sup>+</sup> subset of  $\gamma\delta$  T cells was enriched while the V $\delta$ 2<sup>+</sup> subset was decreased relative to healthy controls in both the blood and liver. Immunofluorescence analysis of tissue sections from PBC patients showed that V $\delta$ 1<sup>+</sup>  $\gamma\delta$  T cells were scattered in the parenchyma and the portal area and no correlations were observed between the proportion of V $\delta$ 1<sup>+</sup>  $\gamma\delta$  T cells and serum markers of tissue damage like ALT and AST. However, circulating V $\delta$ 1<sup>+</sup>  $\gamma\delta$  T cells from PBC patients were highly activated (HLA-DR<sup>+</sup>, CD69<sup>+</sup>, and CD38<sup>+</sup>) (467). Collectively, these observations in patients indicate that  $\gamma\delta$  T cells are altered in several autoimmune liver diseases, but their function is still to be established. Recently, a pro-fibrogenic role was assigned to hepatic  $\gamma\delta$  T cells in a mouse model of PSC. In Mdr2 KO mice, a model of PSC, disease progression led to IL-17 production by hepatic  $\gamma\delta$  T cells and progressive fibrosis. Antibody-mediated depletion of  $\gamma\delta$  T cells in this model reduced secretion of IL-17 and related IL-23, decreased neutrophil and monocyte infiltration, and reduced expression of fibrosis-associated genes suggesting that IL-17-producing  $\gamma\delta$  T cells exacerbate inflammation and fibrosis in PSC. Importantly, intrahepatic  $\gamma\delta$  T cells from human PSC patients undergoing orthotopic liver transplant expressed IL-17 upon stimulation (468).

Although inflammatory Th17 cells are expanded during NAFLD and assumed to be the main IL-17 producers, IL-17-producing  $\gamma\delta$  T cells are much more abundant in both the healthy and the inflamed liver. A study showed that IL-17-producing  $\gamma\delta$  T cells were significantly increased in the liver in a high-fat diet (HFD) model compared to chow diet control mice. In addition, livers from TCR $\delta$ <sup>-/-</sup> mice subjected to HFD exhibited reduced steatosis, decreased number of inflammatory foci and ALT, and had better scores for glucose and insulin tolerance tests compared to their wild-type counterparts demonstrating a pathogenic role of  $\gamma\delta$  T cells in NAFLD. Adoptive transfer experiments demonstrated that this pathogenic effect was mediated by  $\gamma\delta$  T cell-derived IL-17 (251). Even though evidence has accumulated on the role of IL-17 in the pathogenesis of human NAFLD, a definitive link with hepatic  $\gamma\delta$  T cells remains to be established (259, 469-471). The

data from mouse models strongly suggest that IL-17-producing  $\gamma\delta$  T cells are major players in human NAFLD progression and warrant further investigation.

In summary, the study of hepatic  $\gamma\delta$  T cells has revealed their sentinel function during homeostasis and their capacity to protect against a broad range of pathogens including bacteria, viruses, and parasites, as well as their ability to participate in type 1, type 2, and type 3 immune responses. Their capacity to recognize both self and foreign unconventional antigens suggest that they have equally important roles during homeostasis and inflammation. In most chronic conditions hepatic  $\gamma\delta$  T cells exhibit alterations in numbers and function. Delineating the roles of the different  $\gamma\delta$  T cell subpopulations in the pathogenesis of liver diseases will facilitate taking advantage of their broad functional repertoire for the design and customization of  $\gamma\delta$  T cell-based therapies.

### **1.e.3.f Hepatic tissue-resident memory T cells**

The profiling of T cells in non-lymphoid tissue in models of parabiosis, tissue transplantation, and blockade of T cell recirculation has revealed the existence of non-circulating memory T cells called tissue-resident memory T cells or  $T_{RM}$  (239).  $T_{RM}$  are pathogen-specific memory T cells that reside in non-lymphoid organs.  $T_{RM}$  are phenotypically and functionally different from central memory ( $T_{CM}$ ) and effector memory T cells ( $T_{EM}$ ). While  $T_{CM}$  express homing receptors for secondary lymphoid organs (SLOs) (e.g., CCR7 and CD62L), and recirculate between SLOs and the blood, the  $T_{EM}$  and  $T_{RM}$  do not express SLO homing receptors and exhibit different recirculation patterns ( $T_{EM}$ ) or do not recirculate at all ( $T_{RM}$ ). In addition,  $T_{RM}$  differs from  $T_{EM}$  in the expression of tissue retention markers (e.g., CD69, CD49a, and CD103) (472). Therefore, differential expression of chemokine receptors and tissue retention markers underlie the regionalization of T cell-mediated immunosurveillance (258).

$T_{RM}$  are not originally found in healthy/uninjured tissue, but they progressively accumulate and get established in barrier tissues in response to repeated exposure to pathogens. Thus,  $T_{RM}$  cells are typically enriched in chronically inflamed tissue.  $T_{RM}$  cells have been reported in multiple organs including the skin, the gut, the lungs, the urogenital tract, and the liver.  $T_{RM}$  comprise both  $CD4^+$  and  $CD8^+$  T cells but most  $T_{RM}$  described so far are  $CD8^+$  T cells (473-476).

After activation in secondary lymphoid organs, a subset of antigen-experienced T cells differentiates into  $T_{RM}$  in the tissue of pathogen encounter and remains in that tissue (477). Newly

generated  $T_{RM}$  are retained in the tissue due to reduced expression of lymph node homing receptors (e.g., CD62L, CCR7, and S1PR1) and high expression of tissue adhesion molecules (e.g., CD69, CD103, and CD49a) (473, 478). The role of  $T_{RM}$  is to seed the tissues after primary infection with clonally expanded T cells with TCR-specificities for those antigens that have been previously encountered in that location and thereby reinforce the barrier functions of the tissue against reinfection (476, 479). The percentage of hepatic  $T_{RM}$  out of total memory T cells in a model of LCMV infection was higher than 60 % and this was also the case for most organs examined 90 days after viral challenge. Therefore, most memory T cells in the tissue are  $T_{RM}$  (258). The persistence of  $T_{RM}$  cells in the tissue is dependent on tissue-specific factors (e.g., survival like IL-15) and can vary from months to years (241). Interestingly,  $T_{RM}$ -like cells accumulate in several tumors and correlate with better clinical outcomes and patient survival (480). These intratumoral  $T_{RM}$ -like cells express immune checkpoint inhibitors (e.g., PD-1, CTLA-4, and Tim-3), exhibit cytotoxicity, and secrete a variety of tumor-fighting cytokines (480).

$T_{RM}$  in different organs exhibit a different phenotype that is dictated by the tissue of residency but in general, most  $T_{RM}$  can be identified as  $CD69^+ CD103^+ CD49a^+ CD44^+$  T cells. However, *bona fide*  $T_{RM}$  lacking the expression of some of these markers has also been identified (480). In addition to phenotypic markers,  $T_{RM}$  display functional heterogeneity and express type 1, type 2, and type 3 cytokines (473, 481, 482). This functional versatility allows  $T_{RM}$  cells to protect against secondary infections with virtually all types of pathogens at the entry site (241). However, chronic activation of  $T_{RM}$  can also exacerbate autoimmune and inflammatory diseases as observed in vitiligo, psoriasis, inflammatory bowel disease, type I diabetes, Sjogren's syndrome, lupus nephritis, multiple sclerosis, and others (483, 484).

The liver is constantly exposed to a heavy antigenic influx. Multiple pathogens have evolved strategies to exploit the tolerogenic liver microenvironment to establish chronic infections in the hepatic tissue (1). Therefore, it is not surprising the elevated density and variety of phagocytes, conventional and unconventional APCs, and lymphocytes that populate the liver. As expected,  $T_{RM}$  have been shown to accumulate in the liver after systemic infection and vaccination (239, 255, 485).

$T_{RM}$  control hepatotropic viral infections. For instance, in mice, systemic infection with LCMV led to the accumulation of LCMV-specific  $T_{RM}$  in the liver that persisted for at least 120 days

(258). Similarly, the profiling of T<sub>RM</sub> in human hepatic tissue showed expansion of CD8<sup>+</sup>CD69<sup>+</sup>CD103<sup>+</sup>T- bet<sup>lo</sup>Eomes<sup>lo</sup>Blimp-1<sup>hi</sup>Hobit<sup>lo</sup> PD-1<sup>hi</sup> HBV-specific T<sub>RM</sub> cells upon HBV infection (255). Interestingly, enrichment of these HBV-specific T<sub>RM</sub> cells was found in HBV controllers. These hepatic T<sub>RM</sub> cells expressed high levels of the survival factor IL-2 and low GZM B. Although this specific T<sub>RM</sub> population was also present in the healthy human liver, it cannot be concluded that they are part of the naïve repertoire because previous exposure to HBV or HBV vaccination could explain this observation. In addition, *in vitro*, sequential stimulation of PBMCs with IL-15 and TGFβ induced de novo CD8<sup>+</sup> T<sub>RM</sub> expressing both CD69 and CD103 at a similar frequency to that found in the healthy liver (255). Profiling of intrahepatic T cells by CyTOF showed that T<sub>RM</sub> cells were enriched in HBV-associated HCC compared to non-viral HCCs (486). Moreover, the frequency of T<sub>RM</sub> cells in this study correlated with good prognosis paralleling observations in other solid tumors (480).

Hepatic CD69<sup>+</sup> KLRG1<sup>lo</sup> CXCR6<sup>+</sup> T<sub>RM</sub> T cells also accumulated upon vaccination with radiation-attenuated sporozoites (RAS) from *Plasmodium berghei* and persisted in the tissue for at least 100 days, conferring a front-line defense against malaria liver-stage infection (487). Intravital multiphoton microscopy showed that this T<sub>RM</sub> population was intrasinusoidal, and exhibited an amoeboid morphology and a migratory behavior consistent with patrolling activity (487). No preferential location of T<sub>RM</sub> cells was observed along the sinusoidal portal-central axis in this study.

Another recent report showed that hepatic T<sub>RM</sub> cells from explanted liver samples exhibited an increased rate of basal autophagy compared to paired T cells from PBMCs. This adaptation led to increased proliferation and effector functions of hepatic T<sub>RM</sub> cells including cytotoxic activity and cytokine production which was linked to better function in the tolerogenic liver environment (488). Thus, as observed in other organs, hepatic T<sub>RM</sub> cells adopt tissue-specific traits to maximize *in situ* immunity (489).

In summary, T<sub>RM</sub> are principal effector cells in response to reinfection in the liver and other organs. The few reports available in the liver link T<sub>RM</sub> cells with rather positive disease outcomes in viral infections and cancer. However, T<sub>RM</sub> cells hold the potential to perpetuate inflammation and the resultant tissue damage. Therefore, examination of the role of hepatic T<sub>RM</sub> in non-viral non-cancer

diseases is an important previous step to fully assess the potential of hepatic T<sub>RM</sub> cells as therapeutic targets in the future.

### **1.f. The emerging atlas of the hepatic tissue**

The liver is a vital organ in charge of varied essential functions including metabolic homeostasis, biosynthesis of blood factors, removal of toxins from systemic and gut-derived blood, and the induction of peripheral tolerance to harmless antigens. These physiological processes require and involve different cellular and molecular microenvironments and cell populations. Therefore, the liver is a highly organized tissue where the location of parenchymal and non-parenchymal cells, and the interacting networks they form, have evolved to support the formation of several specialized topographical niches.

In this introduction, we have covered the studies that have revealed zonation patterns for hepatocytes, LSECs, and HSCs. Their unique locations are associated with specific transcriptional programs and functions. Similarly, we have presented the evidence of distinctive spatial profiles of several liver resident immune populations during homeostasis (e.g., KCs, LCMs, and NKT cells) and upon injury (e.g., MoMFs). The functional consequences of these topographical distributions are starting to be revealed with the improvement of existing spatial technologies (e.g., intravital microscopy, multiplex immunofluorescence), and the emergence of new ones (e.g., spatial transcriptomics).

The mapping of the cellular networks, and the spatially resolved expression patterns at the single-cell level, will be critical to understanding the homeostatic functions of the liver, and the highly dynamic immune responses to hepatic insults. In the subsequent sections, we will introduce a strategy for higher visualization, quantification, and mapping of immune cells in liver tissue sections (chapter 3). Next, we will present the results of applying the principles of this strategy to the spatio-temporal profiling of hepatic macrophages upon CCl<sub>4</sub> acute injury.



## **Chapter 2: Rationale, Hypothesis, and Objectives**

### **2.a.1. Rationale**

The liver is populated by a large network of innate and innate-like immune cells. The spatial organization of immune populations and their interactions with neighboring tissue cells protect the liver against blood-borne pathogens and support its function as a filter of gut-derived microbes and toxins and as a major enforcer of systemic tolerance to food and commensal-derived antigens. Therefore, the development of methodologies allowing the spatial characterization of immune cells in the tissue environment is required for a deeper understanding of liver physiology and pathology.

In recent years a technological revolution has taken place in the imaging and image analysis field. New multiplex imaging tools have been developed in conjunction with more powerful microscopes, and software solutions (291, 490-495). However, accessibility to these advanced technologies remains restricted to a few laboratories. Specifically, the study of the organization of the hepatic immune cell network has been hampered by the limited multiplexing capability of imaging systems due to the reduced availability and specificity of antibodies, a reduced number of fluorophores suited for imaging, and a limited number of lasers and filters in microscopes. Other limitations include subjectivity and reduced speed of manual counting, and lack of proper representation of the tissue heterogeneity when analyzing fragmented fields of view (FOV). Therefore, the first objective of this thesis was to generate and validate an accessible strategy for increased visualization and unbiased analysis of immune cells in the hepatic tissue.

To overcome limitations associated with inefficient labeling of clinical specimens, we integrated into our immunofluorescence staining protocol several solutions for reducing the autofluorescence and unspecific binding of antibodies (482). To expand the number of markers that can be simultaneously visualized, we combined serial and sequential labeling with digital tissue alignment resulting in the generation of virtual slides allowing the integration of information derived from different images and imaging techniques. In addition, analysis of whole tissue sections, instead of selected FOV, provided a more objective representation of the tissue microenvironment. Also, to reduce the intrinsic subjectivity of manual counting by visual

inspection, we generated protocols for the automated classification of pixels. Furthermore, by incorporating automated counting into our strategy, larger tissue areas were processed in a shorter time (482).

Hepatic macrophages are heterogeneous and are major effector immune cells during homeostasis and in response to injury. Historically, studies on liver macrophages have relied on pan-macrophage markers that cannot discriminate among the different subpopulations (e.g., F4/80 and CD68). More recently, RNA-seq and mass cytometry have revealed the phenotypic heterogeneity and functional plasticity of hepatic macrophages and identified markers unique to each macrophage subset (129, 131-134, 141, 152). However, the distinctive or potentially overlapping spatial and temporal behavior of subpopulations of hepatic macrophages in response to injury is poorly understood. Therefore, the second objective was to use the above-mentioned strategy to dissect the dynamics of the major subpopulations of hepatic macrophages in response to acute liver injury.

We selected the CCl<sub>4</sub>-induced acute injury model in mice because it recapitulates immunological, histological, and pathological features of human toxic liver injury (496). In addition, the immune response to CCl<sub>4</sub>-toxicity is self-limiting, involves considerable tissue reorganization of immune cells, and leads to total healing. Therefore, this is an excellent model to examine the spatio-temporal behavior of hepatic macrophages during different stages of the wound healing response.

In summary, the spatial behavior and interacting partners of immune cells are distinctive features that underlie their capacity to perform their specific effector functions during homeostasis and in response to injury. In this thesis, we developed a strategy allowing the spatial profiling of immune cells and applied it to better understand the unique roles of KCs and MoMFs in response to acute liver injury.

### **2.a.2. Hypothesis**

Our general hypothesis is that immune cells occupy strategic and distinct positions in the hepatic tissue and their locations and interacting partners evolve during the immune response in a cell type-specific manner. Furthermore, the spatial behavior of individual immune cell populations during an immune response is distinctive and underlies its ability to perform its specific effector

functions. In this study, we focused our attention on liver resident KCs and infiltrating MoMFs during the response to CCl<sub>4</sub>-induced acute liver injury. We hypothesize that each of these hepatic macrophage subpopulations exhibits unique spatial and temporal features that are adapted to their characteristic role during the wound-healing response to acute liver injury. We also propose that KCs and MoMFs differentially relate to neighboring cells during the wound-healing response to CCl<sub>4</sub> toxicity.

### **2.a.3. Objectives**

Based on the above rationale and to verify our hypothesis, the objectives of this thesis are as follows:

1. Optimize imaging methods for the visualization of immune cells in the hepatic tissue.
2. Create protocols for the automated quantification and mapping of cells of interest in images from whole tissue sections.
3. Develop a strategy allowing increased multiplexing capabilities and the spatial resolution of immune cells in the hepatic tissue.
4. Validate the strategy by applying it to a concrete example.
5. Characterize spatially and temporally the KCs and MoMFs in response to acute liver injury to gain insight into their unique contributions to inflammation and repair.
6. Determine the origin of hepatic macrophages repopulating the liver upon acute injury.
7. Dissect spatially and temporally the individual contribution of KCs vs. MoMFs to hepatic stellate cell activation, critically implicated in liver repair and healing.

## Chapter 3: Manuscript 1

### Visualization, Quantification, and Mapping of Immune Cell Populations in the Tumor Microenvironment

Published in the Journal of Visualized Experiments (JoVE) on March 25, 2020

doi: 10.3791/60740

Authors: Manuel Flores Molina<sup>1,2</sup>, Thomas Fabre<sup>1,2</sup>, Aurélie Cleret-Buhot<sup>1</sup>, Geneviève Soucy<sup>1,3</sup>, Liliane Meunier<sup>1,4</sup>, Mohamed N. Abdelnabi<sup>1,2</sup>, Nicolas Belforte<sup>1,5</sup>, Simon Turcotte<sup>1,4,6</sup>, Naglaa H. Shoukry<sup>1,4,7</sup>

<sup>1</sup>Centre de Recherche du Centre hospitalier de l'Université de Montréal (CRCHUM)

<sup>2</sup>Département de Microbiologie, Infectiologie et Immunologie, Faculté de Médecine, Université de Montréal

<sup>3</sup>Département de Pathologie et Biologie Cellulaire, Faculté de Médecine, Université de Montréal

<sup>4</sup>Institut du Cancer de Montréal

<sup>5</sup>Département de Neurosciences, Faculté de Médecine, Université de Montréal

<sup>6</sup>Département de Chirurgie, Faculté de Médecine, Université de Montréal

<sup>7</sup>Département de Médecine, Faculté de médecine, Université de Montréal

DOI : doi :10.3791/60740

Keywords: Immunology and Infection, Issue 157, tumor microenvironment, multiplex immunofluorescence, FFPE, image analysis, tissue alignment, tissue heat map, VIS software

Citation: Flores Molina, M., Fabre, T., Cleret-Buhot, A., Soucy, G., Meunier, L., Abdelnabi, M.N., Belforte, N., Turcotte, S., Shoukry, N.H. Visualization, Quantification, and Mapping of Immune Cell Populations in the Tumor Microenvironment. *J. Vis. Exp.* (157), e60740, doi:10.3791/60740 (2020).

Manuel Flores substantially contributed to the conception and design of the study, the optimization of the techniques, the undertaking of experiments, and the acquisition, analysis, and interpretation

of data. He drafted the article and participated in its critical revision for important intellectual content.

**Abstract:**

The immune landscape of the tumor microenvironment (TME) is a determining factor in cancer progression and response to therapy. Specifically, the density and the location of immune cells in the TME have important diagnostic and prognostic values. Multiomic profiling of the TME has exponentially increased our understanding of the numerous cellular and molecular networks regulating tumor initiation and progression. However, these techniques do not provide information about the spatial organization of cells or cell-cell interactions. Affordable, accessible, and easy-to-execute multiplexing techniques that allow spatial resolution of immune cells in tissue sections are needed to complement single-cell-based high-throughput technologies. Here, we describe a strategy that integrates serial imaging, sequential labeling, and image alignment to generate virtual multiparameter slides of whole tissue sections. Virtual slides are subsequently analyzed in an automated fashion using user-defined protocols that enable the identification, quantification, and mapping of cell populations of interest. The image analysis is done, in this case using the analysis modules Tissuealign, Author, and HISTOmap. We present an example where we applied this strategy successfully to one clinical specimen, maximizing the information that can be obtained from limited tissue samples and providing an unbiased view of the TME in the entire tissue section.

The video component of this article can be found at:

<https://www.jove.com/v/60740/visualization-quantification-mapping-immune-cell-populations-tumor>

Or control-click to follow link <https://www.jove.com/video/60740/>

## **Introduction:**

Cancer development is the result of a multistep process involving reciprocal interactions between malignant cells and the TME. Other than tumor cells, the TME is composed of non-malignant cells, stromal cells, immune cell populations, and extracellular matrix (ECM)<sup>1</sup>. The spatial organization of the different cellular and structural components of the tumor tissue and the dynamic exchange between cancer and neighboring non-cancer cells ultimately modulate tumor progression and response to therapy<sup>2,3,4</sup>. It has been shown that the immune response in cancer is spatiotemporally regulated<sup>5,6</sup>. Different immune cell populations infiltrating the neoplastic lesion and the adjacent tissue exhibit distinctive spatial distribution patterns and varied activation and differentiation states associated with different functions (e.g., pro- versus antitumor). These different immune populations and their parameters coevolve over time with the tumor and the stromal compartments.

The emergence of technologies allowing single-cell multiomic profiling has exponentially increased our understanding of the numerous cellular and molecular networks regulating carcinogenesis and tumor progression. However, most single-cell-based high-throughput analytical tools require tissue disruption and single-cell isolation, resulting in a loss of information about the spatial organization of cells and cell-cell interactions<sup>7</sup>. Because the location and arrangement of specific immune cells in the TME have diagnostic and prognostic value, technologies allowing spatial resolution are an essential complement of single-cell-based immune profiling techniques.

Traditionally, imaging techniques like immunohistochemistry (IHC) and multiplex immunofluorescence (mIF) have been restricted to a small number of biomarkers that can be visualized simultaneously. This limitation has hampered the study of the spatiotemporal dynamics of tumor-infiltrating immune cells, which are typically defined by several phenotypic markers. Recent advances in imaging and analytical tools have expanded the possibilities of multiplexing. New antibody-based labeling technologies like histo-cytometry and imaging mass cytometry have been used to spatially separate up to 12 and 32 biomarkers, respectively<sup>8,9</sup>. Mass spectrometry imaging, a technique not requiring labeling, has the potential to image thousands of biomarkers

simultaneously in a single tissue section<sup>10,11</sup>. Although these techniques have already shown great potential for dissecting the tissue immune landscape in cancer, they use highly sophisticated and expensive equipment and software and are not readily accessible to the majority of researchers.

Alternatively, the multiplexing capability of traditional IHC and mIF has been expanded using serial imaging, sequential rounds of labeling, and spectral imaging<sup>7,12,13,14,15,16</sup>. These techniques generate multiple images from the same or from serial tissue sections that can be consolidated into virtual multiparameter slides using image analysis software. As a result, the number of markers that can be visualized and analyzed simultaneously increases.

Here, we propose a strategy for the rational design of tissue multiplex assays using commercially available reagents, affordable microscopy equipment, and user-friendly software (Figure 1). This methodology integrates serial imaging, sequential multiplex labeling, whole tissue imaging, and tissue alignment to generate virtual multiparameter slides that can be used for automated quantification and mapping of immune cells in tissue sections. Using this strategy, we created one virtual slide comprising 11 biomarkers plus two frequently used histological stains: hematoxylin and eosin (H&E) and picosirius red (PSR). Multiple immune cell populations were identified, located, and quantified in different tissue compartments and their spatial distribution was resolved using tissue heatmaps. This strategy maximizes the information that can be gained from limited clinical specimens and applies to formalin-fixed paraffin-embedded (FFPE) archived tissue samples, including whole tissue, core needle biopsies, and tissue microarrays. We propose this methodology as a useful guide for designing custom assays for the identification, quantification, and mapping of immune cell populations in the TME.

## **Protocol**

Three serial FFPE sections from resected hepatitis B virus (HBV)-associated human hepatocellular carcinoma were obtained from the Centre hospitalier de l'Université de Montréal (CHUM) Hepatopancreatobiliary Cancer Clinical Database and Biological Specimen Repository (HBP Biobank). Patients participating in this tissue bank provided informed consent. This study was

approved by the institutional ethics committee (Protocol number 09.237) and performed following the Declaration of Helsinki.

## **1. Hematoxylin and eosin (H&E) staining protocol**

NOTE: The H&E staining was performed by the molecular pathology core facility of the Centre de Recherches du Centre hospitalier de l'Université de Montréal (CRCHUM) using the Shandon multiprogram robotic slide stainer using the following program.

1. For deparaffinization, immerse slides 3x for 2.5 min each in xylene substitute.

CAUTION: Xylene substitutes are flammable, skin irritants, and harmful if inhaled.

2. For rehydration, immerse slides in 100% ethanol 3x for 2.5 min each. Wash for 1 min in double distilled water (ddH<sub>2</sub>O) to rehydrate.
3. Incubate for 1 min in hematoxylin. Wash 3x for 1 min each in ddH<sub>2</sub>O.
4. Incubate for 5 s with eosin. Wash 30 s with 95% ethanol. Wash 2x for 1 min with 100% ethanol.

CAUTION: Ethanol is flammable and an eye irritant. Eosin is an eye irritant.

5. For dehydration, immerse 3x for 1.5 min each in the xylene substitute. Mount slides manually.

NOTE: The estimated time for executing this part of the protocol is 30 min.

## **2. Multiplex immunofluorescence staining protocol for FFPE sections**

NOTE: This protocol was adapted from Robertson et al.<sup>17</sup>.

### **1. Deparaffinization and rehydration**

NOTE: Before antibody-mediated labeling of FFPE sections by IHC or mIF, the paraffin should be removed. Failure to efficiently remove the paraffin results in suboptimal staining.

1. Place 4 µm FFPE tissue section slides into glass slide holders. Under the fume hood, immerse the slides in a Coplin jar containing 37°C prewarmed xylene for 10 min.



CAUTION: Xylene is flammable, a skin irritant, and harmful if inhaled.

2. Manually agitate the slides for 10 s every 2 min. Repeat 1x in fresh xylene for another 5 min.
3. In the chemical hood, immerse the slides sequentially for 5 min in each of the following solutions: 1) xylene: ethanol (1:1 v/v); 2) 100% ethanol; 3) 70% ethanol; 4) 50% ethanol; 5) 30% ethanol; 6) phosphate-buffered saline (PBS).

NOTE: Keep the slides in PBS until ready to perform the antigen retrieval. Keep the dewaxed sections always hydrated. Drying out will cause nonspecific antibody binding and therefore high background staining.

## 2. Heat-induced antigen retrieval

NOTE: Antigens can be masked upon formalin-fixation, preventing antibody binding and consequently visualization. The use of antigen unmasking buffers and procedures partially re-establish the native conformation of epitopes and thereby restore antibody recognition. The type of antigen retrieval buffer and duration should be optimized for the specific assay conditions (e.g., target, antibody, tissue, etc.).

1. Immerse dewaxed slides in a Coplin jar containing the antigen retrieval solution (recipe in Table of Materials).
2. Place the closed Coplin jar into an electric pressure cooker with tap water. The water level should not exceed half the height of the jar so that the water does not mix with the antigen retrieval solution.
3. Close the lid and the pressure valve of the cooker. Select high pressure for 10 min and start. When done, unplug the cooker, release the pressure, open the lid, and keep the jar inside the cooker for 30 min, allowing the slides to cool.

## 3. Blocking of nonspecific binding

1. Transfer the rack with the slides to a Coplin jar filled with PBS. Rinse off the antigen retrieval buffer with PBS 2x for 5 min each.

2. Encircle the tissue sections with a PAP pen to create a hydrophobic barrier. Immerse the slides in a Coplin jar containing 0.1 M glycine in PBS. Incubate for 15 min at room temperature (RT).

NOTE: Glycine saturates the aldehyde groups generated during antigen retrieval. These groups could bind primary and secondary antibodies unspecifically.

3. Rinse off the glycine solution by washing 2x with PBS for 5 min. Place the slides into a humidity chamber and add enough blocking solution to cover all the tissue sections. Avoid overflowing the hydrophobic barrier. Incubate for 30 min at RT.

NOTE: The recipe for the blocking solution can be found in the Table of Materials. The blocking solution should contain a protein (e.g., BSA) to block nonspecific binding sites. It can also incorporate detergents like Triton X-100 or Tween 20 that reduce hydrophobic interactions between antibodies and tissue targets, thereby making antigen recognition more selective. The addition of 10% total serum from the species where the tissue comes from would block Fc receptors and thus reduce nonspecific antibody binding. Finally, the addition of 10% of serum from the species the secondary antibodies were raised in would minimize direct nonspecific attachment of secondary antibodies to the tissue section.

#### 4. Immunofluorescence labeling

1. Rinse with PBS-Tween (0.1% v/v) 2x for 5 min each and place the slides back in the humidity chamber.
2. Add the cocktail of primary antibodies resuspended in the blocking solution. Incubate overnight at 4 °C. Primary and secondary antibodies used for this study are listed in Table of Materials.

NOTE: The cocktail of primary antibodies should contain either antibodies raised in different species, or from the same species but of different isotypes. For a list of the primary-secondary antibody pairs used in this study consult Table 2. Details of all antibodies used are in the Table of Materials and Table 2.

3. Rinse with PBS-Tween (0.1% v/v) 3x for 5 min and place the slides back into the humidity chamber. In the dark, add the cocktail of secondary antibodies and incubate for 1 h at RT.

NOTE: When the primary antibodies are from different species, the secondary antibodies should be selected so that each of them only binds to one of the primary antibodies and not to one another. This is commonly achieved by using secondary antibodies all raised in the same species as long as this species differs from the species where the primary antibodies were generated. In cases where the primary antibodies were raised in the same species but have different isotypes, isotype-specific secondary antibodies should be used.

4. Rinse with PBS-Tween (0.1% v/v) 3x for 5 min each. Rinse with ddH<sub>2</sub>O. Remove excess liquid and mount in mounting media with DAPI. The volume used depends on the size of the section. Usually, 40  $\mu$ L is enough to cover the surface of a regular microscopy slide.
5. Place the cover slide onto the section and gently squeeze out the excess mounting media avoiding bubble formation. Let the slides dry for 20 min at RT in the dark and store at 4 °C until ready for acquisition.
6. Acquire images for all the channels using the whole slide scanner (see Table of Materials).  
NOTE: The antibodies were validated using human hepatocellular carcinoma tissue as a positive control. For each primary antibody, three serial sections were stained with either primary antibody, isotype control, or only blocking solution respectively with no variation in the rest of the staining protocol. The acquired images were compared to establish the specificity of the staining. The staining was considered specific when the signal in the section incubated with the primary antibody had the expected pattern and was easily distinguishable from the background. Primary antibodies giving a high background signal or labeling tissue components in the isotype and no primary antibody sections were considered nonspecific. The estimated time for completing this part of the protocol is 2 days. Required controls include (1) Isotype control to establish the contribution of nonspecific binding of the primary antibody to the background signal. One section is stained in the same way as the other sample tissues except that it is incubated with an antibody with the same isotype and origin of the primary antibody but specific for a target that is absent in the tissue section. If the appropriate isotype control antibody is not available, it can be replaced by total IgG from the same species where the primary antibody was raised in; (2) No primary antibody control (i.e., negative control) to establish the specificity of the staining and to estimate the contribution of nonspecific binding of secondary antibodies to the background signal. In this case, the control section is stained

in the same way as the other sections except that no primary antibody is added; (3) Positive control to establish that the staining works. In this case, the staining is performed on a tissue section that is known to express the marker recognized by the primary antibody.

### **3. Picro-sirius red (PSR)/fast green staining protocol**

NOTE: The goal of this staining is to visualize fibrillar collagens I and III in the FFPE tissue sections. This protocol was adapted from Segnani et al.<sup>18</sup>. All steps are performed in a chemical hood.

1. Perform the deparaffinization and rehydration of tissue sections similar to the multiplex immunofluorescence staining protocol for the FFPE sections (section 2.1).

NOTE: If the section to be stained has previously been used for immunofluorescence labeling and the paraffin has already been removed, the deparaffinization-rehydration steps are useful to remove the mounting media. DAPI is not removed using this procedure, but it does not perceptibly interfere with the PSR staining.

2. Immerse the slides in a jar containing the picro-sirius red/fast green solution (recipe in the table of Materials) and incubate for 30 min at RT (more than 30 min results in nonspecific staining of the nuclei of hepatocytes).
3. Wash slides quickly in ddH<sub>2</sub>O (5 dips). Then, wash quickly in ethanol 100% (5 dips). Wash for 30 s in xylene-100% ethanol (1:1 v/v). Wash for 30 s in xylene. Mount with mounting media (see Table of Materials) before xylene has evaporated (this helps with the mounting).

NOTE: The estimated time for executing this part of the protocol is 1 h.

### **4. Elution of antibodies from tissue sections**

NOTE: To reuse tissue sections in sequential labeling assays, the complete removal of primary and secondary antibodies is required. Bound antibodies were stripped as previously described<sup>13</sup>

Preheat a water bath to 56 °C. Put the sections inside a jar containing stripping buffer (recipe in Table of Materials), close the lid, and seal it with paraffin film tape to prevent leaking during shaking.

1. Put the jar inside the water bath and incubate for 30 min with agitation.
2. Wash 4x for 15 min each in ddH<sub>2</sub>O at RT. Rinse with PBS-Tween (0.1% v/v).

3. Keep the sections hydrated in PBS-Tween or water until ready to reprobe the section with the second round of primary antibodies.

NOTE: The estimated time for executing this part of the protocol is 2 h.

4. Verify the efficiency of the antibody elution procedure.

NOTE: Before using the protocol for antibody elution in a sequential labeling assay, the efficiency of the removal of primary and secondary antibodies should be verified.

1. Perform the staining and image acquisition of a section with a given primary-secondary antibody pair of interest as indicated in the multiplex immunofluorescence staining protocol for FFPE sections (sections 2.1–2.4.6).

2. Upon image acquisition, perform elution of tissue-bound primary-secondary antibody complexes as indicated in sections 4.1–4.3.

3. Incubate the section with the same secondary antibody and the same conditions used in step 2.4.3.

4. Perform washing, mounting, and image acquisition steps as indicated in 2.4.4–2.4.6.

5. Compare side-by-side images acquired before and after the stripping to establish whether or not the specific signal has disappeared.

NOTE: Comparison of images before and after antibody removal will validate the efficiency of the elution procedure. However, it is normal to see an increase in the background signal in all the channels, as well as diffusion of DAPI. This limits the number of rounds of stripping that can be executed on the same tissue section. Three rounds of stripping seem to be the maximum.

## **5. Image acquisition**

1. Generate images using a whole slide scanner.
2. Use a 20x 0.75NA objective lens and a resolution of 0.3225  $\mu\text{m}/\text{pixel}$ .

## 6. Image analysis

NOTE: The method outlined here refers to the current example. Please refer to Table 1 and the text to adapt to other specific samples.

1. Perform tissue alignment using the Tissualign module of the image analysis software (VIS in this protocol, see Table of Materials).

1. Open the image analysis software and click on the Tissuealign tab.
2. Import the images to be aligned into the Slide Tray by going to File | Database and selecting the first image to be aligned. Go back to the Tissuealign tab and load the image by clicking the Load button in the Slide Tray. The image will appear in the Slide Tray and the workspace.
1. NOTE: Only the stack of interest should be loaded into the slide tray.
2. Repeat step 6.1.2 for all the images in the order to be aligned, loading them one by one. Once all the images of interest are loaded onto the slide tray proceed to link the images by pressing Next in the Workflow Steps in the ribbon.
3. Next, drag and drop the second image on top of the first image. The first and second images are now linked. Repeat this step for the other images to be aligned, one by one, in an orderly fashion. The name of the first image will change, indicating that it has been linked to the other images. Simultaneously, the linked images will be displayed in the workspace on the right of the slide tray.
4. At this point, align the images either using automatic alignment, semiautomatic alignment, or manual alignment. It is always preferable to try automatic alignment first. For automatic alignment press the Next button in the workflow steps (step 3) in the ribbon.
5. Review the automatic alignment by navigating different locations of the tissue and visually verifying that the corresponding structures in different images are arranged in the same way in the two dimensions of the image.
6. If the result of the automatic alignment is not satisfactory, improve it using pins (use a minimum of three pins per image) indicating homologous tissue features in the linked images. Once the pins are placed at homologous locations in the linked images, the user

has two choices: semiautomatic alignment or manual alignment. For semiautomatic alignment click on the button Auto-align based on the current pinpoints in the ribbon. For manual alignment, click the button Apply Pins on the ribbon.

7. When satisfied with the alignment click on the Next button in the workflow steps and save the composite image in the database.
8. NOTE: Aligning six slides spanning 11 markers plus the H&E and PSR images took 15 min in the analysis presented.

2. Perform tissue detection using the user-defined protocol Analysis Protocol Package 1 (APP 1, Table 1).

1. Open the Image Analysis module of the software by clicking the Image Analysis tab in the ribbon.
2. Import the composite (aligned) image by going to File | Database and selecting the image of interest and clicking back on the Image Analysis tab.
3. Open the APP selection dialog by clicking on the Open APP icon and select which Analysis Protocol Package (APP) to use. In this case, select APP 1 for tissue detection.
4. Once APP 1 is opened, confirm that APP1 is working properly by going to a selected tissue location and clicking on the Preview button. If the results are satisfactory, go to the next step.
5. Click to run APP 1 and process the image using the selected APP.
6. Export the data (e.g., images, measurements, etc.) when the analysis is done by clicking File/Export.

NOTE: APP 1 creates a region of interest (ROI) delineating the tissue (ROI Tissue) and calculates the area of the tissue.

7. Save the modified image with the newly created ROI by going to File | Save.

NOTE: Detecting the tissue and creating a ROI with APP 1 in the provided example took 5 min in the image analysis station described. The area of the tissue processed was 3.2 cm<sup>2</sup>.

3. Perform tissue segmentation into Stroma and Parenchyma using APP 2 (Table 1).



NOTE: APP 2 works on the predefined ROI Tissue. APP 2 segments the tissue into the ROIs Stroma and Parenchyma.

1. Open the Image Analysis module by clicking the Image Analysis tab in the ribbon.
2. Import the image containing the ROI tissue by going to File | Database and selecting the image saved in step 6.2.7. Go back to the Image Analysis tab and load the image by clicking the Load button in the Slide Tray. The image will appear in the Slide Tray and in the workspace.
3. Open APP 2 using the APP selection dialog as in 6.2.3.
4. Preview APP 2 by processing in a selected field of view. If the results are satisfactory, run APP 2 on the full image by clicking the Run button. As the output of APP 2, the ROI tissue is segmented in the ROIs Stroma and Parenchyma, and their respective areas are determined. Export results as in 6.2.6. Save the modified image as in 6.2.7.

NOTE: Segmenting the tissue in Stroma and Parenchyma using APP 2 took 4 h in the analysis station presented. The area of the tissue processed was 3.2 cm<sup>2</sup>.

4. Identify and quantify FoxP3<sup>hi</sup>CD4<sup>+</sup> cells using the user-defined protocol APP 3 (Table 1).

NOTE: APP 3 works on the predefined ROIs Stroma and Parenchyma.

1. Open the Image Analysis module and import the image containing the ROIs Stroma and Parenchyma as in 6.3.1 and 6.3.2. Open APP 3 using the APP selection dialog as in 6.2.3.
2. Preview APP 3 processing in a selected field of view enriched in FoxP3<sup>hi</sup>CD4<sup>+</sup> cells. If the results are satisfactory, run APP 3 on the full image. As the output of APP 3, all the individual FoxP3<sup>hi</sup>CD4<sup>+</sup> objects will be labeled, and their tissue coordinates stored. Densities of FoxP3<sup>hi</sup>CD4<sup>+</sup> objects in the ROIs Stroma and Parenchyma will be determined. Export the results as in 6.2.6.
3. Perform tissue heatmapping of FoxP3<sup>hi</sup>CD4<sup>+</sup> labeled objects.
  1. Open the user-defined protocol FoxP3<sup>hi</sup>CD4<sup>+</sup> MAP using the APP selection dialog as in 6.2.3.

NOTE: FoxP3<sup>hi</sup>CD4<sup>+</sup> MAP uses the coordinates of FoxP3<sup>hi</sup>CD4<sup>+</sup> labeled objects for generating density heatmaps. Identifying and counting FoxP3<sup>hi</sup>CD4<sup>+</sup> labeled objects using APP 3 took 25 min in the image analysis station described. The area of the tissue processed was 3.2 cm<sup>2</sup>.

2. Run FoxP3<sup>hi</sup>CD4<sup>+</sup> MAP by pressing the Run button. Export the tissue heatmap by clicking File | Export | Working Area.

NOTE: Mapping FoxP3<sup>hi</sup>CD4<sup>+</sup> labeled objects using FoxP3<sup>hi</sup>CD4<sup>+</sup> MAP took 5 min in the image analysis station described.

5. Identify and quantify CD8<sup>+</sup>, CD68<sup>+</sup>, MPO<sup>+</sup>,  $\alpha$ SMA<sup>+</sup>, and CD34<sup>+</sup> objects using the user-defined protocols APP 4, APP5, APP6, APP7, and APP 8, respectively (Table 1) as done in sections 6.4 to 6.4.3.2 loading the APP of interest in each case.

NOTE: APPs 4 to 8 work on the predefined ROIs Stroma and Parenchyma.

## **Representative Results:**

### **Overview of the strategy for visualizing, quantifying, and mapping cell populations of interest in the TME**

To quantify cell populations of interest (COIs) in different tissue compartments (TCs) and to characterize their spatial organization, we designed a workflow that integrates affordable and easy-to-use techniques and maximizes the positional information that can be obtained from precious FFPE clinical specimens (Figure 1). First, serial whole tissue FFPE sections were stained for visualization of COIs (e.g., immune cells) and TCs (e.g., stroma versus parenchyma) (Figure 1, step 1). The number of consecutive sections to be stained should be kept to a minimum that allows visualization of the cells of interest or tissue features needed for addressing the research question. The smaller the number of serial sections, the higher the tissue architecture resemblance and concordance across contiguous sections. In addition, the multiplexing capability can be expanded through the reuse of fluorescently stained sections through stripping and reprobng techniques<sup>19</sup>.

Once the staining steps were done, a whole slide scanner was used to digitize the images. Images acquired from serial sections were aligned and consolidated into a virtual multiplex slide in an automated fashion (Figure 1, section 2). Next, an ROI for the tissue was delineated with a user-defined protocol that identified tissue-associated pixels (TAPs) (Figure 1, step 3). Subsequently, the ROI tissue was segmented into TCs defined as additional ROIs. (Figure 1, step 4). Next, user-defined protocols detected and quantified COIs in different TCs (Figure 1, step 5). Finally, tissue heatmaps of COIs were generated based on their densities and their tissue coordinates (Figure 1, step 6)

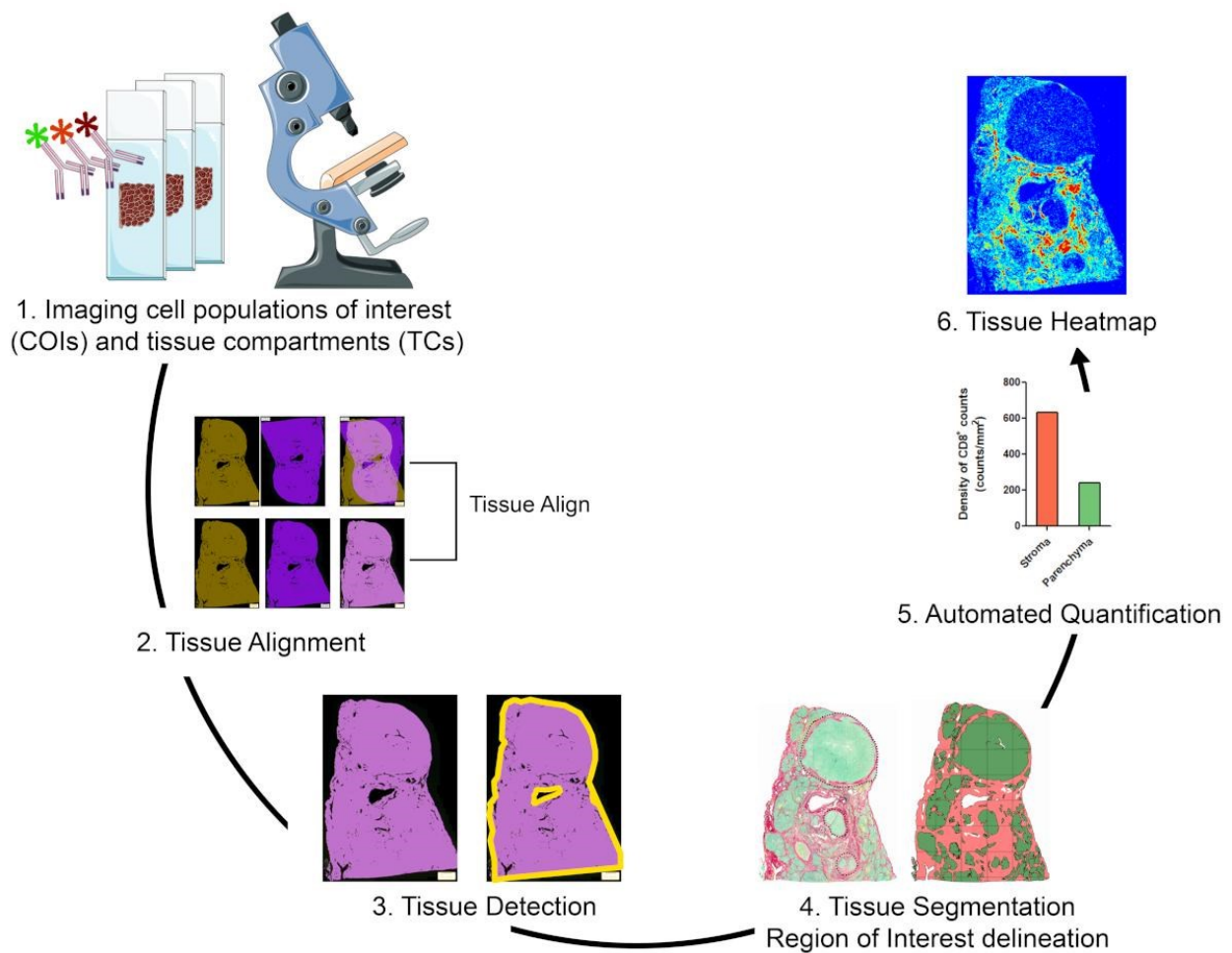


**Figure 1: Schematic representation of the strategy for visualizing, quantifying, and mapping immune cells in the TME.** (1) Serial whole tissue sections were stained for labeling COIs and TCs. Stained whole tissue sections were digitized using a whole slide scanner. (2) Images acquired

*from serial sections were linked, aligned, and coregistered in an automated fashion using a Tissuealign analysis module. A composite image was generated from the high-precision alignment of individual images. (3) A user-defined protocol was used for the automated detection of tissue-associated pixels (TAPs) in the composite image. (4) The tissue was segmented into TCs (e.g., stroma and parenchyma) defined as ROIs. (5) User-defined protocols were used for the automated detection and quantification of COIs in different TCs. (6) Tissue heatmaps of COIs were generated.*

### **Imaging COIs and TCs**

Three serial FFPE whole tissue sections of resected tumor from a subject with HBV-associated hepatocellular carcinoma were stained in one or more rounds of staining as in Figure 2A. Section I was stained with H&E to show the tissue architecture, and cell morphology, and to determine clinically relevant parameters such as type of malignancy, tumor grade, and overall assessment of immune infiltration (Figure 2C). In contiguous section II, two rounds of mIF were used for labeling liver parenchymal and non-parenchymal cells (Figure 2A). In the first round, normal and tumor vessels were visualized using CD34 staining of endothelial cells. Additionally, epithelial cells (hepatocytes and cholangiocytes) were identified using cytokeratin 8/18, and fibrogenic activated hepatic stellate cells were identified as alpha-smooth muscle actin positive ( $\alpha$ SMA<sup>+</sup>) cells (Figure 2C). Following image acquisition, tissue sections were stripped and reprobed with antibodies against macrophages (CD68), and myofibroblasts (desmin). To better characterize the tumor immune infiltrate, adjacent serial section III was stained using two rounds of mIF for the cellular markers CD3, CD4, CD8, forkhead box P3 (FoxP3), and myeloperoxidase (MPO). In all cases, DAPI was used as a nuclear counterstain. Finally, section III was stained with PSR stain and counterstained with fast green to visualize fibrillar collagen and segment the tissue into stroma and parenchyma (Figure 2C).

A whole slide scanner equipped with a 20X objective lens was used to digitize stained sections and create virtual slides. Six images were acquired from the three serial sections (Figure 2B) and the virtual slides were subsequently analyzed using the VIS software according to the schematic representation in Figure 1.

## **Image Analysis**

The image analysis comprised five steps: 1) tissue alignment; 2) tissue detection; 3) tissue segmentation; 4) automated quantification of COIs; and 5) tissue heat mapping. All protocols for image analysis were developed using the Author module of the image analysis software and are referred to in the text as APP.

### **Tissue alignment**

Six virtual slides from three serial sections, spanning 11 markers plus H&E and PSR stains, were loaded into the Tissualign module of the image analysis software. Next, the images were linked, aligned, and coregistered in an automated fashion, generating an 11-plex plus H&E and PSR virtual composite image, containing all the layers of the individual images (Figures 2A–C). Alignment was accurate in the case of images originating from adjacent serial sections, showing corresponding tissue structures positioned and arranged in a homologous fashion upon alignment (Figure 2C and Figure S1A). Furthermore, the alignment was precise at the individual cell level for images originating from the same section (Figure S1B). The time for automatic alignment depends on the number, size, complexity, and similarity of the images to be aligned. The alignment of the above-mentioned six virtual slides took 15 min in our VIS station.

### **Tissue Detection**

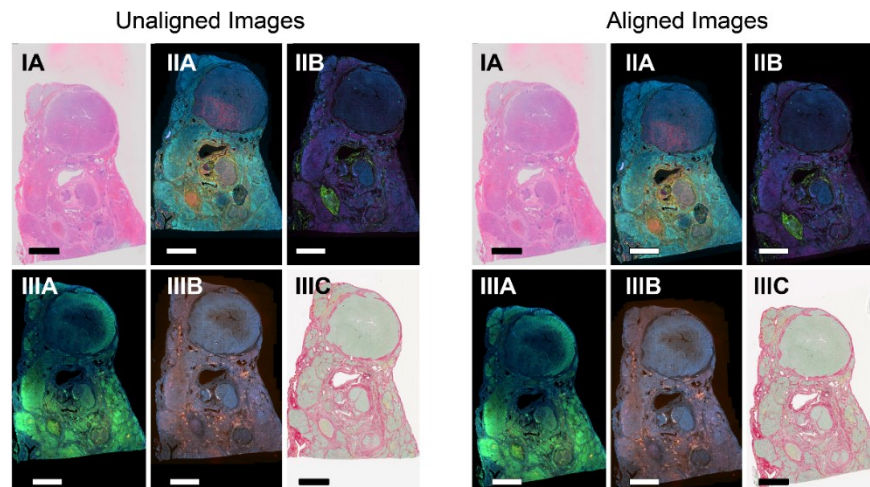
Once the images were linked and aligned, we sought to identify the TAPs (Figure 3A). To design an APP for the automated detection of TAPs (APP 1, Table 1), we took advantage of two properties that differentiate TAPs from pixels not associated with tissue. First, the DAPI signal (blue band) is restricted to the nuclei, which are located exclusively in the tissue, meaning that all DAPI<sup>+</sup> pixels are a subset of TAPs. Second, TAPs have higher autofluorescence signals in the green and yellow bands compared to pixels not associated with the tissue. Consequently, we developed APP 1 for tissue detection (Table 1), which detects the TAPs based on baseline signal in these channels using simple thresholding techniques. Thresholds for the blue, green, and yellow bands were set so that TAPs had background intensity values above the thresholds, while pixels not associated with the tissue had values below. APP 1 for tissue detection was applied to image IIA, which contains

layers in the blue, green, and yellow channels (Figure 3A). As outputs of APP 1, a bright green mask was laid down on top of the TAPs, and a ROI called "Tissue" was delineated (output, Figure 3A). Furthermore, the area of the tissue was determined as a quantitative output variable. Because APP 1 does not incorporate the pixels not associated with the tissue into the ROI Tissue, they were excluded from the subsequent analysis based on this ROI (Figure 3A). The precision of APP 1 at identifying TAPs is shown in Figure 3A.

A

Serial section	1 <sup>st</sup> Staining (A)	2 <sup>nd</sup> Staining (B)	3 <sup>rd</sup> Staining (C)
I	Hematoxylin and Eosin (IA)	---	---
II	DAPI, $\alpha$ SMA, CD34 cytokeratin8/18 (IIA)	DAPI, Desmin, CD68 (IIB)	---
III	DAPI, CD4, FOXP3 MPO (IIIA)	DAPI, CD3, CD8 (IIIB)	Picro Sirius Red (IIIC)

B



C

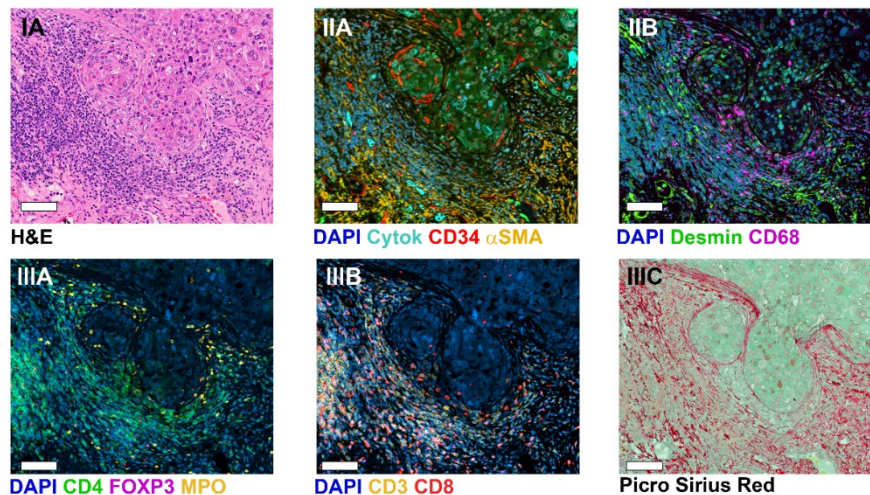


**Figure 2: Staining of serial tissue sections and image alignment.** (A) Summary of stainings done on three serial sections for visualization of COIs and TCs. Numbers in brackets indicate image designation. For sections II and III, tissues were stripped and reprobbed with a second cocktail of antibodies. (B) Overview of six individual whole tissue images before and after tissue alignment (left and right, respectively). Scale bar= 3,500  $\mu\text{m}$ . (C) Zoomed view of aligned images. Scale bar = 80  $\mu\text{m}$ .

### **Tissue segmentation and delineation of ROIs for TCs**

Next, we proceeded to define different compartments inside the ROI tissue by segmenting the tissue into stroma versus parenchyma. We used the PSR stained image (IIIC, Figure 2C), where the stroma can be defined as the area associated with the deposition of fibrillar collagens (red band), the parenchyma as the area where fibrillar collagens are absent, and the fast green counterstaining dye prevails (green band) (Figure 3B). We created APP 2 (Table 1) to digitally delimit the TCs Stroma and Parenchyma. This APP works on the predefined ROI Tissue (output, Figure 3A) and uses representative stroma and parenchyma areas for training the Classifier tool integrated into the Image Analysis module. The trained Classifier assigns the pixels to either a stroma or a parenchyma label (salmon and green, respectively, Figure 3B). Upon classification of pixels, APP 2 executed morphological operations aiming at defining the ROIs Stroma and Parenchyma (Figure 3B and Table 1). The performance of APP 2 at classifying pixels and generating the respective ROIs is shown in Figure 3B. Additionally, APP 2 quantifies the area of the stroma and the parenchyma. Finally, even though the segmentation is done using the PSR stained section, the outlined stroma and parenchyma regions can be transferred to any image aligned with the PSR image.

### **Automated quantification of COIs**

Next, we proceeded to identify, locate, and quantify COIs in the ROIs Stroma and Parenchyma. APPs 3 to 8 (Table 1) were created to locate and count the following COIs:  $\text{CD4}^+ \text{FoxP3}^+$ ,  $\text{CD8}^+$ ,  $\text{CD68}^+$ ,  $\text{MPO}^+$ ,  $\alpha\text{SMA}^+$ , and  $\text{CD34}^+$  cells, respectively. APP 3 was designed to locate and count  $\text{CD4}^+ \text{FoxP3}^+$  cells (image IIIA, Figure 2C) as surrogate markers of regulatory T cells (Tregs). This

protocol detects colocalization of the signal from the nuclear transcription factor FoxP3 (red band) and the DNA labeling dye DAPI (blue band). Given that recently activated T cells upregulate FoxP3, to enrich for Tregs we set thresholds for preselecting only bright FoxP3<sup>hi</sup> cells (FoxP3<sup>hi</sup>). Next, out of all preselected DAPI<sup>+</sup>FoxP3<sup>hi</sup> cells, only those that were surrounded by bright ring-shaped CD4 signals (green band) were labeled and counted as FoxP3<sup>hi</sup>CD4<sup>+</sup> cells (pink label, Figure 4A). The density of FoxP3<sup>hi</sup>CD4<sup>+</sup> cells in the ROIs Stroma and Parenchyma were determined as quantitative output variables of APP 3 (Figure 4A).

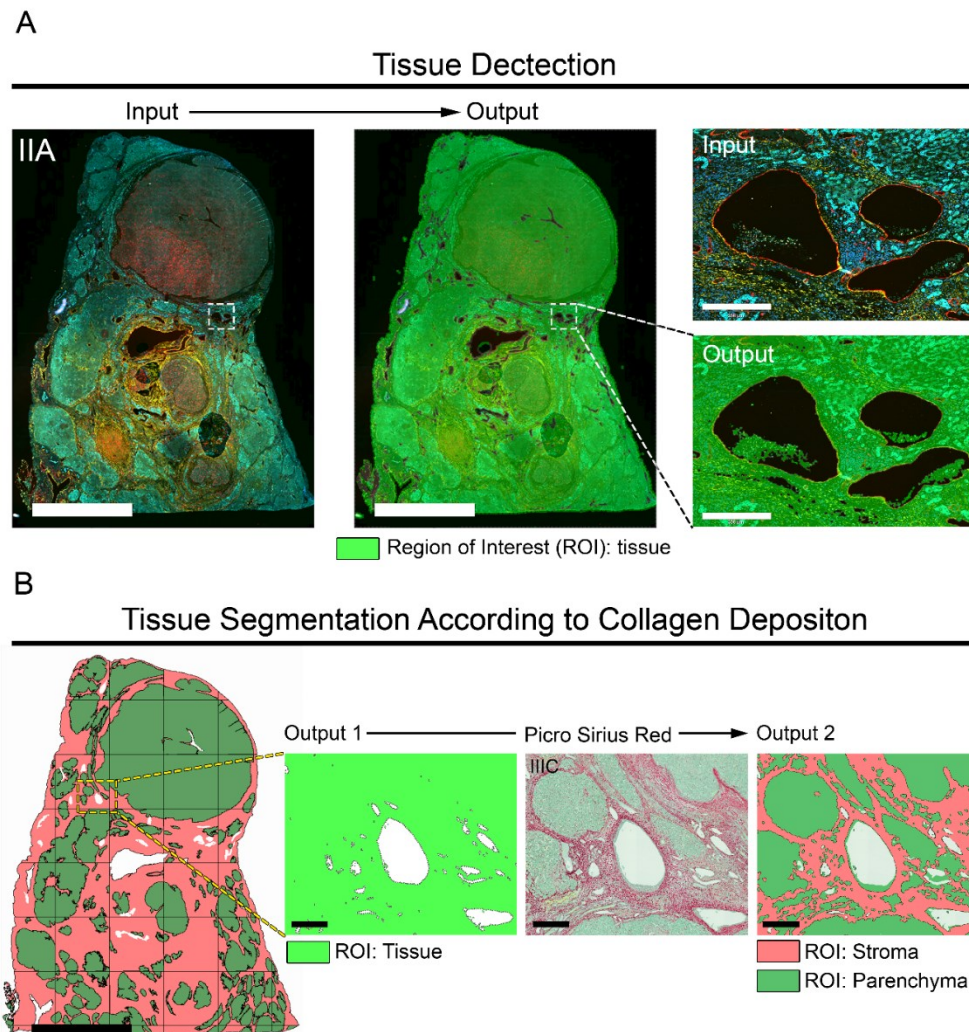


**Figure 3: Automated tissue detection/segmentation and generation of respective ROIs.** (A) Image IIA was used to identify the TAPs (left image, scale bar = 6,000  $\mu\text{m}$ ). A bright green mask was assigned to the TAPs using APP 1 (Table 1) generating a ROI called Tissue (output 1). Right,



*the inset shows zoomed view demonstrating the precision of APP 1 at detecting TAPs. Scale bar = 350  $\mu\text{m}$ . (B) The ROI Tissue (output 1) is segmented into stroma and parenchyma using APP 2. The image on the left shows a view of the ROI Tissue segmented into ROI stroma (salmon) and ROI parenchyma (green). Scale bar = 4,500  $\mu\text{m}$ . On the right, zoomed views of the inset for ROI Tissue, the original PSR staining (image IIC), and the ROIs stroma and parenchyma. Scale bar = 250  $\mu\text{m}$ .*

Similarly, APPs 4 to 6 were designed for the detection of CD8<sup>+</sup>, CD68<sup>+</sup>, and MPO<sup>+</sup> cells. These APPs share the same baseline design for detecting and quantifying COIs. Specifically, COIs are identified based on the signal intensity from the specific cell population biomarker, and then several postprocessing morphological steps are executed to delineate individual cells (Table 1). The individual cells or COIs are labeled, counted, and their tissue coordinates registered. APPs 4 to 6 also determine the density of the COIs in the ROIs Stroma and Parenchyma (Figure 4B–D).

The quality of our DAPI staining was not good enough for integrating nuclei segmentation into APPs 3 to 6, so we cannot ensure that all individually labeled objects are individual cells. For this reason, we expressed the density of cells in counts of labeled objects/ $\text{mm}^2$  (Figure 4). However, cell aggregates were successfully separated into individual cells in the postprocessing steps built into APPs 3 to 6, and extensive visual inspection showed that most labeled objects corresponded to single cells.

For detecting  $\alpha\text{SMA}^+$  and CD34<sup>+</sup> area, we developed APPs 7 and 8, respectively (Table 1). Both APPs detect the specific signal based on thresholds and determine the percentage of positive area in the ROIs Stroma and Parenchyma (Figure 4E–F).

One of the most interesting possibilities for generating virtual multiplex slides is the analysis of colocalization expression. We generated APP 10 to detect colocalization between  $\alpha\text{SMA}$  and desmin, two markers co-expressed by myofibroblasts in the liver. APP 10 uses thresholds for finding pixels positive for  $\alpha\text{SMA}$ , desmin, and  $\alpha\text{SMA}$  plus desmin (Table 1). As quantitative output variables, APP 10 determines the  $\alpha\text{SMA}^+$  area, the desmin<sup>+</sup> area, and the area of colocalized expression of these two markers (Figure S3).

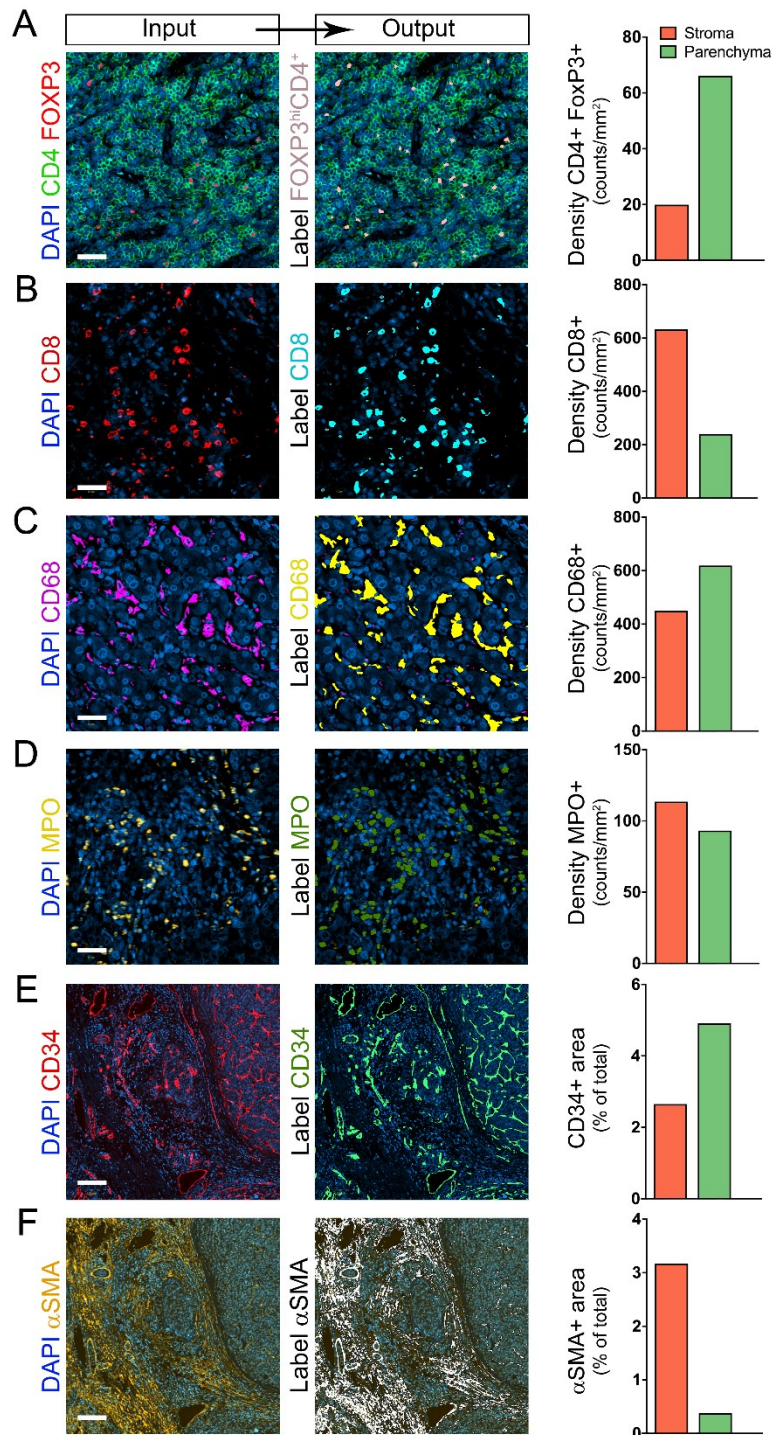


**Figure 4: Identification and quantification of COIs in the TCs stroma and parenchyma. (A–F) Automated detection and quantification of CD4<sup>+</sup>FoxP3<sup>+</sup>, CD8<sup>+</sup>, CD68<sup>+</sup>, MPO<sup>+</sup>,  $\alpha$ SMA<sup>+</sup>, and**

*CD34<sup>+</sup> COIs in the ROIs Stroma and Parenchyma using protocols 3, 4, 5, 6, 7, and 8, respectively (Table 1). Shown on the left are the original images, in the middle are the processed images, and on the right are the quantifications. For Figures 4A–D, scale bar = 40  $\mu$ m. For Figures 4E and F, the scale bar = 350  $\mu$ m. Please click here to view a larger version of this figure.*

As an alternative to quantifying the COIs in the TCs Stroma and Parenchyma, we determined the density of immune cells in the different malignant nodules named 1 to 4 (Figure 5A, H, and I). The ROI for each nodule was manually delineated as indicated in Figure 5A. Distinctive tissue immune signatures characterized each nodule, further revealing the intrinsic heterogeneity of the TME.

### **Tissue Heatmaps**

As mentioned above, APPs 3 to 8 store the tissue coordinates of every individually labeled object. This feature allows the automated generation of tissue maps where regions of a high density of a given cell population are displayed as hot spots (red), and regions with relatively low density as cold spots (dark blue). Intermediate density values are assigned colors according to the color scale shown in Figure 5. Tissue heatmaps were generated by APPs that divided the images into circles of 50  $\mu$ m diameter and assigned a color according to the relative density of a given COI inside the circle. As displayed in Figure 5B–G, the positioning patterns and intensity distribution of the different COIs in the TME were quite varied. Furthermore, at the level of individual nodules, the arrangement of different populations in the tissue area was unique (Figure S2A–C). To provide an example of the power of this technique and to visualize the spatial organization of hot spots from different populations in the same nodule, the hot spots from individual cell types were manually extracted and mapped together onto the outline of nodule 2 (Figure S2, Figure D, and Figure E).

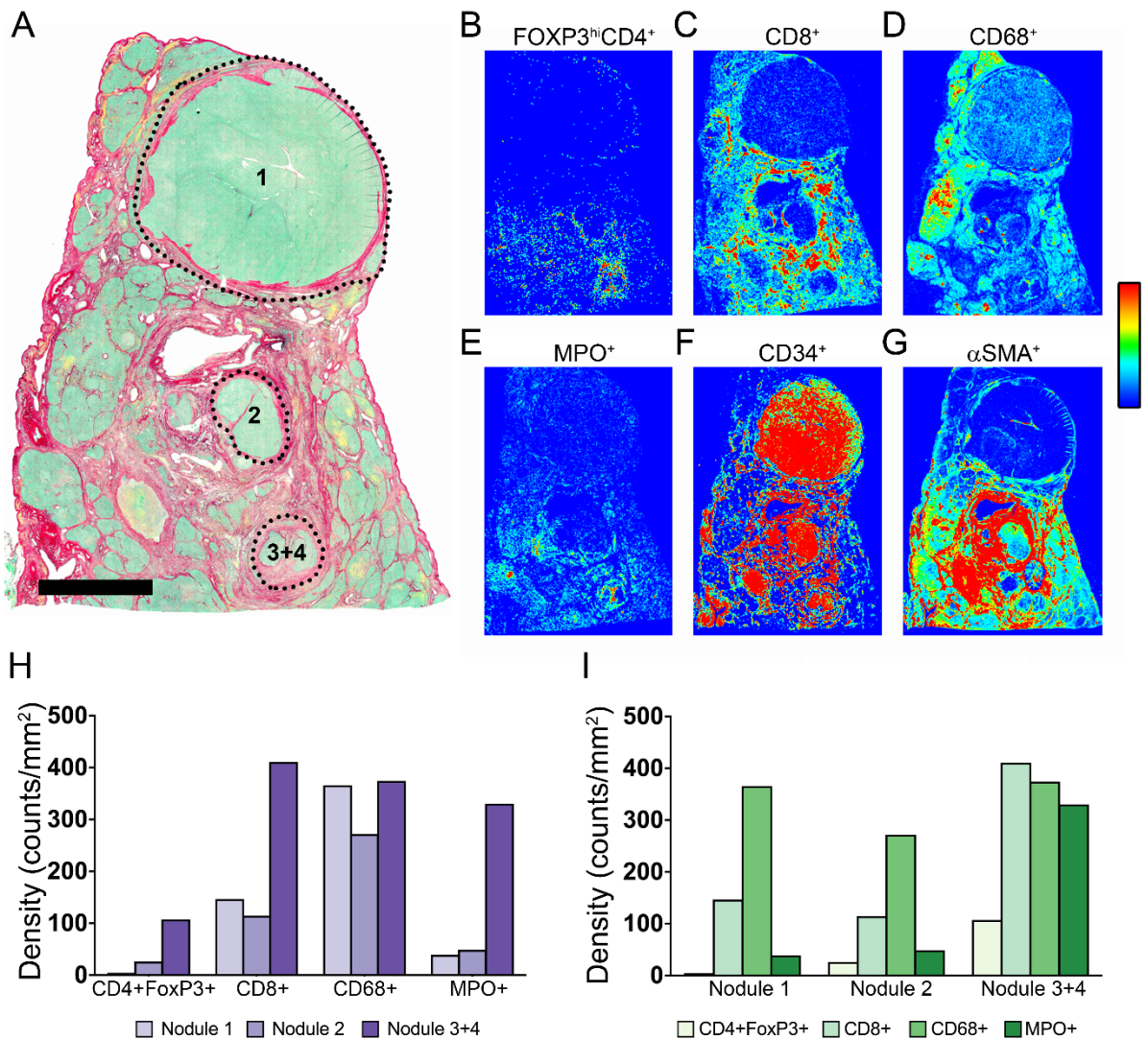
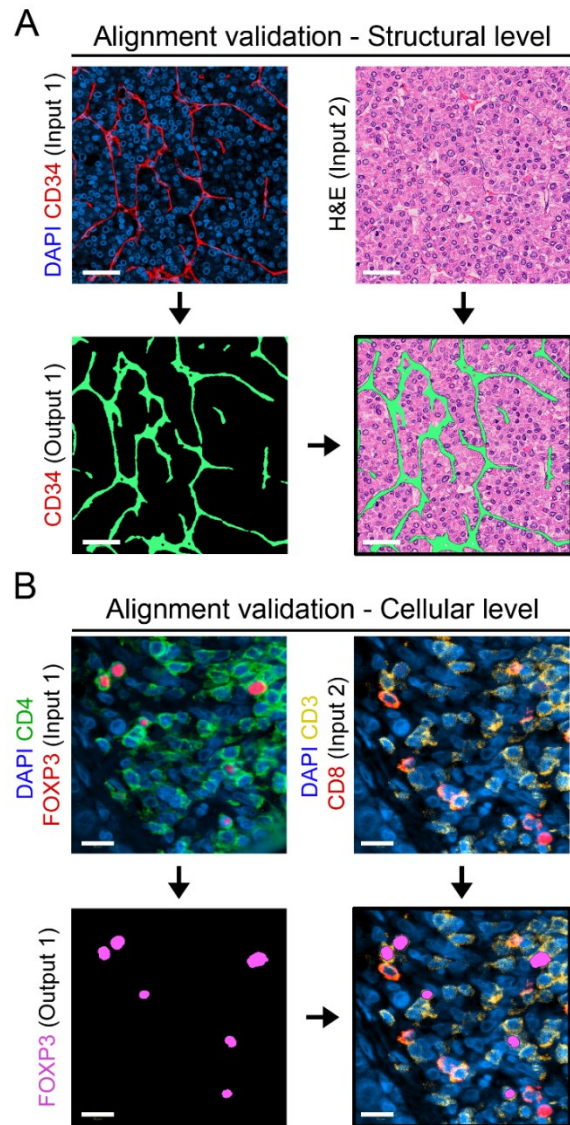
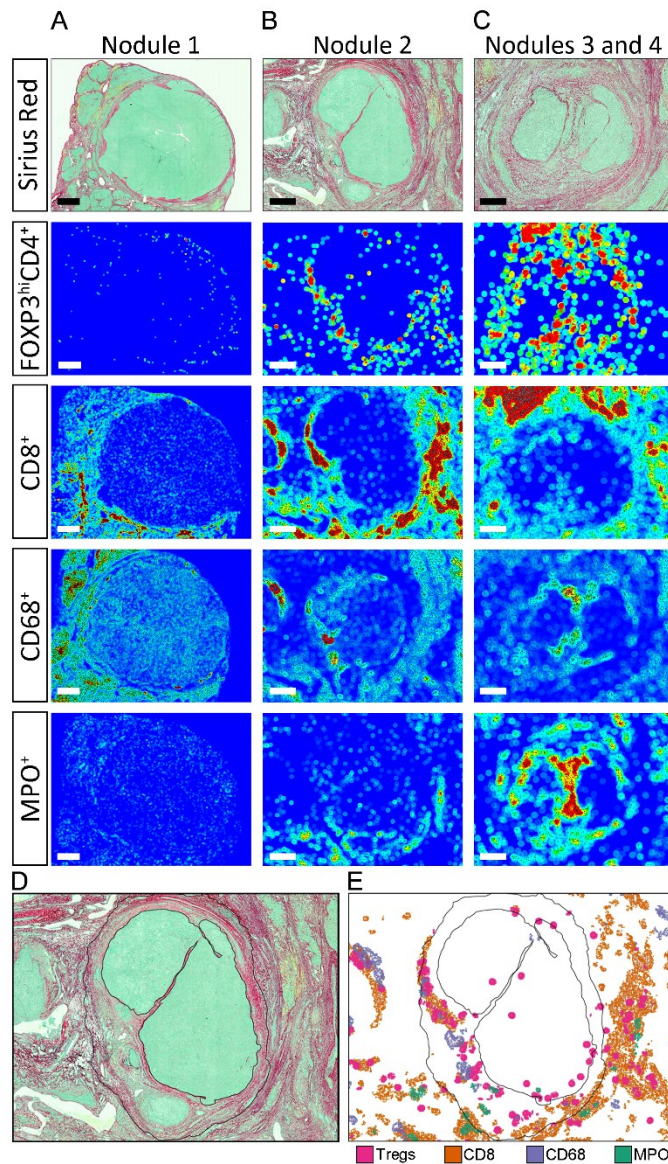


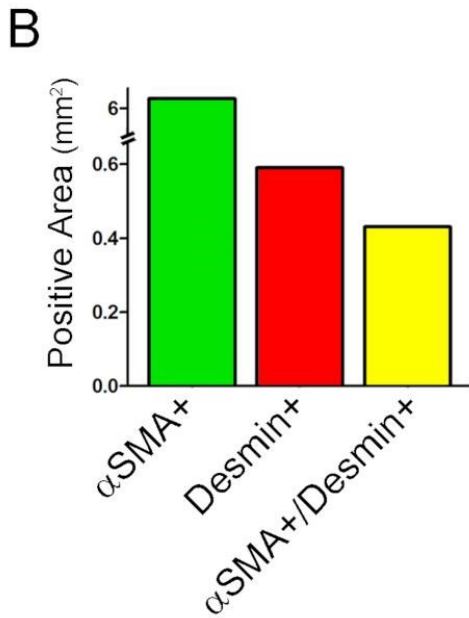
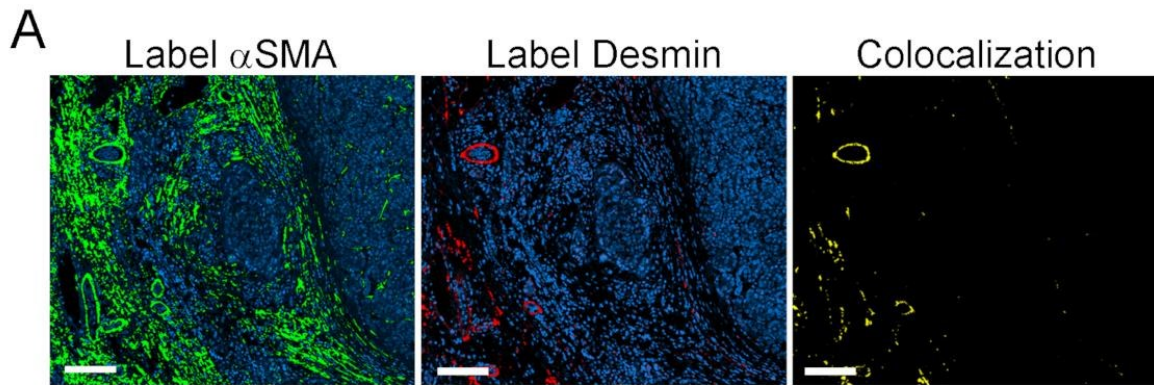
**Figure 5: Tissue heatmaps of COIs in the TME.** (A) Picrosirius Red staining showing the location of nodules 1, 2, 3, and 4. (B–G) Tissue heatmaps for  $CD4^+FoxP3^+$ ,  $CD8^+$ ,  $CD68^+$ ,  $MPO^+$ ,  $CD34^+$ , and  $\alpha SMA^+$  COIs, respectively. Dark blue indicates relatively low density, and red indicates relatively high density. Intermediate density values are assigned colors according to the shown color scale. (H and I) Quantification of COIs in nodules 1, 2, and 3 + 4 organized per cell type and per nodule, respectively.



**Supplementary Figure S1: Validation of tissue alignment.** (A) CD34 staining (in red) done on section II (input 1) is used for generating a CD34 mask in green (output 1). The green mask (output 1) is overlaid on the H&E image from the aligned serial section I (input 2). The merged image shows the perfect correspondence of vascular structures. Scale bar = 50  $\mu\text{m}$ . (B) Image IIIA showing the merge of DAPI, CD4, and FoxP3 (input 1) was used to generate a label for CD4<sup>+</sup>FoxP3<sup>+</sup> cells (output 1 in magenta). Output 1 label was transferred onto aligned image IIIB (input 2) and shows a perfect correspondence between the pairs FoxP3/DAPI, and CD4/CD3 in the merged image. Scale bar = 15  $\mu\text{m}$ .



**Supplementary Figure S2: Zoomed view of tissue heatmaps.** (A–C) Tissue heatmaps for  $CD4^+FoxP3^+$ ,  $CD8^+$ ,  $CD68^+$ , and  $MPO^+$  cells in nodules 1–4. Scale bars in nodules 1, 2, and 3 + 4 represent 1,500  $\mu\text{m}$ , 700  $\mu\text{m}$ , and 500  $\mu\text{m}$  respectively. (D) Outline of nodule 2 with a black solid line. (E) Hot spots for  $CD4^+FoxP3^+$ ,  $CD8^+$ ,  $CD68^+$ , and  $MPO^+$  cells in nodule 2 were extracted and mapped together onto the nodule 2 outline defined in D.



**Supplementary Figure S3: Colocalization Analysis.** (A) On the left and middle are images of  $\alpha$ SMA label in green and the desmin label in red respectively. On the right is a  $\alpha$ SMA/desmin double positive area in yellow. (B) Quantification of  $\alpha$ SMA+ area, desmin + area, and  $\alpha$ SMA/desmin double positive area. Scale bar = 150  $\mu$ m.

APP	Purpose	Classification	Classification	Post-Processing Steps	Output Variables
		Method	Features (pixel value)		
1	Tissue detection	Threshold	Channel DAPI (150)	o Label objects with colocalized above-threshold values for the 3 channels	o ROI Tissue
			Channel FITC/A488 (120)	o Close positive object 5 pixels	o Tissue Area
			Channel TRITC/A568 (40)	o Create ROI Tissue	
2	Tissue Segmentation	Decision Forest	RGB-R median	o Fill holes	o ROI Stroma
			RGB-G median	o Create ROI Stroma	o Stroma Area
			RGB-B median	o Create ROI Parenchyma	o ROI Parenchyma
			IHS-S median		o Parenchyma Area
			H&E Eosin median		
3	To locate and quantify CD4+ FoxP3+ cells	Threshold	Channel DAPI (>600)	o Label objects with colocalization of DAPI and Cy5/A647, surrounded by FITC/A488 signal	o Counts and density of CD4+FoxP3+ cells in ROIs Stroma and Parenchyma
			Channel FITC/A488 poly smoothing (>850)	o Clear objects smaller than 7 $\mu\text{m}^2$	o Coordinates of individual CD4+FoxP3+ cells
			Channel Cy5/A647(>800)		
4	To locate and quantify CD8+ cells	Threshold	Channel DAPI (<1200)	o Clear positive objects smaller than 15 $\mu\text{m}^2$	o Counts and density of CD8+ cells in ROIs Stroma and Parenchyma
			Channel Cy5/A647 median (>80)	o Close positive objects 2 pixels	o Coordinates of individual cells
				o Separate objects	
5	To locate and quantify CD68+ cells	Threshold	Channel FITC/A488 (>200)	o Clear positive objects smaller than 20 $\mu\text{m}^2$	o Counts and density of CD68+ cells in ROIs Stroma and Parenchyma
				o Dilate positive objects 3 pixels	o Coordinates of individual CD68+ cells
				o Separate objects	
6	To locate and quantify MPO+ cells	Threshold	Channel DAPI (>400)	o Clear objects smaller than 5 $\mu\text{m}^2$	o Counts and density of MPO+ cells in ROIs Stroma and Parenchyma.
			Channel TRITC/A568 (900-4000)	o Dilate 3 pixels positive objects	o Coordinates of individual MPO+ cells.
				o Separate objects	
7	To locate and quantify $\alpha\text{SMA+}$ area	Threshold	Channel TRITC/CF568 (>1050)	o Clear positive objects smaller than 25 $\mu\text{m}^2$	o Counts and density of $\alpha\text{SMA+}$ area in ROIs Stroma and Parenchyma
				o Dilate 3 pixels positive objects	o Coordinates of $\alpha\text{SMA+}$ pixels



8	To locate and quantify CD34+ area	Threshold	Channel DAPI (<5000)	o Clear positive objects smaller than 25 $\mu\text{m}^2$	o Counts and density of CD34+ area in ROIs Stroma and Parenchyma
			Channel Cy5/A647 median (>120)	o Dilate 3 pixels positive objects	o Coordinates of CD34+ pixels
9	Create tissue heatmaps for a given cell population	Object Heatmap	Object Heatmap		o Heatmap
			Drawing radius 50 $\mu\text{m}$	---	
10	Quantify colocalization between $\alpha\text{SMA}$ and Desmin	Threshold	Channel TRITC (CF568) (>1050)	o Label objects with above threshold values for TRITC (CF568)	o Quantify colocalized expression of $\alpha\text{SMA}$ and Desmin
			Channel Cy5 (A647) (>1000)	o Label objects with above threshold values for Cy5 (A647)	
				o Label objects with colocalization of above threshold values for TRITC (CF568) and Cy5 (A647)	
				o Clear positive objects smaller than 25 $\mu\text{m}^2$	

**Table 1:** General parameters used for the design of APPs employed for image analysis. The parameters specified in this table are adjusted to the unique characteristics of the images used in this analysis (e.g., background, artifacts, etc.) and may not apply to other images. Because the post-processing steps mentioned were defined for the specific images analyzed in this study, they are intentionally not detailed. The user should customize the APPs to the images to be analyzed.

Section/Staining	Primary Antibody	Secondary Antibody
<b>Section II/1<sup>st</sup> Staining</b>	Mouse IgG2a anti-human $\alpha\text{SMA}$ Mouse IgG1 anti-human CD34 Rabbit anti-human Cytokeratin 8/18	Goat anti-mouse IgG2a CF568 Rat anti-mouse IgG1 A647 Donkey anti-rabbit A488
<b>Section II/2<sup>nd</sup> Staining</b>	Rabbit anti-human Desmin Mouse anti-human CD68	Donkey anti-rabbit A647 Donkey anti-mouse DyLight 755
<b>Section III/1<sup>st</sup> Staining</b>	Mouse anti-human CD4 Rabbit anti-human FoxP3 Goat anti-human MPO	Donkey anti-mouse A488 Donkey anti-rabbit A647 Donkey anti-goat A568
<b>Section III/2<sup>nd</sup> Staining</b>	Rabbit anti-human CD3 Mouse anti-human CD8	Donkey anti-mouse DyLight 755 Donkey anti-rabbit A647

**Table 2:** Primary-Secondary Antibody Pairs for mIF.

## Discussion:

Simple, accessible, and easy-to-execute multiplexing techniques that allow spatial resolution of immune cells in tissue sections are needed to map the immune landscape in cancer and other

immunological disorders. Here, we describe a strategy that integrates widely available labeling and digital analysis techniques to expand the multiplexing capability and multidimensional assessment of imaging assays<sup>12,13,17,19</sup>. The staining of three serial sections for different markers, and the reuse of sections through stripping and reprobing techniques, enabled us to visualize 11 parameters in addition to H&E and PSR stains. Six images from these sections were aligned in an automated fashion using the tissue alignment module. The alignment was precise at the individual cell level for images originating from the same section and highly concordant for images originating from neighboring sections. Virtual multiplexing enabled us to determine how markers visualized in one section relate spatially to markers visualized in another contiguous section. While some of the stainings were labeled COIs, others were labeled TCs, allowing us to quantify COIs in the different TCs. The use of software tools for the automated quantification of COIs greatly simplified and accelerated the processing of images. Moreover, digital analysis was applied to whole tissue sections instead of selected fields of view, resulting in an unbiased representation of the TME. Furthermore, because the tissue coordinates of COIs were registered, it was possible to generate tissue heatmaps.

There are several areas in this protocol where troubleshooting may be needed. First, poor antigen retrieval can affect the quality of mIF, therefore the type of antigen retrieval buffer and duration should be optimized for the specific assay/biomarker conditions used. Second, the type of blocking solution used should be adapted to the tissue/antigen/species of primary and secondary antibodies. In our hands, the addition of 10% total serum from the species where the tissue comes from blocked Fc receptors, and thus reduced nonspecific antibody binding. The addition of 10% of serum from the species the secondary antibodies were raised in would minimize direct nonspecific attachment of secondary antibodies to the tissue section. Third, validation of the specificity of the primary and secondary antibodies using the proper positive and negative controls is essential. Fourth, increased autofluorescence in some channels and diffusion of DAPI upon primary antibody stripping are also common. To address the enhanced autofluorescence, we used primary/secondary antibody pairs where the specific signal had intensity values at least 5x that of the background. Finally, some high-affinity antibodies cannot be eluted with regular stripping procedures. In this case, we recommend using such antibodies in the last round of labeling. The user may have to try different

staining sequences to find the optimal configuration for the antibodies of interest. The efficiency of stripping should be confirmed before proceeding to a second or third round of labeling.

The main limitation and challenge of this strategy are finding the right combinations of primary and secondary fluorescent antibodies for the markers of interest. Finding primary antibodies raised in different species or with different isotypes that could be used simultaneously is limited by what is commercially available. Most whole slide scanners are equipped with lamps and filters that allow imaging a maximum of five channels, and secondary antibodies in the right species and right fluorophore are not always available. We partially overcame these limitations using serial stainings and sequential labeling. Several antibody combinations may need to be tested to arrive at the best combination for the markers of interest. Another limitation is the quality of the DAPI staining because stripping and reprobing may not always allow performing nuclei segmentation.

The tissue align module requires minimal training and no programming skills from users. The software theoretically allows the alignment of an unlimited number of images. However, precise alignment depends on the relatedness of sections, whereas closer sections that are more histologically concordant are more accurately aligned. We used the Author module of VIS for generating the APPs. Basic knowledge of image analysis is needed for creating APPs, but this is equally the case when using any other image analysis software. The unique advantages of VIS as compared to other image analysis software include automated alignment of images from sections prepared using different methods (e.g., IF, histochemistry, IHC). This allows colocalization studies of multiple markers of interest using virtual multiplexing. Furthermore, the flexible and user-friendly design of APPs allows user-specific customization. Automated quantification and mapping, and the possibility of processing whole tissue sections, saves time and reduces bias compared to manual counting by visual inspection.

This strategy is a very useful research tool for tissue immunology in the context of cancer and autoimmunity but remains unvalidated for clinical use. With additional standardization and validation, it can be used in the future for multiple applications (e.g., to map the immune landscape in cancer to predict and monitor the response to immunotherapeutic agents). It can also be adapted to different inflammatory conditions (e.g., inflammatory bowel disease) to combine pathological evaluation with prognostic biomarkers.

The main critical steps in this protocol are the efficiency/specificity of the labeling and the robustness of the designed APPs for the intended use or biomarker. Hence, regular validation by visual inspection, especially upon designing a new APP, is essential. The efficient use of multiple rounds of stripping and reprobing or different types of stains on the same section are critical components and can be tissue or section specific. Verifying the efficiency of such processes before proceeding with large batch analysis is critical.

In summary, we provide a strategy that maximizes the quantitative and spatial information that can be obtained from valuable clinical tissue samples. The resources, equipment, and knowledge required to implement this methodology are widely accessible. We propose this methodology as a useful guide for planning assays aiming at identifying, quantifying, and mapping immune cell populations in the TME.

**Disclosures:**

The authors declare no conflicts of interest.

**Acknowledgments:**

We thank the study participant. We thank Louise Rousseau, coordinator of the HBP biobank for the recovery of the tissue samples and all associated clinical information. We acknowledge the molecular pathology and cell imaging core facilities at the CRCHUM and Michael Persch from Visiopharm for excellent technical assistance. Funding: This study was supported by grants from the Canadian Liver Foundation, Fonds de recherche du Québec–Santé (FRQS) AIDS and Infectious Disease Network (Réseau SIDA-MI), and the Canadian Network on Hepatitis C (CanHepC). CanHepC is funded by a joint initiative from the Canadian Institutes of Health Research (CIHR) (NHC-142832) and the Public Health Agency of Canada. M.F.M. received fellowships from the Université de Montréal, Bourse Gabriel Marquis, and the FRQS. T.F. received doctoral fellowships from CIHR and CanHepC. S.T. holds the Roger-Des-Groseillers Chair in hepatobiliary and pancreatic oncological surgery, Université de Montréal.

Author contributions: M.F.M. designed, performed experiments, and analyzed data. T.F. designed experiments. A.C-B. provided technical guidance. G.S. performed all the pathological assessments of the study subject and provided input on all the pathological aspects. L.M. performed H&E staining, optimized, and performed image acquisition. M.N.A. performed the PSR stain and

provided valuable technical input. N.B. contributed to the image analysis. S.T. is the principal investigator for the HBP biobank and is responsible for overseeing the overall operation of the biobank. He also provided invaluable input on all aspects of the project and its clinical implications. M.F.M, T.F., and N.H.S. conceptualized and designed the study. N.H.S. supervised the work and obtained funding. M.F.M., T.F., A.C-B, and N.H.S. wrote the manuscript. All authors reviewed and approved the manuscript.

### **References:**

1. Greten, F. R., Grivennikov, S. I. Inflammation, and Cancer: Triggers, Mechanisms, and Consequences. *Immunity*. 51, (1), 27-41 (2019).
2. Pages, F., et al. International validation of the consensus Immunoscore for the classification of colon cancer: a prognostic and accuracy study. *Lancet*. 391, (10135), 2128-2139 (2018).
3. Binnewies, M., et al. Understanding the tumor immune microenvironment (TIME) for effective therapy. *Nature Medicine*. 24, (5), 541-550 (2018).
4. Taube, J. M., et al. Implications of the tumor immune microenvironment for staging and therapeutics. *Modern Pathology: an official journal of the United States and Canadian Academy of Pathology, Inc*. 31, (2), 214-234 (2018).
5. Bindea, G., et al. Spatiotemporal dynamics of intratumoral immune cells reveal the immune landscape in human cancer. *Immunity*. 39, (4), 782-795 (2013).
6. Galon, J., et al. Towards the introduction of the 'Immunoscore' in the classification of malignant tumours. *The Journal of Pathology*. 232, (2), 199-209 (2014).
7. Finotello, F., Eduati, F. Multi-Omics Profiling of the Tumor Microenvironment: Paving the Way to Precision Immuno-Oncology. *Frontiers in Oncology*. 8, 430 (2018).
8. Gerner, M. Y., Kastenmuller, W., Ifrim, I., Kabat, J., Germain, R. N. Histo-cytometry: a method for highly multiplex quantitative tissue imaging analysis applied to dendritic cell subset microanatomy in lymph nodes. *Immunity*. 37, (2), 364-376 (2012).
9. Giesen, C., et al. Highly multiplexed imaging of tumor tissues with subcellular resolution by mass cytometry. *Nature Methods*. 11, (4), 417-422 (2014).

10. Porta Siegel, T., et al. Mass Spectrometry Imaging and Integration with Other Imaging Modalities for Greater Molecular Understanding of Biological Tissues. *Molecular Imaging and Biology: MIB: the official publication of the Academy of Molecular Imaging*. 20, (6), 888-901 (2018).
11. Buchberger, A. R., DeLaney, K., Johnson, J., Li, L. Mass Spectrometry Imaging: A Review of Emerging Advancements and Future Insights. *Analytical Chemistry*. 90, (1), 240-265 (2018).
12. Pirici, D., et al. Antibody elution method for multiple immunohistochemistry on primary antibodies raised in the same species and of the same subtype. *Journal of Histochemistry and Cytochemistry*. 57, (6), 567-575 (2009).
13. Gendusa, R., Scalia, C. R., Buscone, S., Cattoretti, G. Elution of High-affinity (>10<sup>9</sup> KD) Antibodies from Tissue Sections: Clues to the Molecular Mechanism and Use in Sequential Immunostaining. *Journal of Histochemistry and Cytochemistry*. 62, (7), 519-531 (2014).
14. van der Loos, C. M. Multiple immunoenzyme staining: methods and visualizations for the observation with spectral imaging. *Journal of Histochemistry and Cytochemistry*. 56, (4), 313-328 (2008).
15. Stack, E. C., Wang, C., Roman, K. A., Hoyt, C. C. Multiplexed immunohistochemistry, imaging, and quantitation: a review, with an assessment of Tyramide signal amplification, multispectral imaging, and multiplex analysis. *Methods*. 70, (1), 46-58 (2014).
16. Toth, Z. E., Mezey, E. Simultaneous visualization of multiple antigens with tyramide signal amplification using antibodies from the same species. *Journal of Histochemistry and Cytochemistry*. 55, (6), 545-554 (2007).
17. Robertson, D., Savage, K., Reis-Filho, J. S., Isacke, C. M. Multiple immunofluorescence labeling of formalin-fixed paraffin-embedded (FFPE) tissue. *BMC Cell Biology*. 9, 13 (2008).
18. Segnani, C., et al. Histochemical Detection of Collagen Fibers by Sirius Red/Fast Green Is More Sensitive than van Gieson or Sirius Red Alone in Normal and Inflamed Rat Colon. *PLoS One*. 10, (12), 0144630 (2015).

19. Bolognesi, M. M., et al. Multiplex Staining by Sequential Immunostaining and Antibody Removal on Routine Tissue Sections. *Journal of Histochemistry and Cytochemistry*. 65, (8), 431-444 (2017).

## Chapter 4: Manuscript 2

### **Distinct spatial distribution and roles of Kupffer cells and monocyte-derived macrophages in mouse acute liver injury**

Published in *Frontiers in Immunology* on September 30, 2022

doi. 10.3389/fimmu.2022.994480

Authors: Manuel Flores Molina<sup>1,2</sup>, Mohamed N. Abdelnabi<sup>1,2</sup>, Sabrina Mazouz<sup>1,2</sup>, Deborah Villafranca Baughman<sup>1,3</sup>, Vincent Quoc-Huy Trinh<sup>1</sup>, Shafi Muhammad<sup>1,4</sup>, Nathalie Bédard<sup>1</sup>, David Osorio Laverde<sup>1</sup>, Ghada S. Hassan<sup>1</sup>, Adriana Di Polo<sup>1,3</sup>, Naglaa H. Shoukry<sup>1,5\*</sup>

<sup>1</sup> Centre de Recherche du Centre hospitalier de l'Université de Montréal (CRCHUM), Montréal, Québec, Canada ;

<sup>2</sup> Département de microbiologie, infectiologie et immunologie, Faculté de médecine, Université de Montréal, Montréal, Québec, Canada ;

<sup>3</sup> Département de neurosciences, Faculté de médecine, Université de Montréal, Montréal, Québec, Canada ;

<sup>4</sup> Department of Biosciences, COMSATS University Islamabad-44000, Pakistan;

<sup>5</sup> Département de médecine, Faculté de médecine, Université de Montréal, Montréal, Québec, Canada.

**Keywords: CCl<sub>4</sub>, intrahepatic leucocytes, necroinflammation, tissue repair**

\*Corresponding author: Dr. Naglaa Shoukry, Centre de Recherche du CHUM (CRCHUM), Tour Viger, Local R09.414, 900 rue St-Denis, Montréal, QC H2X 0A9, Canada, email: [naglaa.shoukry@umontreal.ca](mailto:naglaa.shoukry@umontreal.ca).

Abbreviations: ALT, alanine aminotransferase;  $\alpha$ SMA, alpha smooth muscle actin; BFA, brefeldin A; CCl<sub>4</sub> carbon tetrachloride; CCL2, C-C motif chemokine ligand 2; CCL7, C-C motif 7 chemokine ligand 7; CCR2, C-C motif chemokine receptor 2; CV, central vein; CX3CR1, CX3C chemokine receptor 1; ECM, extracellular matrix; FlowSOM, Flow with Self Organizing Maps; HSC, hepatic stellate cell; IHL, intrahepatic leukocyte; IL-, interleukin-; Ly6C, lymphocyte



antigen 6 complex, locus C; Ly6G, lymphocyte antigen 6 complex, locus G6D; M-CSF, macrophage colony stimulating factor; mIF, Multiplex Immunofluorescence; MoMFs, monocyte derived macrophages; MARCO, macrophage receptor with collagenous domain; NCMs, non classical monocytes; NKT, natural killer T cell; TGF $\beta$ , transforming growth factor- $\beta$ ; TNF $\alpha$ , tumor necrosis factor- $\alpha$ ; t-SNE, t-distributed stochastic neighbor embedding analysis; YS, yolk sac.

Manuel Flores substantially contributed to the conception and design of the study, the optimization of the techniques, the undertaking of experiments, and the acquisition, analysis, and interpretation of data. He drafted the article and participated in its critical revision for important intellectual content.

### **Abstract:**

Macrophages are key regulators of inflammation and repair, but their heterogeneity and multiple roles in the liver are not fully understood. We aimed herein to map the intrahepatic macrophage populations and their function(s) during acute liver injury. We used flow cytometry, gene expression analysis, multiplex-immunofluorescence, 3D-reconstruction, and spatial image analysis to characterize the intrahepatic immune landscape in mice post-CCl<sub>4</sub>-induced acute liver injury during three distinct phases: necroinflammation, and early and late repair. We observed hepatocellular necrosis and a reduction in liver resident lymphocytes during necroinflammation accompanied by the infiltration of circulating myeloid cells and upregulation of inflammatory cytokines and pro-repair chemokines. These parameters returned to baseline levels during the repair phase. We identified resident CLEC4F<sup>+</sup> Kupffer cells (KCs) and infiltrating IBA1<sup>+</sup>CLEC4F<sup>-</sup> monocyte-derived macrophages (MoMFs) as the main hepatic macrophage populations during this response to injury. While occupying most of the necrotic area, KCs and MoMFs exhibited distinctive kinetics, distribution, and morphology at the site of injury. The necroinflammation phase was characterized by low levels of KCs and a remarkable invasion of MoMFs capable of phagocytosing necrotic hepatocytes, while opposite kinetics/distribution were observed during repair. During the early repair phase, KCs originating from the yolk-sac were restored, whereas MoMFs diminished gradually and then dissipated during the late repair. MoMFs interacted with hepatic stellate cells during the necroinflammatory and early repair phases, highly likely modulating their activation state and influencing their fibrogenic and pro-repair functions which are critical for wound healing. Altogether, our study reveals novel and distinct spatial and temporal

distribution of KCs and MoMFs and provides insights into their complementary roles during acute liver injury.

## **Introduction**

Hepatic macrophages are the major liver immune cells. They are a heterogeneous population of cells and have been assigned both beneficial and detrimental roles in human liver disease and experimental models (1). The hepatic macrophage compartment in mice is composed of Kupffer cells (KCs), monocyte-derived macrophages (MoMFs), liver capsular macrophages, and under certain conditions, GATA6<sup>+</sup> peritoneal macrophages (2-4). Despite the tremendous progress made in determining the origin, transcriptional profile, and function of the different subpopulations of liver macrophages, there are significant gaps in knowledge regarding how these subsets are organized within the tissue and how their spatial distribution may impact crosstalk and division of labor in health and disease (2, 5-9).

KCs are the main subset of hepatic macrophages under normal physiological conditions. They are sessile cells that reside in the sinusoids where they perform crucial tasks during homeostasis, including removal of lipopolysaccharides (LPS), efferocytosis of apoptotic cells, induction of T cell tolerance, and the control of iron and lipid metabolism and bilirubin balance (10). In addition, KCs are sentinel cells and first responders to tissue damage (10). They originate from embryonic yolk sac-derived erythro-myeloid progenitors (YS-KCs) and self-maintain throughout adult life independently of hematopoietic stem cells (7, 11, 12). On the other hand, inflammatory monocytes are absent and MoMFs are present in low numbers in the healthy liver (13). However, during acute liver injury, large numbers of recruited inflammatory monocytes and MoMFs take center stage and carry out various effector functions including clearance of debris and pathogens, activation and resolution of inflammation, and extracellular matrix (ECM) remodeling upon injury (1, 6, 8, 10). Notably, infiltrating inflammatory monocytes and MoMFs transition from an inflammatory to a pro-repair phenotype within hours during a typical wound healing response, demonstrating remarkable functional plasticity (6, 8, 13). This conversion occurs at the injury site and depends on IL-4, IL-10, phagocytosis, and neutrophil-derived reactive oxygen species (ROS) (6, 8, 14). Interestingly, KCs and MoMFs, in addition to their differential functionality at various levels of liver disease, exhibit distinct expression of various cell surface markers. In mice, KCs are CD11b<sup>int</sup>, F4/80<sup>hi</sup>, and CLEC4F<sup>+</sup> cells. MoMFs are Ly6C<sup>+</sup> CX3CR1<sup>+</sup> and originate from recruited

inflammatory monocytes (Ly6C<sup>hi</sup> CX3CR1<sup>low</sup>) (1, 6, 8, 10). Another important function of liver macrophages is their capacity to activate hepatic stellate cells (HSCs), which enhances their fibrogenic and pro-repair functions (1). However, the role of the various hepatic macrophage subsets in HSC activation is not fully understood.

In this study, we undertook a spatial and temporal characterization of the liver macrophage compartment to better understand how the different macrophage subsets interact during steady state and in response to injury. We used the carbon tetrachloride (CCl<sub>4</sub>) acute injury model in mice as it recapitulates immunological, histological, and pathological features of human toxic liver injury (15). We established the dynamics of the two largest macrophage subpopulations that spatially overlap in the necrotic areas around central veins (CVs) in response to acute hepatic injury: KCs and MoMFs. Despite their proximity, these subsets exhibited major differences regarding their origin, time of necrotic tissue infiltration, position at the injury site, morphology, capacity to replenish the macrophage pool during tissue repair, and colocalization with HSCs. These results add spatial dimension and tissue context to the interplay between MoMFs and KCs and complement the large body of functional and transcriptomics studies that define these major macrophage subsets and their reciprocal interactions.

## **Materials and Methods**

### **Mice**

Eight- to ten weeks old C57BL/6N male mice were obtained from Charles River Laboratories (Senneville, QC, Canada; strain code 027). Animals were maintained in a specific pathogen-free facility at the Centre de Recherche du Centre hospitalier de l'Université de Montréal (CRCHUM). All animal experiments were approved by the Institutional Animal Care and Use Committee (Protocol IP18035NSs). Mice received a single intraperitoneal injection of CCl<sub>4</sub> (Sigma-Aldrich, Oakville, ON, Canada) at 1 ml/kg resuspended in corn oil (Sigma-Aldrich). Control mice received corn oil only. Mice were terminally euthanized with 400 mg/kg Euthanyl (sodium pentobarbital; CDMV, St-Hyacinthe, QC, Canada) at 0, 12, 24, 48, 72, 96, and 168 h post-injection.

### **Histology**

Hematoxylin and eosin (H&E), Ki67, and IBA1 immunohistochemistry (IHC) stainings were performed by the molecular pathology core platform of the CRCHUM using the Shandon

multiprogram robotic slide stainer on 4 µm formalin-fixed paraffin-embedded (FFPE) hepatic whole tissue sections. Images were acquired with the whole slide scanner Olympus BX61VS. Quantification of the necrotic area was performed with the VIS software (Version 2018.4, Visiopharm, Hørsholm, Denmark) using protocols that automatically detected the tissue and manual delineation of the necrotic area by visual inspection. References for antibodies and H&E reagents are provided in Tables S1 and S2 in the Supplementary Material.

### **Alanine Aminotransferase (ALT) Activity Assay**

ALT test was performed on murine plasma by the clinical laboratory at the Centre hospitalier de l'Université de Montréal. Briefly, mice were bled by cardiac puncture and the blood was anticoagulated using 10 µL of 10% K<sub>2</sub>EDTA in H<sub>2</sub>O per 1 mL of blood. The blood was centrifuged at 13000 rpm for 5 minutes at room temperature, and the upper phase containing the plasma was collected and stored at -80°C until ready for ALT activity measurement.

### **Multiplex Immunofluorescence**

Multiplex immunofluorescence (mIF) for CLEC4F, IBA1, αSMA, GATA-6, and Desmin was performed on 4 µm FFPE tissue sections as previously described (16). mIF for IBA1, CLEC4F, and MARCO was done on frozen 5µm OCT-embedded and fixed liver sections. Briefly, sections were kept at -80°C before usage. Sections were aired for 5 minutes at room temperature (RT) and then immersed in a washing buffer for 10 minutes for OCT removal. Next, sections were transferred to another jar containing antigen retrieval buffer and subjected to high pressure for 5 minutes inside an electric pressure cooker. The pressure was released, the jar was taken out and sections were left for another 20 minutes inside the antigen retrieval buffer to cool down. Afterward, sections were washed and then incubated with glycine solution for 10 minutes at RT, washed two times, and then incubated for 30 minutes with blocking solution at RT. Next, sections were washed and incubated overnight with the cocktail of primary antibodies in a blocking solution at 4°C inside a humidity chamber, to be washed again and incubated with the cocktail of secondary antibodies for 30 minutes at RT in the dark. Finally, washed sections were mounted in Slowfade Gold mounting media plus DAPI and stored in the dark at 4°C up to the acquisition time. mIF for IBA1, CLEC4F, CCR2 and CX3CR1 was performed on 5µm frozen sections. Briefly, sections were kept at -80°C before usage. They were aired for 5 minutes at room temperature (RT) and then immersed in tissufix for 10 minutes at RT for mild fixation. Next, sections were washed and

subjected to the same protocol as described above for OCT sections. All antibodies, solutions, and reagents used are listed in Supplementary Table S1. Whole tissue images were acquired using the whole slide scanner Olympus BX61VS. We performed staining on serial sections when we could not multiplex the primary antibodies of different markers because they were raised in the same species or when the purpose was to align images originated using different techniques (e.g., IHC and H&E).

To mitigate any autofluorescence issues, we tried to use IF channels having the lowest autofluorescence in the liver and/or that have little spillover. In addition, we performed quantification using the VIS software that allows the establishment of thresholds of positivity for every individual channel, with pixel intensity values set well above the background signal and visual artifacts removed from the regions to be analyzed. Non-specific binding of primary antibodies was ruled out using a specific staining pattern for each Ab corresponding to the tissue or cellular location of the marker to be assessed (i.e., nuclear, cytoplasmic, around CV area, etc.). The specificity of the stain was confirmed using other antibodies raised in the same species as negative controls.

### **RNA Isolation and RT-PCR Analysis**

Total RNA was isolated from murine hepatic tissue using RNeasy Mini Kit (Qiagen). cDNA was generated from 2 ug of total RNA using the Transcriptor Universal cDNA Master Mix (Roche Life Science). cDNA was amplified using the LightCycler® 480 SYBR Green I Master (Roche) in the LightCycler 480 instrument (Roche). All the previous procedures were performed according to the manufacturer's protocols. mRNA expression was normalized to the expression of the housekeeping gene 28s and was determined using the  $2^{-\Delta\Delta C_t}$  method. Primer sequences are listed in Supplementary Table S2.

### **Image Analysis**

Image analysis was performed using the image analysis software VIS. The Author™ module was used to design the following protocols: 1) Automated identification and quantification of tissue area. 2) Identification and quantification of IBA1<sup>+</sup>CLEC4F<sup>-</sup> area. 3) Identification and quantification of IBA1<sup>+</sup>CLEC4F<sup>+</sup> area. 4) Quantification of  $\alpha$ SMA<sup>+</sup> area. 5) Quantification of the colocalization between  $\alpha$ SMA<sup>+</sup> cells and CLEC4F<sup>+</sup> cells versus IBA1<sup>+</sup>CLEC4F<sup>-</sup> cells. 6)

Measurement of the distance from nuclei to the central vein. The Tissuealign module of VIS was used for the automated alignment of images from serial sections. The tissue heatmap function of VIS was used for generating heatmaps for CLEC4F<sup>+</sup> KCs and IBA1<sup>+</sup>CLEC4F<sup>-</sup> macrophages. The detection of nuclei was done using the protocol 10169 – Nuclei Detection, AI (Fluorescence) from Visiopharm.

### **Isolation of Intrahepatic Leukocytes (IHLs)**

IHLs were isolated from hepatic tissue in a two-step process: first by mechanical dissociation and next by enzymatic digestion. First, the liver was minced using a scalpel. The dissociated tissue was suspended in cold RPMI media supplemented with 10 % FBS plus benzonase (0.2 U/mL) and collagenase D (0.1 mg/mL) and then incubated at 37°C for 30 minutes with rotation. Upon incubation, the tissue was passed through a 70 µm cell strainer for further mechanical dissociation. The tissue suspension was washed with cold RPMI/FBS, layered on a percoll discontinuous gradient (80% bottom, 40 % top), and centrifuged at 1500 rpm for 25 minutes. The IHLs were recovered from the interphase between the 2 percoll solutions and resuspended in fresh media. The references of all reagents used in this protocol are listed in Supplementary Table S2.

### **Flow Cytometry**

For detection of surface markers, freshly isolated IHLs were washed with FACS buffer (PBS, 1% FBS, 0.02% Sodium Azide) and then transferred to a 96-well plate where they were incubated with a cocktail of fluorescently conjugated antibodies plus aqua vivid and 10% mouse serum for 30 minutes at 4°C in the dark. IHLs were then washed two times with FACS buffer and then fixed in 1% formaldehyde in PBS and kept at 4°C in the dark up to acquisition time. In cases where intracellular staining was required, after labeling cell surface markers, IHLs were incubated with permeabilization/fixation buffer for 30 minutes at 4°C in the dark. Next, IHLs were washed and incubated with the cocktail of antibodies for intracellular targets for 30 minutes at 4°C in the dark. Finally, the samples were washed and fixed and kept at 4°C in the dark up to acquisition time. To detect spontaneous cytokine production, IHLs were incubated with 10 µg/ml of Brefeldin A (Sigma-Aldrich) and 6 µg/ml of monensin sodium salt (Sigma-Aldrich) for 6 h prior to staining.

Samples were acquired on a BD LSRFortessa™ Cytometer equipped with violet (405 nm), blue (488 nm), yellow-green (561 nm), and red (633 nm) lasers and FACSDiva version 8.0.1 (BD

Biosciences, San Diego, CA). Analysis was performed using FlowJo version 10.4 for Mac (BD Biosciences, Ashland, OR) and FlowSOM.

### **Three-dimensional reconstruction**

Sixteen  $\mu\text{m}$  sections from frozen liver OCT embedded sections from 48 h  $\text{CCl}_4$  treated mice were imaged using  $\alpha\text{SMA}$ ,  $\text{CLEC4F}$ , and  $\text{IBA1}$  specific antibodies according to multiplex immunofluorescence protocol described above. Nuclei were counterstained using DAPI. The images or z-stacks were acquired using  $\times 40$  objective, ApoTome 2, Zeiss. Three-dimensional (3D) reconstruction was done using Imaris 8.1.2 software (Bitplane, Zurich, Switzerland).

### **Statistical Analysis**

Statistical analysis was performed with GraphPad Prism 9 software. Data are presented as mean  $\pm$  SEM. The number of samples for each experiment and the number of replicate experiments are indicated in the figure legends. Statistical significance between the two groups was determined by Mann-Whitney Test. When comparing more than two groups, analysis of variance (ANOVA) followed by Dunn's Multiple Comparison Test was performed. A P value  $< 0.05$  was considered statistically significant.

### **Results**

#### **Distinct necroinflammatory and tissue repair phases are observed during acute liver injury**

We sought to understand the wound healing response to acute liver injury in mice using the  $\text{CCl}_4$  model, which is characterized by central vein (CV) injury and a self-limited immune response leading to total healing (15). Herein, 8-10 weeks old C57BL/6 male mice received a single intraperitoneal injection of  $\text{CCl}_4$  (1  $\mu\text{l/g}$  of body weight), and livers and plasma were collected and analyzed at 12, 24, 48-, 72-, 96- and 168 hours post-injection (Figure 1A). Importantly, all imaging labeling, analysis, and quantification are done on whole tissue sections (Figure 1B) with quantification undertaken using automatic protocols with predefined thresholds for signal positivity (16). H&E staining of liver sections demonstrated the hallmark characteristics of CV-associated injury and extensive immune cell infiltration in the necrotic tissue (Figure 1B). We assessed tissue damage by quantifying the percentage of necrotic area and ALT plasma levels. We observed that hepatocellular necrosis was ongoing at 12 h, peaked at 24 h, and persisted up to 48

h post-CCl<sub>4</sub>. At 72 h, both the necrotic area and ALT levels returned to normal suggesting that the period between 48 and 72 h was critical for the transition to tissue repair (Figures 1C, D). The hepatic expression of genes encoding the pro-inflammatory cytokines TNF $\alpha$  and IL-1 $\beta$  closely mirrored the kinetics of plasma ALT, with peak expression at 24 h and return to baseline at 72 h (Figure 1E). In addition, flow cytometric analysis showed a considerable influx of CD11b<sup>+</sup> myeloid cells into the liver between 24 – 48 h, returning to baseline levels at 72 h (Figure 1F). Furthermore, the hepatic gene expression of the pro-resolving chemokine receptor-ligand pair CX3CR1-CX3CL1 was upregulated at 48-72 h post-CCl<sub>4</sub> marking the transition to tissue repair (Figure 1G). Interestingly, the proliferation marker Ki67 was upregulated, both at the mRNA and protein levels, at 48 h and to a lesser extent at 72 h post-injury (Figures 1H, I and Supplementary Figure S1). Immunohistochemical Ki67 staining showed massive and compartmentalized proliferation of parenchymal (hepatocytes with large round nuclei) and non-parenchymal cells (small irregularly shaped nuclei) around portal tracts and CVs, respectively, at 48 h post CCl<sub>4</sub> (Figure 1I). Altogether, these data allowed us to delineate three distinct phases of wound repair during acute liver injury (Figure 1A). First, the necroinflammatory phase, characterized by tissue damage and immune cell infiltration, spans from 0 to 48 h post CCl<sub>4</sub>. Second, the early phase of tissue repair from 48 to 72 h post CCl<sub>4</sub>, is characterized by receding inflammation with the return to baseline levels of inflammatory cytokines and tissue damage markers, and concomitant upregulation of pro-resolving genes and proliferation of tissue cells. Third, the late repair phase is between 72 to 168 h post CCl<sub>4</sub> where inflammation and tissue damage indicators return to homeostatic levels.

### **CCl<sub>4</sub>-mediated acute liver injury caused partial and temporary depletion of hepatic resident immune populations and a massive influx of circulating myeloid cells**

Next, we characterized the intrahepatic leucocytes during the three different phases of acute injury using high-resolution flow cytometry. We observed that the major resident lymphocyte populations including T cells, B cells, and NKT cells, were significantly reduced during necroinflammation and only recovered during tissue repair (Figures 2A, B). Conversely, as demonstrated above, infiltrating CD11b<sup>+</sup> myeloid cells significantly increased during necroinflammation (Figure 1F). These myeloid cells upregulated Ki67 expression suggesting that they underwent *in situ* proliferation (Figure 2C). In addition, we observed that CCl<sub>4</sub>-mediated



injury-induced expression of pro-inflammatory cytokines like TNF $\alpha$ , the pro-fibrogenic cytokine IL-13, and the anti-inflammatory mediators IL-10 and Arg-1 by hepatic myeloid cells, suggesting that they may be functionally implicated in both necroinflammation and tissue repair (Figures 2C, D).

For unbiased identification of the myeloid subpopulations induced upon acute injury, we applied t-distributed stochastic neighbor embedding (t-SNE) analysis and FlowSOM on flow cytometry data for several well-established myeloid markers (17). These analyses were undertaken at 0, 24 h, 48 h, 72 h, and 96 h post-CCl<sub>4</sub> injury. The t-SNE heatmap density plots of the pooled data for each marker are presented in Figure 3A. Unsupervised clustering generated by FlowSOM identified six CD11b<sup>+</sup> populations (Figures 3B-D). Population 0 may represent a subset of hepatic dendritic cells because they are F4/80<sup>-</sup> Ly6C<sup>-</sup> CX3CR1<sup>+</sup> MHCII<sup>hi</sup>, but definitive confirmation requires the inclusion of the CD11c marker that is absent in this analysis (11, 18). Population 1 was classified as MoMFs as they expressed Ly6C and CX3CR1, and moderate levels of F4/80 and MHC II (8, 10). Population 2 was classified as inflammatory monocytes due to its high expression of Ly6C, low to a negative expression of CX3CR1, and no expression of the granulocytic marker Ly6G (6, 10, 14, 19, 20). Population 3 was classified as non-classical monocytes (NCMs) since they were Ly6C<sup>-</sup> Ly6G<sup>-</sup> CX3CR1<sup>hi</sup> MHCII<sup>+</sup> F4/80<sup>+</sup> (21, 22). Population 4 could not be classified with the markers included in this analysis. Population 5 expressed Ly6G and intermediate levels of Ly6C and was classified as neutrophils (10, 23). The kinetics of the different myeloid subpopulations are shown in representative t-SNE plots in Figure 3D. We also validated the FlowSOM population identity for the four phagocytic myeloid populations identified above using manual gating (Supplementary Figure S2A). Representative flow cytometry plots of the kinetics of myeloid populations are presented in Supplementary Figure S2B. Surprisingly, t-SNE FlowSOM analysis did not reveal a population with a phenotype consistent with KCs. The two predominant populations expressing high levels of the macrophage marker F4/80 (populations 2 and 3) also co-expressed markers inconsistent with the KC phenotype (Ly6C and CX3CR1). It is important to note that we also tried gating manually on the CD45<sup>+</sup> CD11b<sup>+</sup> MHCII<sup>+</sup> F4/80<sup>+</sup> CD64<sup>+</sup> population that has been previously reported to contain the KCs (10). However, this population consisted almost exclusively of CX3CR1<sup>+</sup> cells, and therefore could not be KCs (Supplementary Figure S3). Altogether, we identified four different myeloid cell populations implicated in acute liver injury, which is consistent with MoMFs, inflammatory monocytes, NCMs, and neutrophils.

### **Kinetics of myeloid populations at the liver injury site reveal temporally distinct waves of inflammatory monocytes, NCMs, neutrophils, and MoMFs**

Next, we examined the infiltration kinetics of the four main myeloid populations identified. The numbers of inflammatory monocytes and neutrophils were very low in the hepatic tissue at the steady state (Figures 3E, F). This situation dramatically changed during the first half of the necroinflammatory phase, when inflammatory monocytes and a first wave of neutrophils extensively infiltrated the hepatic tissue (Figures 3E, F), consistent with previous reports in the APAP-induced acute hepatic injury model (10, 19). Interestingly, NCMs, normally associated with anti-inflammatory and pro-repair effector functions, also increased during this period, suggesting that they may be involved in preventing collateral damage associated with the inflammatory reaction (21, 22, 24). The second half of the necroinflammatory stage (24 to 48 h post CCl<sub>4</sub>) was characterized by the simultaneous decline of the above-mentioned inflammatory populations and the rapid increase of MoMFs, outnumbering all other phagocytic subsets and prevailing during the early repair phase (Figures 3E, F). We also observed increased expression of the monocyte/macrophage chemokines CCL2 and CCL7 and the growth factor M-CSF during necroinflammation and early repair, suggesting their involvement in the observed monocyte/macrophage recruitment and expansion (Figure 3G), as previously reported (7, 12, 27, 28). Finally, two waves of neutrophils infiltrated the hepatic tissue at the peak of necroinflammation and repair stages at 24 h and 72 h, respectively (Figures 3E, F). In summary, whereas tissue-resident immune populations decreased during necroinflammation, circulating myeloid cells infiltrated the liver in an orchestrated fashion and their presence was temporally associated with the restoration of tissue homeostasis.

### **Acute liver injury induces changes in the composition, density, and spatial distribution pattern of the hepatic macrophages**

To understand the functional and spatial implications of the different macrophage subsets, we proceeded to map the macrophage populations *in situ* in the CCl<sub>4</sub>-injured liver tissue. Even though the characterization of macrophages in acute liver injury has previously been described, the spatial and temporal distribution of the two major subpopulations, KCs and MoMFs, and their interrelation to one another during the wound-healing response are still unknown. In addition,

previous studies on liver macrophages have relied on F4/80 for tissue visualization, however, this marker does not discriminate between different macrophage subpopulations (10, 19, 25).

We assessed liver macrophages using the KC-specific marker, uniquely expressed by KCs regardless of their origin (YS-KCs vs. bone marrow (BM)-KCs) (13), the C-Type Lectin Domain Family 4 Member F (CLEC4F), and the macrophage activation marker, the ionized calcium-binding adapter molecule 1 (IBA1) (26-28). IBA1/CLEC4F multiplex immunofluorescence (mIF) of liver tissue revealed two distinct subpopulations of macrophages infiltrating the necrotic areas around CVs during acute liver injury: IBA1<sup>+</sup>CLEC4F<sup>+</sup> KCs (CLEC4F<sup>+</sup> KCs) and IBA1<sup>+</sup>CLEC4F<sup>-</sup> macrophages (Figure 4A and Supplementary Figure S4). Quantification of the CLEC4F<sup>+</sup> area showed that KCs were partially depleted during necroinflammation and recovered during repair (Figure 4B) (5, 10). In accordance, qPCR data demonstrated decreased CLEC4F gene expression further confirming KC depletion at necroinflammation and suggesting the death of KCs at this phase given the massive tissue damage revealed at 24 h by ALT levels (Figure 4C).

We further generated tissue heatmaps to provide an overview of the tissue distribution pattern and evolution of these subsets during acute liver injury. Tissue heatmaps of CLEC4F<sup>+</sup> KCs showed shrinkage of densely populated red areas during necroinflammation, consistent with KC partial depletion (Figure 4D, 24 h). Conversely, during repair, starting at 48 h and extending to 96 h, CLEC4F<sup>+</sup> KCs proliferated around healing CVs, as shown by the increasing red spot areas (Figure 4D, 48 h, 72 h, and 96 h), their quantification (Figure 4B) and the upregulated Ki67 expression on these KCs, as shown by the multitude of Ki67<sup>+</sup> nuclei in the area occupied by CLEC4F<sup>+</sup> cells (Figure 4E). Indeed, another support of a proliferative phenotype of CLEC4F<sup>+</sup> cells at repair, is that colocalization of CLEC4F and Ki67 at 48 h around CVs preceded the formation of highly packed clusters of KCs at 72h and 96h post CCl<sub>4</sub> (Figures 4E, F). These aggregates of CV-associated CLEC4F<sup>+</sup> KCs dissipated during the late repair phase (96 h-168 h). Tissue mapping also demonstrated that KCs returned to their normal tissue density and distribution by 168 h post-CCl<sub>4</sub> (Figure 4D, 168 h). It is important to note here that we labeled KCs with the specific marker, CLEC4F, and we essentially observed the same staining pattern as observed in previous studies using F4/80 labeling where KCs are enriched around portal tracts in the steady state (29), but their distribution changes during necroinflammation and tissue repair as shown in Figures 4A, D.

In contrast, IBA1<sup>+</sup>CLEC4F<sup>-</sup> macrophages were absent in the uninjured liver and were recruited in large numbers upon injury (Figure 4G). Tissue heatmaps revealed that infiltrating IBA1<sup>+</sup>CLEC4F<sup>-</sup> macrophages were restricted to the necrotic areas around CVs during necroinflammation and early repair and disappeared by the late repair phase (Figures 4G, H). In summary, resident CLEC4F<sup>+</sup> KCs and infiltrating IBA1<sup>+</sup>CLEC4F<sup>-</sup> macrophages exhibited different kinetics and distinctive distribution patterns supporting the notion of unique roles and division of labor between these two subsets of macrophages. Our staining strategy revealed simultaneously the distribution pattern of the two hepatic macrophage populations at the injury site.

### **The necrotic area during acute liver injury is characterized by distinct temporal distribution and microanatomical localization of CLEC4F<sup>+</sup> KCs and IBA1<sup>+</sup>CLEC4F<sup>-</sup> macrophages**

Given that most of the dynamic changes take place around necrotic CVs, we further characterized CLEC4F<sup>+</sup> KCs and IBA1<sup>+</sup>CLEC4F<sup>-</sup> macrophages in this zone. At steady state, areas around non-injured CVs were populated by resident CLEC4F<sup>+</sup> KCs exhibiting weak to negative IBA1 expression (Figure 5A, 0 h) while IBA1<sup>+</sup>CLEC4F<sup>-</sup> macrophages were absent in the healthy liver. These CLEC4F<sup>+</sup> KCs exhibited the typical sinusoidal location, elongated processes, and scattered distribution of KCs. During necroinflammation (at 24 h), CLEC4F<sup>+</sup> KCs were located primarily in the periphery of the necrotic area, and some of them displayed yellow labeling probably due to the upregulation of IBA1 expression. Concomitantly, IBA1<sup>+</sup>CLEC4F<sup>-</sup> macrophages appeared in this region (Figure 5A, 24 h). These two subsets of macrophages exhibited distinct cell morphologies: stellar-shaped in the case of CLEC4F<sup>+</sup> KCs, and globular in the case of IBA1<sup>+</sup>CLEC4F<sup>-</sup> macrophages (Figure 5A, 24 h). At 48 h, CLEC4F<sup>+</sup> KCs (yellow cells) formed ring-shaped structures in the periphery of clusters of IBA1<sup>+</sup>CLEC4F<sup>-</sup> macrophages (red cells) that filled the inner necrotic area closer to CVs (Figure 5A, 48 h). During early repair, the population of IBA1<sup>+</sup>CLEC4F<sup>-</sup> macrophages was markedly reduced to finally disappear by 96 h to 168 h post CCl<sub>4</sub>. Conversely, dense aggregates of CLEC4F<sup>+</sup> KCs moved closer to the CVs between 72 and 96 h and then dispersed by 168 h post CCl<sub>4</sub> (Figure 5A, 96 h, and 168 h).

Next, we measured the relative area occupied by CLEC4F<sup>+</sup> KCs and IBA1<sup>+</sup>CLEC4F<sup>-</sup> macrophages in the necrotic area (around CVs) between 48 to 96 h post CCl<sub>4</sub> (Figure 5B-E). Our data confirm that IBA1<sup>+</sup>CLEC4F<sup>-</sup> macrophages predominate at the necrotic site during the transition from necroinflammation to tissue repair (48 h post-CCl<sub>4</sub>) and declined during late repair (72 h-96 h post

CCl<sub>4</sub>) (Figures 5B-E). We sought to evaluate the microanatomical localization of these macrophages relative to CV structures, at 48 h post CCl<sub>4</sub>, the time point where both subsets are mostly present. We measured the shortest distance from macrophage nuclei to the CV (>4000 nuclei) and found that IBA1<sup>+</sup>CLEC4F<sup>-</sup> macrophages (red) were closer to CVs than CLEC4F<sup>+</sup> KCs (yellow) at 48 h post CCl<sub>4</sub> (Figures 5F-H) suggesting that the two populations occupy different microanatomical locations. To further define cell-cell interactions, we performed three-dimensional (3D) reconstruction and found that stellar-shaped CLEC4F<sup>+</sup> KCs were in intimate contact with globular IBA1<sup>+</sup>CLEC4F<sup>-</sup> macrophages at 48 h post CCl<sub>4</sub>, demonstrating direct contact and suggesting possible interdependence (Video 1, green (KCs) and yellow (MoMFs) cells). Moreover, globularly shaped IBA1<sup>+</sup> macrophages infiltrated the necrotic/inflammatory area around CV at 24 h post-CCl<sub>4</sub> (Supplementary Figure S5, red arrowheads). Interestingly, hepatocytes with big and round nuclei are visible around CVs at 0 and 24 h (Supplementary Figure S5, white arrowheads) but absent at 48 h post CCl<sub>4</sub>. At this time, enucleated hepatocytes around CVs show particulate material inside, indicating that they are necrotic (Supplementary Figure S5, inset, yellow arrowheads). Furthermore, digital alignment of serial H&E and IBA1 IHC images revealed that IBA1<sup>+</sup> macrophages spatially overlapped with necrotic hepatocytes suggesting that these macrophages may be involved in dismantling the nuclei and phagocytosing dead hepatocytes (Supplementary Figure S5, red arrowheads, 48 h). We also investigated whether these two subpopulations of hepatic macrophages are present in a model of chronic liver injury. We found that the fibrotic liver of 12-week CCl<sub>4</sub>-treated mice was infiltrated by IBA1<sup>+</sup>CLEC4F<sup>-</sup> macrophages and IBA1<sup>+</sup>CLEC4F<sup>+</sup> KCs as observed for CCl<sub>4</sub> acute injury (Supplementary Figure S6). In summary, resident CLEC4F<sup>+</sup> KCs and infiltrating IBA1<sup>+</sup>CLEC4F<sup>-</sup> macrophages occupied most of the necrotic area around CVs, suggesting that they may be critical players in the wound healing response to acute injury. These two hepatic macrophage subpopulations differed in their kinetics, phenotype, cell morphology, and microanatomical tissue location.

### **CV-associated IBA1<sup>+</sup>CLEC4F<sup>-</sup> macrophages exhibit characteristics of MoMFs**

The kinetics of IBA1<sup>+</sup>CLEC4F<sup>-</sup> macrophages in the tissue as determined by mIF (Figure 4G), mirrored the kinetics of Ly6C<sup>+</sup> CX3CR1<sup>+</sup> MoMFs as determined by flow cytometry (Figure 3F). In addition, IBA1<sup>+</sup>CLEC4F<sup>-</sup> macrophages did not express the KC marker CLEC4F and were absent in the non-injured liver (Figures 4G, H) (5). Consequently, we hypothesized that the

IBA1<sup>+</sup>CLEC4F<sup>-</sup> macrophages are MoMFs specially recruited to the necrotic tissue in response to injury. Indeed, our additional mIF analysis of liver tissues demonstrated that IBA1<sup>+</sup>CLEC4F<sup>-</sup> cells recruited to the necrotic/inflammatory area around CV at 48 h post-CCl<sub>4</sub> expressed CX3CR1 and the monocytic marker CCR2 (Figure 6A). Consistent with this, our flow cytometry analysis of intrahepatic myeloid IBA1<sup>+</sup> cells showed that this population is expanded at 48 h post CCl<sub>4</sub> compared to controls and expressed the MoMF-associated markers, Ly6C and CX3CR1, as well as the proliferation marker Ki67 (Figure 6B) (5, 6). To rule out the possibility that these IBA1<sup>+</sup>CLEC4F<sup>-</sup> macrophages are of peritoneal origin, we assessed their GATA6 expression, given that F4/80hi GATA6<sup>+</sup> peritoneal macrophages could infiltrate the liver and locate to the centrilobular area in the CCl<sub>4</sub> model (3). Serial labeling and digital tissue alignment of GATA6 and IBA1 staining showed that most CV-associated IBA1<sup>+</sup> macrophages do not express GATA6 (Figure 6C). Collectively, these observations strongly suggest that IBA1<sup>+</sup>CLEC4F<sup>-</sup> macrophages are MoMFs, which are recruited to the necrotic/inflammatory area around CV in response to injury.

#### **CLEC4F<sup>+</sup> KCs of yolk sac origin replenish the hepatic macrophage pool during tissue repair**

Landmark studies have shown that, under physiological conditions, YS-KCs self-maintain independently of circulating progenitors (7, 12). However, in response to injury, opposing results have been reported as to the capacity of monocyte/MoMFs to differentiate into BM-KCs and replace the dead resident YS-KCs (5, 10, 11, 30). Lineage tracing experiments using the APAP-, highly homologous to ours herein, and the radiation-induced hepatic injury models revealed MARCO as a specific marker of YS-KCs and completely absent on infiltrating monocytes or MoMFs (5, 10). Moreover, MARCO was shown to be the marker defining one of the two major subpopulations of resident hepatic macrophages in humans (31). Further support of this notion is the finding identifying *bona fide* KCs across species and revealing that MARCO is expressed by KCs in uninjured livers of pigs, macaques, hamsters, chickens, and zebrafish (152). Thus, to identify the origin of CLEC4F<sup>+</sup> KCs replenishing the KC pool during repair, we used MARCO as the marker of YS-KCs (5, 10, 11). YS-KCs are identified as CLEC4F<sup>+</sup> MARCO<sup>+</sup> while BM-KCs are CLEC4F<sup>+</sup> MARCO<sup>-</sup>. Multiplexing CLEC4F with MARCO showed that CLEC4F<sup>+</sup> KCs are MARCO<sup>+</sup> at all time points examined, from the steady state (Figure 7A) until the late repair phase when the KC pool was replenished (Figures 7B, D). This finding suggests that virtually all KCs

that repopulated the hepatic tissue during repair are of yolk sac origin. Visual inspection showed that the small percentage of CLEC4F<sup>+</sup> MARCO<sup>-</sup> cells (~5%) could be attributed to suboptimal MARCO staining since the signal was weak but present. In addition, we performed digital image alignment of consecutive serial sections and demonstrated that there was no spatial overlap between IBA1<sup>+</sup> macrophages, in direct contact with CVs, and MARCO<sup>+</sup> cells suggesting that IBA1<sup>+</sup>CLEC4F<sup>-</sup> macrophages around CVs are MARCO<sup>-</sup>, and thus are not YS-derived (Figures 7B, C, insets), but rather monocyte-derived. In summary, these observations suggest that the original YS-KCs that die during necroinflammation are replaced by the proliferation of the remaining YS-KCs (CLEC4F<sup>+</sup> MARCO<sup>+</sup>) around the CVs.

### **IBA1<sup>+</sup>CLEC4F<sup>-</sup> macrophages are in closer contact with activated hepatic stellate cells than CLEC4F<sup>+</sup> KCs**

Activated HSCs (aHSCs) are positive for alpha-smooth muscle actin ( $\alpha$ SMA<sup>+</sup>) and are the main source of ECM proteins in self-resolving liver inflammation and fibrosis (33, 34). While all HSCs in mice are Desmin<sup>+</sup>, only aHSCs are  $\alpha$ SMA<sup>+</sup> (35). Several studies have supported the notion that both MoMFs and KCs can activate HSCs (34). Indeed, 3D reconstruction showed that  $\alpha$ SMA<sup>+</sup> aHSCs wrapped themselves around both CLEC4F<sup>+</sup> KCs and IBA1<sup>+</sup>CLEC4F<sup>-</sup> MoMFs suggesting that either macrophage subpopulation could be the source of activating signals (Video 1 in Supplementary information). To further dissect the role of these subsets and evaluate their relative contribution to the activation of HSCs and the kinetics involved, we first analyzed the colocalization of CLEC4F<sup>+</sup> KCs and Desmin<sup>+</sup> HSCs. We observed that HSCs are in direct contact with resident CLEC4F<sup>+</sup> KCs in the steady state (Figure 8A). Some degree of direct contact was observed at all time points post-CCl<sub>4</sub> (Figure 8A). Since there are no infiltrating IBA1<sup>+</sup>CLEC4F<sup>-</sup> macrophages in the uninjured liver, we reasoned that the early activating signals of HSCs upon injury are most likely originating from colocalized CLEC4F<sup>+</sup> KCs.

Next, we established the kinetics of tissue repair as demonstrated by upregulation of the pro-fibrogenic markers TGF $\beta$ , ACTA-2, and collagen between 48-72 h (Figure 8B). This was associated with HSC activation at 48 h post CCl<sub>4</sub> as demonstrated by their increased expression of  $\alpha$ SMA (Figure 8C). At this time point, infiltrating IBA1<sup>+</sup> CLEC4F<sup>-</sup> macrophages colocalized with  $\alpha$ SMA<sup>+</sup> aHSCs to a larger extent than resident CLEC4F<sup>+</sup> KCs, suggesting that this population may be a more significant source of HSC activating signals in the necrotic tissue (Figures 8D, E).

Furthermore, we characterized the inflammatory and pro-resolving profiles of intrahepatic IBA1<sup>+</sup> myeloid cells by flow cytometry. Our data show that they exhibit upregulated levels of TNF $\alpha$ , IL-13, IL-10, and Arg-1 at 48 h post CCl<sub>4</sub> compared to controls, supporting their potential role in modulating the activation and deactivation states of colocalized HSCs (Figure 8F). Collectively, these data suggest that resident CLEC4F<sup>+</sup> KCs may provide early activating signals to colocalized HSCs, which then become motile and migrate to the CV necrotic area where they interact with IBA1<sup>+</sup>CLEC4F<sup>-</sup> macrophages to acquire a fully activated phenotype.

## **Discussion**

While bulk and single-cell transcriptomics have provided a wealth of knowledge on the different subpopulations of hepatic macrophages and their phenotypes and roles during homeostasis and disease, their spatial behavior and cell-cell interactions in the tissue remain to be defined. We examined the spatial distribution of subpopulations of liver macrophages and their temporal association with other immune and non-immune hepatic cells in the context of the wound-healing response to acute liver injury. Our study is dissecting the kinetics and tissue spatial distribution of hepatic macrophages, namely KCs and MoMFs in response to acute liver injury. Mapping the position of these two subpopulations of macrophages relative to one another was essential for the characterization of their neighboring yet different microanatomical niches, highly suggesting non-overlapping functions for each population.

By examining the immune signatures during the response to an acute liver injury, our flow cytometry analysis showed that liver resident immune populations decreased during necroinflammation but recovered during tissue repair, including KCs, B, T, and NKT cells. Conversely, circulating myeloid cells including neutrophils, monocytes, and MoMFs, massively infiltrated the liver during necroinflammation and progressively declined during repair. We observed two different waves of infiltrating neutrophils during necroinflammation and repair. Since neutrophils do not proliferate in the liver, these two waves are likely the result of two independent recruitment events, probably modulating different effector functions of neutrophils at different phases of the wound healing response to acute liver injury (36). Indeed, while a pro-inflammatory profile has been attributed to neutrophils via their production of reactive oxygen species (ROS) and cytokines such as IL-1 $\beta$  and TNF- $\alpha$ , a pro-repair function has also been



assigned to these cells in their response to liver damage (37-39). The exact role of neutrophils in the different phases of liver wound repair should be defined in future studies.

MoMFs became the predominant phagocyte population during the transition from necroinflammation to early repair, in agreement with the current view that these macrophages are highly plastic cells and experience *in situ* switching from an inflammatory to a pro-restorative phenotype (6, 10). This observation supports the notion of MoMFs as dual effectors of inflammation and repair and may explain the divergent outcomes of MoMF depletion during necroinflammation versus repair in different injury models (6, 10, 40-42). Using mIF, we identified two subsets of hepatic macrophages: resident CLEC4F<sup>+</sup> KCs and infiltrating IBA1<sup>+</sup>CLEC4F<sup>-</sup> macrophages, with multiple evidence indicating that the latter is a subset of MoMFs. Since together CLEC4F<sup>+</sup> KCs and IBA1<sup>+</sup>CLEC4F<sup>-</sup> MoMFs occupied most of the necrotic area, they are arguably the predominant macrophage subsets in the response to CCl<sub>4</sub> toxicity, directly suggesting their functional relevance. By further investigating the kinetics and spatial distribution of these subsets, our data demonstrate that while the KC population was partially depleted during necroinflammation and recovered at repair, MoMFs behaved contrariwise in these disease phases. Previous studies have also described these macrophage populations at the injury site in liver disease (43-45), but at the individual level and without further characterization of their distribution in time and space. Characterization of MoMFs using the acute model of sterile hepatic injury detected the classical CCR2<sup>hi</sup>/CX3CR1<sup>-</sup> monocytes at the site of injury as early as 8 h post-injury. Subsequently, at 48h post-injury, these monocytes differentiated into MoMFs in a process that involved upregulation of CX3CR1 and downregulation of CCR2 and LyC. However, this study did not examine the kinetics and distribution of the other major macrophage subpopulation, KCs, and the model used lacked the zoned injury pattern observed in intoxication-induced acute liver injury (6). On the other hand, in the APAP acute injury model, Zigmond et al used flow cytometry to show that KCs are depleted during necroinflammation and recover during the resolution/repair phase by self-renewal with no contribution from circulating Ly6C<sup>hi</sup> inflammatory monocytes (10). Our study expanded these observations by using tissue imaging where we demonstrate the overall spatial behavior of KCs during the healing response to acute liver injury and showed the specific location of KCs around CVs where KCs proliferated during tissue repair. Furthermore, we show that depletion of KCs at the early response phase is followed by the invasion of MoMFs into the site of injury, supporting the notion that signals generated upon activation and depletion of KCs

initiate the recruitment of circulatory monocytes and their differentiation into what is known as restorative macrophage population, herein MoMFs (46, 47). Our further spatial evaluation of these subpopulations revealed distinct microanatomical locations, with MoMFs filling the inner necrotic areas and KCs surrounding them. Other papers, rather than investigating chronic models of liver injuries, have imaged the spatial behavior of KCs or MoMFs but at the individual level and with no reference to the disease stage (6, 11, 19, 32, 48). In addition, most of the tissue work done on acute liver injury has relied on markers that do not allow the proper differentiation of the different macrophage subpopulations like MoMFs, peritoneal macrophages, liver capsular macrophages and resident KCs (e.g., F4/80) (10, 19), while we used in our study more specific markers defined using multiomic technologies (e.g., CLEC4F, GATA6, MARCO) (2, 5, 10, 13). Thus, our observations expand knowledge as to the contribution of hepatic macrophages to liver injury by showing that, during repair, CLEC4F<sup>+</sup> KCs proliferated around healed CVs from where they seemed to have radiated outwards and colonized the partially depleted surrounding areas. Steady state KCs, broadly assumed to be sessile, become thus motile during late repair to move from the CV-associated clusters to the surrounding sinusoidal regions and re-establish the homeostatic density (9, 44).

Fate mapping approaches have revealed that resident YS-KCs persist in the tissue by self-renewal, independently of monocytic hematopoietic progenitors in the steady state (4, 7). However, contradictory reports exist on the capacity of inflammatory monocytes/MoMFs to differentiate into tissue-resident macrophages (BM-KCs) in response to injury and replace the original YS-KCs (5, 10, 11, 13, 30). Here, we demonstrated that CLEC4F<sup>+</sup> KCs that repopulated the liver during tissue repair were yolk sac derived, while MoMFs were not. This suggests that even in the presence of significant tissue damage and KC death, the remaining original YS-KCs retained an advantage over other macrophage populations in terms of replenishing the KC pool. Our results support the emergent view that the generation of BM-KCs depends on niche availability, which is not equal in different injury models, and only models with extensive KC depletion make the niche available for engraftment of infiltrating monocytes/MoMFs (5, 10, 11, 13, 30). Indeed, the repopulation of KCs in the KC-Diphtheria toxin receptor (DTR) mouse model involved the contribution of circulatory monocytes (48). Diphtheria toxin in such a model induced a 100 % depletion of KCs so there are no KCs left to replenish the niche. On the other hand, following our findings, the

APAP liver injury model, where KCs were partially depleted, lineage tracing showed that KCs of yolk sac origin replenish the KC compartment independently of bone marrow-derived cells (10).

Activation of HSCs is a major step in the repair processes during acute liver injury and fibrosis development under chronic injuries (49, 50). Activated HSCs assume a myofibroblast phenotype, upregulating expression of  $\alpha$ SMA and releasing extracellular matrix proteins, including collagen (51). Previous studies have found that both KCs and MoMFs can activate HSCs, but the relative individual contribution and kinetics are still unknown. We took advantage of simultaneous visualization of CLEC4F<sup>+</sup> KCs and IBA1<sup>+</sup>CLEC4F<sup>-</sup> MoMFs to gain insight into the individual contribution of these subsets to HSC activation. We demonstrated that quiescent Desmin<sup>+</sup> $\alpha$ SMA<sup>-</sup> HSCs were in direct contact with KCs in the steady state making the resident macrophages the most likely source of initial activating signals upon damage as previously reported (48). Indeed, KCs are important activators of HSCs via the release of pro-inflammatory mediators and growth factors (43, 52). Through their release of reactive oxygen species, and IL-6 induction KCs were shown to contribute to HSC activation and fibrogenic differentiation (53). KCs are also one of the sources of the major fibrogenic cytokine TGF- $\beta$  (54, 55). Indeed, our data also demonstrated the upregulation of TGF- $\beta$  concomitantly with an activated state of HSCs. As the response to injury progressed,  $\alpha$ SMA<sup>+</sup> aHSCs further colocalized with MoMFs as compared to KCs, in line with previous work showing that recruited macrophages also contribute to the activation of HSCs and, ultimately, fibrosis (56). These results are consistent with a division of labor between these macrophage subsets, where KCs provide early activating signals to colocalized HSCs that may induce their motility and migration into the necrotic zone. Once in this region, monocyte-derived macrophages are likely the major source of the remaining signals that induce the fully activated phenotype observed at 48 h post CCl<sub>4</sub>.

In summary, we showed that CLEC4F<sup>+</sup> KCs and IBA1<sup>+</sup>CLEC4F<sup>-</sup> MoMFs are the predominant hepatic macrophages during CCl<sub>4</sub>-mediated acute liver injury. These two subpopulations exhibited different origins and morphology, infiltrated the necrotic area at different times, and occupied neighboring but unique microanatomical locations. Newly generated KCs proliferated around CVs and colonized the surrounding tissue, whereas infiltrating MoMFs was transient and did not contribute to the replenishment of the KC pool in the liver. Lastly, while KCs colocalized with HSCs in steady-state conditions, MoMFs were responsible for activating HSCs during liver injury,

enhancing their pro-repair functions, and initiating the healing process. Future studies investigating the underlying mechanism(s) are warranted.

### **Authors' Contributions**

M.F.M. substantially contributed to the conception and design of the study, the undertaking of experiments, and the acquisition, analysis, and interpretation of data. He drafted the article and participated in its critical revision for important intellectual content. M.N.A., S.M., Sh.M., and D.O. contributed to the undertaking of experiments and the acquisition, analysis, and interpretation of data. D.V.-B., V.Q.H.T., N.B., and A.D.P. contributed to the acquisition, analysis, and interpretation of data. G.S.H. contributed to writing the article and revising it critically for important intellectual content. N.H.S., the corresponding author, substantially contributed to the conception and design of the study and the critical revision of the article for important intellectual content. She is responsible for the acquisition of funding. All authors approved the final version of the manuscript.

### **Funding**

This study was funded by research grants from the Canadian Liver Foundation and the Canadian Institutes of Health Research (CIHR) (PJ4-169659 and PJT-175134). MFM received a doctoral fellowship from the Fonds de Recherche du Québec-Santé (FRQ-S). MNA received the bourse d'exemption des droits de scolarité supplémentaires from the Université de Montréal and a doctoral fellowship from the Canadian Network on Hepatitis C (CanHepC). CanHepC is funded by a joint initiative of the CIHR and the Public Health Agency of Canada (HPC-178912). S.M. received a doctoral fellowship from CanHepC.

### **Acknowledgments**

We acknowledge the following CRCHUM platforms for excellent technical assistance: animal facility, molecular pathology, microscopy, and flow cytometry. We also thank Rainer Gangnus and Regan Baird from Visiopharm for their technical insights and assistance.

## **Data availability statement**

The original contributions presented in the study are included in the article/Supplementary Material, further inquiries can be directed to the corresponding author/s.

## **Ethics statement**

The animal study was reviewed and approved by the Institutional Animal Care and Use Committee at the CRCHUM.

## **References**

1. Krenkel O, Tacke F. Liver macrophages in tissue homeostasis and disease. *Nat Rev Immunol.* 2017;17(5):306-21.
2. Sierro F, Evrard M, Rizzetto S, Melino M, Mitchell AJ, Florido M, et al. A Liver Capsular Network of Monocyte-Derived Macrophages Restricts Hepatic Dissemination of Intraperitoneal Bacteria by Neutrophil Recruitment. *Immunity.* 2017;47(2):374-88.e6.
3. Wang J, Kubes P. A Reservoir of Mature Cavity Macrophages that Can Rapidly Invade Visceral Organs to Affect Tissue Repair. *Cell.* 2016;165(3):668-78.
4. Yona S, Kim KW, Wolf Y, Mildner A, Varol D, Breker M, et al. Fate mapping reveals origins and dynamics of monocytes and tissue macrophages under homeostasis. *Immunity.* 2013;38(1):79-91.
5. Beattie L, Sawtell A, Mann J, Frame TCM, Teal B, de Labastida Rivera F, et al. Bone marrow-derived and resident liver macrophages display unique transcriptomic signatures but similar biological functions. *J Hepatol.* 2016;65(4):758-68.

6. Dal-Secco D, Wang J, Zeng Z, Kolaczowska E, Wong CH, Petri B, et al. A dynamic spectrum of monocytes arising from the in situ reprogramming of CCR2<sup>+</sup> monocytes at a site of sterile injury. *J Exp Med*. 2015;212(4):447-56.
7. Gomez Perdiguero E, Klapproth K, Schulz C, Busch K, Azzoni E, Crozet L, et al. Tissue-resident macrophages originate from yolk-sac-derived erythro-myeloid progenitors. *Nature*. 2015 ;518(7540) :547-51.
8. Ramachandran P, Pellicoro A, Vernon MA, Boulter L, Aucott RL, Ali A, et al. Differential Ly-6C expression identifies the recruited macrophage phenotype, which orchestrates the regression of murine liver fibrosis. *Proc Natl Acad Sci U S A*. 2012;109(46): E3186-95.
9. Klein I, Cornejo JC, Polakos NK, John B, Wuensch SA, Topham DJ, et al. Kupffer cell heterogeneity: functional properties of bone marrow derived and sessile hepatic macrophages. *Blood*. 2007;110(12):4077-85.
10. Zigmond E, Samia-Grinberg S, Pasmanik-Chor M, Brazowski E, Shibolet O, Halpern Z, et al. Infiltrating monocyte-derived macrophages and resident Kupffer cells display different ontogeny and functions in acute liver injury. *J Immunol*. 2014 ;193(1) :344-53.
11. David BA, Rezende RM, Antunes MM, Santos MM, Freitas Lopes MA, Diniz AB, et al. Combination of Mass Cytometry and Imaging Analysis Reveals Origin, Location, and Functional Repopulation of Liver Myeloid Cells in Mice. *Gastroenterology*. 2016;151(6):1176-91.
12. Hoeffel G, Chen J, Lavin Y, Low D, Almeida FF, See P, et al. C-Myb (+) erythro-myeloid progenitor-derived fetal monocytes give rise to adult tissue-resident macrophages. *Immunity*. 2015;42(4):665-78.
13. Scott CL, Zheng F, De Baetselier P, Martens L, Saeys Y, De Prijck S, et al. Bone marrow-derived monocytes give rise to self-renewing and fully differentiated Kupffer cells. *Nat Commun*. 2016 ;7:10321.

14. Yang W, Tao Y, Wu Y, Zhao X, Ye W, Zhao D, et al. Neutrophils promote the development of reparative macrophages mediated by ROS to orchestrate liver repair. *Nat Commun.* 2019;10(1):1076.
15. Yanguas SC, Cogliati B, Willebrords J, Maes M, Colle I, van den Bossche B, et al. Experimental models of liver fibrosis. *Archives of toxicology.* 2016;90(5):1025-48.
16. Flores Molina M, Fabre T, Cleret-Buhot A, Soucy G, Meunier L, Abdelnabi MN, et al. Visualization, Quantification, and Mapping of Immune Cell Populations in the Tumor Microenvironment. *J Vis Exp.* 2020(157).
17. Van Gassen S, Callebaut B, Van Helden MJ, Lambrecht BN, Demeester P, Dhaene T, et al. FlowSOM: Using self-organizing maps for visualization and interpretation of cytometry data. *Cytometry A.* 2015;87(7):636-45.
18. Kolodziejczyk AA, Federici S, Zmora N, Mohapatra G, Dori-Bachash M, Hornstein S, et al. Acute liver failure is regulated by MYC- and microbiome-dependent programs. *Nat Med.* 2020;26(12):1899-911.
19. Graubardt N, Vugman M, Mouhadeb O, Caliarì G, Pasmanik-Chor M, Reuveni D, et al. Ly6C(hi) Monocytes and Their Macrophage Descendants Regulate Neutrophil Function and Clearance in Acetaminophen-Induced Liver Injury. *Front Immunol.* 2017; 8:626.
20. Guilliams M, Mildner A, Yona S. Developmental and Functional Heterogeneity of Monocytes. *Immunity.* 2018;49(4):595-613.
21. Alkhani A, Levy CS, Tsui M, Rosenberg KA, Polovina K, Mattis AN, et al. Ly6c(Lo) non-classical monocytes promote resolution of rhesus rotavirus-mediated perinatal hepatic inflammation. *Sci Rep.* 2020;10(1):7165.

22. Auffray C, Fogg D, Garfa M, Elain G, Join-Lambert O, Kayal S, et al. Monitoring of blood vessels and tissues by a population of monocytes with patrolling behavior. *Science*. 2007;317(5838):666-70.
23. Wang J, Hossain M, Thanabalasuriar A, Gunzer M, Meininger C, Kubes P. Visualizing the function and fate of neutrophils in sterile injury and repair. *Science*. 2017;358(6359):111-6.
24. Narasimhan PB, Marcovecchio P, Hamers AAJ, Hedrick CC. Nonclassical Monocytes in Health and Disease. *Annu Rev Immunol*. 2019; 37:439-56.
25. Dos Anjos Cassado A. F4/80 as a Major Macrophage Marker: The Case of the Peritoneum and Spleen. *Results Probl Cell Differ*. 2017; 62:161-79.
26. Yang CY, Chen JB, Tsai TF, Tsai YC, Tsai CY, Liang PH, et al. CLEC4F is an inducible C-type lectin in F4/80-positive cells and is involved in alpha-galactosylceramide presentation in liver. *PLoS One*. 2013;8(6): e65070.
27. Ito D, Imai Y, Ohsawa K, Nakajima K, Fukuuchi Y, Kohsaka S. Microglia-specific localization of a novel calcium binding protein, Iba1. *Brain Res Mol Brain Res*. 1998;57(1):1-9.
28. Kohler C. Allograft inflammatory factor-1/Ionized calcium-binding adapter molecule 1 is specifically expressed by most subpopulations of macrophages and spermatids in testis. *Cell Tissue Res*. 2007;330(2):291-302.
29. Gola A, Dorrington MG, Speranza E, Sala C, Shih RM, Radtke AJ, et al. Commensal-driven immune zonation of the liver promotes host defence. *Nature*. 2021;589(7840):131-6.
30. Lavin Y, Winter D, Blecher-Gonen R, David E, Keren-Shaul H, Merad M, et al. Tissue-resident macrophage enhancer landscapes are shaped by the local microenvironment. *Cell*. 2014 ;159(6) :1312-26.



31. MacParland SA, Liu JC, Ma XZ, Innes BT, Bartczak AM, Gage BK, et al. Single cell RNA sequencing of human liver reveals distinct intrahepatic macrophage populations. *Nature communications*. 2018 ;9(1) :4383.
32. Williams M, Bonnardel J, Haest B, Vanderborght B, Wagner C, Remmerie A, et al. Spatial proteogenomics reveals distinct and evolutionarily conserved hepatic macrophage niches. *Cell*. 2022.
33. Mederacke I, Hsu CC, Troeger JS, Huebener P, Mu X, Dapito DH, et al. Fate tracing reveals hepatic stellate cells as dominant contributors to liver fibrosis independent of its aetiology. *Nature communications*. 2013; 4:2823.
34. Tsuchida T, Friedman SL. Mechanisms of hepatic stellate cell activation. *Nat Rev Gastroenterol Hepatol*. 2017;14(7):397-411.
35. Guido M, Rugge M, Leandro G, Fiel IM, Thung SN. Hepatic stellate cell immunodetection and cirrhotic evolution of viral hepatitis in liver allografts. *Hepatology*. 1997;26(2):310-4.
36. Capucetti A, Albano F, Bonecchi R. Multiple Roles for Chemokines in Neutrophil Biology. *Front Immunol*. 2020 ; 11 :1259.
37. Xu R, Huang H, Zhang Z, Wang FS. The role of neutrophils in the development of liver diseases. *Cell Mol Immunol*. 2014;11(3):224-31.
38. Heymann F, Tacke F. Immunology in the liver--from homeostasis to disease. *Nat Rev Gastroenterol Hepatol*. 2016;13(2):88-110.
39. Guillot A, Tacke F. The Unexpected Role of Neutrophils for Resolving Liver Inflammation by Transmitting MicroRNA-223 to Macrophages. *Hepatology*. 2020;71(2):749-51.

40. Karlmark KR, Weiskirchen R, Zimmermann HW, Gassler N, Ginhoux F, Weber C, et al. Hepatic recruitment of the inflammatory Gr1<sup>+</sup> monocyte subset upon liver injury promotes hepatic fibrosis. *Hepatology*. 2009;50(1):261-74.
41. Aoyama T, Inokuchi S, Brenner DA, Seki E. CX3CL1-CX3CR1 interaction prevents carbon tetrachloride-induced liver inflammation and fibrosis in mice. *Hepatology*. 2010;52(4):1390-400.
42. Duffield JS, Forbes SJ, Constandinou CM, Clay S, Partolina M, Vuthoori S, et al. Selective depletion of macrophages reveals distinct, opposing roles during liver injury and repair. *J Clin Invest*. 2005;115(1):56-65.
43. Wen Y, Lambrecht J, Ju C, Tacke F. Hepatic macrophages in liver homeostasis and diseases-diversity, plasticity and therapeutic opportunities. *Cell Mol Immunol*. 2021;18(1):45-56.
44. Blériot C, Ginhoux F. Understanding the Heterogeneity of Resident Liver Macrophages. *Front Immunol*. 2019; 10:2694.
45. Shan Z, Ju C. Hepatic Macrophages in Liver Injury. *Front Immunol*. 2020; 11:322.
46. Tacke F, Zimmermann HW. Macrophage heterogeneity in liver injury and fibrosis. *J Hepatol*. 2014;60(5):1090-6.
47. Ramachandran P, Iredale JP, Fallowfield JA. Resolution of liver fibrosis: basic mechanisms and clinical relevance. *Semin Liver Dis*. 2015 ;35(2) :119-31.
48. Bonnardel J, T'Jonck W, Gaublonne D, Browaeys R, Scott CL, Martens L, et al. Stellate Cells, Hepatocytes, and Endothelial Cells Imprint the Kupffer Cell Identity on Monocytes Colonizing the Liver Macrophage Niche. *Immunity*. 2019;51(4):638-54. e9.
49. Fujita T, Narumiya S. Roles of hepatic stellate cells in liver inflammation: a new perspective. *Inflamm Regen*. 2016; 36:1.

50. Cai X, Wang J, Wang J, Zhou Q, Yang B, He Q, et al. Intercellular crosstalk of hepatic stellate cells in liver fibrosis: New insights into therapy. *Pharmacol Res.* 2020; 155:104720.
51. Gandhi CR. Hepatic stellate cell activation and pro-fibrogenic signals. *J Hepatol.* 2017;67(5):1104-5.
52. Cai B, Dongiovanni P, Corey KE, Wang X, Shmarakov IO, Zheng Z, et al. Macrophage MerTK Promotes Liver Fibrosis in Nonalcoholic Steatohepatitis. *Cell Metab.* 2020;31(2):406-21 e7.
53. Nieto N. Oxidative-stress and IL-6 mediate the fibrogenic effects of [corrected] Kupffer cells on stellate cells. *Hepatology.* 2006;44(6):1487-501.
54. Nakatsukasa H, Nagy P, Evarts RP, Hsia CC, Marsden E, Thorgeirsson SS. Cellular distribution of transforming growth factor-beta 1 and procollagen types I, III, and IV transcripts in carbon tetrachloride-induced rat liver fibrosis. *J Clin Invest.* 1990;85(6):1833-43.
55. Hernandez-Gea V, Friedman SL. Pathogenesis of liver fibrosis. *Annual review of pathology.* 2011; 6:425-56.
56. Krenkel O, Puengel T, Govaere O, Abdallah AT, Mossanen JC, Kohlhepp M, et al. Therapeutic inhibition of inflammatory monocyte recruitment reduces steatohepatitis and liver fibrosis. *Hepatology.* 2018;67(4):1270-83.

## Figures

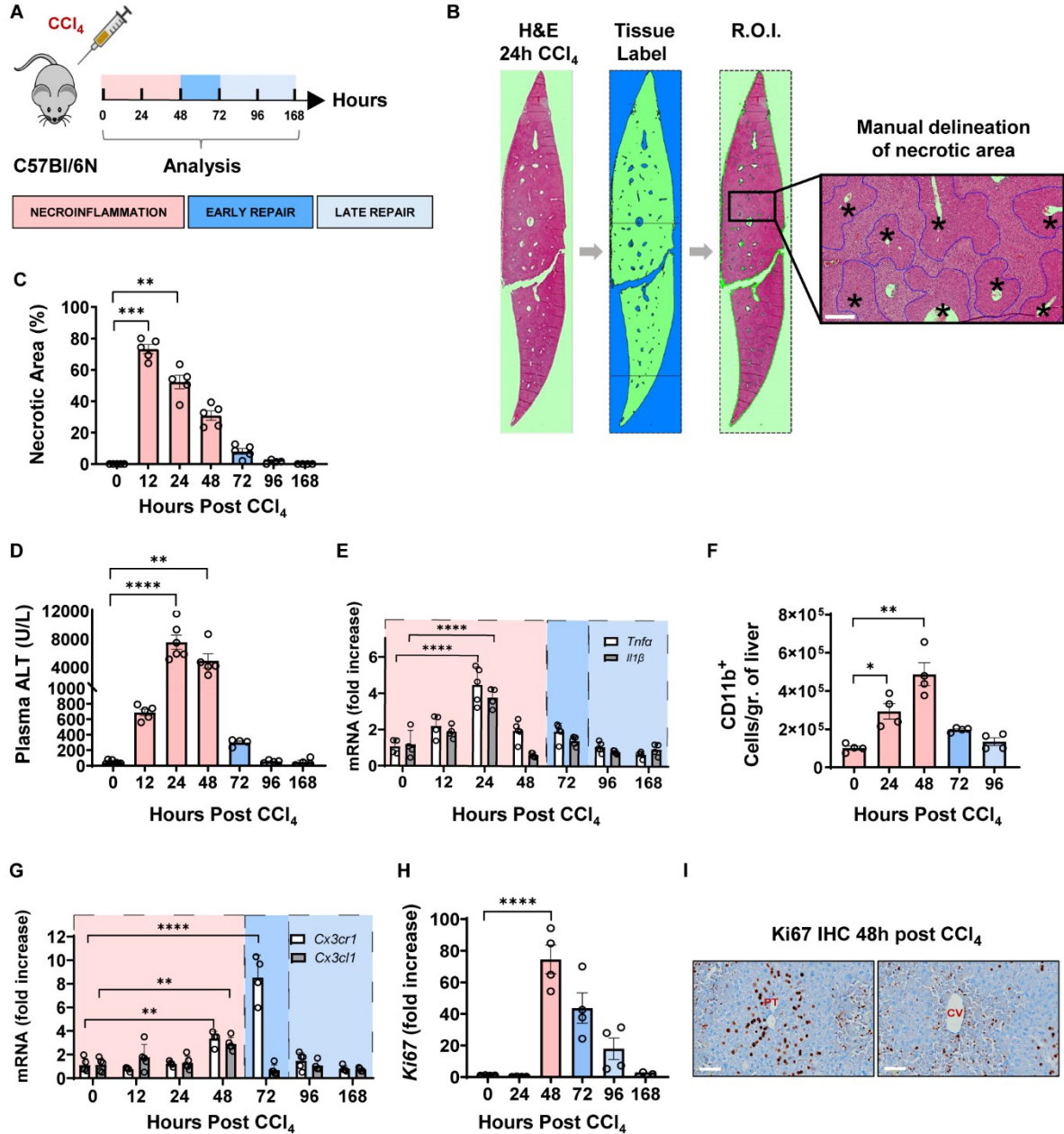


**Figure 1:** *CCl<sub>4</sub>-induced acute liver injury is characterized by a necroinflammatory phase followed, at 48 h post-injury, by an early tissue repair phase and then a late one from 72 hours onward.* (A) Schematics of the experimental design delineating the phases of the wound healing response to one intraperitoneal injection of *CCl<sub>4</sub>* at 1 $\mu$ L/g of body weight. (B) Representative H&E image of one whole liver section covering at least the total surface area of a transverse section of one entire lobe per mouse, at 24 h following *CCl<sub>4</sub>* injection. The necrotic area was delineated

manually around CV as outlined in blue, scale bar=200  $\mu\text{m}$ , \* indicates CV. (C) Percentage of the necrotic area within the total tissue area. (D) Plasma ALT levels. (E) Relative gene expression levels of *Tnf- $\alpha$*  and *Il-1 $\beta$*  determined by qPCR on bulk liver tissue. The mRNA expression data represent fold increase relative to 0 h controls and was normalized to 28s. (F) Kinetics of recruitment of intrahepatic myeloid cells as determined by flow cytometry. (G) Relative gene expression levels of *Cx3cr1* and *Cx3cl1* were determined by qPCR on the bulk liver. (H) Relative gene expression levels of *Ki67* determined by qPCR on the bulk liver. (I) Representative *Ki67* immunohistochemistry images from liver sections of 48 h  $\text{CCl}_4$ -treated mouse showing *Ki67* staining around portal tracts (PT) on the left and CVs on the right, scale bar 75  $\mu\text{m}$ . N=4-5 mice per group. Data are shown as mean  $\pm$  SEM. Statistical analysis was performed using one Way ANOVA and Dunn's Multiple Comparison Test. \* $P < 0.05$ , \*\* $P < 0.01$ , \*\*\* $P < 0.001$ .

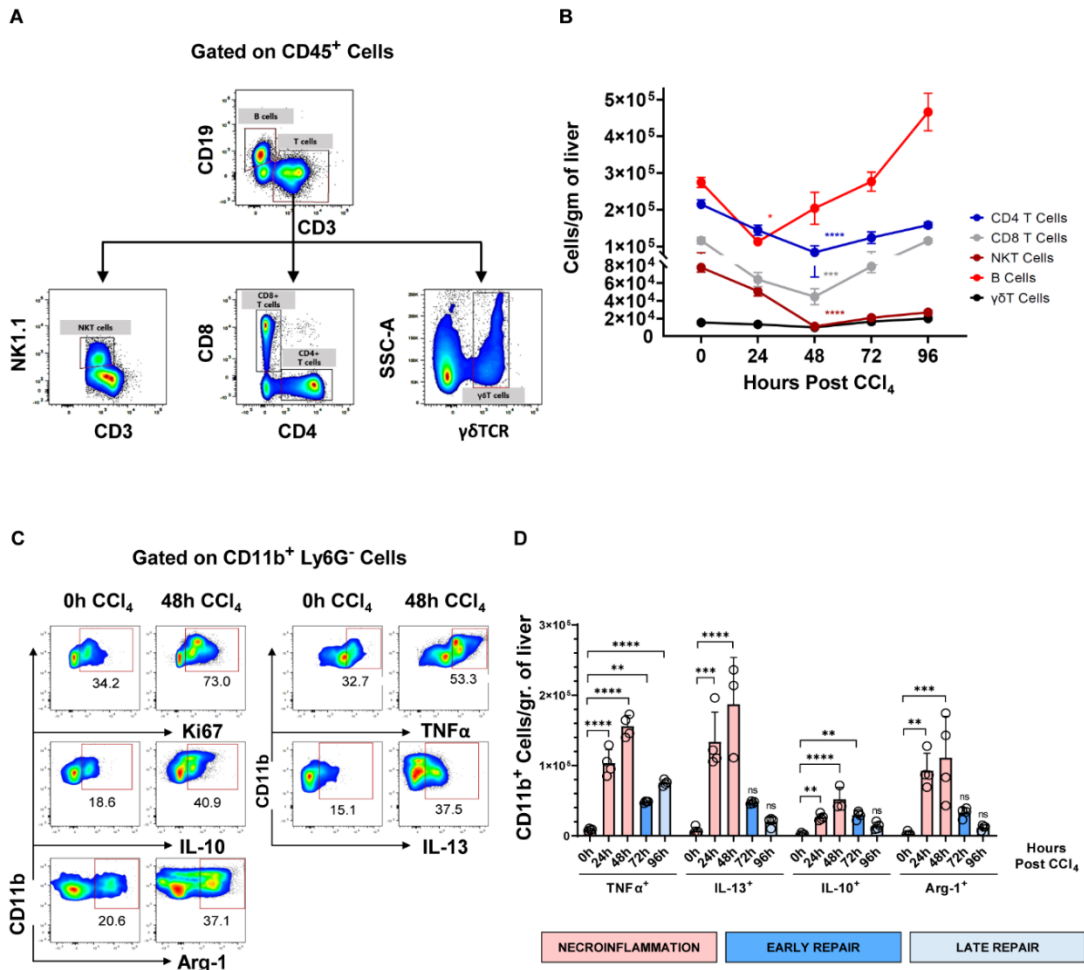


**Figure 2: Hepatic resident lymphocytes are partially depleted during the necroinflammatory phase and recover during the tissue repair phase of CCl<sub>4</sub>-mediated acute liver injury, while intrahepatic myeloid cells respond by inflammatory mediators' release. (A) Gating strategy for flowcytometric analysis of intrahepatic lymphocytes, gated on live CD45<sup>+</sup> lymphocytes. (B) Kinetics of the main hepatic resident lymphocyte populations following one single intraperitoneal injection of CCl<sub>4</sub> at 1μL/g of body weight. (C) Representative pseudocolor plots of analysis spontaneous production of different immune mediators by intrahepatic myeloid cells treated for 6h with BFA and monensin, presented as frequencies of CD11b<sup>+</sup> Ly6G<sup>-</sup> cells. (D) Expression of TNFα, IL-10, IL-13, and Arg-1 normalized to the number of CD11b<sup>+</sup> myeloid cells/gr of liver during the different phases of the response to CCl<sub>4</sub>-mediated acute liver injury. N=4-5 mice per group. Data are shown as mean ± SEM. Statistical analysis was performed using One Way ANOVA and Dunn's Multiple Comparison Test. \*P < 0.05, \*\*P < 0.01, \*\*\*P < 0.001.**

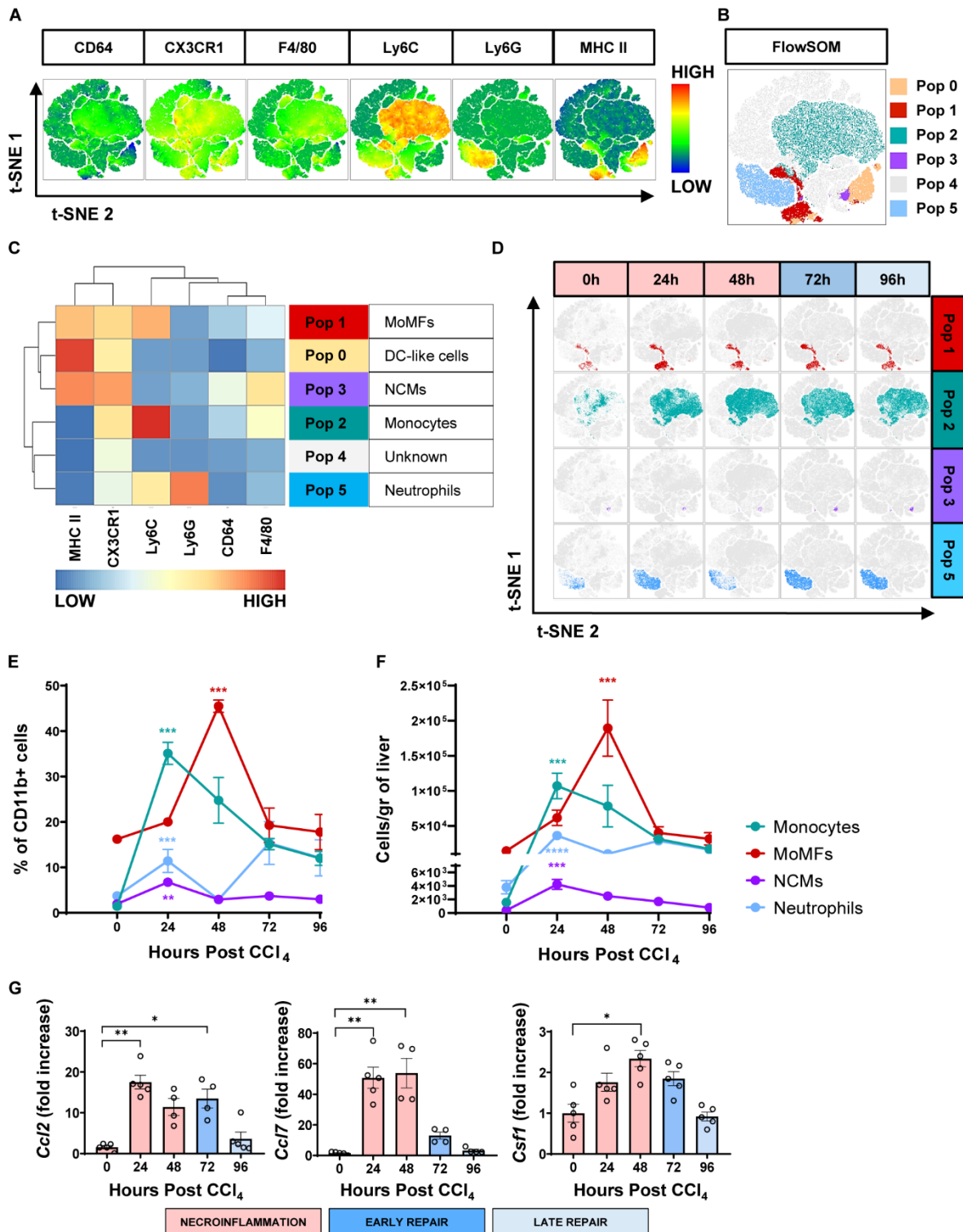


**Figure 3: The wound healing response to acute liver injury is associated with an influx of circulating myeloid cells. (A) t-SNE plots of total myeloid CD11b<sup>+</sup> cells showing pooled**

*expression of myeloid-associated markers from all mice at all time points. (B) t-SNE projection of myeloid cell populations identified by FlowSOM. (C) Heatmap showing relative marker expression associated with the different myeloid populations identified by FlowSOM and their proposed identity. (D) Representative t-SNE plots showing the kinetics of MoMFs, inflammatory monocytes, NCMs, and neutrophils in response to acute liver injury. (E) Frequencies of the different myeloid cell populations as determined by manual gating. (F) The total number of myeloid cell populations per gram of liver as determined by manual gating. (G) Relative gene expression of *Ccl2*, *Ccl7*, and *Csf1* determined by qPCR on bulk liver tissue. The mRNA expression data represent fold increase relative to 0 h controls and was normalized to 28s. N=4 mice per group. Data are shown as mean  $\pm$  SEM. Statistical analysis was performed using one Way ANOVA and Dunn's Multiple Comparison Test. \* $P < 0.05$ , \*\* $P < 0.01$ , \*\*\* $P < 0.001$ .*



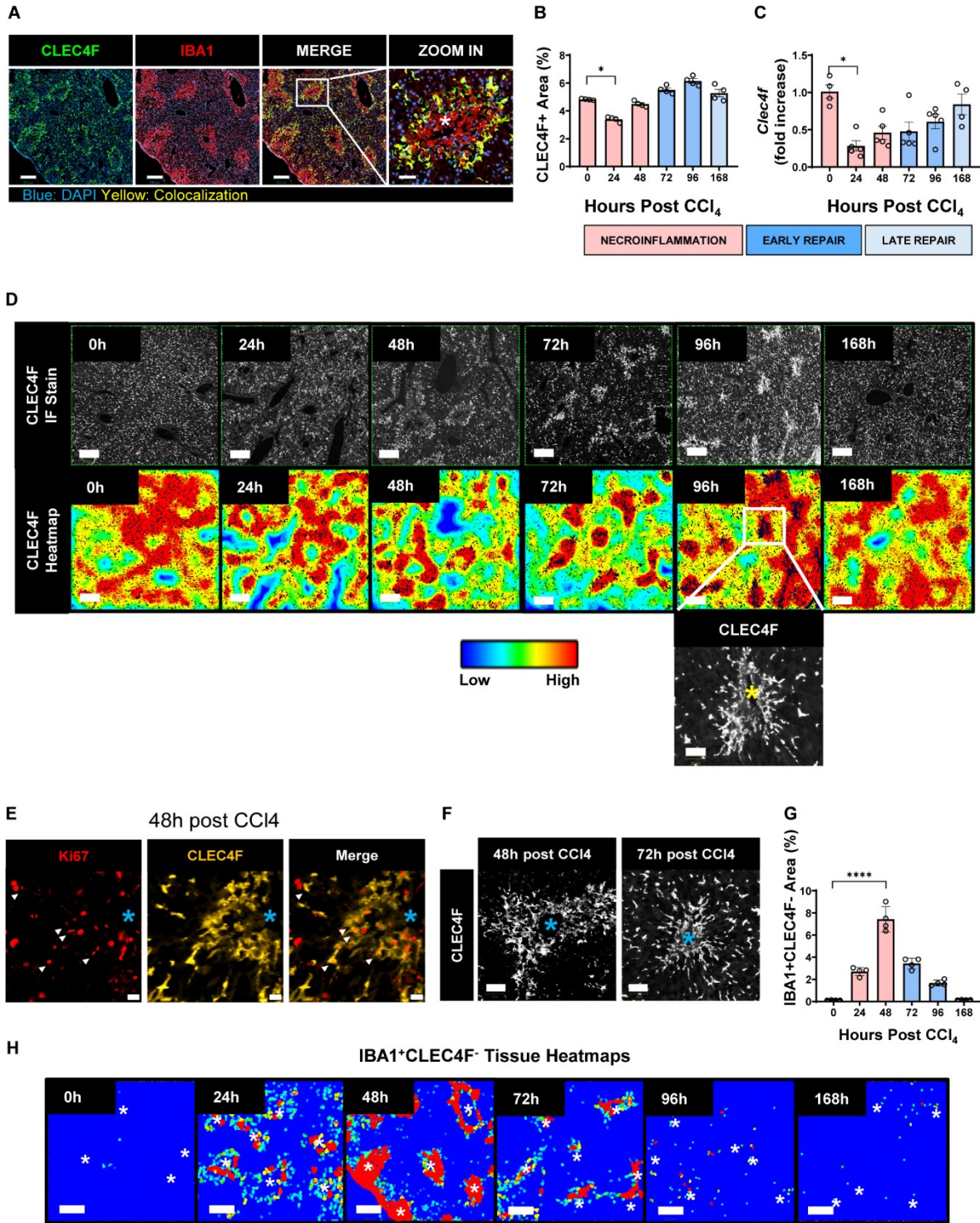
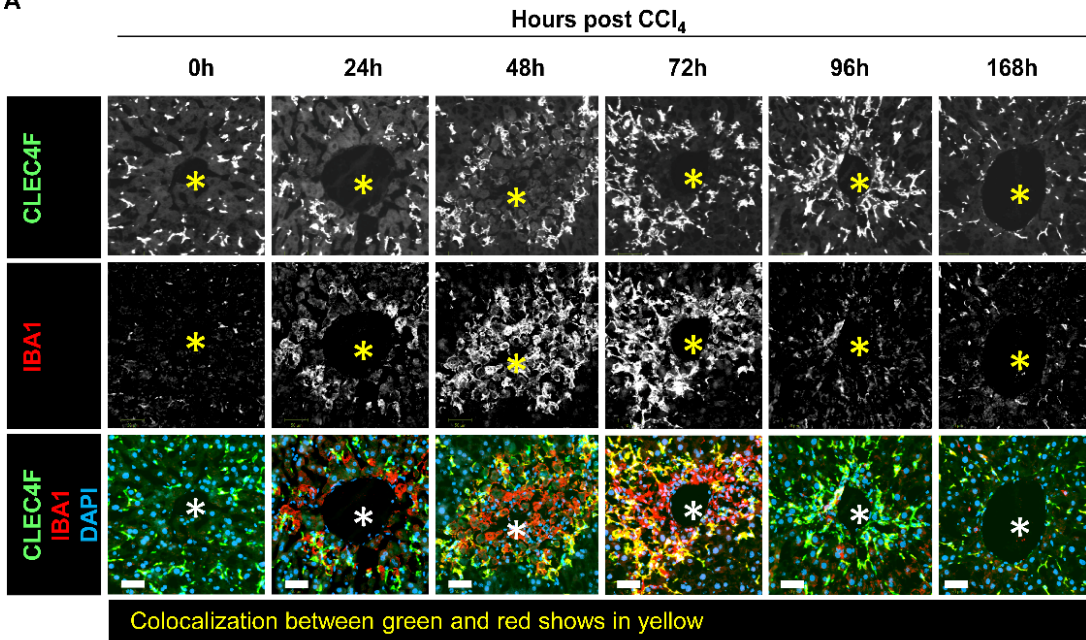
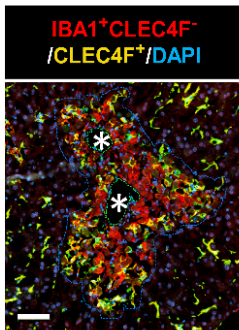


**Figure 4: KCs and MoMFs exhibit different distribution patterns and kinetics during acute liver injury whereby early transient depletion of CLEC4F<sup>+</sup> KCs is followed by recruitment of IBA1<sup>+</sup>CLEC4F<sup>-</sup> macrophages then return to baseline conditions during repair.** (A) mIF representative images of liver tissue at 48 h post CCl<sub>4</sub>. From left to right, CLEC4F (green), IBA1 (red), merge/colocalization (yellow). Nuclei are stained with DAPI (blue) scale bar =250 μm; the inset showing merge image at high magnification, scale bar =60 μm, \* indicates CV. (B) The density of CLEC4F<sup>+</sup> KCs macrophages as assessed by IF and expressed as % of total tissue area. (C) Quantification of the *Clec4f* by qPCR. The mRNA expression data represent fold increase relative to 0 h controls and was normalized to 28s. N=4-5 mice per group (D) Representative CLEC4F immunofluorescence images and their respective tissue heatmaps, indicating density per pre-defined area unit (color assigned according to a density grade), scale bar =250 μm. Inset showing high magnification of original CLEC4F staining, scale bar =50 μm. (E) IF representative images of Ki67 (red), and CLEC4F (yellow) at 48 h, scale bar =20 μm. (F) High magnification of CLEC4F IF at 48 h (left) and 72 h (right) post-CCl<sub>4</sub>, scale bar 70 μm. (G) The density of IBA1<sup>+</sup>CLEC4F<sup>-</sup> macrophages as assessed by IF and expressed as % of total tissue area. (H) Representative tissue heatmaps of IBA1<sup>+</sup>CLEC4F<sup>-</sup> macrophages, scale bar =250 μm. High-density areas are displayed in red and low density displayed in blue, intermediate values are displayed according to the color scale in the figure. N=4-5 mice per group. Data are shown as mean ± SEM. Statistical analysis was performed using one Way ANOVA and Dunn's Multiple Comparison Test. \*P < 0.05, \*\*P < 0.01, \*\*\*P < 0.001.

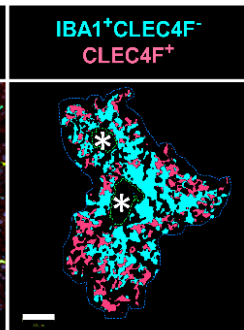
A



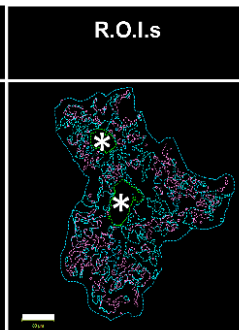
B



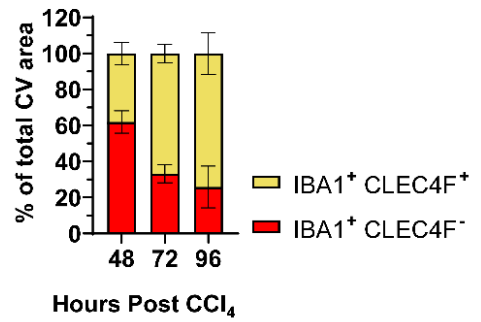
C



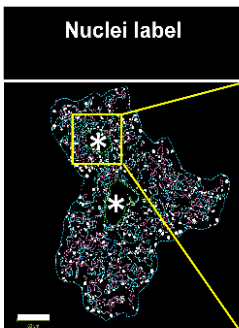
D



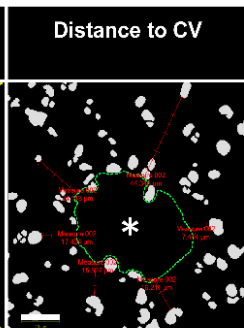
E



F



G



H

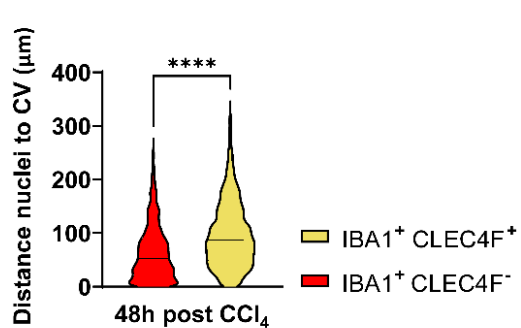
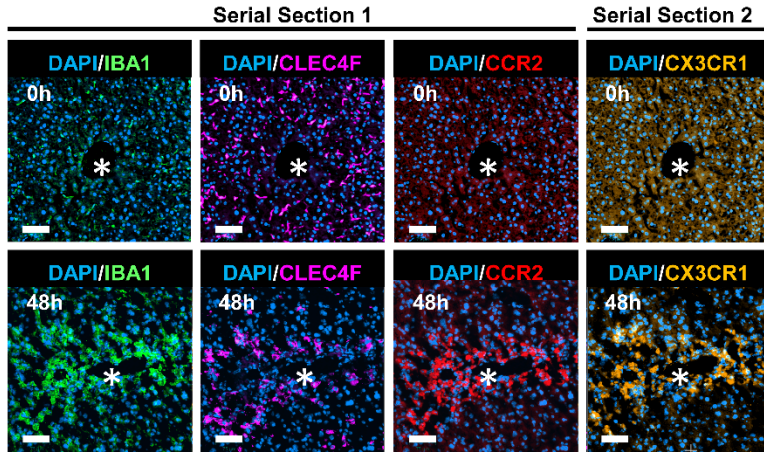
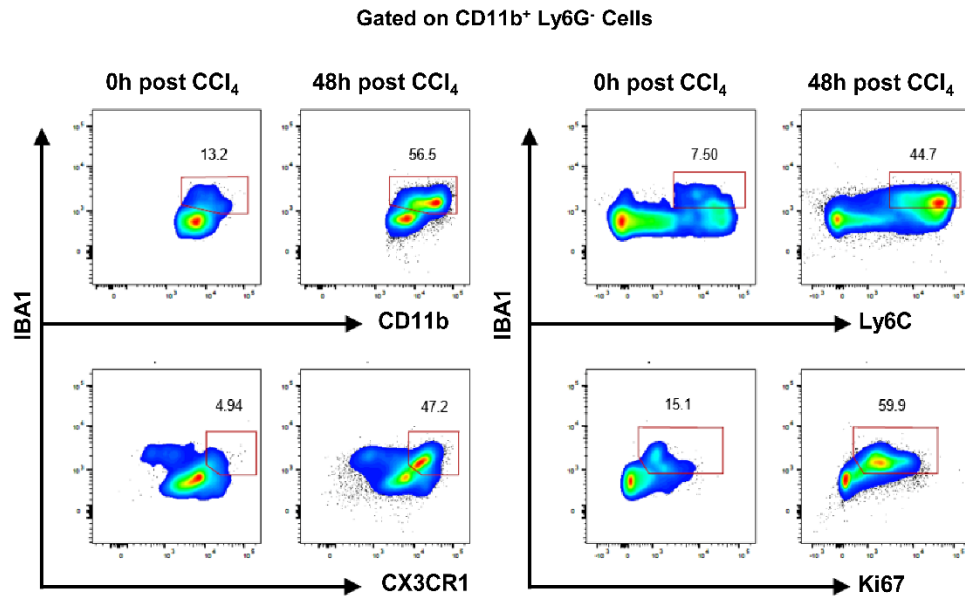


**Figure 5: CLEC4F<sup>+</sup> KCs and IBA1<sup>+</sup>CLEC4F<sup>-</sup> macrophages are in close contact in the necrotic area but exhibit different kinetics, microanatomical location, and morphology.** (A) Representative mIF images of CLEC4F (green), IBA1 (red), and DAPI (blue) around injured CVs. The top, middle, and bottom rows show CLEC4F single channel (grayscale), IBA1 single channel (grayscale), and merge (CLEC4F in green, IBA1 in red, and DAPI in blue), respectively, scale bar =50  $\mu$ m, \* indicates CV. (B) Representative image of CV-associated macrophages at 48 h post CCl<sub>4</sub> with CLEC4F<sup>+</sup> KCs in yellow and IBA1<sup>+</sup>CLEC4F<sup>-</sup> macrophages in red, scale bar =80  $\mu$ m. (C) Digitally generated labels for CLEC4F<sup>+</sup> KCs (pink) and IBA1<sup>+</sup>CLEC4F<sup>-</sup> macrophages (cyan). (D) Automated outlining of R.O.I. with dotted lines for the necrotic area (blue), CLEC4F<sup>+</sup> KCs (pink), IBA1<sup>+</sup>CLEC4F<sup>-</sup> macrophages (cyan), and CV (green). (E) Automated measurement of CLEC4F<sup>+</sup> KCs (pink cells in D) and IBA1<sup>+</sup>CLEC4F<sup>-</sup> macrophages (cyan cells in D) to calculate the percentage of necrotic area occupied by each of these subpopulations. (F) Automated detection of nuclei inside the R.O.I.s. (G) Automated measurement of the shortest distance from each nucleus to CV. (H) Quantification of the distance to the CV from IBA1<sup>+</sup> CLEC4F<sup>-</sup> nuclei vs. IBA1<sup>+</sup> CLEC4F<sup>+</sup> cells nuclei. N=4 mice per group. Data are shown as mean  $\pm$  SEM, n>4000 nuclei. Statistical analysis was performed using Mann–Whitney U test. \*P < 0.05, \*\*P < 0.01, \*\*\*P < 0.001.

A



B



C

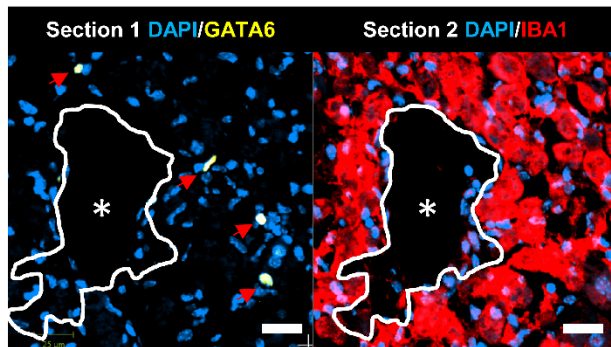


**Figure 6: IBA1<sup>+</sup>CLEC4F<sup>-</sup> macrophages exhibit phenotypic markers of MoMFs.** (A) Representative mIF images of IBA1 (green), CLEC4F (magenta), and the monocytic markers CCR2 (red), CX3CR1 (orange), and DAPI (blue) around CVs at 0 h vs. 48 h post CCl<sub>4</sub>, scale bar= 75 μm. IBA1, CLEC4F, and CCR2 were multiplexed on the same section (section 1), CX3CR1 was imaged in the contiguous section (section 2), and the \* indicates CV. (B) Representative pseudocolor flow cytometry plots of intrahepatic IBA1<sup>+</sup> myeloid cells at 0 h vs. 48 h post-CCl<sub>4</sub>. Cells were gated on CD11b<sup>+</sup> Ly6G<sup>-</sup> cells. The numbers next to the contoured plot graphs represent frequencies in this gate. (C) Representative digital alignment of IF images from serial sections showing on the left GATA6 (yellow), as a marker of peritoneal macrophages, and on the right IBA1 (red). The demarcation (white line) is to facilitate the visual merge. DAPI nuclei are in blue, scale bar =25 μm. The perimeter of the CV is delineated in white. N=4 mice per group.

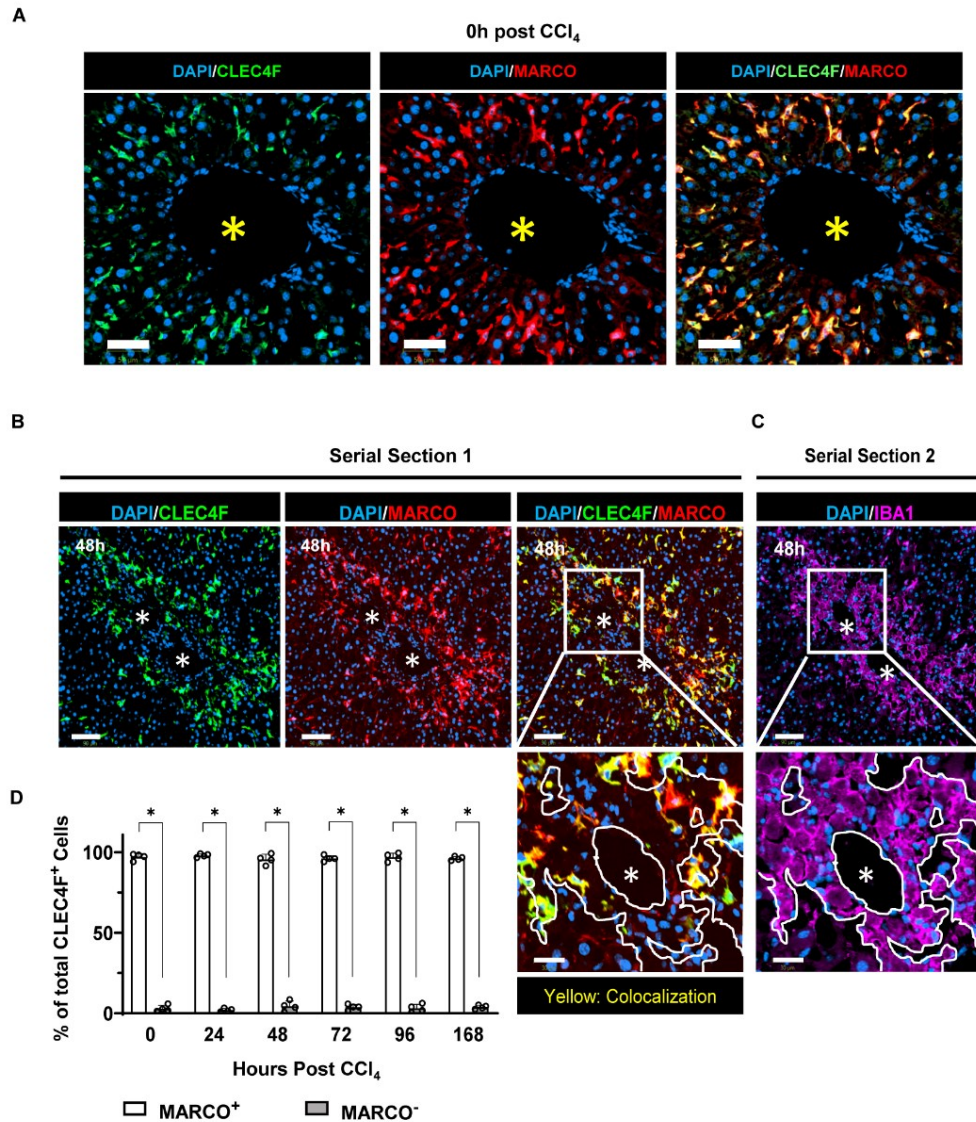
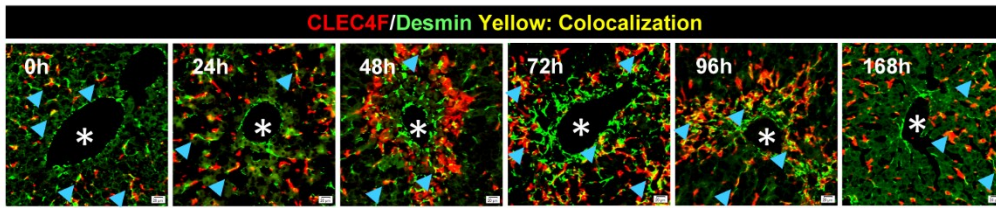
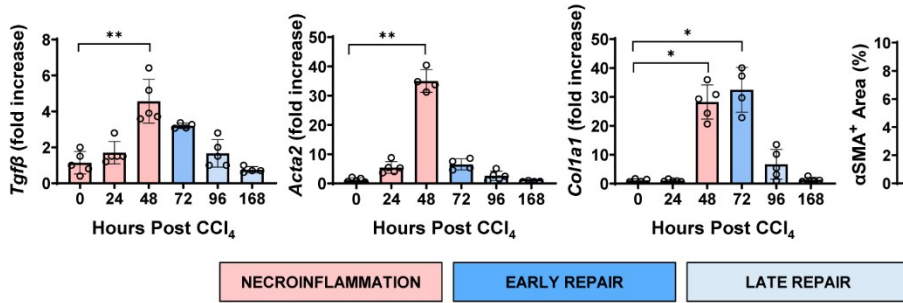


**Figure 7: CLEC4F<sup>+</sup> KCs of yolk sac origin replenish the hepatic macrophage pool during tissue repair.** (A) Representative mIF images from liver sections at steady state (0 h), CLEC4F in green (left), MARCO in red (middle) and merge (right). Nuclei counterstained with DAPI (blue), scale bar 50  $\mu$ m. (B) Representative mIF images from liver sections, CLEC4F in green (left), MARCO in red (middle), and merge (right) on serial section 1. (C) IBA1 IF (magenta) on serial section 2 (upper panel), scale bar = 90  $\mu$ m. The inset shows high magnification of the area delineated in the upper panel, scale bar = 30  $\mu$ m, \* indicates CVs. The demarcation (white lines) delineates the area occupied by IBA1<sup>+</sup> cells around a CV. (D) Quantification of MARCO<sup>+</sup> vs. MARCO<sup>-</sup> CLEC4F<sup>+</sup> KCs. N=4 mice per group. Data are shown as mean  $\pm$  SEM. Statistical analysis was performed using Mann–Whitney U test. \*P < 0.05, \*\*P < 0.01, \*\*\*P < 0.001.

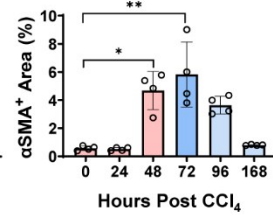
A



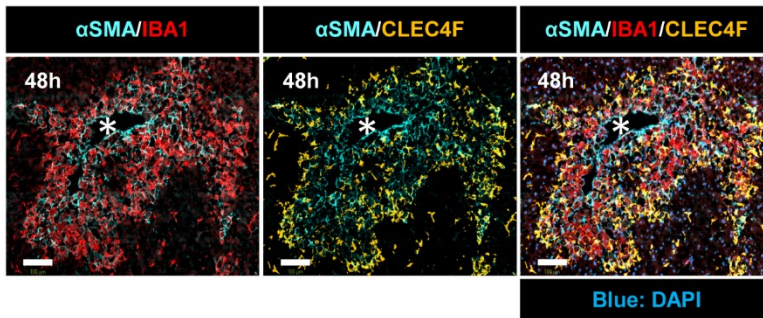
B



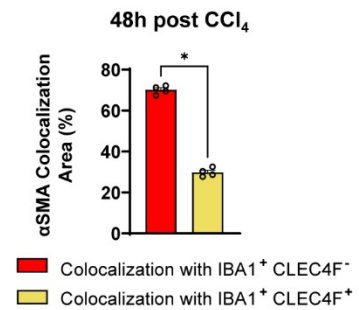
C



D



E



F

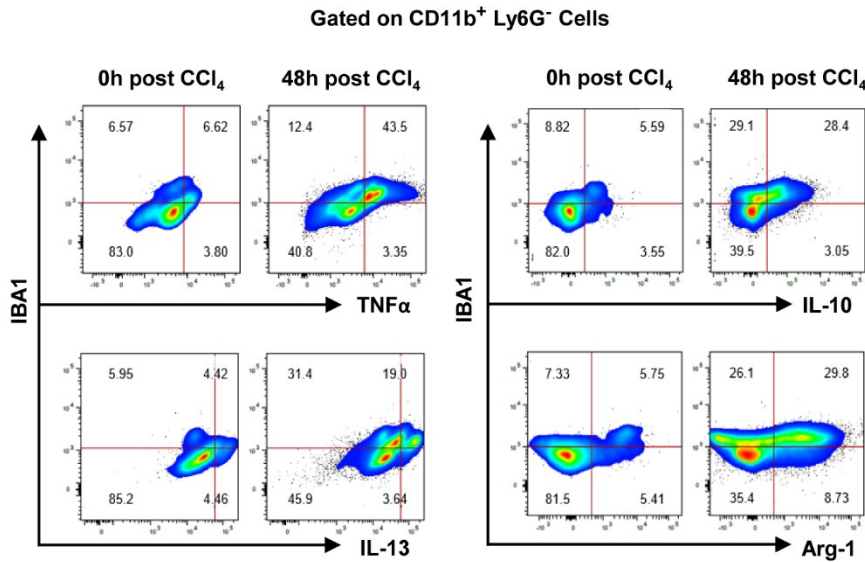




**Figure 8: IBA1<sup>+</sup> CLEC4F<sup>-</sup> macrophages interact with  $\alpha$ HSCs to a greater extent than CLEC4F<sup>+</sup> KCs.** (A) Representative mIF images from liver sections showing CLEC4F (red), Desmin (green), and DAPI (blue). Blue arrowheads point at colocalization between CLEC4F and Desmin, scale bar= 20  $\mu$ m. (B) Hepatic mRNA expression of *Tgfb*, *Acta-2*, and *Colla1*. The mRNA expression data represented fold increase relative to 0 h controls and was normalized to 28s. (C) The density of  $\alpha$ SMA<sup>+</sup> HSCs staining in liver sections expressed as % of total tissue area. (D) Representative mIF images of IBA1 (red), CLEC4F (yellow),  $\alpha$ SMA (cyan), and DAPI (blue), scale bar= 100  $\mu$ m, \* indicates CVs. (E) Percentage of colocalization between  $\alpha$ SMA<sup>+</sup> HSCs and either IBA1<sup>+</sup>CLEC4F<sup>-</sup> cells or CLEC4F<sup>+</sup> KCs. (F) Representative flow cytometry plots of IBA1<sup>+</sup> intrahepatic myeloid cells isolated from the liver at 0 and 48 h post CCl<sub>4</sub> and incubated with BFA and monensin for 6 h prior to staining. The populations shown were pre-gated in CD11b<sup>+</sup> Ly6G<sup>-</sup> and the frequencies indicated are relative to this gate. N=4-5 mice per group. Data are shown as mean  $\pm$  SEM. Statistical analysis was performed using Mann–Whitney U test. \*P < 0.05, \*\*P < 0.01, \*\*\*P < 0.001.

## Supporting Information

**Table S1. Immunofluorescence antibodies and reagents**

<b>Immunohistochemistry Abs</b>	<b>Company</b>	<b>Clone</b>	<b>Catalog #</b>	<b>State, Country</b>
Ki67	Invitrogen	SP6	MA5-14520	Canada
IBA1	Fujifilm WAKO Chemicals	Rabbit Polyclonal	019-19741	USA
<b>Immunofluorescence Primary Abs</b>				
CLEC4F	R&D Systems	Goat Polyclonal	AF2784	Canada
IBA1	Fujifilm WAKO Chemicals	Rabbit Polyclonal	019-19741	USA
MARCO	Abcam	EPR22944-64	ab239369	Canada
$\alpha$ SMA	Sigma Aldrich	1A4	A2547-100UL	Canada
CCR2	R&D Systems	475303	MAB55382-SP	Canada
CX3CR1	ThermoFisher Scientific	1H14L7	702321	Canada
Desmin	Invitrogen	Rabbit Polyclonal	PA5-16705	Canada
GATA-6	Cell Signaling	D61E4	5851T	Ontario, Canada
<b>Immunofluorescence Secondary Abs</b>				
Donkey anti-goat A568	Invitrogen	Donkey Polyclonal	A-11057	Canada
Donkey anti-rabbit A647	Invitrogen	Donkey Polyclonal	A-31573	Canada
Donkey anti-rabbit A488	Invitrogen	Donkey Polyclonal	A-21206	Canada
Donkey anti-mouse A488	Invitrogen	Donkey Polyclonal	A-21202	Canada
Chicken anti-rat A647	Invitrogen	Chicken Polyclonal	A-21472	Canada
<b>Other Reagents for Immunofluorescence</b>				
SlowFade Gold antifade with DAPI	Invitrogen		S36938	Canada
Bovine serum albumin (BSA)	Multicell		800-095-EG	Qc, Canada

Human Serum	Gemini		22210	USA
Sodium Citrate Dihydrate	Millipore Sigma		1545801	Canada
Triton X-100	Sigma Aldrich		T8787- 50ML	Canada
Tris-HCl	BioShop		77-86-1	Canada
Tween 20	Fisher Scientific		BP337-500	Canada
Tissufix	ChapteC		T-50	Montreal, Canada
<b>Solutions for Immunofluorescence</b>	<b>Composition</b>		S36938	
Blocking solution for immunofluorescence	1 % BSA, 10 % human serum, 10 % donkey serum, 0.1 % Tween 20 and 0.3% Triton in PBS			
Glycine solution for saturation of aldehyde groups	Glycine 0,1 M in PBS			
Antigen retrieval solution	Sodium Citrate Buffer (10 mM Sodium Citrate, 0.05% v/v Tween 20, pH 6.0)			
Washing Solution	PBS 0.1% Tween			

**Table S2. Antibodies and reagents of flow cytometry and other techniques**

<b>Flow Cytometry Abs</b>	<b>Company</b>	<b>Clone</b>	<b>Catalog #</b>	<b>State, Country</b>
CD45 SB645	eBioscience	30-F11	64-0451-82	Canada
CD45 BV650	Biolegend	30-F11	103151	USA
CD11b BV 421	BD Biosciences	M1/70	562605	USA
Ly6C PE-CF594	BD Biosciences	AL-21	562728	USA
Ly6G A488	Biolegend	1A8	127626	USA
Gr-1 A488 (Ly6G/Ly6C)	eBioscience	RB6-8C5	53-5931-82	Canada
IBA1/A1F1 A488	Millipore	20A12.1	MABN92-AF488	Canada
CCR2 PE	R&D Systems	475301	FAB5538P	Canada
CD64 APCe780	eBioscience	X54-5/7.1	212838	Canada
F4/80 BUV395	BD Biosciences	T45-2342	565614	USA
CX3CR1 BV785	Biolegend	SA011F11	149029	USA
MHC II (I-A/I-E) BUV 737	BD Biosciences	M5/114,15,2	748845	USA
Arg-1 PE	eBioscience	A1exF5	12-3697-82	Canada
TNF $\alpha$ PE Cy7	BD Biosciences	MP6-XT22	557644	USA
IL-10 BUV 421	Biolegend	JES5-16E3	505022	USA
IL-13 PE Cy5.5	Novus Biologicals	13A	NBP1-43239PECY55	Canada
CD3 BUV 395	BD Biosciences	145-2C11	563565	USA
CD4 BUV 496	BD Biosciences	GK1.5	564667	USA
CD8 BUV 737	BD Biosciences	53-6.7	564297	USA
CD19 APC H7	BD Biosciences	1D3	560245	USA
NK1.1	Biolegend	PK136	108718	USA
TCR $\gamma\delta$	BD Biosciences	GL3	562892	USA
<b>Other Flow Cytometry Reagents</b>				
LIVE/DEAD™ Fixable Aqua Dead Cell Stain Kit	ThermoFisher Scientific		L34957	Canada
Brilliant Stain Buffer	BD Horizon		566349	USA
BFA	Sigma Aldrich		B6542	Canada
Monensin Sodium Salt	Sigma Aldrich		M5273	Canada
Foxp3 / Transcription Factor Staining Buffer Set	ThermoFisher Scientific		00-5523-00	Canada
<b>Reagents for RNA Isolation and RT-PCR</b>				
RNeasy Plus Micro-Kit (50)	Qiagen		74034	USA

Transcriptor Universal cDNA Master	Roche		05893151001	Canada
LightCycler® 480 SYBR Green I Master	Roche		4707516001	Canada
<b>H&amp;E Reagents</b>				
Eosin	Leica Biosystems		3801600	USA
Hematoxylin Stain Sol., Gil 1. Formulation, Reg.	Ricca Chemical Comp.		3535-32	USA
<b>Reagents for Isolation of IHLs</b>				
Benzonase	Millipore Sigma		70664	Canada
Collagenase D	Roche		11088866001	Canada
RPMI 1640	Thermofisher Scientific		11875093	Canada
FBS	Thermofisher Scientific		A31607	Canada
Percoll	Sigma Aldrich		P1644	Canada
Sodium Azide	Fisher Scientific		S-227	Canada
Normal Mouse Serum	Thermofisher Scientific		10410	Canada
Formaldehyde	Sigma Aldrich		F8775	Canada

<b>Primers</b>	<b>Forward</b>	<b>Reverse</b>
TNF-a	5'-ACTCCAGGCGGTGCCTATGT-3'	5'-GTGAGGGTCTGGGCCATAGAA-3'
IL-1B	5'-GGCAGGCAGTATCACTCATT-3'	5'-GAGGATGGGCTCTTCTTCAAA-3'
CX3CL-1	5'-CGCGTTCTTCCAATTTGTGTA-3'	5'-CTGTGTCGTCTCCAGGACAA-3'
CX3CR1	5'-ATTCTTCATCACCGTCATCAG-3'	5'-ACTAATGGTGACACCGTGCT-3'
CCL2	5'-TCTGGACCCATTCCTTCTTGG-3'	5'-TCAGCCAGATGCAGTTAACGC-3'
CCL7	5'-GGCCTCCTCAACCCACTTCT-3'	5'-CCCTGGGAAGCTGTTATCTTCA-3'
M-CSF	5'-CAGCTGCTTCACCAAGGACT-3'	5'-TCATGGAAAGTTCGGACACA-3'
mCLEC4F	5'-CTTCGGGGAAGCAACAAC-3'	5'-CAAGCAACTGCACCAGAGAAC-3'
28s	5'-CGAGATTCCCACTGTCCCTA-3'	5'-GGGGCCTCCCACTTATTCTA-3'
<b>Primers</b>	<b>Company</b>	<b>NCBI reference</b>
Colla1	Qiagen	(NM_007742)
Acta2	Qiagen	(NM_007392)
TGF- $\beta$ 1	Qiagen	(NM_011577)

**Table S3. Primers**

Supplementary Figures:

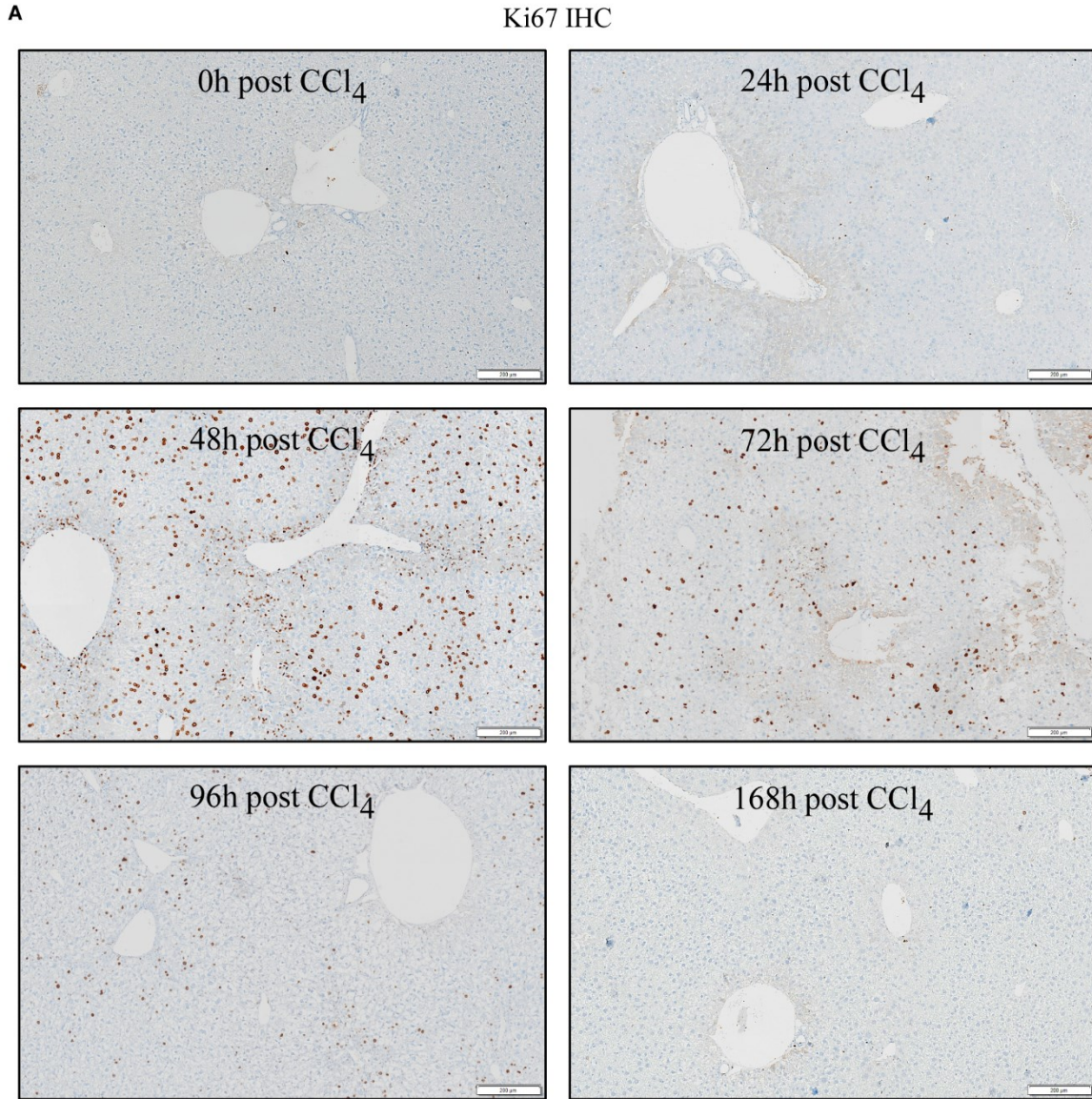


**Figure S1: Ki67 levels are highest at 48 h post CCl<sub>4</sub>.** (A) Representative Ki67 IHC images at 0, 24, 48, 72, 96, and 168 h post-CCl<sub>4</sub>, scale bar = 200 μm.

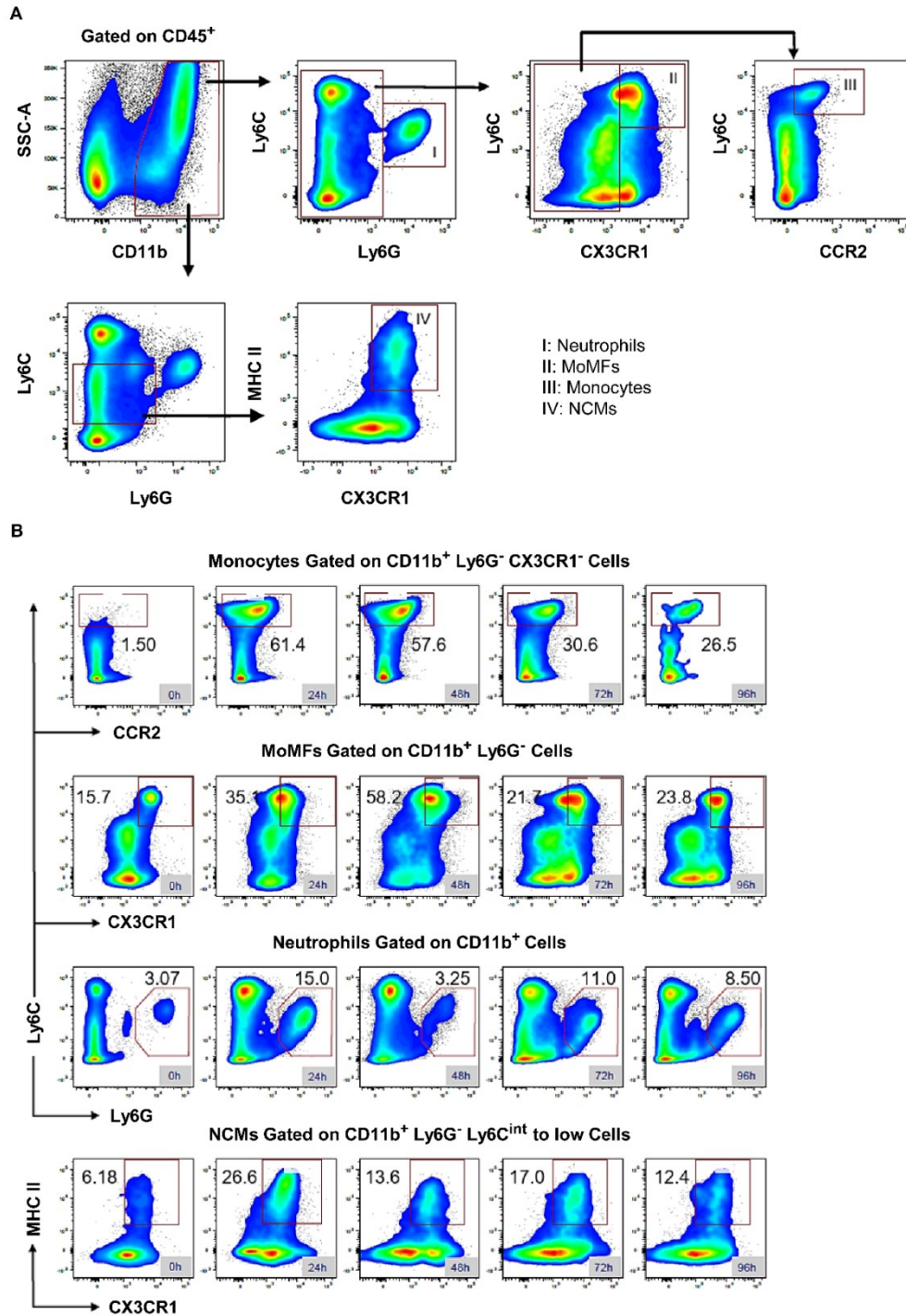
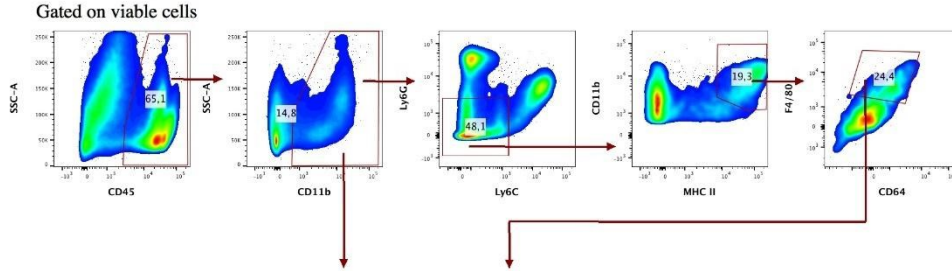


**Figure S2: Circulating phagocytes are recruited to the liver in response to CCl<sub>4</sub>-induced acute injury during the necroinflammatory and tissue repair phases. (A) Gating strategy for intrahepatic phagocytes. (B) Representative pseudocolor plots of the kinetics of major phagocyte populations induced in response to CCl<sub>4</sub> injury. N=4-5 mice per group.**



A

Gating strategy for exclusion of Ly6Chi monocytes and Ly6G+ neutrophils and gating on the KCs  
 KCs are CD45+ CD11b+ MHCII+ F4/80+ CD64+ CX3CR1- Ly6C- Ly6G-



B

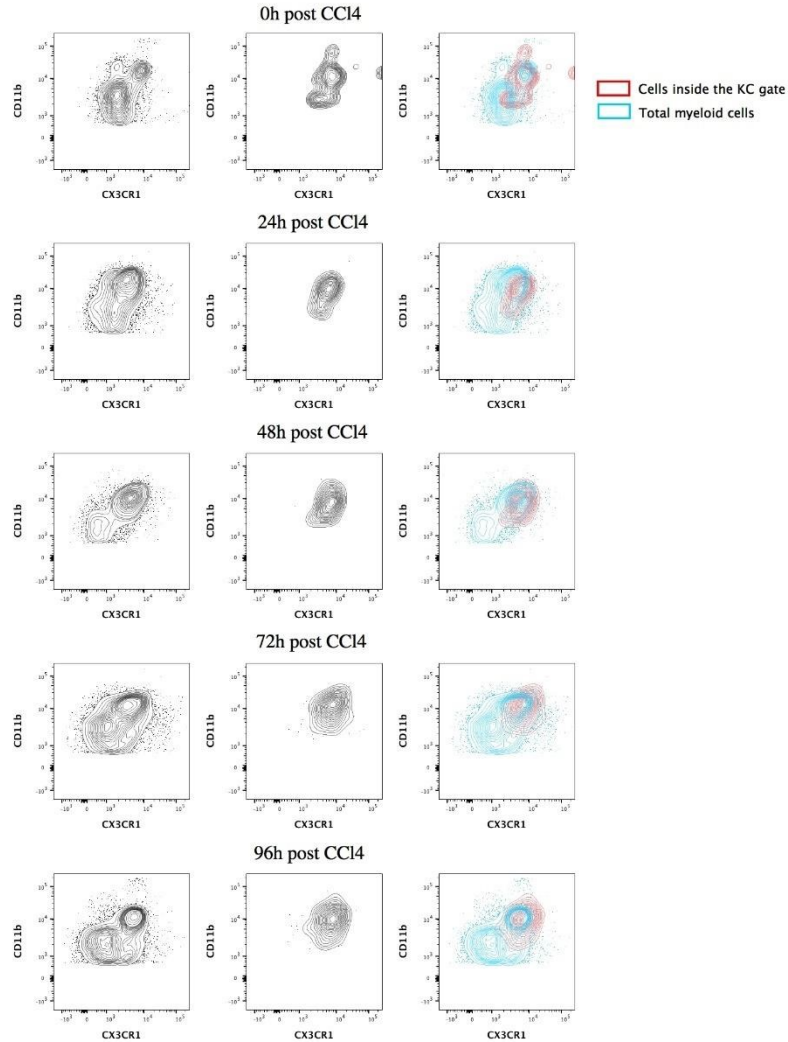


**Figure S3: Recovered  $CD11b^+ MHCII^+ CD64^+ F4/80^+$  cells express  $CX3CR1$ , and therefore are not KCs. (A) Gating strategy to define KCs from total intrahepatic leukocytes. (B) Contour plots showing  $CX3CR1$  expression by total myeloid cells (left column), by  $CD11b^+ MHCII^+ CD64^+ F4/80^+$  cells (center column), and the merge (right column).**

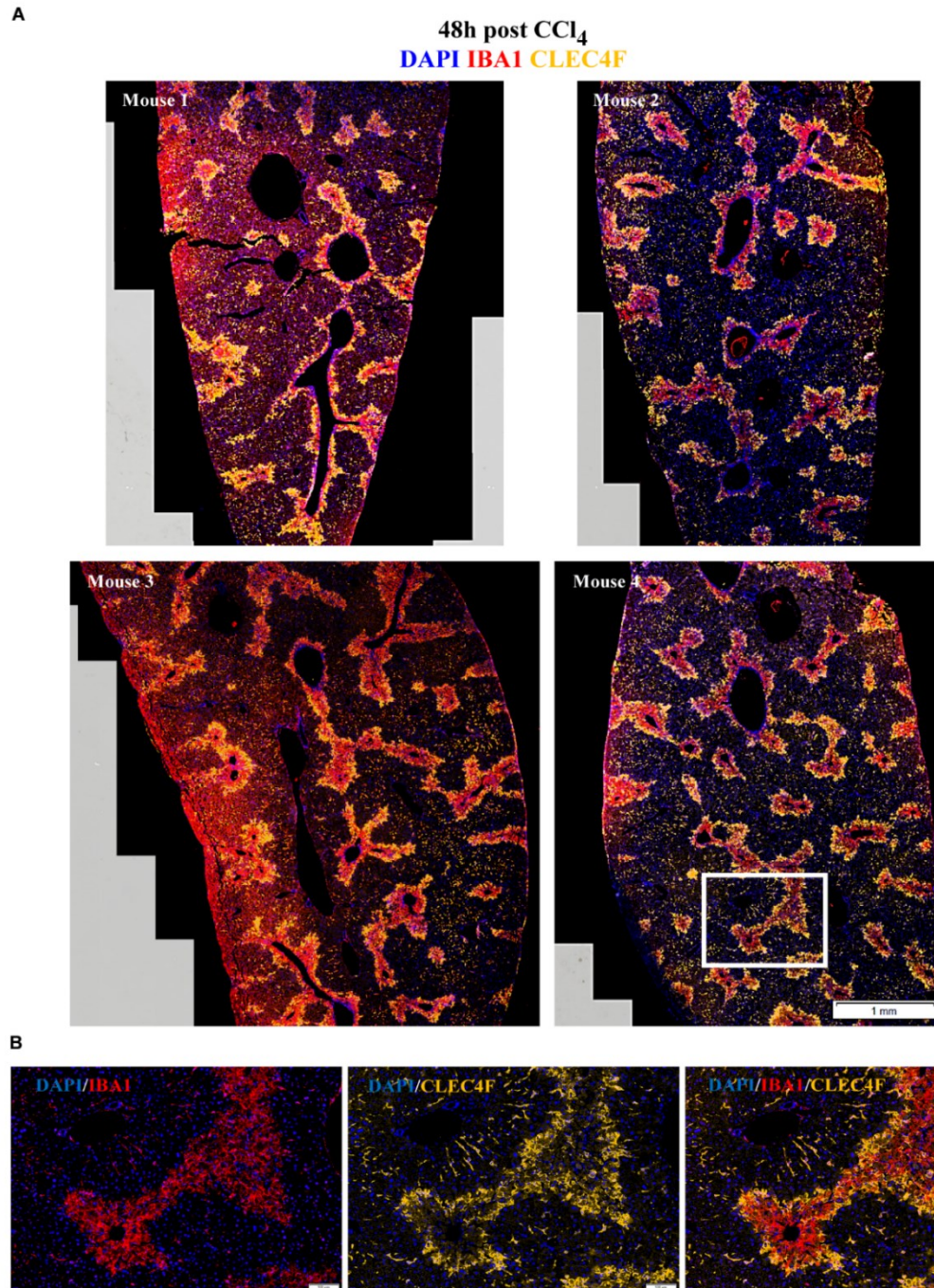


**Figure S4: IBA1<sup>+</sup> CLEC4F<sup>-</sup> macrophages, and CLEC4F<sup>+</sup> KCs exhibit different microanatomical locations in response to CCl<sub>4</sub>-induced acute liver injury. (A) Representative IBA1 (red) and CLEC4F (yellow) IF images of whole tissue at 48 h post CCl<sub>4</sub> at low magnification, scale bar = 1 mm. (B) High magnification of inset from (A) showing DAPI/IBA1 (left), DAPI/CLEC4F (center), and merge (right), scale bar = 100 μm**

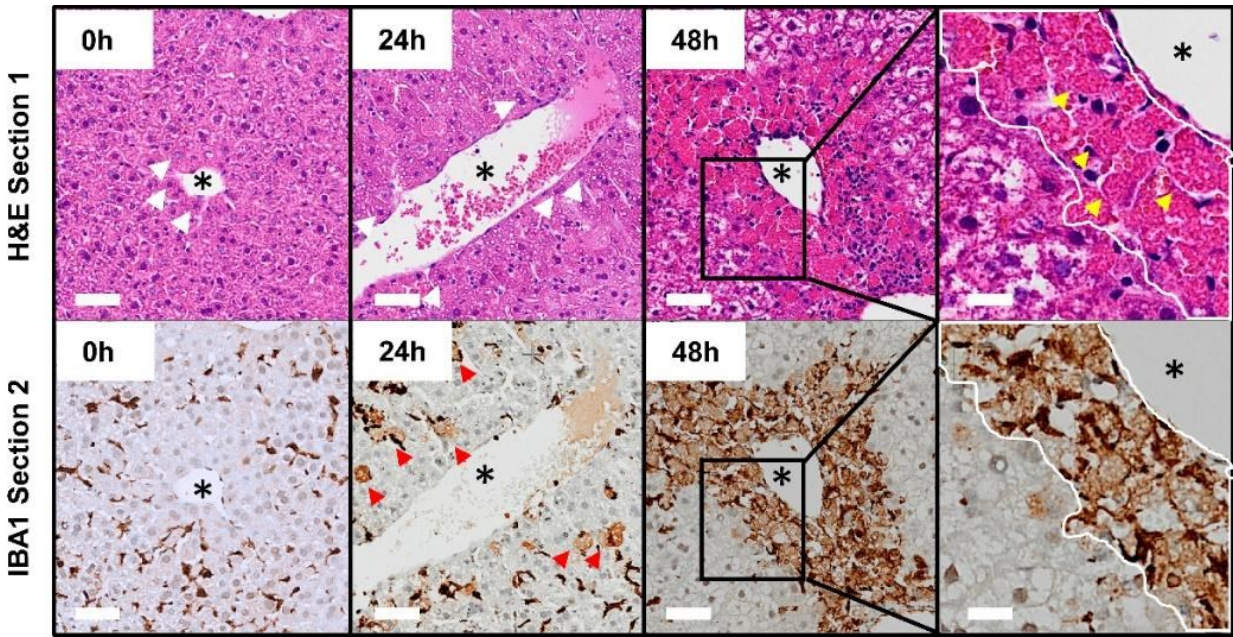
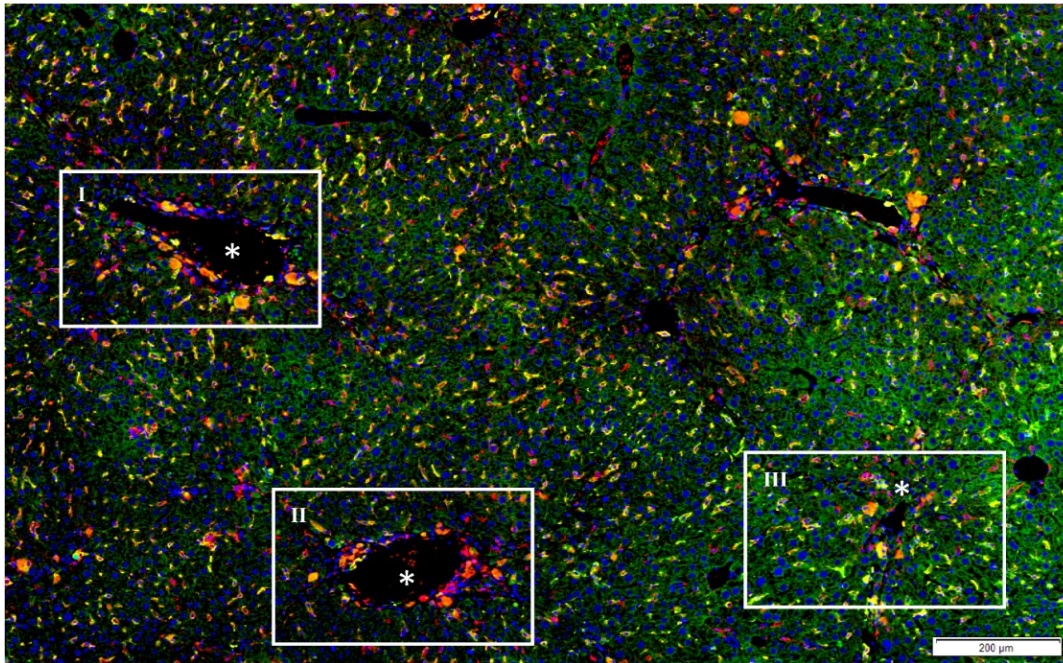


*Figure S5: Globular-shaped IBA1<sup>+</sup> cells infiltrate the necrotic tissue at 24 h and replace hepatocytes in the area surrounding CVs by 48 h post CCl<sub>4</sub>. Aligned serial sections of hepatic tissue: section 1 (H&E) and section 2 (IBA1 IHC). Red arrowheads pointing at infiltrating amoeboid IBA1<sup>+</sup> macrophages at 24 h post CCl<sub>4</sub>, scale bar= 50 μm. Yellow arrowheads pointing at IBA1<sup>+</sup> macrophages at 48 post CCl<sub>4</sub> with particulate material inside and occupying the previous location of hepatocytes around CVs, scale bar= 20 μm (insets). N=4 mice per group.*

A

12 weeks CCl<sub>4</sub>  
DAPI IBA1 CLEC4F



B

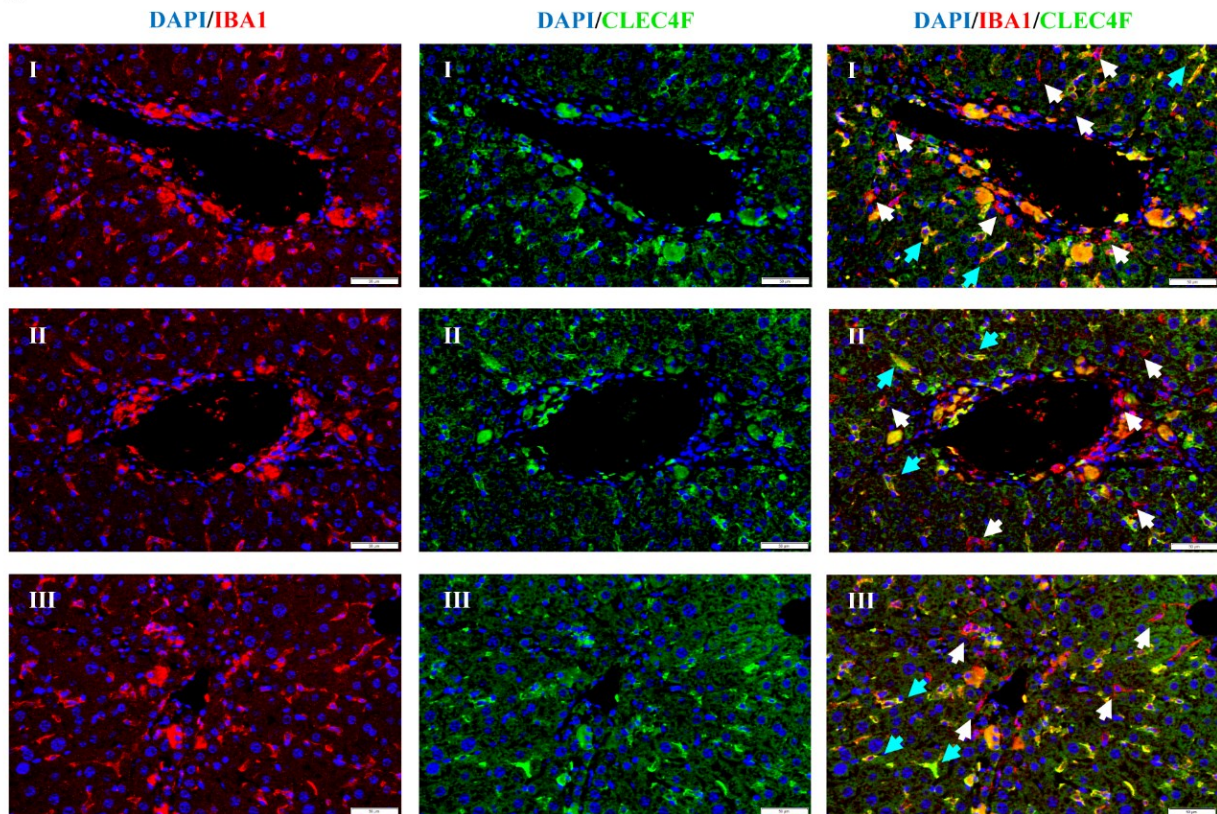


**Figure S6: IBA1<sup>+</sup> CLEC4F<sup>-</sup> macrophages and IBA1<sup>+</sup> CLEC4F<sup>+</sup> KCs are present in the murine fibrotic liver.** (A) Multiplex IF showing IBA1 (red) and CLEC4F (green) on liver section from 12 weeks CCl<sub>4</sub>-treated mouse. Colocalization red and green shows in yellow. Scale bar = 200 μm. \* designates CVs. (B) High magnification of insets I, II, and III from (A). IBA1/DAPI (left column), CLEC4F/DAPI (center column), and merge (right column). White arrowheads pointing at IBA1<sup>+</sup> CLEC4F<sup>-</sup> macrophages (red) and cyan arrowheads pointing at IBA1<sup>+</sup> CLEC4F<sup>+</sup> KCs (green-yellow-orange). Scale bar = 100 μm.

To see the video, follow the link below:

<https://www.frontiersin.org/articles/10.3389/fimmu.2022.994480/full#supplementary-material>

**Video: Activated hepatic stellate cells, IBA1<sup>+</sup>CLEC4F<sup>-</sup> macrophages and CLEC4F<sup>+</sup> KCs establish direct contact around injured central veins at 48 h post CCl<sub>4</sub>.** Three-dimensional (3D) reconstruction of the interaction between an activated HSC in red (based on αSMA signal), an IBA1<sup>+</sup>CLEC4F<sup>-</sup> macrophage in yellow (based on IBA1 signal), and a CLEC4F<sup>+</sup> KC in white and green (based on CLEC4F signal in white). Images or z-stacks were acquired using ×40 objective, ApoTome 2, Zeiss. Three-dimensional reconstruction was done using Imaris 8.1.2 software (Bitplane, Zurich, Switzerland).

### Supplemental References

1. Flores Molina M, Fabre T, Cleret-Buhot A, Soucy G, Meunier L, Abdelnabi MN, et al. Visualization, Quantification, and Mapping of Immune Cell Populations in the Tumor Microenvironment. *J Vis Exp.* 2020(157).

## Chapter 5: Discussion

### 5.a. Summary of the thesis

In this thesis, we generated a strategy for increased visualization, mapping, and profiling of immune cells in the liver tissue. We used this strategy to monitor hepatic macrophage subsets in the tissue to better understand their differential role in response to CCl<sub>4</sub> acute injury. This strategy uncovered unique spatial and temporal signatures of MoMFs vs. KCs.

We established the kinetics of the wound healing response to CCl<sub>4</sub>-induced acute liver injury to be able to relate our observations of macrophages *in situ* to major effector phases like necroinflammation and tissue repair. This approach allowed us to gain insight into the differential roles of macrophage subpopulations at different stages of the wound healing response. We observed that KCs and MoMFs exhibited different kinetics, but they spatially and temporally overlapped in the necrotic tissue. Although KCs and MoMFs converged in the necrotic area, we found that they occupied unique microanatomical locations and exhibited different cellular morphology.

Since hepatic macrophages do not act in isolation but engage in dynamic interactions with other resident and infiltrating cells, we also monitored by flow cytometry the kinetics of the major immune cell populations in response to CCl<sub>4</sub> to achieve a higher perception of the potential interacting partners of hepatic macrophages. This profiling showed that KCs shared the same kinetics of other resident populations (e.g., T, B, and NKT cells) characterized by decreased numbers during necroinflammation and recovery during repair. By contrast, the kinetics of MoMFs was like that of other infiltrating myeloid populations with a transient presence in the liver (e.g., neutrophils, monocytes, NCMs). In addition, we found that KCs but not MoMFs contributed to the replenishment of the KC pool during tissue repair. Finally, colocalization analysis showed that KCs and MoMFs differently interacted with HSCs, suggesting dissimilar effects on their activation status.

In summary, the spatio-temporal profiling of KCs and MoMFs revealed that these two subpopulations exhibited distinctive spatial signatures which suggest different roles during the wound healing response to acute liver injury.

## **5.b. Development of a methodology for increased multiplexing capability and spatial phenotyping in the hepatic tissue**

The immune response is spatially and temporally regulated and relies on cell-cell interactions that take place in SLOs and non-lymphoid parenchymal tissues (2, 490). In the tissues, immune cells are spatially organized in a way that maximizes the encounter of rare relevant cell populations in a timely manner and provides the optimal microenvironment to favor tissue homeostasis and immunity in response to insults. Therefore, the immune response cannot be properly understood by merely analyzing isolated molecules and cells while ignoring their spatial distribution, cell-cell interactions, and the tissue context (490).

In the last two decades, new technologies have been developed interrogating images from tissue sections and from *in vivo* systems to generate single cell-based high-throughput data. Examples of these technologies are histo-cytometry, imaging mass cytometry, mass spectrometry imaging, iterative bleaching extends multiplexity (IBEX), spinning-disk confocal intravital microscopy (SD-IVM), and CODEX (193, 291, 491-495, 497). In addition, technologies combining transcriptome gene expression profiles with histological information are expanding the toolbox of solutions for mapping cells with resolved gene expression (e.g., RNAscope and Visium Spatial Gene Expression) (152, 498). These technologies have revealed how the spatial organization of the immune system supports immune function in SLOs and barrier tissues. However, the use of expensive equipment and/or software has prevented broad access to them for most of the research community. Only a few studies have focused on investigating the spatial behavior of immune cells in the hepatic tissue (7, 45, 148, 152, 193, 497, 499, 500). Therefore, the organization and dynamics of resident and infiltrating immune cells in the healthy and inflamed liver are insufficiently characterized.

There are major challenges for imaging immune cells in tissue sections, including the fact that multiple markers are needed to identify immune subsets; microscopes have a limited number of channels; the availability of fluorophores suited for imaging is low; and the number of species used for antibody production is restricted. To overcome these limitations, we integrated multiple accessible solutions for multiplexing in a strategy for visualization, quantification, and mapping of immune cell populations in hepatic tissue that greatly expanded the number of markers to be visualized and analyzed simultaneously (Figure 1, chapter 3) (501).

As a proof of concept of the feasibility and advantages of the strategy, we visualized 11 parameters (CD3, CD4, CD8, CD34, CD68, FoxP3, MPO, Desmin,  $\alpha$ SMA, cytokeratins 8/18, and DAPI) plus two frequent stains in three serial sections of formalin-fixed paraffin-embedded human HBV-associated HCC tissue (Figure 2, chapter 3). The first step of the strategy is the imaging of cell populations of interest (COIs) and tissue compartments (TC) where the COIs would be analyzed. Next, for enhanced multiplexing, we combined serial imaging and sequential labeling. Serial imaging allowed us to visualize different subsets of immune cells in serial or consecutive sections, and sequential labeling made possible the reuse of sections for several staining cycles targeting different immune populations. In addition, the tissue context of labeled immune cells was determined through the differential staining of distinctive TCs like the stroma and the parenchyma (Figure 3, chapter 3). We also performed H&E staining to spatially relate histopathological information to immune profiling. Overall, 10 biomarkers were distributed into 6 immune populations, and 3 non-parenchymal cell populations were labeled.

Subsequently, whole tissue images from all the stains were acquired and digitally aligned using the software VIS and consolidated into a virtual slide that was used for image analysis (Figure 2, chapter 3). We proved that the precision of the alignment could reach the individual cell level for images derived from the same section making this strategy compatible with virtual multiplexing (Supplementary Figure S1, chapter 3). In addition, the alignment of images derived from serial sections showed clear-cut spatial overlap of structural features (e.g., vessels), confirming the preciseness of the tissue alignment.

Next, we used the module Author of the VIS software for creating customized protocols for tissue detection and segmentation, or the identification, quantification, and mapping of COIs. In total, 15 image analysis protocols were designed and used for various purposes like tissue detection, tissue segmentation, and the specific identification and mapping of COIs in the different tissue compartments (e.g., stroma vs. parenchyma and tumor vs. non-tumor) (Figures 3 and 4, chapter 3). Furthermore, relevant tissue structures like vessels and fibrous septa were also visualized and analyzed to better understand the neighborhoods of immune cells.

In the final step of the strategy, we generated tissue heatmaps to have a panoramic view of the overall tissue distribution of different COIs in the TME, making possible the understanding of how different populations of cells spatially relate with one another and how they relate to tissue features



like vessels and the fibrotic septa, or to tumors (Figure 5, chapter 3). Tissue heatmapping revealed that different neighboring tumors in the same section can exhibit quite dissimilar distribution patterns for the same immune cell population (Supplementary Figure S2, chapter 3). Therefore, the histological complexity of the TME translates into spatial heterogeneity of immune cells, emphasizing the need for whole tissue analysis and tissue heatmapping for the analysis of immune cells in tissue sections.

Among the great features of this strategy is its capacity for the analysis of whole tissue sections. The extensive histological heterogeneity and the uneven distribution of immune cells in the tumor microenvironment cannot be adequately captured by the analysis of fragmented and disconnected fields of view or tissue microarray images (501). By contrast, whole tissue analysis results in an unbiased representation of the immune microenvironment but requires a high computing power that has only become recently available. By integrating the use of VIS and automated analysis into this strategy, hundreds of thousands of immune cells were profiled, quantified, and mapped within a few hours.

Additional advantages of this strategy are the increased multiplexing capability using easily accessible techniques and resources. In addition, the digital alignment of serial images allowed us to analyze how markers or populations visualized in one image spatially related to markers or populations in another image. The fact that the image analysis is automated tremendously increases the tissue area that is covered by the analysis and its speed. Moreover, the use of image analysis protocols with fixed classification criteria of the pixels ensured the consistency of the analysis and removed the subjectivity associated with quantification by visual inspection and the inter-sample variability.

In summary, this strategy increases the spatial information that can be obtained from limited clinical specimens, is easily adaptable to other tissues and biomarkers of interest, and the technical knowledge and resources required to execute it are accessible to most investigators.

### **5.c. Spatio-temporal characterization of the hepatic macrophage compartment in response to acute liver injury**

Hepatic macrophages are key effector cells during homeostasis and in response to injury and are involved in the pathogenesis of several liver diseases (195, 502). The heterogeneity of the

macrophage compartment in the liver has only recently started to be appreciated with the emergence of RNA sequencing, flow cytometry, and mass cytometry (129, 131-133, 148). However, these technologies involve tissue disruption and loss of spatial information and tissue context. Indeed, the spatial and temporal profiling of liver macrophages in tissue samples during the steady state and response to injury will provide non-redundant information on how macrophages relate to neighboring cells and their behavior during immune responses, hence the importance of this characterization of hepatic macrophages in space and time.

In the second part of this study, we combined multiparameter flow cytometry and RNA expression profiling with the imaging techniques and digital analysis tools we had previously developed for spatial phenotyping of immune cells in the liver tissue (chapter 3) to dissect the hepatic macrophage compartment in response to acute injury with CCl<sub>4</sub>. One dose of 1 $\mu$ L of CCl<sub>4</sub> per gram of body weight leads to massive central vein necrosis, increased liver weight, and elevated levels of ALT, AST, and urea in the blood (503). However, in this model, tissue damage and inflammation are followed by a repair response that completely restores the homeostatic structure, composition, and physiology of the hepatic tissue (503, 504). Thus, this model offers an opportunity to monitor the subpopulations of hepatic macrophages spatially and temporally during all the phases of the wound healing response.

We hypothesized that despite the remarkable phenotypic and functional plasticity exhibited by hepatic macrophages, the individual subpopulations evolved to assume distinctive roles in response to injury. Furthermore, we proposed that each subset of macrophages would exhibit unique morphological, spatial, and temporal profiles and would differentially relate to neighboring cells during the response to acute liver injury.

Our approach consisted in first delineating the kinetics of the wound healing response to identify the tissue context at different time points upon CCl<sub>4</sub>-induced injury. We reasoned that this strategy would allow us to link the kinetics, phenotype, cell morphology, and tissue distribution pattern of hepatic macrophages to specific effector programs like inflammation and repair. Next, we characterized the kinetics of the major innate and adaptive hepatic immune populations by multiparameter flow cytometry to understand how these cell populations temporally relate to our observations of hepatic macrophages. Subsequently, we dissected the spatio-temporal dynamics of tissue-resident KCs and infiltrating MoMFs in response to acute injury. Finally, we investigated

how these two subpopulations differentially contributed to the replenishment of the macrophage compartment and the activation of HSCs during the wound-healing response to acute liver injury.

### **5.c.1. Wound healing response to CCl<sub>4</sub>-induced acute liver injury**

In this study we used the CCl<sub>4</sub> model of acute liver injury, using a single dose of 1  $\mu$ L per gram of body weight. The merits of this model include great reproducibility, easy to implement, and the fact that it recapitulates the histological, and pathophysiological features of APAP-induced injury in humans, the most common source of acute liver failure (505). In addition, since CCl<sub>4</sub> intoxication leads to self-limited inflammation, the immune cells involved in the response can be monitored throughout all the phases of the wound healing response. Furthermore, CCl<sub>4</sub> causes centrilobular necrosis, the same spatial pattern of injury observed during APAP, which adds relevance to the spatial profiling of macrophages in this model. Moreover, the CCl<sub>4</sub> model can be used to induce chronic inflammation and fibrosis. Unlike surgical models of acute liver injury (e.g., hepatectomy), the CCl<sub>4</sub> model is easy to implement in small animals. Similarly, the CCl<sub>4</sub> model does not directly activate adaptive immune cells like the immunogenic model of Concanavalin A-induced liver injury and therefore is better suited to study the role of myeloid cells (506). The main limitations of this model are the induction of metabolic alterations, and that it does not recapitulate the hepatic encephalopathy associated with acute liver failure (506).

We profiled the spatial behavior of hepatic macrophages using only male mice for practical reasons (e.g., people available to do the experiments and time). In addition, there is no evidence to our knowledge that macrophage biology in the liver is influenced by sex/gender, but differences may exist. The study of hepatic diseases in men vs. women and experimental models has shown that gender differences are associated with differences in incidence, severity, and clinical outcome in multiple hepatic diseases including autoimmune hepatitis, acute liver injury, ALD, viral hepatitis, and HCC (507). Therefore, the results presented in this study cannot be directly extrapolated to female mice.

We delineated the precise kinetics of the wound healing response to CCl<sub>4</sub>-induced acute liver injury which allowed us to understand the evolving tissue context of hepatic macrophage subpopulations and to gain insight into their roles. Specifically, we identified 3 distinctive phases

of the wound healing response to CCl<sub>4</sub>-induced acute liver injury: necroinflammation, early repair, and late repair (Figure 1, chapter 4).

The wound-healing response to an acute injury is a complex and highly coordinated multicellular tissue response to tissue damage caused by physical trauma or pathogen invasion. During this response, resident and infiltrating immune cells cooperate with tissue cells to bring about the restoration of the normal tissue architecture and physiology upon injury.

The wound healing response has been better conceptualized and studied in the skin and 6 sequential but also overlapping stages have been defined: hemostasis, inflammation, angiogenesis, growth, re-epithelialization, and remodeling (508). In the liver studies, the wound healing response has not been conceptualized in a detailed manner, but the early stages namely hemostasis and inflammation, are grouped under the term necroinflammation, and regeneration and repair encompass the regrowth of vessels, the restoration of the ECM, and the proliferation of tissue cells (509, 510). In the following sections, we will discuss how our observations relate to previous studies characterizing necroinflammation and tissue repair upon acute liver injury, avoiding those aspects already discussed in the manuscript (chapter 4).

#### **5.c.1.a. Necroinflammation in response to CCl<sub>4</sub>-induced acute liver injury**

Necroinflammation is defined as the process of activation of resident immune cells, and the subsequent recruitment of circulating immune cells to the damaged tissue in response to DAMPs and pro-inflammatory cytokines released by cells undergoing necrotic cell death (510).

In our study, signs of hepatic necroinflammation were already detectable at 12 h post-CCl<sub>4</sub> injury and extended up to 48 h when evidence of pro-repair activity started to emerge (Figure 1C and 1D, chapter 4). The necroinflammatory phase of the wound healing response was characterized by extensive tissue damage as measured by ALT and % of the necrotic area, partial depletion of resident immune cell populations, massive myeloid cell infiltration, and upregulated expression of pro-inflammatory cytokines (Figure 1, chapter 4).

Recent research has revealed that necrosis may happen as a programmed and genetically regulated process intended to trigger acute inflammation (e.g., necroptosis, ferroptosis, pyroptosis), or may happen in a non-regulated manner which is known as traumatic necrosis. The release of highly

immunogenic DAMPs during regulated necrosis not only activates the immune system and promotes inflammation, but also triggers pro-repair pathways critical for the re-establishment of tissue homeostasis upon injury. This explains why defects in necrosis-inducing pathways lead to aberrant inflammation and autoimmunity (510, 511). Depending on the dose, CCl<sub>4</sub> injury can induce either regulated or traumatic necrosis in hepatocytes. Administration of 1 μL of CCl<sub>4</sub> per gram of body weight causes a self-limited immune response that leads to total healing within 2 weeks which fits the model of regulated necrosis (510, 511).

Hepatocellular death induced by CCl<sub>4</sub> is attributed to toxic radicals generated by the action of the cytochrome P450 superfamily of monooxygenases. It has been postulated that CCl<sub>4</sub>-derived radicals react with nucleic acids, proteins, and lipids, thereby functionally impairing hepatocytes, inducing necrosis and the release of cellular contents like DAMPs and ALT (512). Importantly, cytochrome P450 enzymes exhibit zoned expression with increased activity in pericentral hepatocytes (513). Accordingly, we observed zoned-specific damage around central veins and elevated levels of plasma ALT during necroinflammation (Figure 1B-D, chapter 4). Overall, the dynamics of necroinflammatory markers like ALT levels, necrotic area, and expression of pro-inflammatory cytokines, were highly consistent with previous reports, emphasizing the great reproducibility of the CCl<sub>4</sub> model (514-519).

Our data also showed a significant induction of pro-inflammatory cytokines TNFα and IL-1β during necroinflammation as previously reported (Figure 1E, chapter 4) (520, 521). Upon liver injury, *Tnfa* activates signaling pathways leading to the secretion of pro-inflammatory cytokines and chemokines, including IL-1α, IL-6, CCL2, CCL3, and CCL4, that mediate recruitment of monocyte/macrophages to the injury site (522, 523). In line with this, in our study, the induction of *Tnfa* upon CCl<sub>4</sub> preceded the upregulation of the transcripts for the inflammatory chemokines *Ccl2*, *Ccl3*, and *Ccl4* (*Ccl2* included in Figure 3G, chapter 4, *Ccl3*, and *Ccl4* not shown).

Although TNFα can be produced by multiple cells like lymphoid cells, endothelial cells, and fibroblasts, KCs have been identified as a major source in response to hepatic tissue damage (521). Studies using mice deficient for TNFα have found opposing roles of this cytokine depending on the nature of the insult. Decreased tissue damage was found in TNFα deficient mice upon LPS injury (524). However, lack of TNFα signaling worsened recovery in the APAP model and during partial hepatectomy due to reduced survival and proliferation of hepatocytes (521, 523, 525).

Similarly, the role of IL-1 $\beta$  in acute liver injury has been established using IL-1 $\beta$  receptor KO mice. These mice exhibited reduced tissue damage in response to thioacetamide (TAA) as determined by ALT and % of necrotic area compared to wild-type counterparts (520). In addition, it has been shown that IL-1 $\beta$  from dying cells induces a pro-inflammatory gene expression program in target immune cells involving increased expression of iNOS, adhesion molecules, and inflammatory chemokines (526, 527). Therefore, the functional outcome of IL-1 $\beta$  signaling is leukocyte trafficking and extravasation into the injury site (527). However, despite its pro-inflammatory properties, evidence has accumulated pointing to the pro-repair functions of IL-1 $\beta$  in the liver. A direct role in ECM remodeling and repair has been demonstrated via matrix metalloproteinases (MMPs) induction in HSCs (520). IL-1 $\beta$  is also an angiogenic factor through induction of VEGF and therefore contributes to the repair of injured vessels (527).

Collectively, these observations indicate that TNF $\alpha$  and IL-1 $\beta$  expression, typically upregulated during necroinflammation, may play dual roles as inflammatory and pro-repair factors upon hepatic injury.

In our study, CCl<sub>4</sub>-induced necroinflammation was also characterized by extensive myeloid infiltration of hepatic tissue (discussed below), indicating that recruited myeloid cells and their descendants perform necroinflammation-related functions (Figures 1F, 2C, 2D, and 3E and 3F, chapter 4). The dissection of myeloid cells, their functional profile, and the kinetics of the different myeloid subpopulations in response to CCl<sub>4</sub> injury will be discussed in subsequent sections.

### **5.c.1.b Tissue repair in response to CCl<sub>4</sub>-induced acute liver injury**

Tissue repair follows and terminates inflammation. Tissue repair is a dynamic process aimed at re-establishing the homeostatic organ structure and function following injury. During tissue repair, the markers of tissue damage and inflammation decrease, and tissue homeostasis is restored through the combination of compensatory cell proliferation, regeneration of the ECM, and angiogenesis that regenerates blood vessels and restores blood supply (528). Cytokines, chemokines, and growth factors provide the mitogenic signals required for cell proliferation and tissue repopulation (528). In agreement with this definition, we observed that the early repair phase of the wound healing response to CCl<sub>4</sub> injury was defined by a return to baseline levels of TNF $\alpha$  and IL-1 $\beta$ , significant reduction of plasma ALT, necrotic tissue contraction, increased expression

of pro-resolving genes (e.g., *Cx3cr1/Cx3cl1*, Figure 1G, chapter 4) and growth factors (e.g., *Tgfb* (Figure 8B, chapter 4), and *Ctgf* (not shown)), parenchymal and non-parenchymal cell proliferation, and upregulation of genes associated with ECM synthesis (e.g., *Colla1* (Figure 8B, chapter 4), and *Timp-1* (not shown)). During late repair, all indicators of tissue damage, inflammation, and cell proliferation returned to baseline levels and the homeostatic composition of liver resident immune populations was restored (Figure 1 and 3, chapter 4).

We observed upregulation of hepatic *Cx3cl1* and *Cx3cr1* restricted to the early repair phase (Figure 1G, chapter 4). CX3CL1, also known as fractalkine, is a chemokine that can be expressed as a membrane-bound or as a soluble peptide (529). While membrane-bound CX3CL1 functions as an adhesion molecule, soluble CX3CL1 is a chemoattractant for CX3CR1<sup>+</sup> leukocytes, including MoMFs, NCMs, NK cells, CD8<sup>+</sup> T cells, and  $\gamma\delta$  T cells (529). CX3CL1 has been associated with the pathogenesis of multiple chronic inflammatory conditions, mostly through the recruitment of cytotoxic effector cells and the resultant collateral tissue damage (530). However, CX3CL1 signaling during acute liver injury contributes to the resolution of inflammation and tissue repair. Mice deficient in CX3CR1 developed increased immune infiltration and higher expression of transcripts for pro-inflammatory cytokines and chemokines (e.g., *Tnfa*, *Ccl2*, *Ccl4*, and *Ccl5*) upon CCl<sub>4</sub> treatment compared to WT counterparts (94). The interaction between CX3CR1 and CX3CL1 mediates the conversion of pro-inflammatory/pro-fibrogenic macrophages (TNF $\alpha$ , IL-1 $\beta$ , iNOS, and TGF $\beta$ -producers) into anti-inflammatory/pro-repair macrophages (IL-10 and Arg-1-producers) upon acute liver injury (94, 201). In addition, the lack of CX3CR1 signaling in infiltrating MoMFs induces cell death and perpetuates inflammation (201).

Although in the liver, multiple cell types express CX3CR1 (e.g., HSCs, NK cells, and T cells) most of this CX3CR1 signal that we detected in the injury site colocalized with IBA1 and CCR2 suggests that MoMFs may be the main CX3CR1<sup>+</sup> population in the lesion (Figure 6A, chapter 4) (94). We observed that increased hepatic expression of *Cx3cr1/Cx3cl1* coincided with reduced expression of pro-inflammatory cytokines, decreased levels of tissue damage markers, and increased cell proliferation, supporting their role in the transition from necroinflammation to tissue repair as previously described (Figure 1, chapter 4) (94, 201).

### **5.c.1.c. Parenchymal and non-parenchymal cell proliferation during early tissue repair in response to CCl<sub>4</sub>-induced acute liver injury**

Another defining feature of tissue repair is the proliferation of tissue cells for the replacement of dead cells (133, 194, 202). In our study, we found hepatic upregulation of the proliferation marker Ki67 by qPCR. Further analysis of whole tissue sections identified the compartmentalized and simultaneous proliferation of parenchymal and non-parenchymal cells around portal tracts and central veins respectively (Figure 1H, 1I, and S1 chapter 4).

Ki67<sup>+</sup> hepatocytes with big round nuclei accumulated exclusively around portal tracts during early tissue repair (Figure 1I, chapter 4). Our observations are aligned with recent fate mapping studies demonstrating that during CCl<sub>4</sub> acute injury, differentiated hepatocytes around portal tracts re-enter the cell cycle, proliferate, and replenish the lost tissue (531). On the other side, Ki67<sup>+</sup> cells with irregularly shaped small nuclei, consistent with non-parenchymal cells, were present exclusively around central veins (Figure 1I, chapter 4). Immunofluorescence analysis showed some of these proliferating cells to be KCs (Figure 4E, chapter 4) and aHSCs (not shown). Together, these observations demonstrated that parenchymal and non-parenchymal cells exhibited the same kinetics of proliferation upon injury but suggested the possibility that spatially compartmentalized signals direct the expansion of these two major groups of cells in the liver during tissue repair.

### **5.c.1.d. Kinetics of the major innate and adaptive immune cell populations in response to CCl<sub>4</sub>-induced acute liver injury**

The liver is populated by relatively large populations of tissue-resident lymphocytes, and myeloid cells at the steady state (1). Tissue injury can rapidly and drastically change the composition of hepatic immune populations through cell depletion, cell recruitment, and differentiation of resident progenitors or infiltrating cells (133, 193, 194, 497). To better understand the dynamics of hepatic immune cells in response to CCl<sub>4</sub>-induced acute injury, we monitored by flow cytometry the major lymphocyte and myeloid populations in the liver (Figure 2 and 3, chapter 4).

During necroinflammation, the resident lymphoid cells were partially depleted (e.g., NKT cells, CD4<sup>+</sup> T cells, CD8<sup>+</sup> T cells, and B cells) and only recovered when the tissue started to heal (Figure 2A and 2B, chapter 4). Image analysis and qPCR data showed that resident CLEC4F<sup>+</sup>KCs also



decreased during necroinflammation, as previously reported in other liver injury models (Figure 4B to 4D) (129, 133, 204). These results suggested that CCl<sub>4</sub> toxicity may affect all the resident populations that are trapped in the damaged tissue, and repopulation is dependent on the healing of the affected zone.

Previous studies have shown that T cell-deficient mice (CD3 $\epsilon$ KO) are protected from ischemia-reperfusion injury (IRI), pointing to the role of T cells in enhancing the severity of IRI (532). In agreement with this, studies in the CCl<sub>4</sub> model revealed that severe combined immunodeficient mice (SCID) that are deficient in mature B and T cells exhibited reduced acute hepatocellular necrosis and ALT compared to their WT counterparts (533). Combined, these studies suggested a role for resident T cells in increasing tissue damage during acute liver injury. Furthermore, the characterization in recent years of liver-resident lymphocytes revealed that they exhibit an effector memory phenotype in the healthy liver, express multiple PRRs, and can respond in a TCR-dependent and TCR-independent manner. Therefore, they may be involved in the early sensing of tissue damage induced by CCl<sub>4</sub> and the rapid release of inflammatory chemokines and cytokines (239). Since T cells are depleted during necroinflammation in our study, it is unlikely that they played a functional role beyond sensing early damage and initial induction of inflammation in the model of acute liver injury with CCl<sub>4</sub> (Figure 2B, chapter 4).

As mentioned, we also observed depletion of intrahepatic B cells during necroinflammation and repopulation during early repair (Figure 2B, chapter 4). B cells in the liver of healthy mice were more abundant than any other lymphoid population in our flow cytometry data set suggesting their relevance (Figure 2B, chapter 4). However, unlike T cells, the lack of B cells had no impact on the development of or resolution of acute liver injury in three injury models (IRI, Con A, and APAP) using the B cell-deficient mice *muMt*<sup>-</sup> (532). Human data showed that during chronic HCV infection, B cells form aggregates around portal tracts (534-536). However, only a small fraction of these cells is HCV-specific, and the hepatic B cell follicles formed during HCV infection are rather composed of polyclonal naïve and memory B cells and do not function as ectopic germinal centers (537). Furthermore, it has been suggested that these B cells play a pathogenic role in the development of lymphoproliferative diseases (538). Intrahepatic B cells also negatively impact the development of AIH, as demonstrated in the context of B cell depletion using Rituximab, which led to a better outcome in patients with AIH and AIH mouse models (539, 540).

In contrast with hepatic resident immune cells, circulating myeloid cells massively infiltrated the liver during necroinflammation, as described in other models of hepatic injury (Figure 1F, 2E, and 2F, chapter 4) (133, 194, 199, 204). Dissection of the myeloid compartment using flow cytometry and t-SNE FlowSOM revealed that the most distinctive myeloid subpopulations accumulating in the liver after CCl<sub>4</sub> were inflammatory monocytes (Ly6C<sup>hi</sup> CX3CR1<sup>low</sup> Ly6G<sup>-</sup> MHC II<sup>-</sup>), neutrophils (Ly6C<sup>int</sup> Ly6G<sup>+</sup>), NCMs (Ly6C<sup>low</sup> CX3CR1<sup>hi</sup> F4/80<sup>+</sup> MHC II<sup>+</sup>), and MoMFs (Ly6C<sup>int</sup> Ly6G<sup>-</sup> CX3CR1<sup>+</sup> F4/80<sup>int</sup>) (Figure 3C, chapter 4).

Unexpectedly, a subpopulation fitting the profile of KCs was not identified even though KCs are the major myeloid population in the uninjured liver and one of the major ones during inflammation (Figure 3C, chapter 4). In this regard, previous reports have found an important discrepancy in the numbers of KCs in murine and human flow cytometry data sets when isolated using enzymatic digestion versus the numbers of KCs detected by *in situ* labeling (130, 541). Indeed, there is a growing realization that methods that combine mechanical tissue disruption with collagenase and benzonase digestion-based protocols are efficient at isolating MoMFs but not KCs (542). The mechanical aspect of our tissue dissociation protocol is in line with standard practices involving mincing the liver into small pieces with a razor blade, incubation at 37 °C in a shaker, and crushing/filtering the tissue fragments through a cell strainer (542, 543). However, our digestion media only contains standard amounts of collagenase D (0.1 mg/mL) and benzonase which may not be enough to dissociate KCs from the endothelium. Some protocols adapted to KC isolation have proposed 10 times increased collagenase concentrations and mixed several types of collagenases in the digestion media (e.g., collagenase D, collagenase V, and dispase that also cleaves fibronectin) (542). In our study, we compensated for this limitation through *in situ* detection of KCs by immunofluorescence (Figure 4A to C, chapter 4).

We observed that neutrophils and inflammatory monocytes represented small populations in the healthy liver (Figure 3F, chapter 4, Figure 19A, 19B, 19F, chapter 5). CCl<sub>4</sub> injury rapidly induced an extensive influx of both inflammatory populations early on during the necroinflammatory phase, as previously reported (133, 160, 192, 193, 497, 544). Neutrophil and monocyte infiltration was preceded and overlapped with an increased hepatic expression of their major chemokines *Cxcl1/2* and *Ccl2/7*, respectively (Figure 19C and 19D, chapter 5, and Figure 3G, chapter 4). Among the cellular sources of these chemoattractants are activated KCs, HSCs, and LSECs (85,

544). Importantly, CCR2 and its ligands CCL2 and CCL7 are required for monocyte egress from the bone marrow and accumulation in the injured liver (85, 192, 545-547). Furthermore, our data showed the upregulation of the monocyte/macrophage growth factor csf-1 (encoding M-CSF) during necroinflammation and early repair, suggesting its involvement in the expansion of the monocyte population in the liver as previously reported in the APAP model (Figure 3G, chapter 4) (133). M-CSF is known to induce the differentiation of bone marrow myeloid progenitors into inflammatory monocytes and is also required for their subsequent differentiation into MoMFs in peripheral tissues both in humans and in mice (548-550).

Despite the temporal overlap, depletion experiments showed that monocyte recruitment is not dependent on neutrophils in the model of sterile injury with a thermal probe (193). Our results also revealed no impact of neutrophil ablation in the recruitment of inflammatory monocytes upon CCl<sub>4</sub> injury (not shown). Similarly, antibody-mediated depletion of monocytes didn't affect neutrophil recruitment in the APAP model (194). Together, these data suggested that neutrophil and monocyte recruitment are independent of one another in liver inflammation. However, early studies showed that neutrophils release monocyte/macrophage chemokines pre-stored in their granules (e.g., cathepsin G and azurocidin) (551, 552). Accordingly, depletion of neutrophils delays inflammatory monocyte recruitment in a model of intramuscular injection of platelet-activating factor in mice (552). Since in the liver, several resident cells produce the major monocyte/macrophage chemokines CCL2 and CCL7 (e.g., KCs, hepatocytes, and HSCs), it is possible that the contribution of neutrophils to monocyte recruitment is relatively modest and difficult to quantify (553-555).

The flow cytometry analysis also showed that NCMs expanded about ten times during necroinflammation in response to CCl<sub>4</sub> toxicity (Figure 3F, chapter 4). Contrary to inflammatory monocytes, NCMs are present in the tissue at the steady state and their tissue trafficking is dependent on CX3CR1 instead of CCR2 (556). NCMs exhibit a unique crawling behavior inside blood vessels that was linked to immune surveillance of endothelial cells during homeostasis and to vessel repair after exposure to irritants, aseptic wounding, and peritoneal infection with *Listeria monocytogenes* (556). In addition, NCMs are involved in vessel protection and repair during homeostasis and pathological conditions in several organ systems including the skin and the central nervous system (203). However, their role in the normal and inflamed liver is still unknown (556-

558). In a recent study, Alkhani et al. profiled perinatal intrahepatic NCMs using scRNA-seq and identified an anti-inflammatory and pro-repair signature characterized by upregulation of *Il4ra* and *Tgfb1* (557). Their study showed an association between hepatic NCMs and the resolution of rhesus rotavirus (RRV)-mediated periportal inflammation, but causation was not established, and the underlying mechanism was not investigated. Since we observed that intrahepatic NCMs peak at the same time as neutrophils and inflammatory monocytes in the CCl<sub>4</sub> model, NCMs may be involved in preventing or repairing immune-mediated collateral damage caused by inflammatory leukocytes (Figure 3F, chapter 4). The recent availability of engineered mice with a reduced number of NCMs (Nr4a1-deficient mice) and reporter mouse models for NCMs (e.g., CX3CR1<sup>GFP</sup>) allow the study of the functional role of NCMs in acute liver injury (559, 560). Further studies are granted to address this relevant question.

During the late part of necroinflammation and early tissue repair, the monocytic and granulocytic populations declined sharply and MoMFs became the most abundant myeloid population (Figure 3F, chapter 4). The decrease of inflammatory monocytes temporally coincided with the increase of MoMFs, in agreement with the former population differentiating into the latter (Figure 3F, chapter 4) (133, 193). In addition, we observed that the peak of MoMF infiltration upon CCl<sub>4</sub> injury coincided with the transition to tissue repair, in agreement with the postulated pro-resolution phenotype assigned to MoMFs in the APAP model and response to a focal thermal injury (Figure 3F, chapter 4) (133, 193). During late repair, MoMFs rapidly decreased to baseline levels demonstrating that this population is transitory as previously reported in other acute liver injury models (Figure 3F, chapter 4) (133, 194). In the hepatic tissue, we identified a population of IBA1<sup>+</sup>CLEC4F<sup>-</sup> macrophages fitting the phenotype and kinetics of flow cytometry-identified MoMFs (Figures 4A, 4G, 4H, and Figures 6A and 6B, chapter 4). The spatial characterization of these tissue MoMFs in response to CCl<sub>4</sub>-induced injury will be discussed in the following sections.

Surprisingly, two waves of neutrophils transiently infiltrated the liver during CCl<sub>4</sub> injury (Figure 3F, chapter 4 and Figure 19B and 19F, chapter 5). This observation will be discussed in more detail in the next section. Finally, during late repair the number of monocytes, neutrophils, and MoMFs returned to baseline bringing the total number of intrahepatic CD11b<sup>+</sup> myeloid cells back to homeostatic levels (Figure 1F and 3F, chapter 4).

In summary, CCl<sub>4</sub>-mediated injury induces partial depletion of resident immune cell populations and recruitment of circulating phagocytes and their presence in the liver temporarily overlaps with the restoration of tissue homeostasis. The rapid changes in the composition of the population of intrahepatic leukocytes emphasize the significance of the temporal dimension for the proper understanding of the immune response to acute liver injury.

#### **5.c.1.e. Profile of myeloid cells during the wound healing response to CCl<sub>4</sub>-induced acute liver injury**

Myeloid cells infiltrated the hepatic tissue during necroinflammation and persisted during the early repair. The functional characterization of these myeloid cells revealed that they are major producers of inflammatory TNF $\alpha$ , pro-fibrogenic IL-13, anti-inflammatory IL-10, and pro-repair Arg-1, as previously reported in models of liver inflammation (Figure 2C and 2D, chapter 4) (523, 561-566). This functional profile and kinetics suggested that the heterogeneous population of hepatic myeloid cells present in the inflamed liver has the potential to mediate inflammation, resolution of inflammation, and repair.

IL-10-producing myeloid cells accumulated in the liver of CCl<sub>4</sub>-treated mice during the transition from necroinflammation to tissue repair (Figure 2C and 2D, chapter 4). IL-10 is an immunoregulatory cytokine that plays important roles in preventing or attenuating hepatic inflammation upon liver injury (566). Several cellular sources of IL-10 have been identified in the healthy and in the inflamed liver demonstrating its immune modulatory activity both during homeostasis and inflammation. Hepatocytes, LSECs, HSCs, KCs, and resident T cells produce IL-10 in response to a variety of danger, infectious, or stress signals (e.g., LPS, TNF $\alpha$ , catecholamines) (99, 566-568). IL-10 deficiency in the CCl<sub>4</sub> model has been linked to increased neutrophilic inflammation and elevated levels of TNF $\alpha$  (569, 570). In addition, *in vitro* assays showed that IL-10 treatment reduced LPS-induced TNF $\alpha$  secretion by KCs (571). In our study, IL-10 and TNF $\alpha$  production by infiltrating myeloid cells temporally overlapped, suggesting that IL-10 may prevent immune-related collateral damage caused by TNF $\alpha$  during CCl<sub>4</sub>-induced inflammation.

We also observed an accumulation of intrahepatic IL-13-producing myeloid cells during the transition from necroinflammation to tissue repair (Figure 2C and 2D, chapter 4). Although not

previously investigated in the CCl<sub>4</sub> model, IL-13 was shown to be a potent activator of HSCs *in vitro*, and in liver infection with Schistosoma species (e.g., *S. mansoni* and *S. japonicum*) (564, 572-575). IL-13 directly induces the expression of  $\alpha$ SMA, type I collagen, and pro-fibrogenic connective tissue growth factor (CTGF) by HSCs (576, 577). Repeated IL-13 signal in the injured liver promotes fibrosis, as seen in murine models of Schistosomiasis (572, 574). In HCV and steatosis/steatohepatitis patients, IL-13 expression positively correlates with the fibrosis stage (578, 579). However, whilst sustained IL-13 signaling leads to hyperactivation of HSCs, and thereby to fibrosis during chronic inflammation, the transient release of IL-13 may be beneficial through temporary induction of HSC activation and subsequent ECM repair upon CCl<sub>4</sub> acute injury. In support of this possibility, our results showed that the increase of IL-13-producing myeloid cells is restricted to the necroinflammatory and early repair phases and temporarily overlapped with HSC activation, as determined by mRNA profiling (ACTA-2, and Colla1) and by quantification of  $\alpha$ SMA<sup>+</sup> HSCs in the hepatic tissue (Figures 2C, 2D, 8B, and 8C, chapter 4). Myeloid cell-derived IL-13 expression also preceded and overlapped with the hepatic expression of fibrogenic markers TGF $\beta$  and CTGF.

As mentioned above, our data showed that Arg-1 expression by myeloid cells increased during necroinflammation and peaked at the transition from necroinflammation to early repair (Figure 2C and 2D, chapter 4). In addition, the mean fluorescent intensity (MFI) of Arg-1 in myeloid cells substantially increased during tissue repair compared to necroinflammation suggesting its involvement in the healing of CCl<sub>4</sub> injury (Figure 18). Moreover, MoMFs specifically showed upregulation of Arg-1 during repair.

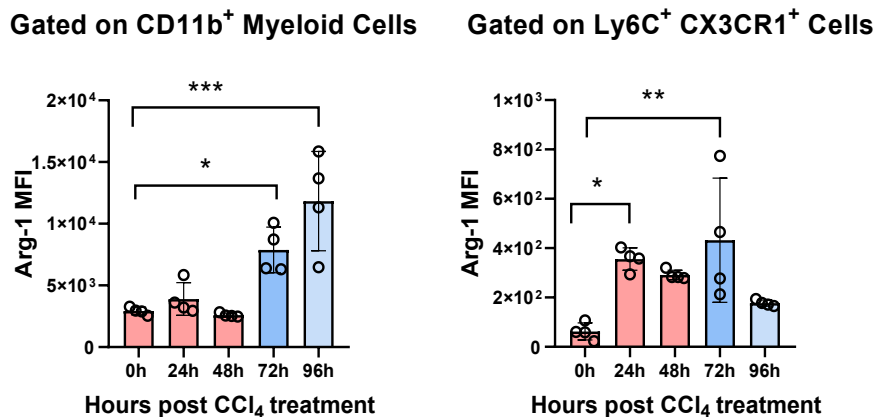


**Figure 18: Myeloid cells and particularly MoMFs increase Arg-1 expression during tissue repair.** (A) Mean fluorescent intensity (MFI) of Arg-1 in intrahepatic myeloid cells upon CCL4 treatment. (B) MFI of Arg-1 in intrahepatic Ly6C<sup>+</sup> CX3CR1<sup>+</sup> MoMFs.

Arg-1 expression by myeloid cells is tightly regulated and is induced by signature Th2 cytokines IL-4 and IL-13. Both iNOS and Arg-1 define two alternate functional states of macrophages known as classically and alternatively activated, or M1 and M2, respectively (580, 581). Arg-1 competes with iNOS for L-arginine, thereby limiting the production of the antimicrobial and cytotoxic molecule nitric oxide (NO) (561, 582). By contrast, Arg-1 converts L-arginine to L-ornithine and urea, and subsequently, L-ornithine can be converted to polyamines and proline. Studies in the skin (surgery wounds and skin ulcers) have shown that while polyamines are required for cell proliferation, proline is needed for collagen synthesis and ECM repair. Thus, Arg-1 is a critical effector molecule for matrix synthesis and re-epithelialization after injury in the skin (583). In the inflamed liver, we observed a temporal association between peak Arg-1 expression in myeloid cells, the proliferation of hepatocytes, and maximal collagen expression, suggesting similar pro-repair functions in the liver to the ones observed in the injured skin (Figure 2C, 2D, 1H, and 8B, chapter 4). Further research is warranted to establish the role of myeloid-associated Arg-1 during hepatic tissue repair.

#### **5.c.1.f. Neutrophils in response to acute liver injury**

Neutrophils are the first line of defense against extracellular bacteria and fungi and are important effector cells in all types of injury that overwhelms the phagocytic capacity of tissue-resident myeloid cells as is the case in severe sterile or toxic injuries. Neutrophils are generated in the bone marrow and constitute the most abundant circulating immune population accounting for up to 70 and 25 % of all leukocytes in human and mice blood, respectively (584, 585). In addition to their innate antimicrobial properties, neutrophils also perform multiple effector functions in response to sterile injury and during homeostasis (497, 586, 587).

Once at the injury site, neutrophils eliminate invading pathogens through the release of granules containing antimicrobial peptides, ROS, and enzymes. In addition, neutrophils can capture pathogens through complement receptors, Fc receptors, and integrins, or can release neutrophil extracellular traps (NETs) for pathogen immobilization (588). Such neutrophil antimicrobial

functions can cause tissue damage and impair wound healing as observed in multiple acute and chronic injury settings (202, 588, 589).

Aside from their antimicrobial and inflammatory functions, neutrophils are also promoters of tissue repair (587). Among the healing functions of neutrophils is their induction of angiogenesis and ECM restoration which are typically dysregulated in non-healing wounds like in diabetes and cancer (590). In addition, in models of skin injury, impaired neutrophil recruitment leads to delayed repair due to decreased neo-vascularization and epithelialization (591). Similarly, in the liver, neutrophils dismantle damaged vessels and create tunnels for new vessel formation thereby initiating healing in response to focal thermal sterile injury (497). Moreover, neutrophils remove apoptotic cells and inflammatory debris, critical processes in proper healing (592). Indeed, neutrophil depletion during acute hepatic injury leads to delayed repair as evidenced by increased ALT levels, augmented injury size, and reduced debris clearance (202, 497).

Neutrophils also indirectly contribute to repair through their effects on other cells. For example, efferocytosis of apoptotic neutrophils reprograms the transition of pro-inflammatory into pro-resolving macrophages (593, 594). In addition, neutrophil-derived ROS trigger the phenotypic conversion of pro-inflammatory  $\text{Ly6C}^{\text{hi}}\text{CX3CR1}^-$  monocytes/macrophages into pro-resolving  $\text{Ly6C}^{\text{int to lo}}\text{CX3CR1}^+$  MoMFs (202).

Regarding the origin of neutrophils in the liver, in a recent report, Casanova-Acebes et al. used a parabiosis model to track neutrophils and monitor them as they leave the bone marrow and infiltrate peripheral tissues during homeostasis. This study demonstrated that neutrophils in the hepatic tissue are derived from circulation. They do not proliferate in the liver at least during the steady state (586).

In our study, we delineated the kinetics of neutrophils in response to  $\text{CCl}_4$  acute liver injury (Figure 3F). We found few neutrophils in the healthy liver. Indeed, and in agreement with previous reports, steady-state neutrophils were sparsely and homogeneously distributed inside the liver sinusoids (not shown) (194, 497, 586). However,  $\text{CCl}_4$  injury induced two temporarily separated neutrophil recruitment events: one during necroinflammation and another during repair (Figures 3F, 4, and 19A, 19B and 19F, 5). The characterization of the tissue context during necroinflammation versus repair revealed two significantly different tissue environments in terms of immune cell composition, tissue damage markers, expression of pro-inflammatory cytokines, and proliferation



of cells (Figures 1, chapter 4). These differences suggested that neutrophils infiltrating the liver during necroinflammation vs. repair may have different interacting partners and perform different functions.

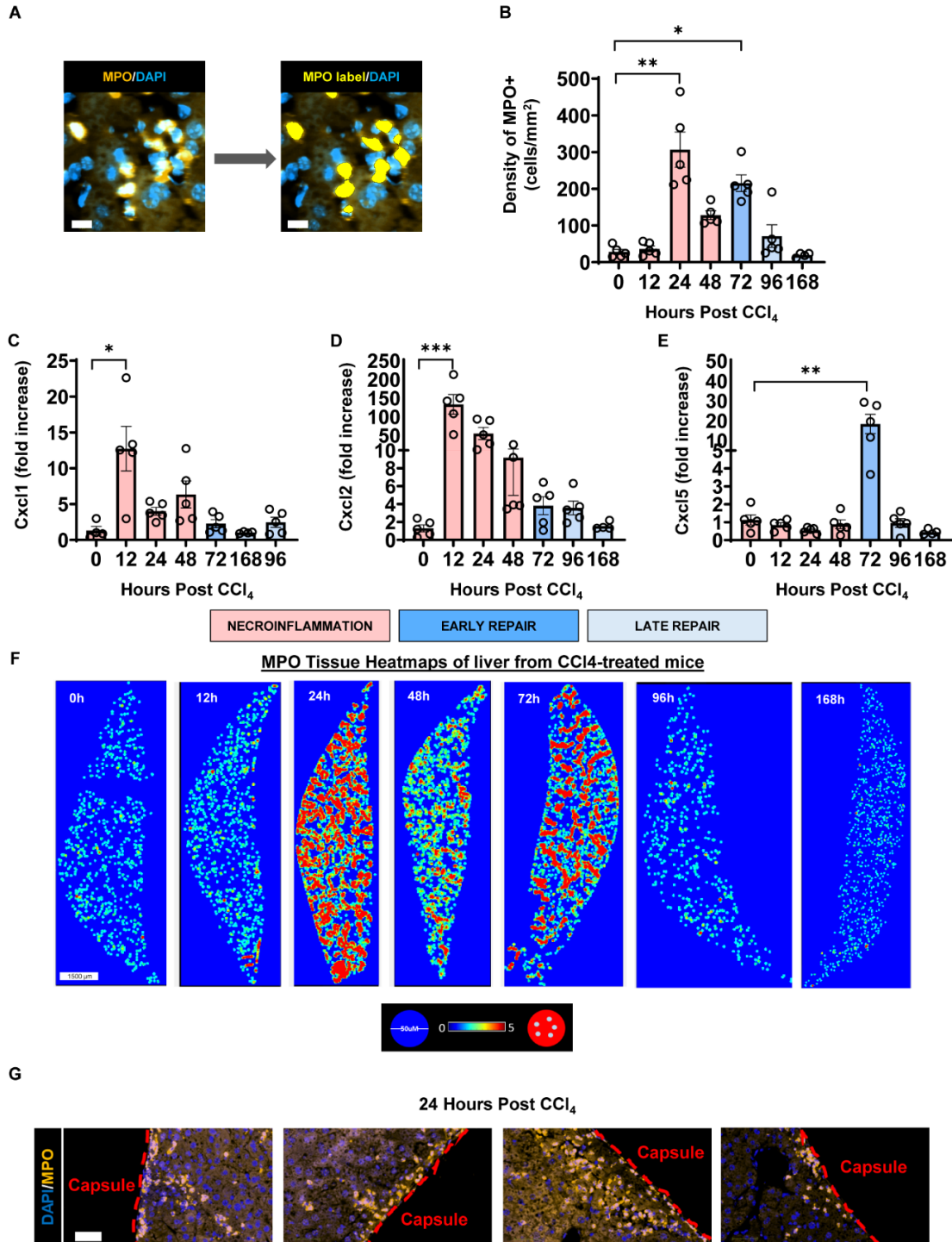


**Figure 19: CCl<sub>4</sub> injury induces two temporarily separated waves of neutrophil infiltration.** (A) On the left is a representative image of immunofluorescence staining for MPO (yellow) and DAPI (blue), and on the right is the processed image with a yellow label on the MPO<sup>+</sup> neutrophils. Scale bar is 10  $\mu$ m (B) Quantification of the tissue density of MPO<sup>+</sup> cells. (C-E) Relative gene expression

levels determined by qPCR on bulk liver tissue: (C) *Cxcl1*, (D) *Cxcl2*, and (E) *Cxcl5*. mRNA expression data represent fold increase relative to 0 h controls and was normalized to 28s. (F) Representative tissue heatmaps of MPO<sup>+</sup> cells (neutrophils) in hepatic tissue sections at 0, 12, 24, 48, 72, 96, and 168 h post CCl<sub>4</sub>. High density areas are represented in red and have 5 neutrophils or more per 50 μm diameter circles. Areas with 0 neutrophils are represented in dark blue. Areas with intermediate density values are represented according to the scale provided in figure F. (G) Representative images from liver of 24 h CCl<sub>4</sub>-treated mouse showing aggregates of MPO<sup>+</sup> cells (yellow) around the liver capsule (dotted red lines). Scale bar is 40 μm. Data are representative of 2 independent experiments (n=4-5 per group). Data are shown as mean ± SEM. One Way ANOVA. Dunn's Multiple Comparison Test. \*P < 0.05, \*\*P < 0.01, \*\*\*P < 0.001.

Recently, neutrophil subsets with different transcriptional, functional, and phenotypic properties have been identified (595). Indeed, our preliminary characterization supports the hypothesis that the neutrophils recruited during necroinflammation and those recruited during repair are two different subpopulations (596). While neutrophil infiltration during necroinflammation was preceded and overlapped with elevated transcript levels of the major neutrophil chemoattractants *Cxcl1* and *Cxcl2*, and baseline levels of *Cxcl5*, the second wave of neutrophils was associated with a significant decrease of *Cxcl1*, restoration to baseline levels of *Cxcl2*, and elevated *Cxcl5* (Figure 19 C to E). Previous studies have found activated KCs, HSCs, and LSECs to be the main cellular sources of these chemokines (85, 594). Moreover, LCMs were recently added to the list of tissue macrophages that recruit neutrophils in response to invading bacteria (intraperitoneal *Listeria monocytogenes*) and were shown to produce CXCL1 and CXCL2 (131). In this regard, our observations in the CCl<sub>4</sub> model support the notion of the involvement of LCMs in neutrophil recruitment. We found that during necroinflammation, pockets of neutrophils accumulated in the liver capsule, colocalized with IBA1<sup>+</sup> capsular macrophages, and seemingly accessed the liver through discontinuation points in the network formed by these macrophages (Figures 19G and 20). Interestingly, accumulation of neutrophils in the hepatic capsule was not observed for the second wave of neutrophils infiltrating the liver during tissue repair. These observations suggest that LCMs may mediate neutrophil recruitment during necroinflammation and constitute a gateway for access to the liver also in non-infectious models of hepatic injury (131).

## 24h CCl<sub>4</sub>

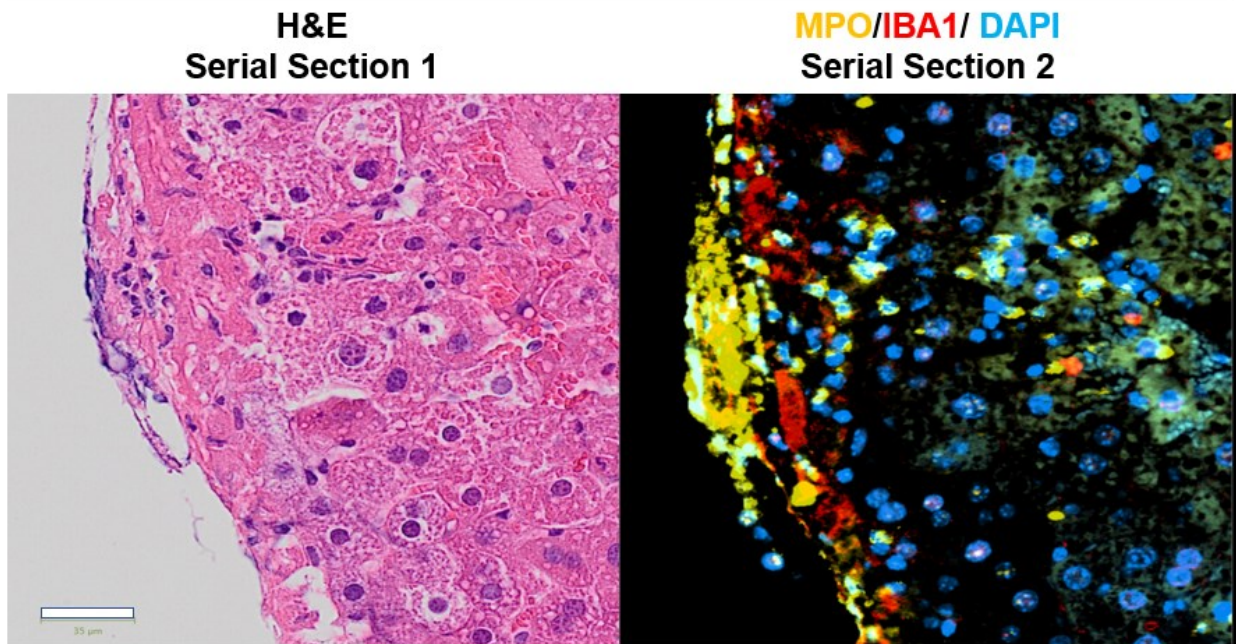


**Figure 20:** Neutrophils accumulate in the capsule of CCl<sub>4</sub>-injured mice during necroinflammation and seem to access the parenchyma through discontinuation points in the network of IBA1<sup>+</sup> capsular macrophages. Digital alignment of two serial sections from livers of 24h CCl<sub>4</sub>-treated mouse. On the left H&E staining on section 1, and on the right immunofluorescence showing neutrophils (MPO<sup>+</sup>) in yellow, LCMs (IBA1<sup>+</sup>) in red, and DAPI in blue on serial section 2. Scale bar, 35 μm.

The heterogeneity of neutrophils also involves their site of origin and differentiation pathways (597). Under homeostatic conditions, the bone marrow is the primary site of granulopoiesis from where most circulating and tissue-infiltrating neutrophils are derived. These classical neutrophils are mostly mature neutrophils exhibiting hypersegmented nuclei and an inflammatory and antimicrobial profile (598-600). Classical neutrophils have also been called high or normal-density neutrophils (HDNs) because of their density properties when analyzed using discontinuous gradient centrifugation (596). However, in recent years, new evidence has shown that during acute infections, cancer, severe trauma, and pregnancy, normal granulopoiesis can be switched into an emergency mode (600). Emergency granulopoiesis can take place both in the bone marrow and in the spleen (extramedullary granulopoiesis) (597, 599). By contrast to normal granulopoiesis, this alternative pathway generates a larger cellular output and a more heterogeneous population of

peripheral neutrophils including immature neutrophils with horseshoe-shaped nuclei and an anti-inflammatory/immunosuppressive profile (598). These neutrophils can be separated from the HDN fraction using discontinuous gradient centrifugation and are known as low-density neutrophils (LDNs) (601). In our study, we used a combination of two successive discontinuous gradient centrifugation methods and flow cytometry and determined that while infiltrating neutrophils are mostly HDNs during necroinflammation, there is a significant enrichment of LDNs during tissue repair (Figure 21).

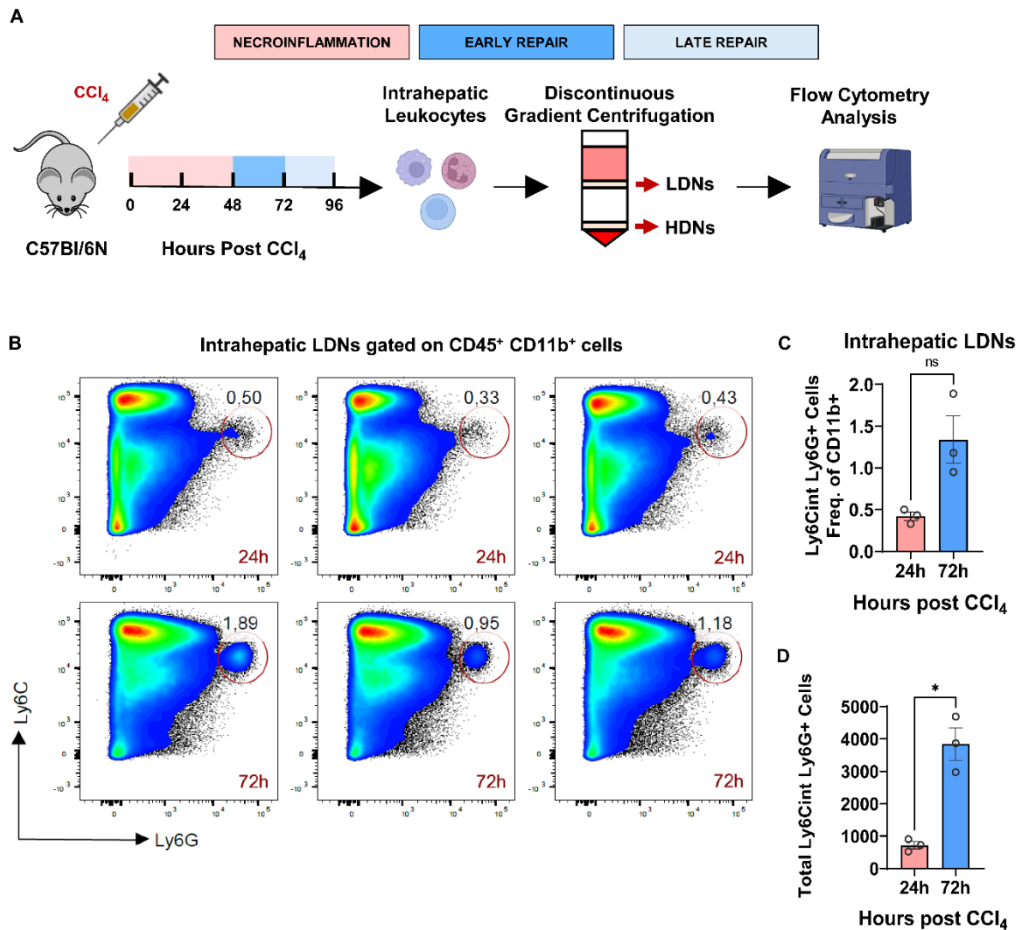


**Figure 21: The neutrophils that infiltrate the liver during necroinflammation exhibit different cellular density than neutrophils infiltrating the liver during repair. (A) Schematics of the experimental design. (B) Representative pseudocolor plots of intrahepatic LDNs at 24 and 72 hours post CCl<sub>4</sub>. (C) Quantification of frequency intrahepatic LDNs relative to total myeloid cells. (D) Quantification of total numbers of intrahepatic LDNs per gram of liver tissue. Data are shown as mean  $\pm$  SEM. Mann-Whitney Test. \* $P < 0.05$ , \*\* $P < 0.01$ , \*\*\* $P < 0.001$ .**

The population of LDNs is highly heterogeneous and its composition varies in different disease contexts. In this regard, granulocytic myeloid-derived suppressor cells (gMDSCs) are the most conspicuous LDN subpopulation in advanced cancer and have been extensively studied (602). gMDSCs are pathogenic in the context of cancer through a variety of effector mechanisms including suppression of anti-tumoral T cells, induction of Tregs, inhibition of DC, and macrophage activation. In addition, gMDSCs can promote cancer progression through non-immune effector mechanisms as well, like induction of vessel formation and ECM remodeling which are typical pro-repair functions. Since tumor cells hijack existing mechanisms, it has been proposed that the evolutionary role of gMDSCs is not tumor promotion but the resolution of inflammation, prevention of immune-mediated tissue damage, and tissue repair during chronic inflammation and wound healing (597).

Considering that the second wave of neutrophils infiltrate the liver during tissue repair and are enriched in LDNs, we propose that this is a subset of pro-repair neutrophils phenotypically and functionally different from necroinflammation-associated neutrophils. To gain insight into the contribution of neutrophils to tissue repair, we depleted neutrophils during CCl<sub>4</sub>-induced acute liver injury using anti-Ly6G antibodies (Figures 22A and 22B). We found that anti-Ly6G-mediated depletion of neutrophils was only partially efficient in the liver with a reduction of about 50 % of infiltrating neutrophils at 48 h post CCl<sub>4</sub>, but no reduction at 72h post CCl<sub>4</sub>. Neutrophil depletion did not affect the levels of tissue damage as assessed by ALT and % of the necrotic area, but significantly reduced the hepatic expression of the proliferation marker *Ki67*, the growth factor *Tgfβ*, and the markers of HSC activation *ACTA-2* and *Coll1a1* (Figure 22B to D). Indeed, we detected colocalization of neutrophils and HSCs in the necrotic area of the livers of CCl<sub>4</sub>-treated mice during early repair (Figures 22E, and 23). These results suggested that neutrophils are involved in the induction of pro-repair functions like cell proliferation and ECM repair, but the experimental design did not allow to dissect the effect of necroinflammation-associated neutrophils vs. repair-associated neutrophils which would require selective depletion of each subpopulation. Further spatial characterization showed that neutrophils colocalized with IBA1<sup>+</sup> CLEC4F<sup>-</sup> MoMFs and IBA1<sup>+</sup> CLEC4F<sup>+</sup> KCs during tissue repair (Figure 24).

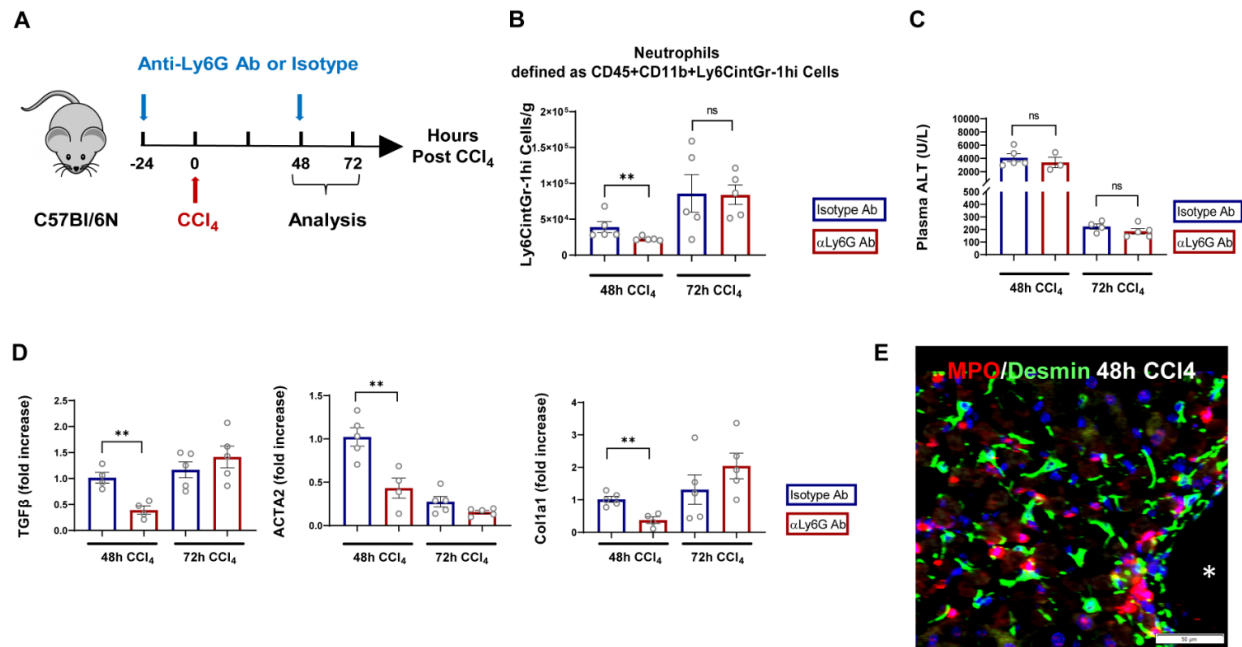


**Figure 22: Neutrophil depletion before CCl<sub>4</sub> injury has no impact on tissue damage but decreases the expression of fibrogenic cytokines and activation markers of HSCs during early repair.** (A) Schematics of the experimental design. (B) Quantification of intrahepatic neutrophils by flow cytometry at 48 and 72 hours post CCl<sub>4</sub> with and without neutrophil depletion (C) Quantification of plasma ALT levels at 48 and 72 hours post CCl<sub>4</sub> with and without neutrophil depletion (D) Relative gene expression levels determined by qPCR on bulk liver tissue for TGFβ, ACTA-2, and Col1a1. mRNA expression data represent fold increase relative to 48 h isotype controls and was normalized to 28s. Data are shown as mean ± SEM. Mann-Whitney Test. \*P < 0.05, \*\*P < 0.01, \*\*\*P < 0.001.

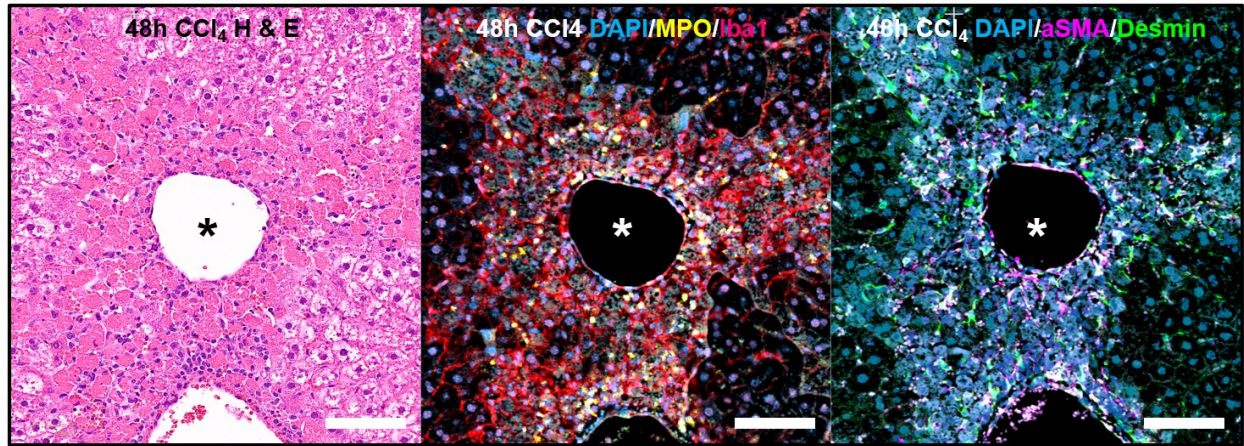


**Figure 23: Neutrophils, Macrophages, and aHSCs spatially and temporally overlap in the centrilobular necrotic area at 48h post CCl<sub>4</sub> treatment.** Digitally aligned serial sections showing on the left H&E staining; in the middle, multiplex immunofluorescence (mIF) for neutrophils (MPO in yellow), and macrophages (IBA1 in red); and on the right, mIF for HSCs (desmin in green), and aHSCs ( $\alpha$ SMA in magenta). Green and magenta colocalization is shown in white. Nuclei were stained with DAPI (blue). Scale bar is 75  $\mu$ m. \* indicates central vein.

72 h post CCl<sub>4</sub>

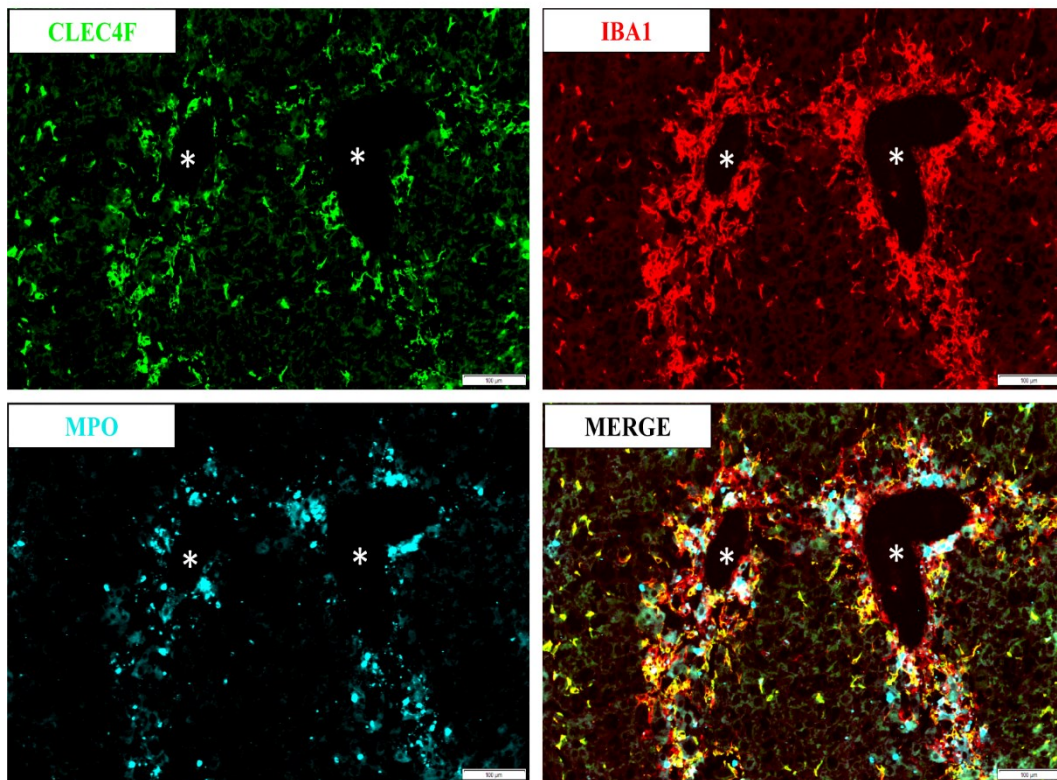




**Figure 24: Neutrophils colocalize with IBA1<sup>+</sup> CLEC4F<sup>-</sup> MoMFs and IBA1<sup>+</sup> CLEC4F<sup>+</sup> KCs during tissue repair.** Representative image of *mIF* for neutrophils (MPO in cyan), IBA1 (in red, and CLEC4F (in green) at 72 h post CCl<sub>4</sub>. Red and green colocalization shows in yellow, and green and cyan colocalization is shown in white. Scale bar is 100 μm. \* indicates central vein.

In summary, we have identified two waves of neutrophils that are induced at different stages in the wound-healing response to acute liver injury. These two waves are temporarily associated with different patterns of chemokines and have a different composition relative to HDNs vs. LDNs. Our preliminary results are not sufficient to establish whether they merely represent two different subpopulations with transient phenotypes or activation states sharing the same origin, or real different subsets exhibiting divergent profiles and committed to distinctive effector functions (596). Ongoing efforts by our team are focusing on transcriptional profiling of sorted necroinflammation-associated vs. repair-associated neutrophils. In addition, methods for the selective and efficient depletion of each of these populations will be optimized to establish their contribution to tissue repair *in vivo* models of acute liver injury, and assays for assessing their effector functions will be carried out.

### **5.c.1.g. Inflammatory monocytes and MoMFs in response to acute liver injury**

Monocytes are mononuclear phagocytes present in the blood and constitute about 10% of peripheral leukocytes in humans and 4% in mice (203). Inflammatory monocytes develop in the bone marrow and are defined as CD115<sup>+</sup>Ly6C<sup>hi</sup> CCR2<sup>+</sup>CD62<sup>+</sup>Ly6G<sup>-</sup>CX3CR1<sup>low</sup> blood cells in mice (545, 546, 603). These Ly6C<sup>hi</sup> monocytes are rapidly recruited to peripheral tissues upon damage or pathogen invasion where they perform a variety of effector functions and differentiate into MoMFs and monocyte-derived DCs (203). Homing of inflammatory monocytes to the hepatic lesion is dependent on CCR2 (133, 193). Once at the injury site, they can perform both pro-inflammatory and pro-resolving functions depending on the cues present in the tissue microenvironment (133, 193, 194).

Upon sterile or toxic acute liver injury, liver infiltrating inflammatory monocytes reprogram themselves into MoMFs as demonstrated using lineage tracing (e.g., CCR2<sup>RFP</sup>CX3CR1<sup>GFP</sup> mice), adoptive transfer, and antibody-mediated depletion models of inflammatory monocytes (133, 193). This phenotypic switch takes place at the injury site and involves the downregulation of CCR2 and

Ly6C and the upregulation of CX3CR1. Several factors drive this conversion including CX3CL1, IL-4, and IL-10 signaling, neutrophil-derived ROS, and phagocytosis of necrotic cells (94, 133, 134, 181, 193, 199, 202).

The spatial and temporal behavior of infiltrating inflammatory monocytes and their MoMF progeny has been delineated in the model of sterile injury with a thermal probe. In this model, Ly6C<sup>hi</sup>CCR2<sup>+</sup> CX3CR1<sup>-</sup> inflammatory monocytes colonize the necrotic tissue as early as 8 h post-injury but only start to differentiate into Ly6C<sup>int</sup>CCR2<sup>+</sup>CX3CR1<sup>+</sup> MoMFs at 48 h (Figure 15, chapter 1) (193). The phenotypic switch from inflammatory monocytes to MoMFs takes place at the border of the injury. Subsequently, the newly generated MoMFs crawl inside the core of the lesion where they clear necrotic tissue (193). While this model is very informative regarding the kinetics of monocyte/macrophage infiltration and differentiation, and their relative topographical distribution, the fact remains that this model lacks the zone-specific characteristics of most liver injuries (e.g., CV lesion in toxic injury, portal tract inflammation in cholangiopathies). The distribution of MoMFs has also been analyzed in more relevant models like APAP intoxication using monocyte reporter mice. This study showed that MoMFs infiltrated the region surrounding injured CVs and localized in the deeper regions (Figure 14, chapter 1). These MoMFs exhibited a gorged appearance that suggested the engulfment of large particles or dead cells (133).

In our study, we identified a population of IBA1<sup>+</sup>CLEC4F<sup>-</sup> macrophages that infiltrate the CV region upon CCl<sub>4</sub> injury (Figure 4A, 4G, and 4H, chapter 4). IBA1<sup>+</sup>CLEC4F<sup>-</sup> macrophages exhibited characteristics of MoMFs including expression of Ly6C, CX3CR1, and CCR2 (Figure 6A and 6B, chapter 4). Furthermore, we showed that IBA1<sup>+</sup>CLEC4F<sup>-</sup> macrophages were not YSKCs because they lacked expression of CLEC4F and MARCO. IBA1<sup>+</sup>CLEC4F<sup>-</sup> macrophages were not peritoneal macrophages because they did not express GATA6 (Figure 6A and 6C, chapter 4). In addition, image analysis showed that, unlike resident CLEC4F<sup>+</sup> KCs, IBA1<sup>+</sup>CLEC4F<sup>-</sup> MoMFs were absent in the uninjured liver and massively infiltrate the necrotic tissue during necroinflammation and early repair, to subsequently disappear during late repair (Figures 4G and 4H, chapter 4). These macrophages were closer to the CVs when compared to CLEC4F<sup>+</sup> resident KCs and exhibited a globular morphology different from the stellar shape of KCs (Figure 5, chapter 4). In addition, serial imaging showed that IBA1<sup>+</sup>CLEC4F<sup>-</sup> MoMFs overlapped with enucleated apoptotic hepatocytes suggesting that they are involved in the clearance of dead cells around

injured CVs (Figure S5, chapter 4). Importantly, these two subpopulations of macrophages established intimate contact all along the wound healing response as demonstrated by imaging and 3D reconstruction (video 1, chapter 4), suggesting functional interdependence and cooperation.

Our data showed that CLEC4F<sup>+</sup> KCs interacted with HSCs during the steady state and are therefore the most likely source of early signals for hepatic stellate cell activation upon injury (0-24 h post CCl<sub>4</sub>) (Figure 8A, chapter 4). By contrast, IBA1<sup>+</sup>CLEC4F<sup>-</sup> MoMFs infiltrated the deep necrotic area during the transition from necroinflammation to tissue repair (48h post CCl<sub>4</sub>) and further colocalized with HSCs at the time of their peak of activation (Figure 8B to E, chapter 4). These observations demonstrated that resident infiltrating MoMFs and resident KCs exhibited different timing for interaction with HSCs and may therefore differentially modulate their phenotype and effector functions during healing. In summary, different kinetics, morphology, and spatial distribution suggested that infiltrating IBA1<sup>+</sup>CLEC4F<sup>-</sup> MoMFs and resident CLEC4F<sup>+</sup> KCs perform unique and non-overlapping functions during the response to CCl<sub>4</sub>-induced acute liver injury.

#### **5.c.1.h. Kupffer cells in acute liver injury:**

KCs are the most abundant macrophage population of the body. They play important roles during homeostasis and in response to damage. In the steady state, KCs perform such diverse functions as phagocytosis of aged cells and platelets, removal of LPS, processing of iron and lipids, and induction of T cell tolerance to food-derived and commensal bacteria-derived antigens (163-173, 176).

KCs are located inside the liver sinusoids and express a large repertoire of PPRs that allows them to sense incoming threats or damage signals from injured hepatocytes or LSECs (164, 179, 604). The detection of tissue damage or pathogen invasion by KCs leads to their activation and subsequent release of inflammatory cytokines and chemokines that initiates inflammation (162, 163, 164). In addition to their sentinel and inflammatory properties, KCs have been shown to promote tissue repair as discussed below (189, 190). KCs exhibit a zoned distribution along the porto-central sinusoidal axis with a higher concentration of KCs around portal triads and slightly different sizes, morphology, and functional properties between periportal vs. pericentral KCs (7,

149-151). Even though KCs are broadly assumed to be stationary, their spatial behavior in response to injury has not been sufficiently investigated (53, 130, 143).

In our study, we monitored the quantity and spatial distribution of KCs in liver tissue sections to better understand their role during the wound-healing response to CCl<sub>4</sub>-induced acute liver injury. We used CLEC4F as a specific marker of KCs (153-155). We observed partial depletion of KCs during necroinflammation as determined by CLEC4F immunofluorescence and mRNA expression (Figure 4B to D, chapter 4, and Figure 25, chapter 5). A similar reduction in KCs was reported in the APAP model and the model of radiation-induced hepatic injury (129, 133, 194). Using multiplex immunofluorescence, we showed that during necroinflammation, the remaining KCs got located at the periphery of the injury forming ring-like structures surrounding and in intimate contact with MoMFs that filled the innermost region of the necrotic tissue (Figure 5A chapter 4, and Figure 25, chapter 5). With the progression of the healing response, KCs moved closer to the injured CVs where they proliferated and formed dense aggregates during early repair. These aggregates dissipated by the end of the repair phase and the homeostatic distribution of KCs was restored (Figure 4D to F, chapter 4, and Figure 25, chapter 5).

### Hepatic tissue from CCl<sub>4</sub>-treated mice

DAPI/CLEC4F/Desmin

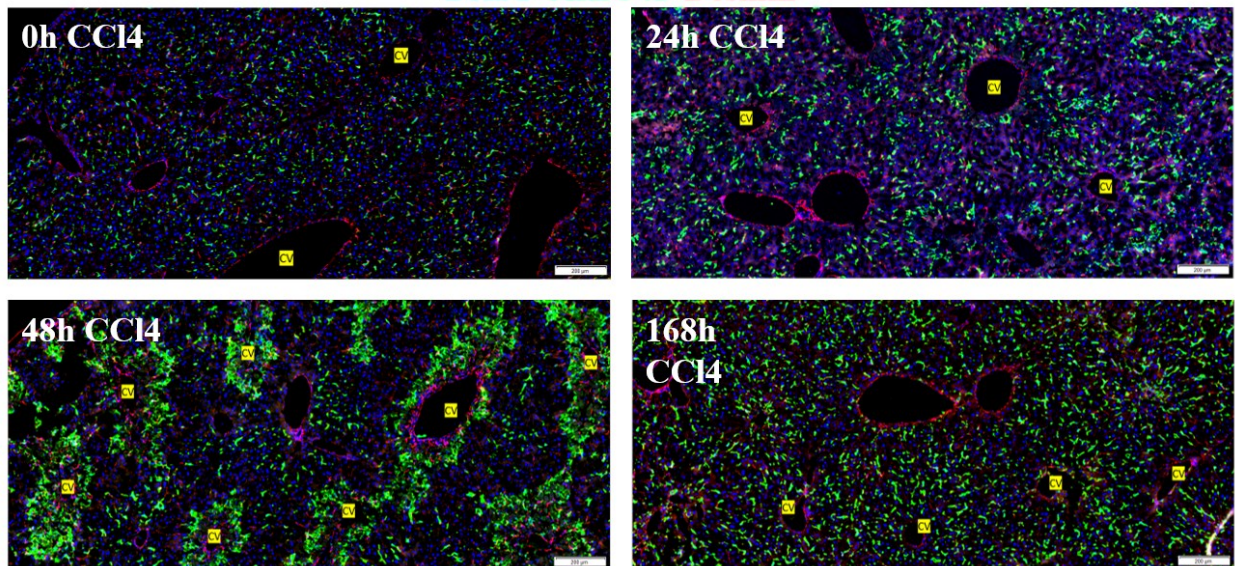


**Figure 25:** *KCs change their tissue distribution pattern in response to acute liver injury with CCl<sub>4</sub>. Multiplex immunofluorescence showing CLEC4F<sup>+</sup> KCs (green) and Desmin<sup>+</sup> HSCs (red) at*

*0, 24, 48, and 168 h post CCl<sub>4</sub> in liver tissue sections. Nuclei were counterstained with DAPI (blue). CV indicates central veins (yellow square). Scale bar is 200 μm.*

Our observations of the relocation of KCs during the response to acute liver injury conflict with the notion of KCs being sessile-stationary cells that are anchored to fixed positions in the lumen of hepatic sinusoids (53, 130, 143). Interestingly, the idea of stationary KCs derives from a limited set of observations and experimental conditions. For instance, the monitoring of KCs at the steady state by intravital microscopy revealed that they didn't change their positions for several hours (143). In addition, it was shown that KCs did not migrate towards inflammatory foci composed of influenza-induced CD8<sup>+</sup> T cells in a model of hepatic inflammation (130). These two observations are the basis of the assumption that KCs lack motility. However, we observed an obvious change of position of the KCs in fixed images both during necroinflammation and repair that can only be explained by the migration of KCs (Figures 4D, 5A, 8A, and Figure 25) (143). However, the relocation of KCs during the wound healing response may be relatively slow compared to infiltrating phagocytes (e.g., neutrophils and MoMFs) and may be technically challenging to record using intravital microscopy. What seems to be clear is that the notion of stationary KCs does not apply to all types of injuries and should be challenged with modern imaging techniques and using more varied and representative models of hepatic inflammation.

While several injury models lead to partial or complete depletion of KCs, the origin of the KCs repopulating the liver during repair can differ from model to model (129, 133, 148, 154). To understand the origin of repopulating KCs in response to CCl<sub>4</sub>-induced acute liver injury, we used MARCO as a specific marker of YS-KCs (129, 133, 154). We observed that all CLEC4F<sup>+</sup> KCs coexpressed MARCO, both in the healthy liver and during tissue repair, indicating that the original YS-KCs that died during necroinflammation are replaced by the proliferation of remaining YS-KCs (Figure 7, chapter 4). Similarly, it was also reported in the APAP model that YS-KCs recover by self-renewal, with no contribution from infiltrating Ly6G<sup>hi</sup> inflammatory monocytes (133). The CCl<sub>4</sub> and the APAP model have in common the partial depletion of KCs due to CV toxic injury with the mid and periportal regions being spared. By contrast, in the model of radiation-induced injury, the whole tissue is exposed to the damaging agent and the pool of KCs recovers by engraftment of infiltrating bone marrow-derived MoMFs (BM-KCs) (129, 130). In this case, the newly generated BM-KCs were transcriptionally similar but not identical to the original YS-KCs

they replaced (129). While BM-KCs exhibited early expression of CLEC4F, and other typical features of YS-KCs like stellar morphology, sinusoidal location, and stationary behavior at steady state, they displayed some minor transcriptional differences like the reduced expression of genes associated with iron homeostasis including scavenger receptors like MARCO (129). At the functional level, BM-KCs and YS-KCs exhibited comparable clearance of effete red blood cells but differential uptake of bacteria with BM-KCs exhibiting a higher efficiency (129, 130). Similarly, in a model of diphtheria toxin (DT) mediated depletion of YS-KCs (DTR-KC mice), the BM-KCs permanently replaced YS-KCs (154). In contrast to toxic or radiation-induced depletion of KCs, administration of DT did not result in hepatic inflammation and was 100 % efficient at removing KCs. In this non-inflammatory model, engrafted BM-KCs were highly homologous to original YS-KCs, even more than the homology observed upon radiation-induced depletion of KCs. For instance, BM-KCs in the DTR-KC mice expressed similar levels of genes associated with iron and lipid metabolism compared to original YS-KCs. In addition, BM-KCs acquired the capacity to self-renew, a property previously believed to be unique to embryonic-derived macrophages like YS-KCs (154). A subsequent study in this model revealed that signals originating in LSECs, hepatocytes, and HSCs imprint the KC identity on infiltrating monocytes and direct their differentiation into BM-KCs (85). In summary, the origin of KCs repopulating the liver during tissue repair is dependent on the type of injury (e.g., toxic vs. radiation), niche availability (partial vs. total depletion of resident KCs), and probably the degree of preservation of other tissue cells like LSECs, hepatocytes, and HSCs that can provide signals for differentiation of infiltrating monocytes into BM-KCs.

We showed the dynamic nature of the interactions between KCs and neighboring cells (e.g., MoMFs and HSCs) (Figure 8A and 8D, chapter 4; video chapter 4). For instance, the interaction of KCs with MoMFs was mostly restricted to the last part of necroinflammation and early repair and took place at the injury site (24 to 72h post CCl<sub>4</sub>) (Figure 5A, chapter 4). By contrast, at steady state, virtually all HSCs were in contact with KCs. This distribution significantly changed during necroinflammation and early repair, when KCs relocated to the border of the injury and the HSCs occupied the innermost regions around CVs (Figure 8A and 8D, chapter 4). In addition, KCs, MoMFs, and aHSCs occupied most of the area around CVs during repair suggesting that their reciprocal interactions may be crucial for wound healing (Figure 8D, chapter 4). In support of this, the combined absence of resident KCs and infiltrating macrophages (most likely MoMFs)

markedly delayed liver repair in APAP-treated mice compared to mice lacking either one of the individual populations, demonstrating that these two subsets of macrophages contribute to tissue repair (189).

In summary, the spatial and temporal profiling of KCs revealed that their numbers, distribution pattern, and interaction with neighboring cells change during the wound-healing response to CCl<sub>4</sub>-induced acute liver injury. Further studies are granted to interrogate how the interplay between KCs, MoMFs, and HSCs brings about the restoration of tissue homeostasis upon acute liver injury.

#### **5.d. Conclusions**

The immune response is a spatially and temporally coordinated process. While scRNA-seq, flow cytometry, and mass cytometry have been useful to dissect the transcriptional, and proteomic signatures of major immune subsets in the liver during health and disease, studies defining their spatial signatures have been lagging (48). During the last decade, technological advances in the fields of tissue processing, fluorescent labeling, image acquisition, and digital analysis have considerably increased our knowledge of the spatial behavior of immune cells (e.g., intravital imaging, histo-cytometry, and recently CODEX and Visium Spatial Gene Expression). However, these technologies are still difficult to implement and generalize because of elevated costs and the need for highly specialized knowledge (193, 291, 491-494, 497). In this study, we proposed a methodology for increased visualization, quantification, and mapping of immune cells in liver tissue sections that can be implemented with resources and equipment widely accessible (Chapter 3) (501).

This strategy integrated several solutions that maximized the quantity and quality of information that can be collected from tissue sections including serial and sequential labeling, tissue alignment, and virtual multiplexing. Through the incorporation of digital protocols for the classification of pixels and identification of cells of interest, our strategy overcame the subjectivity associated with manual counting by visual inspection. In addition, the analysis of whole tissue sections provided a more comprehensive and unbiased characterization of the tissue microenvironment compared to traditional analysis of representative fields of view. Furthermore, the use of computers and software for image analysis tremendously increased the speed and extent of the analysis.

In the second part of the study, we applied the principles of this methodology to the spatial and temporal profiling of liver macrophages during acute liver injury. We delineated the phases of the wound healing response and showed that myeloid cells were recruited to the injury site during necroinflammation and produced factors functionally associated with inflammation, resolution, and repair. We showed that MoMFs and KCs both localized to the lesion where they occupied most of the necrotic area. The necrotic tissue was characterized by highly dynamic changes in the composition and positioning of immune and non-immune cells including MoMFs, KCs, neutrophils, and HSCs. Despite the proximity between MoMFs and KCs, they occupied different microanatomical locations, exhibited partially different kinetics, and displayed different morphology. Furthermore, MoMFs and KCs were differentially involved in the replenishment of the macrophage compartment and the degree and timing of their interactions with HSCs during tissue repair (graphical abstract, page 201). Thus, our results validated the hypothesis that MoMFs and KCs exhibit distinct spatial signatures, strongly suggesting non-overlapping roles during the wound-healing response to acute liver injury.

### **5.e. Limitations and Future Directions**

Our work demonstrated that MoMFs and KCs have different spatial and temporal profiles. One of the main limitations of this study derives from the uncertainty associated with the identity of IBA1<sup>+</sup> CLEC4F<sup>-</sup> macrophages. While, by flow cytometry, we defined MoMFs as Ly6C<sup>+</sup> CX3CR1<sup>+</sup> myeloid cells, as it is widely accepted, in the tissue they were defined as IBA1<sup>+</sup> CLEC4F<sup>-</sup> macrophages. This mismatch between the markers used for flow cytometry and imaging was the consequence of lacking good antibodies to label Ly6C, and CX3CR1 in tissue sections which is a limitation of the field and not uniquely ours. Even though we presented considerable evidence that IBA1<sup>+</sup> CLEC4F<sup>-</sup> macrophages are MoMFs, lineage tracing experiments need to be performed to prove it. This can be done using the CCR2<sup>GFP/+</sup>- CCR2<sup>GFP/GFP</sup> mice, or the CX3CR1 reporter/KO mice.

Another limitation was the inability to efficiently isolate KCs. The functional profiling of KCs by flow cytometry can provide valuable insights into their unique roles during the different stages of the wound-healing response to acute liver injury.



This study lacks experiments interrogating the underlying mechanisms explaining the observed spatial profiles of KCs and MoMFs and their functional consequences. For instance, we observed spatial overlap of globularly shaped MoMFs and necrotic hepatocytes suggesting that MoMFs phagocytose dead hepatocytes. In addition, we showed that both KCs and MoMFs colocalize with HSCs but at different times during the wound healing response suggesting a differential impact of HSC activity. To understand the significance of these interactions, experiments depleting the individual macrophage subpopulations (KCs vs. MoMFs) need to be carried out. Below are some examples:

- Antibody-mediated depletion of inflammatory monocytes or the use of CCR2 KO mice, that has a reduced number of inflammatory monocytes in inflamed tissue, can be used to establish if IBA1<sup>+</sup> CLEC4F<sup>-</sup> macrophages phagocytose necrotic hepatocytes as suggested by their colocalization at 24 h post CCl<sub>4</sub> and the globular morphology of these macrophages.
- Depletion of KCs could be used to interrogate their role in providing early activation signals to HSCs upon injury as suggested by the colocalization of KCs and HSCs and the virtual absence of IBA1<sup>+</sup> CLEC4F<sup>-</sup> MoMFs at the steady state.
- Depletion of MoMFs or the CCR2 KO mice can be used to interrogate the functional impact of MoMFs on activation of HSC as suggested by their colocalization during the transition from necroinflammation to tissue repair.
- Depletion of MoMFs or the CCR2 KO mice can be used to investigate the potential impact of MoMFs in the position and kinetics of KCs in the injury site.

Another experimental approach to investigate the specific function of IBA1<sup>+</sup> CLEC4F<sup>-</sup> MoMFs vs. KCs would be the use of precision-cut liver slices (605). This model preserves the integrity of the tissue environment and its cell composition and can be used to interrogate the role of KCs in HSC activation and necrotic hepatocyte clearing, in response to CCl<sub>4</sub> intoxication (606). Specifically, slides from the KC-depleted liver and slides from the normal liver can be stimulated with CCl<sub>4</sub>, and the kinetics of HSC activation determined by imaging, qPCR, and flow cytometry. KCs can then be sorted from the normal slices at the relevant time point and profiled to identify potential HSC-activating mediators produced by KCs. Similarly, the kinetics of necrotic hepatocyte clearing can be assessed in the presence and absence of KCs, and the relevant receptors

and pathways identified. Since MoMFs are infiltrating cells upon CCl<sub>4</sub> injury, this model cannot be directly used to interrogate their role during wound healing.

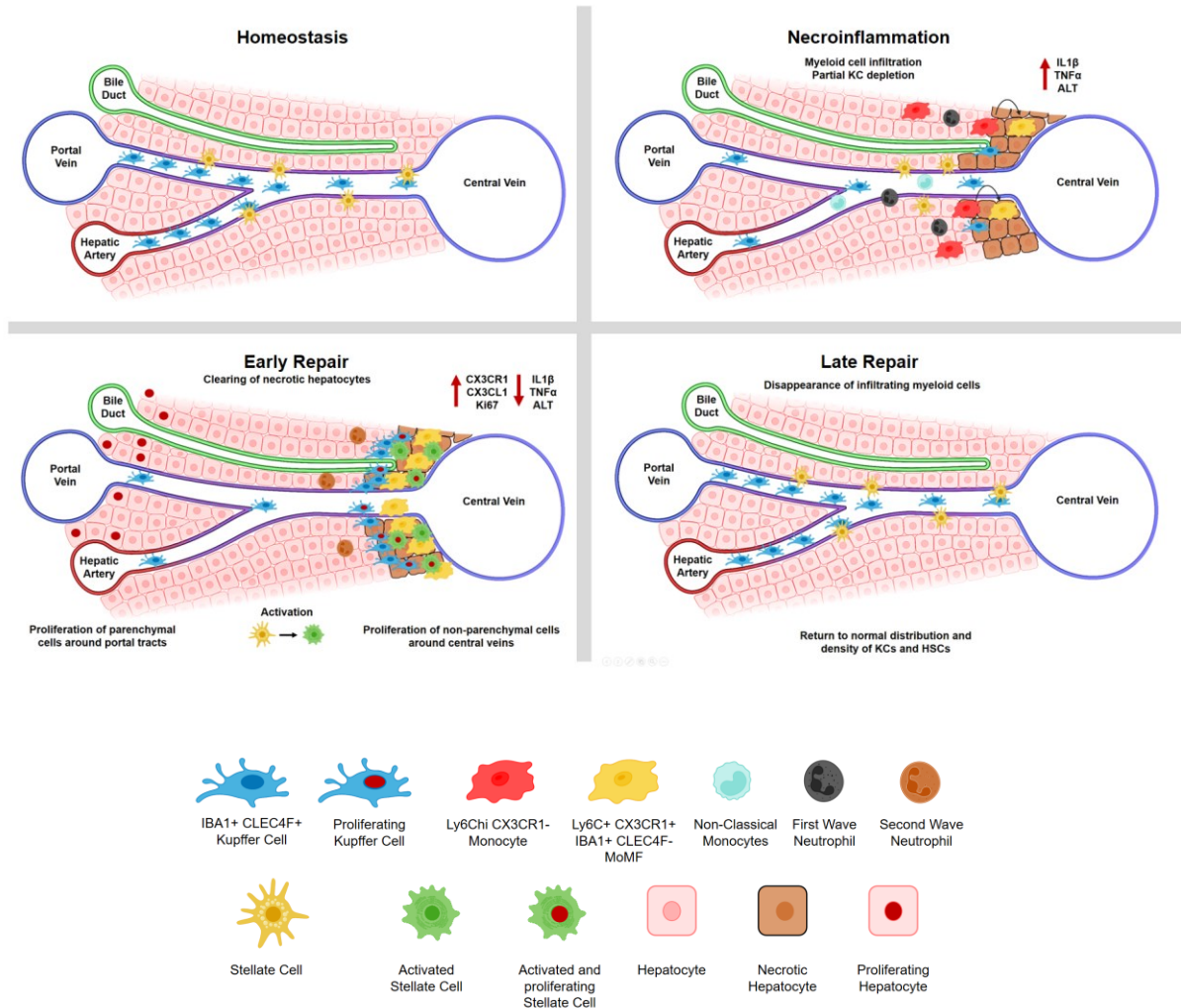
Another limitation of the study is that we relied on MARCO expression to classify the macrophages as YS-KCs. However, in the KC-DTR mice model, infiltrating monocytes can engraft in the KC-depleted livers and differentiate into BM-KCs which are transcriptionally indistinguishable from the original YS-KCs including MARCO expression (85). Therefore, a lineage tracing model is required to validate our observations.

Other relevant questions to address in future experiments are whether the same subpopulations of macrophages are present in other models of hepatic injury (IRI, NASH, ASH models, infectious models, etc.) and humans, and how they spatially relate between themselves, and relative to the lesions.

One of the most surprising observations of this study was the existence of two separate waves of neutrophils infiltrating the hepatic tissue during necroinflammation and repair. Although we have gathered evidence suggesting that there are different subpopulations of neutrophils committed to different effector functions during the wound-healing response to acute liver injury, this remains to be established using transcriptome profiling and selective depletion.

In summary, spatial, and temporal profiling of KCs and MoMFs revealed how these subsets are organized in the tissue and where and when they were in contact between themselves or with HSCs. This information is critical for designing future experiments to interrogate the functional significance of the observed distribution, interactions, and kinetics.

## 5.f. Graphical Abstract



During homeostasis (0h post CCl<sub>4</sub>), Kupffer cells are enriched in the periportal areas and are in direct contact with hepatic stellate cells. Upon CCl<sub>4</sub> injury, and during necroinflammation (0-48h post CCl<sub>4</sub>), Kupffer cells are partially depleted, and the liver is infiltrated by Ly6C<sup>hi</sup> CX3CR1<sup>-</sup> inflammatory monocytes, non-classical monocytes, and a first wave of neutrophils that locate to the area inside and around the necrotic tissue surrounding central veins. During early repair (48-72h post CCl<sub>4</sub>), hepatic stellate cells get activated, and necrotic hepatocytes are cleared. Both, the clearing of necrotic hepatocytes and the activation of hepatic stellate cells, are temporally associated with their colocalization with MoMFs (Ly6C<sup>+</sup> CX3CR1<sup>+</sup> IBA1<sup>+</sup> CLEC4F<sup>-</sup>). At early repair, MoMFs relocate to the innermost regions around central veins and are surrounded by proliferating and non-proliferating Kupffer cells. At the same time, a second wave of neutrophils

infiltrates the centrilobular area. During late repair, MoMFs and neutrophils disappear. Simultaneously, the clusters of hepatic stellate cells and Kupffer cells around central veins dissipate to regenerate the homeostatic spatial distribution of these resident cell subsets. Created with BioRender.com

### 5.g. Phenotype of main myeloid and lymphoid liver resident populations included in this thesis

Intrahepatic Leukocyte subset	Phenotype (Mice)	Phenotype (Human)
YS-KCs	F4/80 <sup>hi</sup> CD11b <sup>int</sup> Clec4F <sup>+</sup> TIM4 <sup>+</sup> Clec2 <sup>hi</sup> VSIG4 <sup>+</sup> CD64 <sup>+</sup> CD207 <sup>+</sup> CD163 <sup>+</sup> MARCO <sup>+</sup> Stab2 <sup>+</sup>	CD68 <sup>+</sup> MARCO <sup>+</sup> VSIG4 <sup>+</sup> CD163 <sup>+</sup> CD5L <sup>+</sup> HMOX1 <sup>+</sup>
MoMFs	CD11b <sup>+</sup> Ly6C <sup>hi</sup> CCR2 <sup>+</sup> CX3CR1 <sup>low</sup>	CD68 <sup>+</sup> MARCO <sup>-</sup> CD163 <sup>low</sup> PLBD1 <sup>+</sup> LYZ <sup>+</sup> CD74 <sup>+</sup>
LCMs	CD11b <sup>+</sup> F4/80 <sup>+</sup> CD64 <sup>+</sup> , CSF-1R <sup>+</sup> , and CD14 <sup>+</sup>	Not included
pDCs	Lineage <sup>-</sup> CD11c <sup>int</sup> B220 <sup>+</sup> , CD11b <sup>-</sup>	Lineage <sup>-</sup> CD303 <sup>+</sup> CD304 <sup>+</sup> ILT7 <sup>+</sup> CD4 <sup>+</sup> CD45RA <sup>+</sup> CD68 <sup>+</sup> ILT3 <sup>+</sup> CD123 <sup>+</sup>
cDC immature	CD11c <sup>int</sup> CD11b <sup>+</sup> B220 <sup>-</sup> CD40 <sup>lo</sup> CD80 <sup>lo</sup> CD86 <sup>lo</sup> MHC class II <sup>lo</sup>	Not included
cDC mature	CD11c <sup>hi</sup> CD11b <sup>+</sup> B220 <sup>-</sup> CD40 <sup>hi</sup> CD80 <sup>hi</sup> CD86 <sup>hi</sup> MHC class II <sup>hi</sup>	Not included
cDC		Lineage <sup>-</sup> CD123 <sup>-</sup> BDCA2 <sup>-</sup> MHCII <sup>high</sup>
ILC1	CD45 <sup>+</sup> Lin <sup>-</sup> CD62L <sup>-</sup> Eomes <sup>-</sup> Tbet <sup>+</sup> Hobit <sup>+</sup> CD49b <sup>-</sup> CD49a <sup>+</sup> TRAIL <sup>+</sup> CD69 <sup>+</sup> NK1.1 <sup>+</sup> NKp46 <sup>+</sup> CD127 <sup>+</sup> IL1Rβ <sup>+</sup> Sca-1 <sup>+</sup> CD90 <sup>+</sup> CD200R1 <sup>+</sup> and CXCR6 <sup>+</sup> .	Not included
ILC2	CD45 <sup>+</sup> Lin <sup>-</sup> CD62L <sup>-</sup> KLRG1 <sup>+</sup> ST2 <sup>+</sup> Sca-1 <sup>+</sup> CD49b <sup>-</sup> CD49a <sup>+</sup> TRAIL <sup>+</sup> IL-25R <sup>+</sup> CD69 <sup>+</sup> NK1.1 <sup>-</sup> GATA-3 <sup>+</sup> CD127 <sup>+</sup> c-Kit <sup>+</sup> Sca-1 <sup>+</sup> ICOS <sup>+</sup> MHC II <sup>+</sup> IL-33R <sup>+</sup> .	Not included

ILC3	CD45 <sup>+</sup> Lin <sup>-</sup> RORγt <sup>+</sup> CD4 <sup>-</sup> CD127 <sup>+</sup> NK1.1 <sup>+</sup> and NKp46 <sup>+/-</sup>	Not included
LTi cells	CD45 <sup>+</sup> Lin <sup>-</sup> RORγt <sup>+</sup> CD4 <sup>+</sup> IL- 23R <sup>+</sup> CCR6 <sup>+</sup> and AhR <sup>+</sup>	Not included
cNK cells	Lineage <sup>-</sup> CD49a <sup>-</sup> DX5 <sup>+</sup>	CD56 <sup>dim</sup> CD69 <sup>-</sup> , CCR5 <sup>-</sup> , CXCR6 <sup>-</sup> CCR7 <sup>hi</sup> CD62L <sup>hi</sup>
lr-NK cells	Lineage <sup>-</sup> CD49a <sup>+</sup> DX5 <sup>-</sup>	CD56 <sup>bright</sup> CD69 <sup>+</sup> CXCR6 <sup>+</sup> CCR5 <sup>+</sup> CCR7 <sup>-</sup>
NKT cells	Lineage <sup>-</sup> CD3 <sup>int</sup> NK1.1 <sup>+</sup>	CD3 <sup>+</sup> CD161 <sup>+</sup> CD56 <sup>+</sup> CD69 <sup>+</sup> CD16 <sup>+</sup>
MAIT cells	CD45RA <sup>-</sup> CD45RO <sup>+</sup> CD95 <sup>hi</sup> CD62L <sup>low</sup> CCR7 <sup>-</sup> CD44 <sup>hi</sup>	CD45RA <sup>-</sup> CD45RO <sup>+</sup> CD95 <sup>hi</sup> CD62L <sup>low</sup> CCR7 <sup>-</sup> CD44 <sup>hi</sup> CXCR6 <sup>+</sup> , CCR6 <sup>+</sup> , αEβ7 <sup>+</sup>
γδT cells	CD3 <sup>+</sup> TCRδ <sup>+</sup> CD44 <sup>hi</sup> CD62L <sup>-</sup> CD24 <sup>low</sup>	Not included
T <sub>RM</sub> cells	CD3 <sup>+</sup> CD69 <sup>+</sup> , CD49a <sup>+</sup> CD103 <sup>+</sup> CD62L <sup>low</sup> CCR7 <sup>-</sup>	CD3 <sup>+</sup> CD69 <sup>+</sup> , CD49a <sup>+</sup> CD103 <sup>+</sup> CD62L <sup>low</sup> CCR7 <sup>-</sup>

## Chapter 6: References

1. Crispe IN. The liver as a lymphoid organ. *Annu Rev Immunol.* 2009 ;27 :147-63.
2. Galon J, Costes A, Sanchez-Cabo F, Kirilovsky A, Mlecnik B, Lagorce-Pagès C, et al. Type, density, and location of immune cells within human colorectal tumors predict clinical outcome. *Science.* 2006;313(5795):1960-4.
3. Krijgsman D, van Leeuwen MB, van der Ven J, Almeida V, Vlutters R, Halter D, et al. Quantitative Whole Slide Assessment of Tumor-Infiltrating CD8-Positive Lymphocytes in ER-Positive Breast Cancer in Relation to Clinical Outcome. *IEEE J Biomed Health Inform.* 2021;25(2):381-92.
4. Kubes P, Jenne C. Immune Responses in the Liver. *Annu Rev Immunol.* 2018 ;36 :247-77.
5. Pagès F, Kirilovsky A, Mlecnik B, Asslaber M, Tosolini M, Bindea G, et al. In situ cytotoxic and memory T cells predict outcome in patients with early-stage colorectal cancer. *J Clin Oncol.* 2009;27(35):5944-51.
6. Tang J, van Panhuys N, Kastenmüller W, Germain RN. The future of immunoimaging--deeper, bigger, more precise, and definitively more colorful. *Eur J Immunol.* 2013;43(6):1407-12.
7. Gola A, Dorrington MG, Speranza E, Sala C, Shih RM, Radtke AJ, et al. Commensal-driven immune zonation of the liver promotes host defence. *Nature.* 2021;589(7840):131-6.
8. Guilliams M, Bonnardel J, Haest B, Vanderborcht B, Wagner C, Remmerie A, et al. Spatial proteogenomics reveals distinct and evolutionarily conserved hepatic macrophage niches. *Cell.* 2022;185(2):379-96.e38.
9. Dobie R, Wilson-Kanamori JR, Henderson BEP, Smith JR, Matchett KP, Portman JR, et al. Single-Cell Transcriptomics Uncovers Zonation of Function in the Mesenchyme during Liver Fibrosis. *Cell Rep.* 2019;29(7):1832-47.e8.
10. Gebhardt R, Matz-Soja M. Liver zonation: Novel aspects of its regulation and its impact on homeostasis. *World J Gastroenterol.* 2014;20(26):8491-504.
11. Halpern KB, Shenhav R, Massalha H, Toth B, Egozi A, Massasa EE, et al. Paired-cell sequencing enables spatial gene expression mapping of liver endothelial cells. *Nat Biotechnol.* 2018;36(10):962-70.

12. Halpern KB, Shenhav R, Matcovitch-Natan O, Toth B, Lemze D, Golan M, et al. Single-cell spatial reconstruction reveals global division of labour in the mammalian liver. *Nature*. 2017 ;542(7641) :352-6.
13. MacParland SA, Liu JC, Ma XZ, Innes BT, Bartczak AM, Gage BK, et al. Single cell RNA sequencing of human liver reveals distinct intrahepatic macrophage populations. *Nat Commun*. 2018 ;9(1) :4383.
14. Payen VL, Lavergne A, Alevra Sarika N, Colonval M, Karim L, Deckers M, et al. Single-cell RNA sequencing of human liver reveals hepatic stellate cell heterogeneity. *JHEP Rep*. 2021;3(3):100278.
15. Cavalli M, Diamanti K, Pan G, Spalinskas R, Kumar C, Deshmukh AS, et al. A Multi-Omics Approach to Liver Diseases: Integration of Single Nuclei Transcriptomics with Proteomics and HiCap Bulk Data in Human Liver. *Omics*. 2020;24(4):180-94.
16. Chappell L, Russell AJC, Voet T. Single-Cell (Multi)omics Technologies. *Annu Rev Genomics Hum Genet*. 2018;19:15-41.
17. Ho DW, Tsui YM, Sze KM, Chan LK, Cheung TT, Lee E, et al. Single-cell transcriptomics reveals the landscape of intra-tumoral heterogeneity and stemness-related subpopulations in liver cancer. *Cancer Lett*. 2019;459:176-85.
18. Liu X, Xu J, Rosenthal S, Zhang LJ, McCubbin R, Meshgin N, et al. Identification of Lineage-Specific Transcription Factors That Prevent Activation of Hepatic Stellate Cells and Promote Fibrosis Resolution. *Gastroenterology*. 2020 ;158(6) :1728-44.e14.
19. Ramachandran P, Dobie R, Wilson-Kanamori JR, Dora EF, Henderson BEP, Luu NT, et al. Resolving the fibrotic niche of human liver cirrhosis at single-cell level. *Nature*. 2019 ;575(7783) :512-8.
20. Su X, Shi Y, Zou X, Lu ZN, Xie G, Yang JYH, et al. Single-cell RNA-Seq analysis reveals dynamic trajectories during mouse liver development. *BMC Genomics*. 2017;18(1):946.
21. Zhang W, Conway SJ, Liu Y, Snider P, Chen H, Gao H, et al. Heterogeneity of Hepatic Stellate Cells in Fibrogenesis of the Liver: Insights from Single-Cell Transcriptomic Analysis in Liver Injury. *Cells*. 2021;10(8).
22. Zhu D, Rostami MR, Zuo WL, Leopold PL, Crystal RG. Single-Cell Transcriptome Analysis of Mouse Liver Cell-Specific Tropism and Transcriptional Dysregulation Following Intravenous Administration of AAVrh.10 Vectors. *Hum Gene Ther*. 2020;31(9-10):590-604.

23. Mr. Kiernan on the Anatomy and Physiology of the Liver. *Med Chir Rev.* 1834;20(40):305-15.
24. Kietzmann T. Metabolic zonation of the liver: The oxygen gradient revisited. *Redox Biol.* 2017;11:622-30.
25. Burt AD, Portmann B, Ferrell LD, MacSween RNM. MacSween's pathology of the liver. 2012.
26. Rappaport AM, Borowy ZJ, Loughheed WM, Lotto WN. Subdivision of hexagonal liver lobules into a structural and functional unit; role in hepatic physiology and pathology. *Anat Rec.* 1954;119(1):11-33.
27. Shetty S, Lalor PF, Adams DH. Liver sinusoidal endothelial cells - gatekeepers of hepatic immunity. *Nat Rev Gastroenterol Hepatol.* 2018;15(9):555-67.
28. Hernandez-Gea V, Friedman SL. Pathogenesis of liver fibrosis. *Annu Rev Pathol.* 2011;6:425-56.
29. Chen Y, Tian Z. Innate lymphocytes: pathogenesis and therapeutic targets of liver diseases and cancer. *Cell Mol Immunol.* 2021;18(1):57-72.
30. Racanelli V, Rehermann B. The liver as an immunological organ. *Hepatology.* 2006;43(2 Suppl 1):S54-62.
31. Schulze RJ, Schott MB, Casey CA, Tuma PL, McNiven MA. The cell biology of the hepatocyte: A membrane trafficking machine. *J Cell Biol.* 2019;218(7):2096-112.
32. Zanger UM, Schwab M. Cytochrome P450 enzymes in drug metabolism: regulation of gene expression, enzyme activities, and impact of genetic variation. *Pharmacol Ther.* 2013;138(1):103-41.
33. Soto-Gutierrez A, Gough A, Verneti LA, Taylor DL, Monga SP. Pre-clinical and clinical investigations of metabolic zonation in liver diseases: The potential of microphysiology systems. *Exp Biol Med (Maywood).* 2017;242(16):1605-16.
34. Debois D, Bralet MP, Le Naour F, Brunelle A, Laprévotte O. In situ lipidomic analysis of nonalcoholic fatty liver by cluster TOF-SIMS imaging. *Anal Chem.* 2009;81(8):2823-31.
35. Hinson JA, Roberts DW, James LP. Mechanisms of acetaminophen-induced liver necrosis. *Handb Exp Pharmacol.* 2010(196):369-405.



36. Watterich J, Seeley EH, Angel P, Chen H, Bowen BP, Lanciault C, et al. Differential intrahepatic phospholipid zonation in simple steatosis and nonalcoholic steatohepatitis. *PLoS One*. 2013;8(2):e57165.
37. Aizarani N, Saviano A, Sagar, Mailly L, Durand S, Herman JS, et al. A human liver cell atlas reveals heterogeneity and epithelial progenitors. *Nature*. 2019;572(7768):199-204.
38. Ben-Moshe S, Itzkovitz S. Spatial heterogeneity in the mammalian liver. *Nat Rev Gastroenterol Hepatol*. 2019;16(7):395-410.
39. Ben-Moshe S, Shapira Y, Moor AE, Manco R, Veg T, Bahar Halpern K, et al. Spatial sorting enables comprehensive characterization of liver zonation. *Nat Metab*. 2019;1(9):899-911.
40. Birnbaum KD. Power in Numbers: Single-Cell RNA-Seq Strategies to Dissect Complex Tissues. *Annu Rev Genet*. 2018;52:203-21.
41. Xiong X, Kuang H, Liu T, Lin JD. A Single-Cell Perspective of the Mammalian Liver in Health and Disease. *Hepatology*. 2020;71(4):1467-73.
42. Yin L, Lynch D, Ilic Z, Sell S. Proliferation and differentiation of ductular progenitor cells and littoral cells during the regeneration of the rat liver to CCl<sub>4</sub>/2-AAF injury. *Histol Histopathol*. 2002;17(1):65-81.
43. Han Y, Glaser S, Meng F, Francis H, Marzioni M, McDaniel K, et al. Recent advances in the morphological and functional heterogeneity of the biliary epithelium. *Exp Biol Med (Maywood)*. 2013;238(5):549-65.
44. Banales JM, Huebert RC, Karlsen T, Strazzabosco M, LaRusso NF, Gores GJ. Cholangiocyte pathobiology. *Nat Rev Gastroenterol Hepatol*. 2019;16(5):269-81.
45. Andrews TS, Atif J, Liu JC, Perciani CT, Ma XZ, Thoeni C, et al. Single-Cell, Single-Nucleus, and Spatial RNA Sequencing of the Human Liver Identifies Cholangiocyte and Mesenchymal Heterogeneity. *Hepatol Commun*. 2022;6(4):821-40.
46. Lazaridis KN, Strazzabosco M, LaRusso NF. The cholangiopathies: disorders of biliary epithelia. *Gastroenterology*. 2004;127(5):1565-77.
47. Yokoda RT, Rodriguez EA. Review: Pathogenesis of cholestatic liver diseases. *World J Hepatol*. 2020;12(8):423-35.
48. Ramachandran P, Matchett KP, Dobie R, Wilson-Kanamori JR, Henderson NC. Single-cell technologies in hepatology: new insights into liver biology and disease pathogenesis. *Nat Rev Gastroenterol Hepatol*. 2020;17(8):457-72.

49. Wilkinson AL, Qurashi M, Shetty S. The Role of Sinusoidal Endothelial Cells in the Axis of Inflammation and Cancer Within the Liver. *Front Physiol.* 2020;11:990.
50. Wisse E, De Zanger RB, Charels K, Van Der Smissen P, McCuskey RS. The liver sieve: considerations concerning the structure and function of endothelial fenestrae, the sinusoidal wall and the space of Disse. *Hepatology.* 1985;5(4):683-92.
51. Stan RV, Tse D, Deharvengt SJ, Smits NC, Xu Y, Luciano MR, et al. The diaphragms of fenestrated endothelia: gatekeepers of vascular permeability and blood composition. *Dev Cell.* 2012 ;23(6) :1203-18.
52. Guidotti LG, Inverso D, Sironi L, Di Lucia P, Fioravanti J, Ganzer L, et al. Immunosurveillance of the liver by intravascular effector CD8(+) T cells. *Cell.* 2015;161(3):486-500.
53. McCuskey RS. Morphological mechanisms for regulating blood flow through hepatic sinusoids. *Liver.* 2000;20(1):3-7.
54. McCuskey RS. The hepatic microvascular system in health and its response to toxicants. *Anat Rec (Hoboken).* 2008;291(6):661-71.
55. Warren A, Le Couteur DG, Fraser R, Bowen DG, McCaughan GW, Bertolino P. T lymphocytes interact with hepatocytes through fenestrations in murine liver sinusoidal endothelial cells. *Hepatology.* 2006;44(5):1182-90.
56. Li R, Oteiza A, Sørensen KK, McCourt P, Olsen R, Smedsrød B, et al. Role of liver sinusoidal endothelial cells and stabilins in elimination of oxidized low-density lipoproteins. *Am J Physiol Gastrointest Liver Physiol.* 2011;300(1):G71-81.
57. Mates JM, Yao Z, Cheplowitz AM, Suer O, Phillips GS, Kwiek JJ, et al. Mouse Liver Sinusoidal Endothelium Eliminates HIV-Like Particles from Blood at a Rate of 100 Million per Minute by a Second-Order Kinetic Process. *Front Immunol.* 2017;8:35.
58. Løvdal T, Andersen E, Brech A, Berg T. Fc receptor mediated endocytosis of small soluble immunoglobulin G immune complexes in Kupffer and endothelial cells from rat liver. *J Cell Sci.* 2000;113 ( Pt 18):3255-66.
59. Ganesan LP, Mohanty S, Kim J, Clark KR, Robinson JM, Anderson CL. Rapid and efficient clearance of blood-borne virus by liver sinusoidal endothelium. *PLoS Pathog.* 2011;7(9):e1002281.

60. Breiner KM, Schaller H, Knolle PA. Endothelial cell-mediated uptake of a hepatitis B virus: a new concept of liver targeting of hepatotropic microorganisms. *Hepatology*. 2001;34(4 Pt 1):803-8.
61. Rowe IA, Galsinh SK, Wilson GK, Parker R, Durant S, Lazar C, et al. Paracrine signals from liver sinusoidal endothelium regulate hepatitis C virus replication. *Hepatology*. 2014;59(2):375-84.
62. Deleve LD, Wang X, Guo Y. Sinusoidal endothelial cells prevent rat stellate cell activation and promote reversion to quiescence. *Hepatology*. 2008;48(3):920-30.
63. Xie G, Wang X, Wang L, Wang L, Atkinson RD, Kanel GC, et al. Role of differentiation of liver sinusoidal endothelial cells in progression and regression of hepatic fibrosis in rats. *Gastroenterology*. 2012;142(4):918-27.e6.
64. Huang S, Wu J, Gao X, Zou S, Chen L, Yang X, et al. LSECs express functional NOD1 receptors: A role for NOD1 in LSEC maturation-induced T cell immunity in vitro. *Mol Immunol*. 2018;101:167-75.
65. Martin-Armas M, Simon-Santamaria J, Pettersen I, Moens U, Smedsrød B, Sveinbjørnsson B. Toll-like receptor 9 (TLR9) is present in murine liver sinusoidal endothelial cells (LSECs) and mediates the effect of CpG-oligonucleotides. *J Hepatol*. 2006;44(5):939-46.
66. Wu J, Meng Z, Jiang M, Zhang E, Trippler M, Broering R, et al. Toll-like receptor-induced innate immune responses in non-parenchymal liver cells are cell type-specific. *Immunology*. 2010;129(3):363-74.
67. Yao Z, Mates JM, Cheplowitz AM, Hammer LP, Maiseyeu A, Phillips GS, et al. Blood-Borne Lipopolysaccharide Is Rapidly Eliminated by Liver Sinusoidal Endothelial Cells via High-Density Lipoprotein. *J Immunol*. 2016;197(6):2390-9.
68. Knolle PA, Uhrig A, Hegenbarth S, Löser E, Schmitt E, Gerken G, et al. IL-10 down-regulates T cell activation by antigen-presenting liver sinusoidal endothelial cells through decreased antigen uptake via the mannose receptor and lowered surface expression of accessory molecules. *Clin Exp Immunol*. 1998;114(3):427-33.
69. Uhrig A, Banafsche R, Kremer M, Hegenbarth S, Hamann A, Neurath M, et al. Development and functional consequences of LPS tolerance in sinusoidal endothelial cells of the liver. *J Leukoc Biol*. 2005;77(5):626-33.

70. Amersfoort J, Eelen G, Carmeliet P. Immunomodulation by endothelial cells - partnering up with the immune system? *Nat Rev Immunol* 22, 576–588 (2022).
71. Burgdorf S, Kautz A, Böhnert V, Knolle PA, Kurts C. Distinct pathways of antigen uptake and intracellular routing in CD4 and CD8 T cell activation. *Science*. 2007;316(5824):612-6.
72. Limmer A, Ohl J, Wingender G, Berg M, Jüngerkes F, Schumak B, et al. Cross-presentation of oral antigens by liver sinusoidal endothelial cells leads to CD8 T cell tolerance. *Eur J Immunol*. 2005;35(10):2970-81.
73. Knolle PA, Limmer A. Neighborhood politics: the immunoregulatory function of organ-resident liver endothelial cells. *Trends Immunol*. 2001;22(8):432-7.
74. von Oppen N, Schurich A, Hegenbarth S, Stabenow D, Tolba R, Weiskirchen R, et al. Systemic antigen cross-presented by liver sinusoidal endothelial cells induces liver-specific CD8 T-cell retention and tolerization. *Hepatology*. 2009;49(5):1664-72.
75. Diehl L, Schurich A, Grochtmann R, Hegenbarth S, Chen L, Knolle PA. Tolerogenic maturation of liver sinusoidal endothelial cells promotes B7-homolog 1-dependent CD8+ T cell tolerance. *Hepatology*. 2008;47(1):296-305.
76. Höchst B, Schildberg FA, Böttcher J, Metzger C, Huss S, Türler A, et al. Liver sinusoidal endothelial cells contribute to CD8 T cell tolerance toward circulating carcinoembryonic antigen in mice. *Hepatology*. 2012;56(5):1924-33.
77. Limmer A, Ohl J, Kurts C, Ljunggren HG, Reiss Y, Groettrup M, et al. Efficient presentation of exogenous antigen by liver endothelial cells to CD8+ T cells results in antigen-specific T-cell tolerance. *Nat Med*. 2000;6(12):1348-54.
78. Böttcher JP, Schanz O, Garbers C, Zaremba A, Hegenbarth S, Kurts C, et al. IL-6 trans-signaling-dependent rapid development of cytotoxic CD8+ T cell function. *Cell Rep*. 2014;8(5):1318-27.
79. Knolle PA, Wohlleber D. Immunological functions of liver sinusoidal endothelial cells. *Cell Mol Immunol*. 2016;13(3):347-53.
80. Schurich A, Berg M, Stabenow D, Böttcher J, Kern M, Schild HJ, et al. Dynamic regulation of CD8 T cell tolerance induction by liver sinusoidal endothelial cells. *J Immunol*. 2010 ;184(8) :4107-14.

81. Baiocchini A, Del Nonno F, Taibi C, Visco-Comandini U, D'Offizi G, Piacentini M, et al. Liver sinusoidal endothelial cells (LSECs) modifications in patients with chronic hepatitis C. *Sci Rep.* 2019;9(1):8760.
82. Greuter T, Shah VH. Hepatic sinusoids in liver injury, inflammation, and fibrosis: new pathophysiological insights. *J Gastroenterol.* 2016;51(6):511-9.
83. Iwakiri Y, Shah V, Rockey DC. Vascular pathobiology in chronic liver disease and cirrhosis - current status and future directions. *J Hepatol.* 2014;61(4):912-24.
84. Wake K. "Sternzellen" in the liver: perisinusoidal cells with special reference to storage of vitamin A. *Am J Anat.* 1971;132(4):429-62.
85. Bonnardel J, T'Jonck W, Gaublomme D, Browaeys R, Scott CL, Martens L, et al. Stellate Cells, Hepatocytes, and Endothelial Cells Imprint the Kupffer Cell Identity on Monocytes Colonizing the Liver Macrophage Niche. *Immunity.* 2019;51(4):638-54.e9.
86. Geerts A. History, heterogeneity, developmental biology, and functions of quiescent hepatic stellate cells. *Semin Liver Dis.* 2001;21(3):311-35.
87. Friedman SL. Hepatic stellate cells: protean, multifunctional, and enigmatic cells of the liver. *Physiol Rev.* 2008;88(1):125-72.
88. Mederacke I, Hsu CC, Troeger JS, Huebener P, Mu X, Dapito DH, et al. Fate tracing reveals hepatic stellate cells as dominant contributors to liver fibrosis independent of its aetiology. *Nat Commun.* 2013;4:2823.
89. Tsuchida T, Friedman SL. Mechanisms of hepatic stellate cell activation. *Nat Rev Gastroenterol Hepatol.* 2017;14(7):397-411.
90. Bachem MG, Melchior R, Gressner AM. The role of thrombocytes in liver fibrogenesis: effects of platelet lysate and thrombocyte-derived growth factors on the mitogenic activity and glycosaminoglycan synthesis of cultured rat liver fat storing cells. *J Clin Chem Clin Biochem.* 1989;27(9):555-65.
91. Canbay A, Taimr P, Torok N, Higuchi H, Friedman S, Gores GJ. Apoptotic body engulfment by a human stellate cell line is profibrogenic. *Lab Invest.* 2003;83(5):655-63.
92. Jarnagin WR, Rockey DC, Koteliansky VE, Wang SS, Bissell DM. Expression of variant fibronectins in wound healing: cellular source and biological activity of the EIIIA segment in rat hepatic fibrogenesis. *J Cell Biol.* 1994;127(6 Pt 2):2037-48.

93. Novo E, Marra F, Zamara E, Valfrè di Bonzo L, Caligiuri A, Cannito S, et al. Dose dependent and divergent effects of superoxide anion on cell death, proliferation, and migration of activated human hepatic stellate cells. *Gut*. 2006;55(1):90-7.
94. Aoyama T, Inokuchi S, Brenner DA, Seki E. CX3CL1-CX3CR1 interaction prevents carbon tetrachloride-induced liver inflammation and fibrosis in mice. *Hepatology*. 2010;52(4):1390-400.
95. Bourd-Boittin K, Basset L, Bonnier D, L'Helgoualc'h A, Samson M, Théret N. CX3CL1/fractalkine shedding by human hepatic stellate cells: contribution to chronic inflammation in the liver. *J Cell Mol Med*. 2009;13(8a):1526-35.
96. Schwabe RF, Bataller R, Brenner DA. Human hepatic stellate cells express CCR5 and RANTES to induce proliferation and migration. *Am J Physiol Gastrointest Liver Physiol*. 2003;285(5):G949-58.
97. Thompson KC, Trowern A, Fowell A, Marathe M, Haycock C, Arthur MJ, et al. Primary rat and mouse hepatic stellate cells express the macrophage inhibitor cytokine interleukin-10 during the course of activation *In vitro*. *Hepatology*. 1998;28(6):1518-24.
98. Tiggelman AM, Boers W, Linthorst C, Brand HS, Sala M, Chamuleau RA. Interleukin-6 production by human liver (myo)fibroblasts in culture. Evidence for a regulatory role of LPS, IL-1 beta and TNF alpha. *J Hepatol*. 1995;23(3):295-306.
99. Wang SC, Ohata M, Schrum L, Rippe RA, Tsukamoto H. Expression of interleukin-10 by *in vitro* and *in vivo* activated hepatic stellate cells. *J Biol Chem*. 1998;273(1):302-8.
100. Viñas O, Bataller R, Sancho-Bru P, Ginès P, Berenguer C, Enrich C, et al. Human hepatic stellate cells show features of antigen-presenting cells and stimulate lymphocyte proliferation. *Hepatology*. 2003;38(4):919-29.
101. Winau F, Hegasy G, Weiskirchen R, Weber S, Cassan C, Sieling PA, et al. Ito cells are liver-resident antigen-presenting cells for activating T cell responses. *Immunity*. 2007;26(1):117-29.
102. Yu MC, Chen CH, Liang X, Wang L, Gandhi CR, Fung JJ, et al. Inhibition of T-cell responses by hepatic stellate cells via B7-H1-mediated T-cell apoptosis in mice. *Hepatology*. 2004;40(6):1312-21.

103. Fujio K, Evarts RP, Hu Z, Marsden ER, Thorgeirsson SS. Expression of stem cell factor and its receptor, c-kit, during liver regeneration from putative stem cells in adult rat. *Lab Invest.* 1994;70(4):511-6.
104. Paradis V, Dargere D, Bonvoust F, Vidaud M, Segarini P, Bedossa P. Effects and regulation of connective tissue growth factor on hepatic stellate cells. *Lab Invest.* 2002 ;82(6) :767-74.
105. Paradis V, Perlemuter G, Bonvoust F, Dargere D, Parfait B, Vidaud M, et al. High glucose and hyperinsulinemia stimulate connective tissue growth factor expression: a potential mechanism involved in progression to fibrosis in nonalcoholic steatohepatitis. *Hepatology.* 2001;34(4 Pt 1):738-44.
106. Pinzani M, Abboud HE, Aron DC. Secretion of insulin-like growth factor-I and binding proteins by rat liver fat-storing cells: regulatory role of platelet-derived growth factor. *Endocrinology.* 1990;127(5):2343-9.
107. Pinzani M, Abboud HE, Gesualdo L, Abboud SL. Regulation of macrophage colony-stimulating factor in liver fat-storing cells by peptide growth factors. *Am J Physiol.* 1992;262(4 Pt 1):C876-81.
108. Win KM, Charlotte F, Mallat A, Cherqui D, Martin N, Mavier P, et al. Mitogenic effect of transforming growth factor-beta 1 on human Ito cells in culture: evidence for mediation by endogenous platelet-derived growth factor. *Hepatology.* 1993;18(1):137-45.
109. Zindy F, Lamas E, Schmidt S, Kirn A, Brechot C. Expression of insulin-like growth factor II (IGF-II) and IGF-II, IGF-I and insulin receptors mRNAs in isolated non-parenchymal rat liver cells. *J Hepatol.* 1992 ;14(1) :30-4.
110. Xu J, Liu X, Koyama Y, Wang P, Lan T, Kim IG, et al. The types of hepatic myofibroblasts contributing to liver fibrosis of different etiologies. *Front Pharmacol.* 2014;5:167.
111. Dranoff JA, Wells RG. Portal fibroblasts: Underappreciated mediators of biliary fibrosis. *Hepatology.* 2010;51(4):1438-44.
112. Tang L, Tanaka Y, Marumo F, Sato C. Phenotypic change in portal fibroblasts in biliary fibrosis. *Liver.* 1994;14(2):76-82.
113. Fausther M, Goree JR, Lavoie É G, Graham AL, Sévigny J, Dranoff JA. Establishment and characterization of rat portal myofibroblast cell lines. *PLoS One.* 2015;10(3):e0121161.
114. Bataller R, Brenner DA. Liver fibrosis. *J Clin Invest.* 2005;115(2):209-18.

115. Kinnman N, Housset C. Peribiliary myofibroblasts in biliary type liver fibrosis. *Front Biosci.* 2002;7:d496-503.
116. Parola M, Marra F, Pinzani M. Myofibroblast - like cells and liver fibrogenesis: Emerging concepts in a rapidly moving scenario. *Mol Aspects Med.* 2008;29(1-2):58-66.
117. Tuchweber B, Desmoulière A, Bochaton-Piallat ML, Rubbia-Brandt L, Gabbiani G. Proliferation and phenotypic modulation of portal fibroblasts in the early stages of cholestatic fibrosis in the rat. *Lab Invest.* 1996;74(1):265-78.
118. Desmoulière A, Darby I, Costa AM, Raccurt M, Tuchweber B, Sommer P, et al. Extracellular matrix deposition, lysyl oxidase expression, and myofibroblastic differentiation during the initial stages of cholestatic fibrosis in the rat. *Lab Invest.* 1997;76(6):765-78.
119. Kinnman N, Francoz C, Barbu V, Wendum D, Rey C, Hultcrantz R, et al. The myofibroblastic conversion of peribiliary fibrogenic cells distinct from hepatic stellate cells is stimulated by platelet-derived growth factor during liver fibrogenesis. *Lab Invest.* 2003;83(2):163-73.
120. Li Z, Dranoff JA, Chan EP, Uemura M, Sévigny J, Wells RG. Transforming growth factor-beta and substrate stiffness regulate portal fibroblast activation in culture. *Hepatology.* 2007;46(4):1246-56.
121. Perepelyuk M, Terajima M, Wang AY, Georges PC, Janmey PA, Yamauchi M, et al. Hepatic stellate cells and portal fibroblasts are the major cellular sources of collagens and lysyl oxidases in normal liver and early after injury. *Am J Physiol Gastrointest Liver Physiol.* 2013;304(6):G605-14.
122. Wells RG. The portal fibroblast: not just a poor man's stellate cell. *Gastroenterology.* 2014;147(1):41-7.
123. Nishio T, Hu R, Koyama Y, Liang S, Rosenthal SB, Yamamoto G, et al. Activated hepatic stellate cells and portal fibroblasts contribute to cholestatic liver fibrosis in MDR2 knockout mice. *J Hepatol.* 2019;71(3):573-85.
124. Lua I, Li Y, Zagory JA, Wang KS, French SW, Sévigny J, et al. Characterization of hepatic stellate cells, portal fibroblasts, and mesothelial cells in normal and fibrotic livers. *J Hepatol.* 2016;64(5):1137-46.
125. Huang H, Lu Y, Zhou T, Gu G, Xia Q. Innate Immune Cells in Immune Tolerance After Liver Transplantation. *Front Immunol.* 2018;9:2401.



126. Protzer U, Maini MK, Knolle PA. Living in the liver: hepatic infections. *Nat Rev Immunol*. 2012;12(3):201-13.
127. Perlman RL. Mouse models of human disease: An evolutionary perspective. *Evol Med Public Health*. 2016;2016(1):170-6.
128. Guillot A, Tacke F. Liver Macrophages: Old Dogmas and New Insights. *Hepatol Commun*. 2019;3(6):730-43.
129. Beattie L, Sawtell A, Mann J, Frame TCM, Teal B, de Labastida Rivera F, et al. Bone marrow-derived and resident liver macrophages display unique transcriptomic signatures but similar biological functions. *J Hepatol*. 2016;65(4):758-68.
130. Klein I, Cornejo JC, Polakos NK, John B, Wuensch SA, Topham DJ, et al. Kupffer cell heterogeneity: functional properties of bone marrow derived and sessile hepatic macrophages. *Blood*. 2007;110(12):4077-85.
131. Sierro F, Evrard M, Rizzetto S, Melino M, Mitchell AJ, Florido M, et al. A Liver Capsular Network of Monocyte-Derived Macrophages Restricts Hepatic Dissemination of Intraperitoneal Bacteria by Neutrophil Recruitment. *Immunity*. 2017;47(2):374-88.e6.
132. Wang J, Kubes P. A Reservoir of Mature Cavity Macrophages that Can Rapidly Invade Visceral Organs to Affect Tissue Repair. *Cell*. 2016;165(3):668-78.
133. Zigmond E, Samia-Grinberg S, Pasmanik-Chor M, Brazowski E, Shibolet O, Halpern Z, et al. Infiltrating monocyte-derived macrophages and resident kupffer cells display different ontogeny and functions in acute liver injury. *J Immunol*. 2014 ;193(1) :344-53.
134. Ramachandran P, Pellicoro A, Vernon MA, Boulter L, Aucott RL, Ali A, et al. Differential Ly-6C expression identifies the recruited macrophage phenotype, which orchestrates the regression of murine liver fibrosis. *Proc Natl Acad Sci U S A*. 2012;109(46):E3186-95.
135. Wynn TA, Vannella KM. Macrophages in Tissue Repair, Regeneration, and Fibrosis. *Immunity*. 2016;44(3):450-62.
136. Nguyen-Lefebvre AT, Horuzsko A. Kupffer Cell Metabolism and Function. *J Enzymol Metab*. 2015;1(1).
137. Szymańska R, Schmidt-Pospuła M. [Studies of liver's reticuloendothelial cells by Tadeusz Browicz and Karl Kupffer. A historical outline]. *Arch Hist Med (Warsz)*. 1979;42(3):331-6.

138. Gomez Perdiguero E, Klapproth K, Schulz C, Busch K, Azzoni E, Crozet L, et al. Tissue-resident macrophages originate from yolk-sac-derived erythro-myeloid progenitors. *Nature*. 2015;518(7540):547-51.
139. Hashimoto D, Chow A, Noizat C, Teo P, Beasley MB, Leboeuf M, et al. Tissue-resident macrophages self-maintain locally throughout adult life with minimal contribution from circulating monocytes. *Immunity*. 2013;38(4):792-804.
140. Hoeffel G, Chen J, Lavin Y, Low D, Almeida FF, See P, et al. C-Myb(+) erythro-myeloid progenitor-derived fetal monocytes give rise to adult tissue-resident macrophages. *Immunity*. 2015;42(4):665-78.
141. Yona S, Kim KW, Wolf Y, Mildner A, Varol D, Breker M, et al. Fate mapping reveals origins and dynamics of monocytes and tissue macrophages under homeostasis. *Immunity*. 2013;38(1):79-91.
142. Wake K, Decker K, Kirn A, Knook DL, McCuskey RS, Bouwens L, et al. Cell biology and kinetics of Kupffer cells in the liver. *Int Rev Cytol*. 1989;118:173-229.
143. Frevert U, Usynin I, Baer K, Klotz C. Nomadic or sessile: can Kupffer cells function as portals for malaria sporozoites to the liver? *Cell Microbiol*. 2006;8(10):1537-46.
144. MacPhee PJ, Schmidt EE, Groom AC. Evidence for Kupffer cell migration along liver sinusoids, from high-resolution in vivo microscopy. *Am J Physiol*. 1992;263(1 Pt 1):G17-23.
145. Bertolino P, McCaughan GW, Bowen DG. Role of primary intrahepatic T-cell activation in the 'liver tolerance effect'. *Immunol Cell Biol*. 2002;80(1):84-92.
146. Mackay IR. Hepatoimmunology: a perspective. *Immunol Cell Biol*. 2002;80(1):36-44.
147. Markiewski MM, DeAngelis RA, Lambris JD. Liver inflammation and regeneration: two distinct biological phenomena or parallel pathophysiologic processes? *Mol Immunol*. 2006 ;43(1-2) :45-56.
148. David BA, Rezende RM, Antunes MM, Santos MM, Freitas Lopes MA, Diniz AB, et al. Combination of Mass Cytometry and Imaging Analysis Reveals Origin, Location, and Functional Repopulation of Liver Myeloid Cells in Mice. *Gastroenterology*. 2016;151(6):1176-91.
149. Sleyster EC, Knook DL. Relation between localization and function of rat liver Kupffer cells. *Lab Invest*. 1982;47(5):484-90.
150. Bouwens L, Baekeland M, De Zanger R, Wisse E. Quantitation, tissue distribution and proliferation kinetics of Kupffer cells in normal rat liver. *Hepatology*. 1986 ;6(4) :718-22.

151. Itoh Y, Okanoué T, Morimoto M, Nagao Y, Mori T, Hori N, et al. Functional heterogeneity of rat liver macrophages: interleukin-1 secretion and Ia antigen expression in contrast with phagocytic activity. *Liver*. 1992;12(1):26-33.
152. Guilliams M, Bonnardel J, Haest B, Vanderborght B, Wagner C, Remmerie A, et al. Spatial proteogenomics reveals distinct and evolutionarily conserved hepatic macrophage niches. *Cell*. 2022.
153. Lavin Y, Winter D, Blecher-Gonen R, David E, Keren-Shaul H, Merad M, et al. Tissue-resident macrophage enhancer landscapes are shaped by the local microenvironment. *Cell*. 2014;159(6):1312-26.
154. Scott CL, Zheng F, De Baetselier P, Martens L, Saeys Y, De Prijck S, et al. Bone marrow-derived monocytes give rise to self-renewing and fully differentiated Kupffer cells. *Nat Commun*. 2016;7:10321.
155. Yang CY, Chen JB, Tsai TF, Tsai YC, Tsai CY, Liang PH, et al. CLEC4F is an inducible C-type lectin in F4/80-positive cells and is involved in alpha-galactosylceramide presentation in liver. *PLoS One*. 2013 ;8(6) : e65070.
156. Jiang Y, Tang Y, Hoover C, Kondo Y, Huang D, Restagno D, et al. Kupffer cell receptor CLEC4F is important for the destruction of desialylated platelets in mice. *Cell Death Differ*. 2021;28(11):3009-21.
157. Johnson DB, Balko JM, Compton ML, Chalkias S, Gorham J, Xu Y, et al. Fulminant Myocarditis with Combination Immune Checkpoint Blockade. *N Engl J Med*. 2016;375(18):1749-55.
158. Lehrman MA, Hill RL. The binding of fucose-containing glycoproteins by hepatic lectins. Purification of a fucose-binding lectin from rat liver. *J Biol Chem*. 1986;261(16):7419-25.
159. Taylor ME, Snelling T, Smith DF, Drickamer K. Absence of a human ortholog of rodent Kupffer cell galactose-binding receptor encoded by the CLEC4f gene. *Glycobiology*. 2019;29(4):332-45.
160. Blériot C, Barreby E, Dunsmore G, Ballaire R, Chakarov S, Ficht X, et al. A subset of Kupffer cells regulates metabolism through the expression of CD36. *Immunity*. 2021 ;54(9) :2101-16.e6.

161. De Simone G, Andreatta F, Bleriot C, Fumagalli V, Laura C, Garcia-Manteiga JM, et al. Identification of a Kupffer cell subset capable of reverting the T cell dysfunction induced by hepatocellular priming. *Immunity*. 2021;54(9):2089-100.e8.
162. Shan Z, Ju C. Hepatic Macrophages in Liver Injury. *Front Immunol*. 2020;11:322.
163. Deppermann C, Kratoofil RM, Peiseler M, David BA, Zindel J, Castanheira F, et al. Macrophage galactose lectin is critical for Kupffer cells to clear aged platelets. *J Exp Med*. 2020;217(4).
164. Terpstra V, van Berkel TJ. Scavenger receptors on liver Kupffer cells mediate the in vivo uptake of oxidatively damaged red blood cells in mice. *Blood*. 2000;95(6):2157-63.
165. Willekens FL, Werre JM, Kruijt JK, Roerdinkholder-Stoelwinder B, Groenen-Döpp YA, van den Bos AG, et al. Liver Kupffer cells rapidly remove red blood cell-derived vesicles from the circulation by scavenger receptors. *Blood*. 2005;105(5):2141-5.
166. Scott CL, Guilliams M. The role of Kupffer cells in hepatic iron and lipid metabolism. *J Hepatol*. 2018;69(5):1197-9.
167. Theurl I, Hilgendorf I, Nairz M, Tymoszuk P, Haschka D, Asshoff M, et al. On-demand erythrocyte disposal and iron recycling requires transient macrophages in the liver. *Nat Med*. 2016;22(8):945-51.
168. Wang Y, van der Tuin S, Tjeerdema N, van Dam AD, Rensen SS, Hendrikx T, et al. Plasma cholesteryl ester transfer protein is predominantly derived from Kupffer cells. *Hepatology*. 2015;62(6):1710-22.
169. Knolle P, Schlaak J, Uhrig A, Kempf P, Meyer zum Büschenfelde KH, Gerken G. Human Kupffer cells secrete IL-10 in response to lipopolysaccharide (LPS) challenge. *J Hepatol*. 1995;22(2):226-9.
170. Everett ML, Collins BH, Parker W. Kupffer cells: another player in liver tolerance induction. *Liver Transpl*. 2003;9(5):498-9.
171. Heymann F, Peusquens J, Ludwig-Portugall I, Kohlhepp M, Ergen C, Niemietz P, et al. Liver inflammation abrogates immunological tolerance induced by Kupffer cells. *Hepatology*. 2015;62(1):279-91.
172. Sun Z, Wada T, Maemura K, Uchikura K, Hoshino S, Diehl AM, et al. Hepatic allograft-derived Kupffer cells regulate T cell response in rats. *Liver Transpl*. 2003;9(5):489-97.

173. Tay SS, Wong YC, McDonald DM, Wood NA, Roediger B, Sierro F, et al. Antigen expression level threshold tunes the fate of CD8 T cells during primary hepatic immune responses. *Proc Natl Acad Sci U S A*. 2014;111(25):E2540-9.
174. Erhardt A, Biburger M, Papadopoulos T, Tiegs G. IL-10, regulatory T cells, and Kupffer cells mediate tolerance in concanavalin A-induced liver injury in mice. *Hepatology*. 2007;45(2):475-85.
175. Jung K, Kang M, Park C, Hyun Choi Y, Jeon Y, Park SH, et al. Protective role of V-set and immunoglobulin domain-containing 4 expressed on kupffer cells during immune-mediated liver injury by inducing tolerance of liver T- and natural killer T-cells. *Hepatology*. 2012;56(5):1838-48.
176. Chen Y, Liu Z, Liang S, Luan X, Long F, Chen J, et al. Role of Kupffer cells in the induction of tolerance of orthotopic liver transplantation in rats. *Liver Transpl*. 2008;14(6):823-36.
177. Yan ML, Wang YD, Tian YF, Lai ZD, Yan LN. Inhibition of allogeneic T-cell response by Kupffer cells expressing indoleamine 2,3-dioxygenase. *World J Gastroenterol*. 2010;16(5):636-40.
178. Dou L, Shi X, He X, Gao Y. Macrophage Phenotype and Function in Liver Disorder. *Front Immunol*. 2019;10:3112.
179. Nakamoto N, Kanai T. Role of toll-like receptors in immune activation and tolerance in the liver. *Front Immunol*. 2014;5:221.
180. Marra F, Tacke F. Roles for chemokines in liver disease. *Gastroenterology*. 2014;147(3):577-94.e1.
181. McDonald B, Pittman K, Menezes GB, Hirota SA, Slaba I, Waterhouse CC, et al. Intravascular danger signals guide neutrophils to sites of sterile inflammation. *Science*. 2010;330(6002):362-6.
182. Wen Y, Lambrecht J, Ju C, Tacke F. Hepatic macrophages in liver homeostasis and diseases-diversity, plasticity and therapeutic opportunities. *Cell Mol Immunol*. 2021;18(1):45-56.
183. Elchaninov AV, Fat Chudinov TK, Vishnyakova PA, Lokhonina AV, Sukhikh GT. Phenotypical and Functional Polymorphism of Liver Resident Macrophages. *Cells*. 2019;8(9).

184. Van Rooijen N, Sanders A. Kupffer cell depletion by liposome-delivered drugs: comparative activity of intracellular clodronate, propamidine, and ethylenediaminetetraacetic acid. *Hepatology*. 1996;23(5):1239-43.
185. Golbar HM, Izawa T, Wijesundera KK, Bondoc A, Tennakoon AH, Kuwamura M, et al. Depletion of Hepatic Macrophages Aggravates Liver Lesions Induced in Rats by Thioacetamide (TAA). *Toxicol Pathol*. 2016;44(2):246-58.
186. Holt MP, Yin H, Ju C. Exacerbation of acetaminophen-induced disturbances of liver sinusoidal endothelial cells in the absence of Kupffer cells in mice. *Toxicol Lett*. 2010;194(1-2):34-41.
187. Sato A, Nakashima H, Nakashima M, Ikarashi M, Nishiyama K, Kinoshita M, et al. Involvement of the TNF and FasL produced by CD11b Kupffer cells/macrophages in CCl<sub>4</sub>-induced acute hepatic injury. *PLoS One*. 2014;9(3):e92515.
188. Mossanen JC, Tacke F. Acetaminophen-induced acute liver injury in mice. *Lab Anim*. 2015;49(1 Suppl):30-6.
189. You Q, Holt M, Yin H, Li G, Hu CJ, Ju C. Role of hepatic resident and infiltrating macrophages in liver repair after acute injury. *Biochem Pharmacol*. 2013;86(6):836-43.
190. Miura A, Hosono T, Seki T. Macrophage potentiates the recovery of liver zonation and metabolic function after acute liver injury. *Sci Rep*. 2021;11(1):9730.
191. Wong CH, Jenne CN, Petri B, Chrobok NL, Kubes P. Nucleation of platelets with blood-borne pathogens on Kupffer cells precedes other innate immunity and contributes to bacterial clearance. *Nat Immunol*. 2013;14(8):785-92.
192. Blériot C, Dupuis T, Jouvion G, Eberl G, Disson O, Lecuit M. Liver-resident macrophage necroptosis orchestrates type 1 microbicidal inflammation and type-2-mediated tissue repair during bacterial infection. *Immunity*. 2015;42(1):145-58.
193. Dal-Secco D, Wang J, Zeng Z, Kołaczowska E, Wong CH, Petri B, et al. A dynamic spectrum of monocytes arising from the in situ reprogramming of CCR2<sup>+</sup> monocytes at a site of sterile injury. *J Exp Med*. 2015;212(4):447-56.
194. Graubardt N, Vugman M, Mouhadeb O, Caliarì G, Pasmanik-Chor M, Reuveni D, et al. Ly6C(hi) Monocytes and Their Macrophage Descendants Regulate Neutrophil Function and Clearance in Acetaminophen-Induced Liver Injury. *Front Immunol*. 2017;8:626.

195. Krenkel O, Tacke F. Liver macrophages in tissue homeostasis and disease. *Nat Rev Immunol.* 2017;17(5):306-21.
196. Tacke F, Kurts C. Infiltrating monocytes versus resident Kupffer cells: do alternatively activated macrophages need to be targeted alternatively? *Hepatology.* 2011;54(6):2267-70.
197. Baeck C, Wehr A, Karlmark KR, Heymann F, Vucur M, Gassler N, et al. Pharmacological inhibition of the chemokine CCL2 (MCP-1) diminishes liver macrophage infiltration and steatohepatitis in chronic hepatic injury. *Gut.* 2012;61(3):416-26.
198. Heymann F, Hammerich L, Storch D, Bartneck M, Huss S, Rüsseler V, et al. Hepatic macrophage migration and differentiation critical for liver fibrosis is mediated by the chemokine receptor C-C motif chemokine receptor 8 in mice. *Hepatology.* 2012;55(3):898-909.
199. Karlmark KR, Weiskirchen R, Zimmermann HW, Gassler N, Ginhoux F, Weber C, et al. Hepatic recruitment of the inflammatory Gr1<sup>+</sup> monocyte subset upon liver injury promotes hepatic fibrosis. *Hepatology.* 2009;50(1):261-74.
200. Miura K, Yang L, van Rooijen N, Ohnishi H, Seki E. Hepatic recruitment of macrophages promotes nonalcoholic steatohepatitis through CCR2. *Am J Physiol Gastrointest Liver Physiol.* 2012;302(11):G1310-21.
201. Karlmark KR, Zimmermann HW, Roderburg C, Gassler N, Wasmuth HE, Luedde T, et al. The fractalkine receptor CX<sub>3</sub>CR1 protects against liver fibrosis by controlling differentiation and survival of infiltrating hepatic monocytes. *Hepatology.* 2010 ; 52(5) :1769-82.
202. Yang W, Tao Y, Wu Y, Zhao X, Ye W, Zhao D, et al. Neutrophils promote the development of reparative macrophages mediated by ROS to orchestrate liver repair. *Nat Commun.* 2019;10(1):1076.
203. Williams M, Mildner A, Yona S. Developmental and Functional Heterogeneity of Monocytes. *Immunity.* 2018;49(4):595-613.
204. Devisscher L, Scott CL, Lefere S, Raevens S, Bogaerts E, Paridaens A, et al. Non-alcoholic steatohepatitis induces transient changes within the liver macrophage pool. *Cell Immunol.* 2017;322:74-83.
205. Liew PX, Lee WY, Kuberski P. iNKT Cells Orchestrate a Switch from Inflammation to Resolution of Sterile Liver Injury. *Immunity.* 2017;47(4):752-65.e5.

206. Souza COS, Gardinassi LG, Rodrigues V, Faccioli LH. Monocyte and Macrophage-Mediated Pathology and Protective Immunity During Schistosomiasis. *Front Microbiol.* 2020;11:1973.
207. Barron L, Wynn TA. Macrophage activation governs schistosomiasis-induced inflammation and fibrosis. *Eur J Immunol.* 2011;41(9):2509-14.
208. Girgis NM, Gundra UM, Ward LN, Cabrera M, Frevert U, Loke P. Ly6C(high) monocytes become alternatively activated macrophages in schistosome granulomas with help from CD4+ cells. *PLoS Pathog.* 2014;10(6):e1004080.
209. Herbert DR, Hölscher C, Mohrs M, Arendse B, Schwegmann A, Radwanska M, et al. Alternative macrophage activation is essential for survival during schistosomiasis and down modulates T helper 1 responses and immunopathology. *Immunity.* 2004;20(5):623-35.
210. Xu J, Chi F, Guo T, Punj V, Lee WN, French SW, et al. NOTCH reprograms mitochondrial metabolism for proinflammatory macrophage activation. *J Clin Invest.* 2015;125(4):1579-90.
211. Liaskou E, Zimmermann HW, Li KK, Oo YH, Suresh S, Stamataki Z, et al. Monocyte subsets in human liver disease show distinct phenotypic and functional characteristics. *Hepatology.* 2013;57(1):385-98.
212. Naik SH, Sathe P, Park HY, Metcalf D, Proietto AI, Dakic A, et al. Development of plasmacytoid and conventional dendritic cell subtypes from single precursor cells derived in vitro and in vivo. *Nat Immunol.* 2007;8(11):1217-26.
213. Lian ZX, Okada T, He XS, Kita H, Liu YJ, Ansari AA, et al. Heterogeneity of dendritic cells in the mouse liver: identification and characterization of four distinct populations. *J Immunol.* 2003;170(5):2323-30.
214. Waisman A, Lukas D, Clausen BE, Yogev N. Dendritic cells as gatekeepers of tolerance. *Semin Immunopathol.* 2017;39(2):153-63.
215. Pierre P, Turley SJ, Gatti E, Hull M, Meltzer J, Mirza A, et al. Developmental regulation of MHC class II transport in mouse dendritic cells. *Nature.* 1997;388(6644):787-92.
216. Bilsborough J, George TC, Norment A, Viney JL. Mucosal CD8 alpha DC, with a plasmacytoid phenotype, induce differentiation and support function of T cells with regulatory properties. *Immunology.* 2003;108(4):481-92.
217. Boonstra A, Asselin-Paturel C, Gilliet M, Crain C, Trinchieri G, Liu YJ, et al. Flexibility of mouse classical and plasmacytoid-derived dendritic cells in directing T helper type 1 and 2 cell



development: dependency on antigen dose and differential toll-like receptor ligation. *J Exp Med.* 2003;197(1):101-9.

218. Ito T, Yang M, Wang YH, Lande R, Gregorio J, Perng OA, et al. Plasmacytoid dendritic cells prime IL-10-producing T regulatory cells by inducible costimulator ligand. *J Exp Med.* 2007;204(1):105-15.

219. Kuwana M. Induction of anergic and regulatory T cells by plasmacytoid dendritic cells and other dendritic cell subsets. *Hum Immunol.* 2002;63(12):1156-63.

220. Martín P, Del Hoyo GM, Anjuère F, Arias CF, Vargas HH, Fernández LA, et al. Characterization of a new subpopulation of mouse CD8 $\alpha$ <sup>+</sup> B220<sup>+</sup> dendritic cells endowed with type 1 interferon production capacity and tolerogenic potential. *Blood.* 2002;100(2):383-90.

221. Hsu W, Shu SA, Gershwin E, Lian ZX. The current immune function of hepatic dendritic cells. *Cell Mol Immunol.* 2007 ;4(5) :321-8.

222. Shu SA, Lian ZX, Chuang YH, Yang GX, Moritoki Y, Comstock SS, et al. The role of CD11c(+) hepatic dendritic cells in the induction of innate immune responses. *Clin Exp Immunol.* 2007;149(2):335-43.

223. Dou L, Ono Y, Chen YF, Thomson AW, Chen XP. Hepatic Dendritic Cells, the Tolerogenic Liver Environment, and Liver Disease. *Semin Liver Dis.* 2018;38(2):170-80.

224. Steiniger B, Klempnauer J, Wonigeit K. Phenotype and histological distribution of interstitial dendritic cells in the rat pancreas, liver, heart, and kidney. *Transplantation.* 1984;38(2):169-74.

225. Thomson AW, Lu L, Murase N, Demetris AJ, Rao AS, Starzl TE. Microchimerism, dendritic cell progenitors and transplantation tolerance. *Stem Cells.* 1995;13(6):622-39.

226. Rutella S, Bonanno G, Procoli A, Mariotti A, de Ritis DG, Curti A, et al. Hepatocyte growth factor favors monocyte differentiation into regulatory interleukin (IL)-10<sup>++</sup>IL-12<sup>low</sup>/neg accessory cells with dendritic-cell features. *Blood.* 2006;108(1):218-27.

227. Zhang XJ, Olsavszky V, Yin Y, Wang B, Engleitner T, Öllinger R, et al. Angiocrine Hepatocyte Growth Factor Signaling Controls Physiological Organ and Body Size and Dynamic Hepatocyte Proliferation to Prevent Liver Damage during Regeneration. *Am J Pathol.* 2020;190(2):358-71.

228. O'Connell PJ, Logar AJ, Thomson AW. Differential regulation of T-cell proliferation and apoptosis by hepatic CD8 $\alpha$ (+) (lymphoid-related) and CD8 $\alpha$ (-) (myeloid) dendritic cells. *Transplant Proc.* 2001;33(1-2):250-1.
229. Jomantaite I, Dikopoulos N, Kröger A, Leithäuser F, Hauser H, Schirmbeck R, et al. Hepatic dendritic cell subsets in the mouse. *Eur J Immunol.* 2004;34(2):355-65.
230. Abe M, Zahorchak AF, Colvin BL, Thomson AW. Migratory responses of murine hepatic myeloid, lymphoid-related, and plasmacytoid dendritic cells to CC chemokines. *Transplantation.* 2004;78(5):762-5.
231. Akbar SM, Onji M, Inaba K, Yamamura K, Ohta Y. Low responsiveness of hepatitis B virus-transgenic mice in antibody response to T-cell-dependent antigen: defect in antigen-presenting activity of dendritic cells. *Immunology.* 1993;78(3):468-75.
232. Auffermann-Gretzinger S, Keeffe EB, Levy S. Impaired dendritic cell maturation in patients with chronic, but not resolved, hepatitis C virus infection. *Blood.* 2001;97(10):3171-6.
233. Chen S, Akbar SM, Tanimoto K, Ninomiya T, Iuchi H, Michitaka K, et al. Absence of CD83-positive mature and activated dendritic cells at cancer nodules from patients with hepatocellular carcinoma: relevance to hepatocarcinogenesis. *Cancer Lett.* 2000 ;148(1) :49-57.
234. Kanto T, Hayashi N, Takehara T, Tatsumi T, Kuzushita N, Ito A, et al. Impaired allostimulatory capacity of peripheral blood dendritic cells recovered from hepatitis C virus-infected individuals. *J Immunol.* 1999;162(9):5584-91.
235. Lee WC, Chiang YJ, Wang HC, Wang MR, Lia SR, Chen MF. Functional impairment of dendritic cells caused by murine hepatocellular carcinoma. *J Clin Immunol.* 2004 ;24(2) :145-54.
236. Jiao J, Sastre D, Fiel MI, Lee UE, Ghiassi-Nejad Z, Ginhoux F, et al. Dendritic cell regulation of carbon tetrachloride-induced murine liver fibrosis regression. *Hepatology.* 2012;55(1):244-55.
237. Henning JR, Graffeo CS, Rehman A, Fallon NC, Zambirinis CP, Ochi A, et al. Dendritic cells limit fibroinflammatory injury in nonalcoholic steatohepatitis in mice. *Hepatology.* 2013;58(2):589-602.
238. Doherty DG. Immunity, tolerance and autoimmunity in the liver: A comprehensive review. *J Autoimmun.* 2016;66:60-75.
239. Wang Y, Zhang C. The Roles of Liver-Resident Lymphocytes in Liver Diseases. *Front Immunol.* 2019;10:1582.

240. Pasman L, Kasper DL. Building conventions for unconventional lymphocytes. *Immunol Rev.* 2017;279(1):52-62.
241. Sun H, Sun C, Xiao W, Sun R. Tissue-resident lymphocytes: from adaptive to innate immunity. *Cell Mol Immunol.* 2019;16(3):205-15.
242. Crosby CM, Kronenberg M. Tissue-specific functions of invariant natural killer T cells. *Nat Rev Immunol.* 2018;18(9):559-74.
243. Cuff AO, Robertson FP, Stegmann KA, Pallett LJ, Maini MK, Davidson BR, et al. Eomeshi NK Cells in Human Liver Are Long-Lived and Do Not Recirculate but Can Be Replenished from the Circulation. *J Immunol.* 2016;197(11):4283-91.
244. Daussy C, Faure F, Mayol K, Viel S, Gasteiger G, Charrier E, et al. T-bet and Eomes instruct the development of two distinct natural killer cell lineages in the liver and in the bone marrow. *J Exp Med.* 2014 ;211(3) :563-77.
245. Fernandez-Ruiz D, Ng WY, Holz LE, Ma JZ, Zaid A, Wong YC, et al. Liver-Resident Memory CD8(+) T Cells Form a Front-Line Defense against Malaria Liver-Stage Infection. *Immunity.* 2019;51(4):780.
246. Haas JD, González FH, Schmitz S, Chennupati V, Föhse L, Kremmer E, et al. CCR6 and NK1.1 distinguish between IL-17A and IFN-gamma-producing gammadelta effector T cells. *Eur J Immunol.* 2009;39(12):3488-97.
247. Hu Y, Fang K, Wang Y, Lu N, Sun H, Zhang C. Single-cell analysis reveals the origins and intrahepatic development of liver-resident IFN- $\gamma$ -producing  $\gamma\delta$  T cells. *Cell Mol Immunol.* 2021;18(4):954-68.
248. Jeffery HC, van Wilgenburg B, Kurioka A, Parekh K, Stirling K, Roberts S, et al. Biliary epithelium and liver B cells exposed to bacteria activate intrahepatic MAIT cells through MR1. *J Hepatol.* 2016;64(5):1118-27.
249. Kumar H, Belperron A, Barthold SW, Bockenstedt LK. Cutting edge: CD1d deficiency impairs murine host defense against the spirochete, *Borrelia burgdorferi*. *J Immunol.* 2000;165(9):4797-801.
250. Lee WY, Moriarty TJ, Wong CH, Zhou H, Strieter RM, van Rooijen N, et al. An intravascular immune response to *Borrelia burgdorferi* involves Kupffer cells and iNKT cells. *Nat Immunol.* 2010 ;11(4) :295-302.

251. Li F, Hao X, Chen Y, Bai L, Gao X, Lian Z, et al. The microbiota maintain homeostasis of liver-resident  $\gamma\delta$ T-17 cells in a lipid antigen/CD1d-dependent manner. *Nat Commun.* 2017 ;7 :13839.
252. Marquardt N, Béziat V, Nyström S, Hengst J, Ivarsson MA, Kekäläinen E, et al. Cutting edge: identification and characterization of human intrahepatic CD49a+ NK cells. *J Immunol.* 2015;194(6):2467-71.
253. Mikulak J, Bruni E, Oriolo F, Di Vito C, Mavilio D. Hepatic Natural Killer Cells: Organ-Specific Sentinels of Liver Immune Homeostasis and Physiopathology. *Front Immunol.* 2019 ;10 :946.
254. Olson CM, Jr., Bates TC, Izadi H, Radolf JD, Huber SA, Boyson JE, et al. Local production of IFN-gamma by invariant NKT cells modulates acute Lyme carditis. *J Immunol.* 2009;182(6):3728-34.
255. Pallett LJ, Davies J, Colbeck EJ, Robertson F, Hansi N, Easom NJW, et al. IL-2(high) tissue-resident T cells in the human liver: Sentinels for hepatotropic infection. *J Exp Med.* 2017;214(6):1567-80.
256. Peng H, Jiang X, Chen Y, Sojka DK, Wei H, Gao X, et al. Liver-resident NK cells confer adaptive immunity in skin-contact inflammation. *J Clin Invest.* 2013 ;123(4) :1444-56.
257. Stegmann KA, Robertson F, Hansi N, Gill U, Pallant C, Christophides T, et al. CXCR6 marks a novel subset of T-bet(lo)Eomes(hi) natural killer cells residing in human liver. *Sci Rep.* 2016;6:26157.
258. Steinert EM, Schenkel JM, Fraser KA, Beura LK, Manlove LS, Igyártó BZ, et al. Quantifying Memory CD8 T Cells Reveals Regionalization of Immunosurveillance. *Cell.* 2015;161(4):737-49.
259. Tang XZ, Jo J, Tan AT, Sandalova E, Chia A, Tan KC, et al. IL-7 licenses activation of human liver intrasinusoidal mucosal-associated invariant T cells. *J Immunol.* 2013;190(7):3142-52.
260. Zhang LH, Shin JH, Haggadone MD, Sunwoo JB. The aryl hydrocarbon receptor is required for the maintenance of liver-resident natural killer cells. *J Exp Med.* 2016;213(11):2249-57.
261. Zhu S, Zhang H, Bai L. NKT cells in liver diseases. *Front Med.* 2018 ;12(3) :249-61.

262. Mackay LK, Minnich M, Kragten NA, Liao Y, Nota B, Seillet C, et al. Hobit and Blimp1 instruct a universal transcriptional program of tissue residency in lymphocytes. *Science*. 2016;352(6284):459-63.
263. Gasteiger G, Fan X, Dikiy S, Lee SY, Rudensky AY. Tissue residency of innate lymphoid cells in lymphoid and nonlymphoid organs. *Science*. 2015 ;350(6263) :981-5.
264. Vivier E, Artis D, Colonna M, Diefenbach A, Di Santo JP, Eberl G, et al. Innate Lymphoid Cells: 10 Years On. *Cell*. 2018;174(5):1054-66.
265. Murphy JM, Ngai L, Mortha A, Crome SQ. Tissue-Dependent Adaptations and Functions of Innate Lymphoid Cells. *Front Immunol*. 2022;13:836999.
266. Forkel M, Berglin L, Kekäläinen E, Carlsson A, Svedin E, Michaëlsson J, et al. Composition and functionality of the intrahepatic innate lymphoid cell-compartment in human nonfibrotic and fibrotic livers. *Eur J Immunol*. 2017;47(8):1280-94.
267. Liu M, Zhang C. The Role of Innate Lymphoid Cells in Immune-Mediated Liver Diseases. *Front Immunol*. 2017 ;8 :695.
268. Matsumoto A, Kanai T, Mikami Y, Chu PS, Nakamoto N, Ebinuma H, et al. IL-22-producing ROR $\gamma$ t-dependent innate lymphoid cells play a novel protective role in murine acute hepatitis. *PLoS One*. 2013;8(4):e62853.
269. McHedlidze T, Waldner M, Zopf S, Walker J, Rankin AL, Schuchmann M, et al. Interleukin-33-dependent innate lymphoid cells mediate hepatic fibrosis. *Immunity*. 2013;39(2):357-71.
270. Artis D, Spits H. The biology of innate lymphoid cells. *Nature*. 2015;517(7534):293-301.
271. Eberl G, Colonna M, Di Santo JP, McKenzie AN. Innate lymphoid cells. Innate lymphoid cells: a new paradigm in immunology. *Science*. 2015;348(6237):aaa6566.
272. Spits H, Artis D, Colonna M, Diefenbach A, Di Santo JP, Eberl G, et al. Innate lymphoid cells--a proposal for uniform nomenclature. *Nat Rev Immunol*. 2013 ;13(2) :145-9.
273. Klose CS, Kiss EA, Schwierzeck V, Ebert K, Hoyler T, d'Hargues Y, et al. A T-bet gradient controls the fate and function of CCR6-ROR $\gamma$ t<sup>+</sup> innate lymphoid cells. *Nature*. 2013;494(7436):261-5.
274. Klose CSN, Flach M, Möhle L, Rogell L, Hoyler T, Ebert K, et al. Differentiation of type 1 ILCs from a common progenitor to all helper-like innate lymphoid cell lineages. *Cell*. 2014;157(2):340-56.

275. Neill DR, Wong SH, Bellosi A, Flynn RJ, Daly M, Langford TK, et al. Nuocytes represent a new innate effector leukocyte that mediates type-2 immunity. *Nature*. 2010;464(7293):1367-70.
276. Pelly VS, Kannan Y, Coomes SM, Entwistle LJ, Rückerl D, Seddon B, et al. IL-4-producing ILC2s are required for the differentiation of T(H)2 cells following *Heligmosomoides polygyrus* infection. *Mucosal Immunol*. 2016;9(6):1407-17.
277. Monticelli LA, Osborne LC, Noti M, Tran SV, Zaiss DM, Artis D. IL-33 promotes an innate immune pathway of intestinal tissue protection dependent on amphiregulin-EGFR interactions. *Proc Natl Acad Sci U S A*. 2015;112(34):10762-7.
278. Monticelli LA, Sonnenberg GF, Abt MC, Alenghat T, Ziegler CG, Doering TA, et al. Innate lymphoid cells promote lung-tissue homeostasis after infection with influenza virus. *Nat Immunol*. 2011;12(11):1045-54.
279. Annunziato F, Romagnani C, Romagnani S. The 3 major types of innate and adaptive cell-mediated effector immunity. *J Allergy Clin Immunol*. 2015 ;135(3) :626-35.
280. Ibiza S, García-Cassani B, Ribeiro H, Carvalho T, Almeida L, Marques R, et al. Glial-cell-derived neuroregulators control type 3 innate lymphoid cells and gut defence. *Nature*. 2016;535(7612):440-3.
281. Okada S, Markle JG, Deenick EK, Mele F, Averbuch D, Lagos M, et al. IMMUNODEFICIENCIES. Impairment of immunity to *Candida* and *Mycobacterium* in humans with bi-allelic RORC mutations. *Science*. 2015;349(6248):606-13.
282. Colonna M. Innate Lymphoid Cells: Diversity, Plasticity, and Unique Functions in Immunity. *Immunity*. 2018 ;48(6) :1104-17.
283. Hou L, Jie Z, Desai M, Liang Y, Soong L, Wang T, et al. Early IL-17 production by intrahepatic T cells is important for adaptive immune responses in viral hepatitis. *J Immunol*. 2013 ;190(2) :621-9.
284. Jie Z, Liang Y, Hou L, Dong C, Iwakura Y, Soong L, et al. Intrahepatic innate lymphoid cells secrete IL-17A and IL-17F that are crucial for T cell priming in viral infection. *J Immunol*. 2014;192(7):3289-300.
285. Valle-Noguera A, Ochoa-Ramos A, Gomez-Sánchez MJ, Cruz-Adalia A. Type 3 Innate Lymphoid Cells as Regulators of the Host-Pathogen Interaction. *Front Immunol*. 2021;12:748851.
286. Wang S, Li J, Wu S, Cheng L, Shen Y, Ma W, et al. Type 3 innate lymphoid cell: a new player in liver fibrosis progression. *Clin Sci (Lond)*. 2018;132(24):2565-82.

287. Kim CH, Hashimoto-Hill S, Kim M. Migration and Tissue Tropism of Innate Lymphoid Cells. *Trends Immunol.* 2016;37(1):68-79.
288. Steinmann S, Schoedsack M, Heinrich F, Breda PC, Ochel A, Tiegs G, et al. Hepatic ILC2 activity is regulated by liver inflammation-induced cytokines and effector CD4(+) T cells. *Sci Rep.* 2020;10(1):1071.
289. Jeffery HC, McDowell P, Lutz P, Wawman RE, Roberts S, Bagnall C, et al. Human intrahepatic ILC2 are IL-13positive amphiregulinpositive and their frequency correlates with model of end stage liver disease score. *PLoS One.* 2017;12(12):e0188649.
290. Krueger PD, Narayanan S, Surette FA, Brown MG, Sung SJ, Hahn YS. Murine liver-resident group 1 innate lymphoid cells regulate optimal priming of anti-viral CD8+ T cells. *J Leukoc Biol.* 2017;101(1):329-38.
291. Goltsev Y, Samusik N, Kennedy-Darling J, Bhate S, Hale M, Vazquez G, et al. Deep Profiling of Mouse Splenic Architecture with CODEX Multiplexed Imaging. *Cell.* 2018;174(4):968-81.e15.
292. Weizman OE, Adams NM, Schuster IS, Krishna C, Pritykin Y, Lau C, et al. ILC1 Confer Early Host Protection at Initial Sites of Viral Infection. *Cell.* 2017 ;171(4) :795-808.e12.
293. Bai L, Vienne M, Tang L, Kerdiles Y, Etiennot M, Escalière B, et al. Liver type 1 innate lymphoid cells develop locally via an interferon- $\gamma$ -dependent loop. *Science.* 2021;371(6536).
294. Chen Y, Wang X, Hao X, Li B, Tao W, Zhu S, et al. Ly49E separates liver ILC1s into embryo-derived and postnatal subsets with different functions. *J Exp Med.* 2022;219(5).
295. Weizman OE, Song E, Adams NM, Hildreth AD, Riggan L, Krishna C, et al. Mouse cytomegalovirus-experienced ILC1s acquire a memory response dependent on the viral glycoprotein m12. *Nat Immunol.* 2019;20(8):1004-11.
296. Nabekura T, Riggan L, Hildreth AD, O'Sullivan TE, Shibuya A. Type 1 Innate Lymphoid Cells Protect Mice from Acute Liver Injury via Interferon- $\gamma$  Secretion for Upregulating Bcl-xL Expression in Hepatocytes. *Immunity.* 2020;52(1):96-108.e9.
297. Yang Z, Tang T, Wei X, Yang S, Tian Z. Type 1 innate lymphoid cells contribute to the pathogenesis of chronic hepatitis B. *Innate Immun.* 2015;21(6):665-73.
298. Neumann K, Karimi K, Meiners J, Voetlaue R, Steinmann S, Dammermann W, et al. A Proinflammatory Role of Type 2 Innate Lymphoid Cells in Murine Immune-Mediated Hepatitis. *J Immunol.* 2017 ;198(1) :128-37.

299. Louis H, Le Moine A, Flamand V, Nagy N, Quertinmont E, Paulart F, et al. Critical role of interleukin 5 and eosinophils in concanavalin A-induced hepatitis in mice. *Gastroenterology*. 2002;122(7):2001-10.
300. Nakamura R, Yoshizawa A, Moriyasu T, Deloer S, Senba M, Kikuchi M, et al. Group 2 Innate Lymphoid Cells Exacerbate Amebic Liver Abscess in Mice. *iScience*. 2020 ;23(9) :101544.
301. Sonnenberg GF, Monticelli LA, Alenghat T, Fung TC, Hutnick NA, Kunisawa J, et al. Innate lymphoid cells promote anatomical containment of lymphoid-resident commensal bacteria. *Science*. 2012 ;336(6086) :1321-5.
302. Liu Y, Song Y, Lin D, Lei L, Mei Y, Jin Z, et al. NCR(-) group 3 innate lymphoid cells orchestrate IL-23/IL-17 axis to promote hepatocellular carcinoma development. *EBioMedicine*. 2019;41:333-44.
303. van de Pavert SA. Lymphoid Tissue inducer (LTi) cell ontogeny and functioning in embryo and adult. *Biomed J*. 2021;44(2):123-32.
304. Abel AM, Yang C, Thakar MS, Malarkannan S. Natural Killer Cells: Development, Maturation, and Clinical Utilization. *Front Immunol*. 2018;9:1869.
305. Rosenau W, Moon HD. Lysis of homologous cells by sensitized lymphocytes in tissue culture. *J Natl Cancer Inst*. 1961;27:471-83.
306. Smith HJ. Antigenicity of carcinogen-induced and spontaneous tumours in inbred mice. *Br J Cancer*. 1966;20(4):831-7.
307. Scoville SD, Freud AG, Caligiuri MA. Modeling Human Natural Killer Cell Development in the Era of Innate Lymphoid Cells. *Front Immunol*. 2017;8:360.
308. Orr MT, Lanier LL. Natural killer cell education and tolerance. *Cell*. 2010;142(6):847-56.
309. Parham P. MHC class I molecules and KIRs in human history, health and survival. *Nat Rev Immunol*. 2005;5(3):201-14.
310. Vivier E, Tomasello E, Baratin M, Walzer T, Ugolini S. Functions of natural killer cells. *Nat Immunol*. 2008;9(5):503-10.
311. Yokoyama WM, Plougastel BF. Immune functions encoded by the natural killer gene complex. *Nat Rev Immunol*. 2003;3(4):304-16.
312. Degli-Esposti M. To die or not to die--the quest of the TRAIL receptors. *J Leukoc Biol*. 1999;65(5):535-42.



313. Fauriat C, Long EO, Ljunggren HG, Bryceson YT. Regulation of human NK-cell cytokine and chemokine production by target cell recognition. *Blood*. 2010;115(11):2167-76.
314. Screpanti V, Wallin RP, Ljunggren HG, Grandien A. A central role for death receptor-mediated apoptosis in the rejection of tumors by NK cells. *J Immunol*. 2001;167(4):2068-73.
315. Morvan MG, Lanier LL. NK cells and cancer: you can teach innate cells new tricks. *Nat Rev Cancer*. 2016;16(1):7-19.
316. Arase H, Mocarski ES, Campbell AE, Hill AB, Lanier LL. Direct recognition of cytomegalovirus by activating and inhibitory NK cell receptors. *Science*. 2002;296(5571):1323-6.
317. Dokun AO, Kim S, Smith HR, Kang HS, Chu DT, Yokoyama WM. Specific and nonspecific NK cell activation during virus infection. *Nat Immunol*. 2001 ;2(10) :951-6.
318. Vivier E, Raulet DH, Moretta A, Caligiuri MA, Zitvogel L, Lanier LL, et al. Innate or adaptive immunity? The example of natural killer cells. *Science*. 2011;331(6013):44-9.
319. Paust S, Gill HS, Wang BZ, Flynn MP, Moseman EA, Senman B, et al. Critical role for the chemokine receptor CXCR6 in NK cell-mediated antigen-specific memory of haptens and viruses. *Nat Immunol*. 2010;11(12):1127-35.
320. Sun JC, Beilke JN, Lanier LL. Adaptive immune features of natural killer cells. *Nature*. 2009 ;457(7229) :557-61.
321. Hudspeth K, Donadon M, Cimino M, Pontarini E, Tentorio P, Preti M, et al. Human liver-resident CD56(bright)/CD16(neg) NK cells are retained within hepatic sinusoids via the engagement of CCR5 and CXCR6 pathways. *J Autoimmun*. 2016;66:40-50.
322. Heydtmann M, Lalor PF, Eksteen JA, Hübscher SG, Briskin M, Adams DH. CXC chemokine ligand 16 promotes integrin-mediated adhesion of liver-infiltrating lymphocytes to cholangiocytes and hepatocytes within the inflamed human liver. *J Immunol*. 2005;174(2):1055-62.
323. Zheng M, Sun R, Wei H, Tian Z. NK Cells Help Induce Anti-Hepatitis B Virus CD8+ T Cell Immunity in Mice. *J Immunol*. 2016;196(10):4122-31.
324. Bukowski JF, Woda BA, Habu S, Okumura K, Welsh RM. Natural killer cell depletion enhances virus synthesis and virus-induced hepatitis in vivo. *J Immunol*. 1983 ;131(3) :1531-8.
325. Dunn C, Peppas D, Khanna P, Nebbia G, Jones M, Brendish N, et al. Temporal analysis of early immune responses in patients with acute hepatitis B virus infection. *Gastroenterology*. 2009;137(4):1289-300.

326. Maini MK, Peppas D. NK cells: a double-edged sword in chronic hepatitis B virus infection. *Front Immunol.* 2013 ;4 :57.
327. Li F, Wei H, Wei H, Gao Y, Xu L, Yin W, et al. Blocking the natural killer cell inhibitory receptor NKG2A increases activity of human natural killer cells and clears hepatitis B virus infection in mice. *Gastroenterology.* 2013;144(2):392-401.
328. Tjwa ET, van Oord GW, Hegmans JP, Janssen HL, Woltman AM. Viral load reduction improves activation and function of natural killer cells in patients with chronic hepatitis B. *J Hepatol.* 2011 ;54(2) :209-18.
329. Sun C, Fu B, Gao Y, Liao X, Sun R, Tian Z, et al. TGF- $\beta$ 1 down-regulation of NKG2D/DAP10 and 2B4/SAP expression on human NK cells contributes to HBV persistence. *PLoS Pathog.* 2012;8(3):e1002594.
330. Ahlenstiel G, Titerence RH, Koh C, Edlich B, Feld JJ, Rotman Y, et al. Natural killer cells are polarized toward cytotoxicity in chronic hepatitis C in an interferon- $\alpha$ -dependent manner. *Gastroenterology.* 2010;138(1):325-35.e1-2.
331. Amadei B, Urbani S, Cazaly A, Fiscicaro P, Zerbini A, Ahmed P, et al. Activation of natural killer cells during acute infection with hepatitis C virus. *Gastroenterology.* 2010 ;138(4) :1536-45.
332. Oliviero B, Varchetta S, Paudice E, Michelone G, Zaramella M, Mavilio D, et al. Natural killer cell functional dichotomy in chronic hepatitis B and chronic hepatitis C virus infections. *Gastroenterology.* 2009;137(3):1151-60, 60.e1-7.
333. Alter G, Jost S, Rihn S, Reyor LL, Nolan BE, Ghebremichael M, et al. Reduced frequencies of NKp30+NKp46+, CD161+, and NKG2D+ NK cells in acute HCV infection may predict viral clearance. *J Hepatol.* 2011;55(2):278-88.
334. Nattermann J, Feldmann G, Ahlenstiel G, Langhans B, Sauerbruch T, Spengler U. Surface expression and cytolytic function of natural killer cell receptors is altered in chronic hepatitis C. *Gut.* 2006;55(6):869-77.
335. Pelletier S, Drouin C, Bédard N, Khakoo SI, Bruneau J, Shoukry NH. Increased degranulation of natural killer cells during acute HCV correlates with the magnitude of virus-specific T cell responses. *J Hepatol.* 2010;53(5):805-16.
336. Dong Z, Wei H, Sun R, Hu Z, Gao B, Tian Z. Involvement of natural killer cells in PolyI:C-induced liver injury. *J Hepatol.* 2004;41(6):966-73.

337. Zou Y, Chen T, Han M, Wang H, Yan W, Song G, et al. Increased killing of liver NK cells by Fas/Fas ligand and NKG2D/NKG2D ligand contributes to hepatocyte necrosis in virus-induced liver failure. *J Immunol.* 2010;184(1):466-75.
338. Okazaki A, Hiraga N, Imamura M, Hayes CN, Tsuge M, Takahashi S, et al. Severe necroinflammatory reaction caused by natural killer cell-mediated Fas/Fas ligand interaction and dendritic cells in human hepatocyte chimeric mouse. *Hepatology.* 2012;56(2):555-66.
339. Zheng Q, Zhu YY, Chen J, Ye YB, Li JY, Liu YR, et al. Activated natural killer cells accelerate liver damage in patients with chronic hepatitis B virus infection. *Clin Exp Immunol.* 2015 ;180(3) :499-508.
340. Bonorino P, Ramzan M, Camous X, Dufeu-Duchesne T, Thélou MA, Sturm N, et al. Fine characterization of intrahepatic NK cells expressing natural killer receptors in chronic hepatitis B and C. *J Hepatol.* 2009;51(3):458-67.
341. Gorelik E, Wiltrout RH, Okumura K, Habu S, Herberman RB. Role of NK cells in the control of metastatic spread and growth of tumor cells in mice. *Int J Cancer.* 1982;30(1):107-12.
342. Orange JS. Natural killer cell deficiency. *J Allergy Clin Immunol.* 2013 ;132(3) :515-25.
343. Roder JC, Haliotis T, Klein M, Korec S, Jett JR, Ortaldo J, et al. A new immunodeficiency disorder in humans involving NK cells. *Nature.* 1980;284(5756):553-5.
344. Sullivan JL, Byron KS, Brewster FE, Purtilo DT. Deficient natural killer cell activity in x-linked lymphoproliferative syndrome. *Science.* 1980;210(4469):543-5.
345. Talmadge JE, Meyers KM, Prieur DJ, Starkey JR. Role of natural killer cells in tumor growth and metastasis: C57BL/6 normal and beige mice. *J Natl Cancer Inst.* 1980;65(5):929-35.
346. Cai L, Zhang Z, Zhou L, Wang H, Fu J, Zhang S, et al. Functional impairment in circulating and intrahepatic NK cells and relative mechanism in hepatocellular carcinoma patients. *Clin Immunol.* 2008;129(3):428-37.
347. Fathy A, Eldin MM, Metwally L, Eida M, Abdel-Rehim M. Diminished absolute counts of CD56dim and CD56bright natural killer cells in peripheral blood from Egyptian patients with hepatocellular carcinoma. *Egypt J Immunol.* 2009;16(2):17-25.
348. Liu P, Chen L, Zhang H. Natural Killer Cells in Liver Disease and Hepatocellular Carcinoma and the NK Cell-Based Immunotherapy. *J Immunol Res.* 2018;2018:1206737.

349. Wu Y, Kuang DM, Pan WD, Wan YL, Lao XM, Wang D, et al. Monocyte/macrophage-elicited natural killer cell dysfunction in hepatocellular carcinoma is mediated by CD48/2B4 interactions. *Hepatology*. 2013;57(3):1107-16.
350. Hoechst B, Voigtlaender T, Ormandy L, Gamrekelashvili J, Zhao F, Wedemeyer H, et al. Myeloid derived suppressor cells inhibit natural killer cells in patients with hepatocellular carcinoma via the NKp30 receptor. *Hepatology*. 2009 ;50(3) :799-807.
351. Li T, Yang Y, Hua X, Wang G, Liu W, Jia C, et al. Hepatocellular carcinoma-associated fibroblasts trigger NK cell dysfunction via PGE2 and IDO. *Cancer Lett*. 2012;318(2):154-61.
352. Godfrey DI, MacDonald HR, Kronenberg M, Smyth MJ, Van Kaer L. NKT cells: what's in a name? *Nat Rev Immunol*. 2004;4(3):231-7.
353. Makino Y, Kanno R, Ito T, Higashino K, Taniguchi M. Predominant expression of invariant V alpha 14+ TCR alpha chain in NK1.1+ T cell populations. *Int Immunol*. 1995;7(7):1157-61.
354. Cohen NR, Garg S, Brenner MB. Antigen Presentation by CD1 Lipids, T Cells, and NKT Cells in Microbial Immunity. *Adv Immunol*. 2009;102:1-94.
355. Long X, Deng S, Mattner J, Zang Z, Zhou D, McNary N, et al. Synthesis and evaluation of stimulatory properties of Sphingomonadaceae glycolipids. *Nat Chem Biol*. 2007;3(9):559-64.
356. Swain MG. Hepatic NKT cells: friend or foe? *Clin Sci (Lond)*. 2008;114(7):457-66.
357. Kim EY, Lynch L, Brennan PJ, Cohen NR, Brenner MB. The transcriptional programs of iNKT cells. *Semin Immunol*. 2015;27(1):26-32.
358. Akbari O, Stock P, Meyer E, Kronenberg M, Sidobre S, Nakayama T, et al. Essential role of NKT cells producing IL-4 and IL-13 in the development of allergen-induced airway hyperreactivity. *Nat Med*. 2003;9(5):582-8.
359. Milpied P, Massot B, Renand A, Diem S, Herbelin A, Leite-de-Moraes M, et al. IL-17-producing invariant NKT cells in lymphoid organs are recent thymic emigrants identified by neuropilin-1 expression. *Blood*. 2011;118(11):2993-3002.
360. Monteiro M, Almeida CF, Agua-Doce A, Graca L. Induced IL-17-producing invariant NKT cells require activation in presence of TGF- $\beta$  and IL-1 $\beta$ . *J Immunol*. 2013;190(2):805-11.
361. Sakuishi K, Oki S, Araki M, Porcelli SA, Miyake S, Yamamura T. Invariant NKT cells biased for IL-5 production act as crucial regulators of inflammation. *J Immunol*. 2007;179(6):3452-62.

362. Webster KE, Kim HO, Kyparissoudis K, Corpuz TM, Pinget GV, Uldrich AP, et al. IL-17-producing NKT cells depend exclusively on IL-7 for homeostasis and survival. *Mucosal Immunol.* 2014;7(5):1058-67.
363. Bai L, Constantinides MG, Thomas SY, Reboulet R, Meng F, Koentgen F, et al. Distinct APCs explain the cytokine bias of  $\alpha$ -galactosylceramide variants in vivo. *J Immunol.* 2012;188(7):3053-61.
364. Trobonjaca Z, Leithäuser F, Möller P, Schirmbeck R, Reimann J. Activating immunity in the liver. I. Liver dendritic cells (but not hepatocytes) are potent activators of IFN-gamma release by liver NKT cells. *J Immunol.* 2001;167(3):1413-22.
365. Santodomingo-Garzon T, Swain MG. Role of NKT cells in autoimmune liver disease. *Autoimmun Rev.* 2011;10(12):793-800.
366. Geissmann F, Cameron TO, Sidobre S, Manlongat N, Kronenberg M, Briskin MJ, et al. Intravascular immune surveillance by CXCR6<sup>+</sup> NKT cells patrolling liver sinusoids. *PLoS Biol.* 2005;3(4):e113.
367. Ichikawa S, Mucida D, Tyznik AJ, Kronenberg M, Cheroutre H. Hepatic stellate cells function as regulatory bystanders. *J Immunol.* 2011;186(10):5549-55.
368. Zeissig S, Peucker K, Iyer S, Gensollen T, Dougan SK, Olszak T, et al. CD1d-Restricted pathways in hepatocytes control local natural killer T cell homeostasis and hepatic inflammation. *Proc Natl Acad Sci U S A.* 2017;114(39):10449-54.
369. Gao B, Radaeva S, Park O. Liver natural killer and natural killer T cells: immunobiology and emerging roles in liver diseases. *J Leukoc Biol.* 2009;86(3):513-28.
370. Velázquez P, Cameron TO, Kinjo Y, Nagarajan N, Kronenberg M, Dustin ML. Cutting edge: activation by innate cytokines or microbial antigens can cause arrest of natural killer T cell patrolling of liver sinusoids. *J Immunol.* 2008;180(4):2024-8.
371. Tupin E, Benhnia MR, Kinjo Y, Patsey R, Lena CJ, Haller MC, et al. NKT cells prevent chronic joint inflammation after infection with *Borrelia burgdorferi*. *Proc Natl Acad Sci U S A.* 2008;105(50):19863-8.
372. Ishigami M, Nishimura H, Naiki Y, Yoshioka K, Kawano T, Tanaka Y, et al. The roles of intrahepatic Valpha14(+) NK1.1(+) T cells for liver injury induced by *Salmonella* infection in mice. *Hepatology.* 1999 ;29(6) :1799-808.

373. Miyaki E, Hiraga N, Imamura M, Uchida T, Kan H, Tsuge M, et al. Interferon alpha treatment stimulates interferon gamma expression in type I NKT cells and enhances their antiviral effect against hepatitis C virus. *PLoS One*. 2017;12(3):e0172412.
374. Lucas M, Gadola S, Meier U, Young NT, Harcourt G, Karadimitris A, et al. Frequency and phenotype of circulating Valpha24/Vbeta11 double-positive natural killer T cells during hepatitis C virus infection. *J Virol*. 2003;77(3):2251-7.
375. Ye L, Wang X, Wang S, Wang Y, Song L, Hou W, et al. CD56+ T cells inhibit hepatitis C virus replication in human hepatocytes. *Hepatology*. 2009;49(3):753-62.
376. Deignan T, Curry MP, Doherty DG, Golden-Mason L, Volkov Y, Norris S, et al. Decrease in hepatic CD56(+) T cells and V alpha 24(+) natural killer T cells in chronic hepatitis C viral infection. *J Hepatol*. 2002 ;37(1) :101-8.
377. Yamagiwa S, Matsuda Y, Ichida T, Honda Y, Takamura M, Sugahara S, et al. Sustained response to interferon-alpha plus ribavirin therapy for chronic hepatitis C is closely associated with increased dynamism of intrahepatic natural killer and natural killer T cells. *Hepatol Res*. 2008;38(7):664-72.
378. Zeissig S, Murata K, Sweet L, Publicover J, Hu Z, Kaser A, et al. Hepatitis B virus-induced lipid alterations contribute to natural killer T cell-dependent protective immunity. *Nat Med*. 2012 ;18(7) :1060-8.
379. Jiang X, Zhang M, Lai Q, Huang X, Li Y, Sun J, et al. Restored circulating invariant NKT cells are associated with viral control in patients with chronic hepatitis B. *PLoS One*. 2011;6(12):e28871.
380. Vilarinho S, Ogasawara K, Nishimura S, Lanier LL, Baron JL. Blockade of NKG2D on NKT cells prevents hepatitis and the acute immune response to hepatitis B virus. *Proc Natl Acad Sci U S A*. 2007;104(46):18187-92.
381. Bhattacharjee J, Kirby M, Softic S, Miles L, Salazar-Gonzalez RM, Shivakumar P, et al. Hepatic Natural Killer T-cell and CD8+ T-cell Signatures in Mice with Nonalcoholic Steatohepatitis. *Hepatol Commun*. 2017;1(4):299-310.
382. Syn WK, Agboola KM, Swiderska M, Michelotti GA, Liaskou E, Pang H, et al. NKT-associated hedgehog and osteopontin drive fibrogenesis in non-alcoholic fatty liver disease. *Gut*. 2012 ;61(9) :1323-9.

383. Syn WK, Oo YH, Pereira TA, Karaca GF, Jung Y, Omenetti A, et al. Accumulation of natural killer T cells in progressive nonalcoholic fatty liver disease. *Hepatology*. 2010;51(6):1998-2007.
384. Tajiri K, Shimizu Y, Tsuneyama K, Sugiyama T. Role of liver-infiltrating CD3+CD56+ natural killer T cells in the pathogenesis of nonalcoholic fatty liver disease. *Eur J Gastroenterol Hepatol*. 2009;21(6):673-80.
385. Chiaramonte MG, Donaldson DD, Cheever AW, Wynn TA. An IL-13 inhibitor blocks the development of hepatic fibrosis during a T-helper type 2-dominated inflammatory response. *J Clin Invest*. 1999;104(6):777-85.
386. Fichtner-Feigl S, Strober W, Kawakami K, Puri RK, Kitani A. IL-13 signaling through the IL-13alpha2 receptor is involved in induction of TGF-beta1 production and fibrosis. *Nat Med*. 2006 ;12(1) :99-106.
387. Kaneko Y, Harada M, Kawano T, Yamashita M, Shibata Y, Gejyo F, et al. Augmentation of Valpha14 NKT cell-mediated cytotoxicity by interleukin 4 in an autocrine mechanism resulting in the development of concanavalin A-induced hepatitis. *J Exp Med*. 2000 ;191(1) :105-14.
388. Osman Y, Kawamura T, Naito T, Takeda K, Van Kaer L, Okumura K, et al. Activation of hepatic NKT cells and subsequent liver injury following administration of alpha-galactosylceramide. *Eur J Immunol*. 2000;30(7):1919-28.
389. Takeda K, Hayakawa Y, Van Kaer L, Matsuda H, Yagita H, Okumura K. Critical contribution of liver natural killer T cells to a murine model of hepatitis. *Proc Natl Acad Sci U S A*. 2000;97(10):5498-503.
390. Dennert G, Aswad F. The role of NKT cells in animal models of autoimmune hepatitis. *Crit Rev Immunol*. 2006 ;26(5) :453-73.
391. Wondimu Z, Santodomingo-Garzon T, Le T, Swain MG. Protective role of interleukin-17 in murine NKT cell-driven acute experimental hepatitis. *Am J Pathol*. 2010;177(5):2334-46.
392. Hinks TSC, Zhang XW. MAIT Cell Activation and Functions. *Front Immunol*. 2020 ;11 :1014.
393. Tilloy F, Treiner E, Park SH, Garcia C, Lemonnier F, de la Salle H, et al. An invariant T cell receptor alpha chain defines a novel TAP-independent major histocompatibility complex class Ib-restricted alpha/beta T cell subpopulation in mammals. *J Exp Med*. 1999;189(12):1907-21.

394. Eckle SB, Corbett AJ, Keller AN, Chen Z, Godfrey DI, Liu L, et al. Recognition of Vitamin B Precursors and Byproducts by Mucosal Associated Invariant T Cells. *J Biol Chem.* 2015;290(51):30204-11.
395. Kjer-Nielsen L, Patel O, Corbett AJ, Le Nours J, Meehan B, Liu L, et al. MR1 presents microbial vitamin B metabolites to MAIT cells. *Nature.* 2012 ;491(7426) :717-23.
396. Dusseaux M, Martin E, Serriari N, Péguillet I, Premel V, Louis D, et al. Human MAIT cells are xenobiotic-resistant, tissue-targeted, CD161hi IL-17-secreting T cells. *Blood.* 2011;117(4):1250-9.
397. Rahimpour A, Koay HF, Enders A, Clanchy R, Eckle SB, Meehan B, et al. Identification of phenotypically and functionally heterogeneous mouse mucosal-associated invariant T cells using MR1 tetramers. *J Exp Med.* 2015;212(7):1095-108.
398. Chen Z, Wang H, D'Souza C, Sun S, Kostenko L, Eckle SB, et al. Mucosal-associated invariant T-cell activation and accumulation after in vivo infection depends on microbial riboflavin synthesis and co-stimulatory signals. *Mucosal Immunol.* 2017;10(1):58-68.
399. Kurioka A, Walker LJ, Klenerman P, Willberg CB. MAIT cells: new guardians of the liver. *Clin Transl Immunology.* 2016;5(8):e98.
400. Bánki Z, Krabbendam L, Klaver D, Leng T, Kruis S, Mehta H, et al. Antibody opsonization enhances MAIT cell responsiveness to bacteria via a TNF-dependent mechanism. *Immunol Cell Biol.* 2019;97(6):538-51.
401. Lamichhane R, Galvin H, Hannaway RF, de la Harpe SM, Munro F, Tyndall JD, et al. Type I interferons are important co-stimulatory signals during T cell receptor mediated human MAIT cell activation. *Eur J Immunol.* 2020;50(2):178-91.
402. Turtle CJ, Delrow J, Joslyn RC, Swanson HM, Basom R, Tabellini L, et al. Innate signals overcome acquired TCR signaling pathway regulation and govern the fate of human CD161(hi) CD8 $\alpha$ <sup>+</sup> semi-invariant T cells. *Blood.* 2011;118(10):2752-62.
403. Wang H, Kjer-Nielsen L, Shi M, D'Souza C, Pediongco TJ, Cao H, et al. IL-23 costimulates antigen-specific MAIT cell activation and enables vaccination against bacterial infection. *Sci Immunol.* 2019;4(41).
404. Bernal I, Hofmann JD, Bulitta B, Klawonn F, Michel AM, Jahn D, et al. Clostridioides difficile Activates Human Mucosal-Associated Invariant T Cells. *Front Microbiol.* 2018;9:2532.



405. Gold MC, Cerri S, Smyk-Pearson S, Cansler ME, Vogt TM, Delepine J, et al. Human mucosal associated invariant T cells detect bacterially infected cells. *PLoS Biol.* 2010;8(6):e1000407.
406. Jahreis S, Böttcher S, Hartung S, Rachow T, Rummeler S, Dietl AM, et al. Human MAIT cells are rapidly activated by *Aspergillus* spp. in an APC-dependent manner. *Eur J Immunol.* 2018 ;48(10) :1698-706.
407. Le Bourhis L, Dusseaux M, Bohineust A, Bessoles S, Martin E, Premel V, et al. MAIT cells detect and efficiently lyse bacterially-infected epithelial cells. *PLoS Pathog.* 2013 ;9(10) : e1003681.
408. Le Bourhis L, Martin E, Péguillet I, Guihot A, Froux N, Coré M, et al. Antimicrobial activity of mucosal-associated invariant T cells. *Nat Immunol.* 2010;11(8):701-8.
409. Meermeier EW, Harriff MJ, Karamooz E, Lewinsohn DM. MAIT cells and microbial immunity. *Immunol Cell Biol.* 2018;96(6):607-17.
410. Napier RJ, Adams EJ, Gold MC, Lewinsohn DM. The Role of Mucosal Associated Invariant T Cells in Antimicrobial Immunity. *Front Immunol.* 2015;6:344.
411. van Wilgenburg B, Scherwitzl I, Hutchinson EC, Leng T, Kurioka A, Kulicke C, et al. MAIT cells are activated during human viral infections. *Nat Commun.* 2016;7:11653.
412. Leeansyah E, Svärd J, Dias J, Buggert M, Nyström J, Quigley MF, et al. Arming of MAIT Cell Cytolytic Antimicrobial Activity Is Induced by IL-7 and Defective in HIV-1 Infection. *PLoS Pathog.* 2015;11(8):e1005072.
413. Loh L, Wang Z, Sant S, Koutsakos M, Jegaskanda S, Corbett AJ, et al. Human mucosal-associated invariant T cells contribute to antiviral influenza immunity via IL-18-dependent activation. *Proc Natl Acad Sci U S A.* 2016;113(36):10133-8.
414. Sattler A, Dang-Heine C, Reinke P, Babel N. IL-15 dependent induction of IL-18 secretion as a feedback mechanism controlling human MAIT-cell effector functions. *Eur J Immunol.* 2015 ;45(8) :2286-98.
415. Ussher JE, Bilton M, Attwod E, Shadwell J, Richardson R, de Lara C, et al. CD161<sup>++</sup> CD8<sup>+</sup> T cells, including the MAIT cell subset, are specifically activated by IL-12+IL-18 in a TCR-independent manner. *Eur J Immunol.* 2014;44(1):195-203.
416. van Wilgenburg B, Loh L, Chen Z, Pediongco TJ, Wang H, Shi M, et al. MAIT cells contribute to protection against lethal influenza infection in vivo. *Nat Commun.* 2018;9(1):4706.

417. Lepore M, Kalinichenko A, Colone A, Paleja B, Singhal A, Tschumi A, et al. Parallel T-cell cloning and deep sequencing of human MAIT cells reveal stable oligoclonal TCR $\beta$  repertoire. *Nat Commun.* 2014 ;5 :3866.
418. Balmer ML, Slack E, de Gottardi A, Lawson MA, Hapfelmeier S, Miele L, et al. The liver may act as a firewall mediating mutualism between the host and its gut commensal microbiota. *Sci Transl Med.* 2014;6(237):237ra66.
419. Grant AJ, Lalor PF, Salmi M, Jalkanen S, Adams DH. Homing of mucosal lymphocytes to the liver in the pathogenesis of hepatic complications of inflammatory bowel disease. *Lancet.* 2002;359(9301):150-7.
420. Oo YH, Banz V, Kavanagh D, Liaskou E, Withers DR, Humphreys E, et al. CXCR3-dependent recruitment and CCR6-mediated positioning of Th-17 cells in the inflamed liver. *J Hepatol.* 2012 ;57(5) :1044-51.
421. Li Y, Huang B, Jiang X, Chen W, Zhang J, Wei Y, et al. Mucosal-Associated Invariant T Cells Improve Nonalcoholic Fatty Liver Disease Through Regulating Macrophage Polarization. *Front Immunol.* 2018;9:1994.
422. Riva A, Patel V, Kurioka A, Jeffery HC, Wright G, Tarff S, et al. Mucosa-associated invariant T cells link intestinal immunity with antibacterial immune defects in alcoholic liver disease. *Gut.* 2018;67(5):918-30.
423. Llopis M, Cassard AM, Wrzosek L, Boschat L, Bruneau A, Ferrere G, et al. Intestinal microbiota contributes to individual susceptibility to alcoholic liver disease. *Gut.* 2016;65(5):830-9.
424. Ribot JC, Lopes N, Silva-Santos B.  $\gamma\delta$  T cells in tissue physiology and surveillance. *Nat Rev Immunol.* 2021;21(4):221-32.
425. Lafaille JJ, DeCloux A, Bonneville M, Takagaki Y, Tonegawa S. Junctional sequences of T cell receptor gamma delta genes: implications for gamma delta T cell lineages and for a novel intermediate of V-(D)-J joining. *Cell.* 1989;59(5):859-70.
426. Crowley MP, Reich Z, Mavaddat N, Altman JD, Chien Y. The recognition of the nonclassical major histocompatibility complex (MHC) class I molecule, T10, by the gammadelta T cell, G8. *J Exp Med.* 1997;185(7):1223-30.
427. Groh V, Steinle A, Bauer S, Spies T. Recognition of stress-induced MHC molecules by intestinal epithelial gammadelta T cells. *Science.* 1998;279(5357):1737-40.

428. Janeway CA, Jr., Jones B, Hayday A. Specificity and function of T cells bearing gamma delta receptors. *Immunol Today*. 1988;9(3):73-6.
429. Kong Y, Cao W, Xi X, Ma C, Cui L, He W. The NKG2D ligand ULBP4 binds to TCRgamma9/delta2 and induces cytotoxicity to tumor cells through both TCRgammadelta and NKG2D. *Blood*. 2009;114(2):310-7.
430. Shin S, El-Diwany R, Schaffert S, Adams EJ, Garcia KC, Pereira P, et al. Antigen recognition determinants of gammadelta T cell receptors. *Science*. 2005;308(5719):252-5.
431. Bai L, Picard D, Anderson B, Chaudhary V, Luoma A, Jabri B, et al. The majority of CD1d-sulfatide-specific T cells in human blood use a semiinvariant Vδ1 TCR. *Eur J Immunol*. 2012 ;42(9) :2505-10.
432. Luoma AM, Castro CD, Adams EJ. γδ T cell surveillance via CD1 molecules. *Trends Immunol*. 2014;35(12):613-21.
433. Russano AM, Bassotti G, Agea E, Bistoni O, Mazzocchi A, Morelli A, et al. CD1-restricted recognition of exogenous and self-lipid antigens by duodenal gammadelta+ T lymphocytes. *J Immunol*. 2007;178(6):3620-6.
434. Gustafsson K, Herrmann T, Dieli F. Editorial: Understanding Gamma Delta T Cell Multifunctionality - Towards Immunotherapeutic Applications. *Front Immunol*. 2020;11:921.
435. Vantourout P, Hayday A. Six-of-the-best: unique contributions of γδ T cells to immunology. *Nat Rev Immunol*. 2013;13(2):88-100.
436. Bonneville M, O'Brien RL, Born WK. Gammadelta T cell effector functions: a blend of innate programming and acquired plasticity. *Nat Rev Immunol*. 2010;10(7):467-78.
437. Wen L, Barber DF, Pao W, Wong FS, Owen MJ, Hayday A. Primary gamma delta cell clones can be defined phenotypically and functionally as Th1/Th2 cells and illustrate the association of CD4 with Th2 differentiation. *J Immunol*. 1998;160(4):1965-74.
438. Dieli F, Troye-Blomberg M, Ivanyi J, Fournié JJ, Krensky AM, Bonneville M, et al. Granulysin-dependent killing of intracellular and extracellular *Mycobacterium tuberculosis* by Vgamma9/Vdelta2 T lymphocytes. *J Infect Dis*. 2001 ;184(8) :1082-5.
439. Dudal S, Turriere C, Bessoles S, Fontes P, Sanchez F, Liautard J, et al. Release of LL-37 by activated human Vgamma9Vdelta2 T cells: a microbicidal weapon against *Brucella suis*. *J Immunol*. 2006;177(8):5533-9.

440. Qin G, Mao H, Zheng J, Sia SF, Liu Y, Chan PL, et al. Phosphoantigen-expanded human gammadelta T cells display potent cytotoxicity against monocyte-derived macrophages infected with human and avian influenza viruses. *J Infect Dis.* 2009;200(6):858-65.
441. Hammerich L, Tacke F. Role of gamma-delta T cells in liver inflammation and fibrosis. *World J Gastrointest Pathophysiol.* 2014;5(2):107-13.
442. Hou W, Wu X. Diverse Functions of  $\gamma\delta$  T Cells in the Progression of Hepatitis B Virus and Hepatitis C Virus Infection. *Front Immunol.* 2020;11:619872.
443. Jensen KD, Su X, Shin S, Li L, Youssef S, Yamasaki S, et al. Thymic selection determines gammadelta T cell effector fate: antigen-naive cells make interleukin-17 and antigen-experienced cells make interferon gamma. *Immunity.* 2008;29(1):90-100.
444. Kenna T, Golden-Mason L, Norris S, Hegarty JE, O'Farrelly C, Doherty DG. Distinct subpopulations of gamma delta T cells are present in normal and tumor-bearing human liver. *Clin Immunol.* 2004;113(1):56-63.
445. Hunter S, Willcox CR, Davey MS, Kasatskaya SA, Jeffery HC, Chudakov DM, et al. Human liver infiltrating  $\gamma\delta$  T cells are composed of clonally expanded circulating and tissue-resident populations. *J Hepatol.* 2018;69(3):654-65.
446. Groh V, Rhinehart R, Secrist H, Bauer S, Grabstein KH, Spies T. Broad tumor-associated expression and recognition by tumor-derived gamma delta T cells of MICA and MICB. *Proc Natl Acad Sci U S A.* 1999;96(12):6879-84.
447. Bukowski JF, Morita CT, Brenner MB. Human gamma delta T cells recognize alkylamines derived from microbes, edible plants, and tea: implications for innate immunity. *Immunity.* 1999 ;11(1) :57-65.
448. Constant P, Davodeau F, Peyrat MA, Poquet Y, Puzo G, Bonneville M, et al. Stimulation of human gamma delta T cells by nonpeptidic mycobacterial ligands. *Science.* 1994;264(5156):267-70.
449. Tanaka Y, Morita CT, Tanaka Y, Nieves E, Brenner MB, Bloom BR. Natural and synthetic non-peptide antigens recognized by human gamma delta T cells. *Nature.* 1995;375(6527):155-8.
450. Khairallah C, Netzer S, Villacreces A, Juzan M, Rousseau B, Dulanto S, et al.  $\gamma\delta$  T cells confer protection against murine cytomegalovirus (MCMV). *PLoS Pathog.* 2015 ;11(3) : e1004702.

451. Lu Y, Wang X, Yan W, Wang H, Wang M, Wu D, et al. Liver TCR $\gamma\delta$ (+) CD3(+) CD4(-) CD8(-) T cells contribute to murine hepatitis virus strain 3-induced hepatic injury through a TNF- $\alpha$ -dependent pathway. *Mol Immunol*. 2012 ;52(3-4) :229-36.
452. Gardner T, Chen Q, Jin Y, Ajuebor MN. Characterization of the role of TCR gammadelta in NK cell accumulation during viral liver inflammation. *Exp Mol Pathol*. 2009;86(1):32-5.
453. Li Y, Wu X, Chen L, Lyu S, Zhang J, Wang F. [Decrease in  $\gamma\delta$  T cells correlates with severity of liver injury and fibrosis in patients with chronic hepatitis B]. *Zhonghua Gan Zang Bing Za Zhi*. 2015;23(2):94-8.
454. Wu X, Zhang JY, Huang A, Li YY, Zhang S, Wei J, et al. Decreased V $\delta$ 2  $\gamma\delta$  T cells associated with liver damage by regulation of Th17 response in patients with chronic hepatitis B. *J Infect Dis*. 2013;208(8):1294-304.
455. Chen M, Hu P, Peng H, Zeng W, Shi X, Lei Y, et al. Enhanced peripheral  $\gamma\delta$ T cells cytotoxicity potential in patients with HBV-associated acute-on-chronic liver failure might contribute to the disease progression. *J Clin Immunol*. 2012;32(4):877-85.
456. Yin W, Tong S, Zhang Q, Shao J, Liu Q, Peng H, et al. Functional dichotomy of V $\delta$ 2  $\gamma\delta$  T cells in chronic hepatitis C virus infections: role in cytotoxicity but not for IFN- $\gamma$  production. *Sci Rep*. 2016;6:26296.
457. Agrati C, D'Offizi G, Narciso P, Abrignani S, Ippolito G, Colizzi V, et al. Vdelta1 T lymphocytes expressing a Th1 phenotype are the major gammadelta T cell subset infiltrating the liver of HCV-infected persons. *Mol Med*. 2001;7(1):11-9.
458. Tramonti D, Rhodes K, Martin N, Dalton JE, Andrew E, Carding SR. gammadeltaT cell-mediated regulation of chemokine producing macrophages during *Listeria monocytogenes* infection-induced inflammation. *J Pathol*. 2008;216(2):262-70.
459. Rhodes KA, Andrew EM, Newton DJ, Tramonti D, Carding SR. A subset of IL-10-producing gammadelta T cells protect the liver from *Listeria*-elicited, CD8(+) T cell-mediated injury. *Eur J Immunol*. 2008;38(8):2274-83.
460. Hamada S, Umemura M, Shiono T, Tanaka K, Yahagi A, Begum MD, et al. IL-17A produced by gammadelta T cells plays a critical role in innate immunity against *Listeria monocytogenes* infection in the liver. *J Immunol*. 2008;181(5):3456-63.

461. Tsuji M, Mombaerts P, Lefrancois L, Nussenzweig RS, Zavala F, Tonegawa S. Gamma delta T cells contribute to immunity against the liver stages of malaria in alpha beta T-cell-deficient mice. *Proc Natl Acad Sci U S A*. 1994;91(1):345-9.
462. Chen D, Luo X, Xie H, Gao Z, Fang H, Huang J. Characteristics of IL-17 induction by *Schistosoma japonicum* infection in C57BL/6 mouse liver. *Immunology*. 2013 ;139(4) :523-32.
463. Zheng L, Hu Y, Wang Y, Huang X, Xu Y, Shen Y, et al. Recruitment of Neutrophils Mediated by  $V\gamma 2 \gamma\delta$  T Cells Deteriorates Liver Fibrosis Induced by *Schistosoma japonicum* Infection in C57BL/6 Mice. *Infect Immun*. 2017;85(8).
464. Zhou QH, Wu FT, Pang LT, Zhang TB, Chen Z. Role of  $\gamma\delta$ T cells in liver diseases and its relationship with intestinal microbiota. *World J Gastroenterol*. 2020;26(20):2559-69.
465. Martins EB, Graham AK, Chapman RW, Fleming KA. Elevation of gamma delta T lymphocytes in peripheral blood and livers of patients with primary sclerosing cholangitis and other autoimmune liver diseases. *Hepatology*. 1996 ;23(5) :988-93.
466. Ferri S, Longhi MS, De Molo C, Lalanne C, Muratori P, Granito A, et al. A multifaceted imbalance of T cells with regulatory function characterizes type 1 autoimmune hepatitis. *Hepatology*. 2010;52(3):999-1007.
467. Hua F, Wang L, Rong X, Hu Y, Zhang JM, He W, et al. Elevation of  $V\delta 1$  T cells in peripheral blood and livers of patients with primary biliary cholangitis. *Clin Exp Immunol*. 2016;186(3):347-55.
468. Tedesco D, Thapa M, Chin CY, Ge Y, Gong M, Li J, et al. Alterations in Intestinal Microbiota Lead to Production of Interleukin 17 by Intrahepatic  $\gamma\delta$  T-Cell Receptor-Positive Cells and Pathogenesis of Cholestatic Liver Disease. *Gastroenterology*. 2018;154(8):2178-93.
469. Giles DA, Moreno-Fernandez ME, Divanovic S. IL-17 Axis Driven Inflammation in Non-Alcoholic Fatty Liver Disease Progression. *Curr Drug Targets*. 2015;16(12):1315-23.
470. Harley IT, Stankiewicz TE, Giles DA, Softic S, Flick LM, Cappelletti M, et al. IL-17 signaling accelerates the progression of nonalcoholic fatty liver disease in mice. *Hepatology*. 2014;59(5):1830-9.
471. Xu R, Tao A, Zhang S, Zhang M. Neutralization of interleukin-17 attenuates high fat diet-induced non-alcoholic fatty liver disease in mice. *Acta Biochim Biophys Sin (Shanghai)*. 2013;45(9):726-33.

472. Farber DL, Yudanin NA, Restifo NP. Human memory T cells: generation, compartmentalization and homeostasis. *Nat Rev Immunol.* 2014 ;14(1) :24-35.
473. Cheuk S, Schlums H, Gallais S  rezal I, Martini E, Chiang SC, Marquardt N, et al. CD49a Expression Defines Tissue-Resident CD8(+) T Cells Poised for Cytotoxic Function in Human Skin. *Immunity.* 2017;46(2):287-300.
474. Hogan RJ, Usherwood EJ, Zhong W, Roberts AA, Dutton RW, Harmsen AG, et al. Activated antigen-specific CD8+ T cells persist in the lungs following recovery from respiratory virus infections. *J Immunol.* 2001;166(3):1813-22.
475. Masopust D, Vezys V, Marzo AL, Lefran  ois L. Preferential localization of effector memory cells in nonlymphoid tissue. *Science.* 2001;291(5512):2413-7.
476. Sl  tter B, Pewe LL, Kaech SM, Harty JT. Lung airway-surveilling CXCR3(hi) memory CD8(+) T cells are critical for protection against influenza A virus. *Immunity.* 2013;39(5):939-48.
477. Mackay LK, Rahimpour A, Ma JZ, Collins N, Stock AT, Hafon ML, et al. The developmental pathway for CD103(+)CD8+ tissue-resident memory T cells of skin. *Nat Immunol.* 2013;14(12):1294-301.
478. Carbone FR, Mackay LK, Heath WR, Gebhardt T. Distinct resident and recirculating memory T cell subsets in non-lymphoid tissues. *Curr Opin Immunol.* 2013;25(3):329-33.
479. Wu T, Hu Y, Lee YT, Bouchard KR, Benechet A, Khanna K, et al. Lung-resident memory CD8 T cells (TRM) are indispensable for optimal cross-protection against pulmonary virus infection. *J Leukoc Biol.* 2014;95(2):215-24.
480. Park SL, Gebhardt T, Mackay LK. Tissue-Resident Memory T Cells in Cancer Immunosurveillance. *Trends Immunol.* 2019;40(8):735-47.
481. Harrison OJ, Linehan JL, Shih HY, Bouladoux N, Han SJ, Smelkinson M, et al. Commensal-specific T cell plasticity promotes rapid tissue adaptation to injury. *Science.* 2019;363(6422).
482. Schenkel JM, Fraser KA, Beura LK, Pauken KE, Vezys V, Masopust D. T cell memory. Resident memory CD8 T cells trigger protective innate and adaptive immune responses. *Science.* 2014;346(6205):98-101.
483. Ryan GE, Harris JE, Richmond JM. Resident Memory T Cells in Autoimmune Skin Diseases. *Front Immunol.* 2021;12:652191.

484. Samat AAK, van der Geest J, Vastert SJ, van Loosdregt J, van Wijk F. Tissue-Resident Memory T Cells in Chronic Inflammation-Local Cells with Systemic Effects? *Cells*. 2021;10(2).
485. Ishizuka AS, Lyke KE, DeZure A, Berry AA, Richie TL, Mendoza FH, et al. Protection against malaria at 1 year and immune correlates following PfSPZ vaccination. *Nat Med*. 2016;22(6):614-23.
486. Lim CJ, Lee YH, Pan L, Lai L, Chua C, Wasser M, et al. Multidimensional analyses reveal distinct immune microenvironment in hepatitis B virus-related hepatocellular carcinoma. *Gut*. 2019 ;68(5) :916-27.
487. Fernandez-Ruiz D, Ng WY, Holz LE, Ma JZ, Zaid A, Wong YC, et al. Liver-Resident Memory CD8(+) T Cells Form a Front-Line Defense against Malaria Liver-Stage Infection. *Immunity*. 2016;45(4):889-902.
488. Swadling L, Pallett LJ, Diniz MO, Baker JM, Amin OE, Stegmann KA, et al. Human Liver Memory CD8(+) T Cells Use Autophagy for Tissue Residence. *Cell Rep*. 2020;30(3):687-98.e6.
489. Kumar BV, Ma W, Miron M, Granot T, Guyer RS, Carpenter DJ, et al. Human Tissue-Resident Memory T Cells Are Defined by Core Transcriptional and Functional Signatures in Lymphoid and Mucosal Sites. *Cell Rep*. 2017;20(12):2921-34.
490. Germain RN. Imaging the immune system redux. *Immunol Rev*. 2022;306(1):5-7.
491. Gerner MY, Kastenmuller W, Ifrim I, Kabat J, Germain RN. Histo-cytometry: a method for highly multiplex quantitative tissue imaging analysis applied to dendritic cell subset microanatomy in lymph nodes. *Immunity*. 2012;37(2):364-76.
492. Giesen C, Wang HA, Schapiro D, Zivanovic N, Jacobs A, Hattendorf B, et al. Highly multiplexed imaging of tumor tissues with subcellular resolution by mass cytometry. *Nat Methods*. 2014;11(4):417-22.
493. Pirici D, Mogoanta L, Kumar-Singh S, Pirici I, Margaritescu C, Simionescu C, et al. Antibody elution method for multiple immunohistochemistry on primary antibodies raised in the same species and of the same subtype. *J Histochem Cytochem*. 2009;57(6):567-75.
494. Porta Siegel T, Hamm G, Bunch J, Cappell J, Fletcher JS, Schwamborn K. Mass Spectrometry Imaging and Integration with Other Imaging Modalities for Greater Molecular Understanding of Biological Tissues. *Mol Imaging Biol*. 2018;20(6):888-901.



495. Radtke AJ, Kandov E, Lowekamp B, Speranza E, Chu CJ, Gola A, et al. IBEX: A versatile multiplex optical imaging approach for deep phenotyping and spatial analysis of cells in complex tissues. *Proc Natl Acad Sci U S A*. 2020;117(52):33455-65.
496. Yanguas SC, Cogliati B, Willebrords J, Maes M, Colle I, van den Bossche B, et al. Experimental models of liver fibrosis. *Arch Toxicol*. 2016;90(5):1025-48.
497. Wang J, Hossain M, Thanabalasuriar A, Gunzer M, Meininger C, Kubes P. Visualizing the function and fate of neutrophils in sterile injury and repair. *Science*. 2017;358(6359):111-6.
498. Wang F, Flanagan J, Su N, Wang LC, Bui S, Nielson A, et al. RNAscope: a novel in situ RNA analysis platform for formalin-fixed, paraffin-embedded tissues. *J Mol Diagn*. 2012;14(1):22-9.
499. Saldarriaga OA, Freiberg B, Krishnan S, Rao A, Burks J, Booth AL, et al. Multispectral Imaging Enables Characterization of Intrahepatic Macrophages in Patients With Chronic Liver Disease. *Hepatol Commun*. 2020;4(5):708-23.
500. Traum D, Wang YJ, Schwarz KB, Schug J, Wong DK, Janssen H, et al. Highly multiplexed 2-dimensional imaging mass cytometry analysis of HBV-infected liver. *JCI Insight*. 2021 ;6(7).
501. Flores Molina M, Fabre T, Cleret-Buhot A, Soucy G, Meunier L, Abdelnabi MN, et al. Visualization, Quantification, and Mapping of Immune Cell Populations in the Tumor Microenvironment. *J Vis Exp*. 2020(157).
502. Blériot C, Ginhoux F. Understanding the Heterogeneity of Resident Liver Macrophages. *Front Immunol*. 2019;10:2694.
503. Scholten D, Trebicka J, Liedtke C, Weiskirchen R. The carbon tetrachloride model in mice. *Lab Anim*. 2015;49(1 Suppl):4-11.
504. Hoehme S, Brulport M, Bauer A, Bedawy E, Schormann W, Hermes M, et al. Prediction and validation of cell alignment along microvessels as order principle to restore tissue architecture in liver regeneration. *Proc Natl Acad Sci U S A*. 2010;107(23):10371-6.
505. McGill MR, Jaeschke H. Animal models of drug-induced liver injury. *Biochim Biophys Acta Mol Basis Dis*. 2019;1865(5):1031-9.
506. Hefler J, Marfil-Garza BA, Pawlick RL, Freed DH, Karvellas CJ, Bigam DL, et al. Preclinical models of acute liver failure: a comprehensive review. *PeerJ*. 2021;9:e12579.
507. Sayaf K, Gabbia D, Russo FP, De Martin S. The Role of Sex in Acute and Chronic Liver Damage. *Int J Mol Sci*. 2022;23(18).

508. Broughton G, 2nd, Janis JE, Attinger CE. Wound healing: an overview. *Plast Reconstr Surg.* 2006;117(7 Suppl):1e-S-32e-S.
509. Clemens MM, McGill MR, Apte U. Mechanisms and biomarkers of liver regeneration after drug-induced liver injury. *Adv Pharmacol.* 2019;85:241-62.
510. Sarhan M, Land WG, Tonnus W, Hugo CP, Linkermann A. Origin and Consequences of Necroinflammation. *Physiol Rev.* 2018;98(2):727-80.
511. Kim EH, Wong SW, Martinez J. Programmed Necrosis and Disease: We interrupt your regular programming to bring you necroinflammation. *Cell Death Differ.* 2019;26(1):25-40.
512. Weber LW, Boll M, Stampfl A. Hepatotoxicity and mechanism of action of haloalkanes: carbon tetrachloride as a toxicological model. *Crit Rev Toxicol.* 2003;33(2):105-36.
513. Lindros KO. Zonation of cytochrome P450 expression, drug metabolism and toxicity in liver. *Gen Pharmacol.* 1997 ;28(2) :191-6.
514. Cong M, Zhao W, Liu T, Wang P, Fan X, Zhai Q, et al. Protective effect of human serum amyloid P on CCl<sub>4</sub>-induced acute liver injury in mice. *Int J Mol Med.* 2017 ;40(2) :454-64.
515. Dai C, Xiao X, Li D, Tun S, Wang Y, Velkov T, et al. Chloroquine ameliorates carbon tetrachloride-induced acute liver injury in mice via the concomitant inhibition of inflammation and induction of apoptosis. *Cell Death Dis.* 2018;9(12):1164.
516. Endig J, Unrau L, Sprezyna P, Rading S, Karsak M, Goltz D, et al. Acute Liver Injury after CCl<sub>4</sub> Administration is Independent of Smad7 Expression in Myeloid Cells. *Int J Mol Sci.* 2019 ;20(22).
517. Lin D, Sun Z, Jin Z, Lei L, Liu Y, Hu B, et al. Matrix Remodeling Associated 7 Deficiency Alleviates Carbon Tetrachloride-Induced Acute Liver Injury in Mice. *Front Immunol.* 2018;9:773.
518. Munakarmi S, Chand L, Shin HB, Jang KY, Jeong YJ. Indole-3-Carbinol Derivative DIM Mitigates Carbon Tetrachloride-Induced Acute Liver Injury in Mice by Inhibiting Inflammatory Response, Apoptosis and Regulating Oxidative Stress. *Int J Mol Sci.* 2020;21(6).
519. Otsuka T, Takagi H, Horiguchi N, Toyoda M, Sato K, Takayama H, et al. CCl<sub>4</sub>-induced acute liver injury in mice is inhibited by hepatocyte growth factor overexpression but stimulated by NK2 overexpression. *FEBS Lett.* 2002;532(3):391-5.
520. Gieling RG, Wallace K, Han YP. Interleukin-1 participates in the progression from liver injury to fibrosis. *Am J Physiol Gastrointest Liver Physiol.* 2009;296(6):G1324-31.

521. Schwabe RF, Brenner DA. Mechanisms of Liver Injury. I. TNF-alpha-induced liver injury: role of IKK, JNK, and ROS pathways. *Am J Physiol Gastrointest Liver Physiol*. 2006;290(4):G583-9.
522. Connolly MK, Bedrosian AS, Mallen-St Clair J, Mitchell AP, Ibrahim J, Stroud A, et al. In liver fibrosis, dendritic cells govern hepatic inflammation in mice via TNF-alpha. *J Clin Invest*. 2009;119(11):3213-25.
523. Yang YM, Seki E. TNF $\alpha$  in liver fibrosis. *Curr Pathobiol Rep*. 2015;3(4):253-61.
524. Zhao S, Jiang J, Jing Y, Liu W, Yang X, Hou X, et al. The concentration of tumor necrosis factor- $\alpha$  determines its protective or damaging effect on liver injury by regulating Yap activity. *Cell Death Dis*. 2020;11(1):70.
525. Yamada Y, Fausto N. Deficient liver regeneration after carbon tetrachloride injury in mice lacking type 1 but not type 2 tumor necrosis factor receptor. *Am J Pathol*. 1998;152(6):1577-89.
526. Alegre F, Pelegrin P, Feldstein AE. Inflammasomes in Liver Fibrosis. *Semin Liver Dis*. 2017;37(2):119-27.
527. Dinarello CA. Immunological and inflammatory functions of the interleukin-1 family. *Annu Rev Immunol*. 2009;27:519-50.
528. Mehendale HM. Tissue repair: an important determinant of final outcome of toxicant-induced injury. *Toxicol Pathol*. 2005;33(1):41-51.
529. Jones BA, Beamer M, Ahmed S. Fractalkine/CX3CL1: a potential new target for inflammatory diseases. *Mol Interv*. 2010;10(5):263-70.
530. D'Haese JG, Demir IE, Friess H, Ceyhan GO. Fractalkine/CX3CR1: why a single chemokine-receptor duo bears a major and unique therapeutic potential. *Expert Opin Ther Targets*. 2010;14(2):207-19.
531. Font-Burgada J, Shalpour S, Ramaswamy S, Hsueh B, Rossell D, Umemura A, et al. Hybrid Periportal Hepatocytes Regenerate the Injured Liver without Giving Rise to Cancer. *Cell*. 2015;162(4):766-79.
532. Richards JA, Bucsaiova M, Hesketh EE, Ventre C, Henderson NC, Simpson K, et al. Acute Liver Injury Is Independent of B Cells or Immunoglobulin M. *PLoS One*. 2015;10(9):e0138688.
533. Shi Z, Wakil AE, Rockey DC. Strain-specific differences in mouse hepatic wound healing are mediated by divergent T helper cytokine responses. *Proc Natl Acad Sci U S A*. 1997;94(20):10663-8.

534. Curry MP, Golden-Mason L, Doherty DG, Deignan T, Norris S, Duffy M, et al. Expansion of innate CD5pos B cells expressing high levels of CD81 in hepatitis C virus infected liver. *J Hepatol.* 2003;38(5):642-50.
535. Mosnier JF, Degott C, Marcellin P, Hénin D, Erlinger S, Benhamou JP. The intraportal lymphoid nodule and its environment in chronic active hepatitis C: an immunohistochemical study. *Hepatology.* 1993;17(3):366-71.
536. Racanelli V, Sansonno D, Piccoli C, D'Amore FP, Tucci FA, Dammacco F. Molecular characterization of B cell clonal expansions in the liver of chronically hepatitis C virus-infected patients. *J Immunol.* 2001;167(1):21-9.
537. Tucci FA, Broering R, Lutterbeck M, Schlaak JF, Küppers R. Intrahepatic B-cell follicles of chronically hepatitis C virus-infected individuals lack signs of an ectopic germinal center reaction. *Eur J Immunol.* 2014;44(6):1842-50.
538. Agnello V, De Rosa FG. Extrahepatic disease manifestations of HCV infection: some current issues. *J Hepatol.* 2004;40(2):341-52.
539. Béland K, Marceau G, Labardy A, Bourbonnais S, Alvarez F. Depletion of B cells induces remission of autoimmune hepatitis in mice through reduced antigen presentation and help to T cells. *Hepatology.* 2015;62(5):1511-23.
540. Than NN, Hodson J, Schmidt-Martin D, Taubert R, Wawman RE, Botter M, et al. Efficacy of rituximab in difficult-to-manage autoimmune hepatitis: Results from the International Autoimmune Hepatitis Group. *JHEP Rep.* 2019;1(6):437-45.
541. Woltman AM, Boonstra A, Naito M, Leenen PJM. Kupffer Cells in Health and Disease. In: Biswas SK, Mantovani A, editors. *Macrophages: Biology and Role in the Pathology of Diseases.* New York, NY: Springer New York; 2014. p. 217-47.
542. Lynch RW, Hawley CA, Pellicoro A, Bain CC, Iredale JP, Jenkins SJ. An efficient method to isolate Kupffer cells eliminating endothelial cell contamination and selective bias. *J Leukoc Biol.* 2018;104(3):579-86.
543. Li PZ, Li JZ, Li M, Gong JP, He K. An efficient method to isolate and culture mouse Kupffer cells. *Immunol Lett.* 2014;158(1-2):52-6.
544. Dambach DM, Watson LM, Gray KR, Durham SK, Laskin DL. Role of CCR2 in macrophage migration into the liver during acetaminophen-induced hepatotoxicity in the mouse. *Hepatology.* 2002;35(5):1093-103.

545. Geissmann F, Jung S, Littman DR. Blood monocytes consist of two principal subsets with distinct migratory properties. *Immunity*. 2003;19(1):71-82.
546. Ingersoll MA, Spanbroek R, Lottaz C, Gautier EL, Frankenberger M, Hoffmann R, et al. Comparison of gene expression profiles between human and mouse monocyte subsets. *Blood*. 2010;115(3):e10-9.
547. Serbina NV, Pamer EG. Monocyte emigration from bone marrow during bacterial infection requires signals mediated by chemokine receptor CCR2. *Nat Immunol*. 2006;7(3):311-7.
548. Breen FN, Hume DA, Weidemann MJ. Interactions among granulocyte-macrophage colony-stimulating factor, macrophage colony-stimulating factor, and IFN-gamma lead to enhanced proliferation of murine macrophage progenitor cells. *J Immunol*. 1991;147(5):1542-7.
549. Hume DA, MacDonald KP. Therapeutic applications of macrophage colony-stimulating factor-1 (CSF-1) and antagonists of CSF-1 receptor (CSF-1R) signaling. *Blood*. 2012;119(8):1810-20.
550. Hume DA, Pavli P, Donahue RE, Fidler IJ. The effect of human recombinant macrophage colony-stimulating factor (CSF-1) on the murine mononuclear phagocyte system in vivo. *J Immunol*. 1988;141(10):3405-9.
551. Chertov O, Ueda H, Xu LL, Tani K, Murphy WJ, Wang JM, et al. Identification of human neutrophil-derived cathepsin G and azurocidin/CAP37 as chemoattractants for mononuclear cells and neutrophils. *J Exp Med*. 1997;186(5):739-47.
552. Soehnlein O, Zernecke A, Eriksson EE, Rothfuchs AG, Pham CT, Herwald H, et al. Neutrophil secretion products pave the way for inflammatory monocytes. *Blood*. 2008 ;112(4) :1461-71.
553. Degré D, Lemmers A, Gustot T, Ouziel R, Trépo E, Demetter P, et al. Hepatic expression of CCL2 in alcoholic liver disease is associated with disease severity and neutrophil infiltrates. *Clin Exp Immunol*. 2012;169(3):302-10.
554. Fantuzzi L, Tagliamonte M, Gauzzi MC, Lopalco L. Dual CCR5/CCR2 targeting: opportunities for the cure of complex disorders. *Cell Mol Life Sci*. 2019;76(24):4869-86.
555. Xi S, Zheng X, Li X, Jiang Y, Wu Y, Gong J, et al. Activated Hepatic Stellate Cells Induce Infiltration and Formation of CD163(+) Macrophages via CCL2/CCR2 Pathway. *Front Med (Lausanne)*. 2021;8:627927.

556. Auffray C, Fogg D, Garfa M, Elain G, Join-Lambert O, Kayal S, et al. Monitoring of blood vessels and tissues by a population of monocytes with patrolling behavior. *Science*. 2007;317(5838):666-70.
557. Alkhani A, Levy CS, Tsui M, Rosenberg KA, Polovina K, Mattis AN, et al. Ly6c(Lo) non-classical monocytes promote resolution of rhesus rotavirus-mediated perinatal hepatic inflammation. *Sci Rep*. 2020;10(1):7165.
558. Arnold L, Henry A, Poron F, Baba-Amer Y, van Rooijen N, Plonquet A, et al. Inflammatory monocytes recruited after skeletal muscle injury switch into antiinflammatory macrophages to support myogenesis. *J Exp Med*. 2007;204(5):1057-69.
559. Hanna RN, Shaked I, Hubbeling HG, Punt JA, Wu R, Herrley E, et al. NR4A1 (Nur77) deletion polarizes macrophages toward an inflammatory phenotype and increases atherosclerosis. *Circ Res*. 2012;110(3):416-27.
560. Hilgendorf I, Gerhardt LM, Tan TC, Winter C, Holderried TA, Chousterman BG, et al. Ly-6Chigh monocytes depend on Nr4a1 to balance both inflammatory and reparative phases in the infarcted myocardium. *Circ Res*. 2014;114(10):1611-22.
561. El Kasmi KC, Qualls JE, Pesce JT, Smith AM, Thompson RW, Henao-Tamayo M, et al. Toll-like receptor-induced arginase 1 in macrophages thwarts effective immunity against intracellular pathogens. *Nat Immunol*. 2008;9(12):1399-406.
562. Gieseck RL, 3rd, Ramalingam TR, Hart KM, Vannella KM, Cantu DA, Lu WY, et al. Interleukin-13 Activates Distinct Cellular Pathways Leading to Ductular Reaction, Steatosis, and Fibrosis. *Immunity*. 2016;45(1):145-58.
563. Hammerich L, Tacke F. Interleukins in chronic liver disease: lessons learned from experimental mouse models. *Clin Exp Gastroenterol*. 2014;7:297-306.
564. Liu Y, Munker S, Müllenbach R, Weng HL. IL-13 Signaling in Liver Fibrogenesis. *Front Immunol*. 2012;3:116.
565. Munder M. Arginase: an emerging key player in the mammalian immune system. *Br J Pharmacol*. 2009;158(3):638-51.
566. Zhang LJ, Wang XZ. Interleukin-10 and chronic liver disease. *World J Gastroenterol*. 2006;12(11):1681-5.
567. Alexiou D, Karayiannakis AJ, Syrigos KN, Zbar A, Kremmyda A, Bramis I, et al. Serum levels of E-selectin, ICAM-1 and VCAM-1 in colorectal cancer patients: correlations with

- clinicopathological features, patient survival and tumour surgery. *Eur J Cancer*. 2001;37(18):2392-7.
568. Stijlemans B, Korf H, De Baetselier P, Brys L, Van Ginderachter JA, Magez S, et al. Hepatocyte-derived IL-10 plays a crucial role in attenuating pathogenicity during the chronic phase of *T. congolense* infection. *PLoS Pathog*. 2020;16(2):e1008170.
569. Huang YH, Shi MN, Zheng WD, Zhang LJ, Chen ZX, Wang XZ. Therapeutic effect of interleukin-10 on CCl<sub>4</sub>-induced hepatic fibrosis in rats. *World J Gastroenterol*. 2006;12(9):1386-91.
570. Louis H, Van Laethem JL, Wu W, Quertinmont E, Degraef C, Van den Berg K, et al. Interleukin-10 controls neutrophilic infiltration, hepatocyte proliferation, and liver fibrosis induced by carbon tetrachloride in mice. *Hepatology*. 1998;28(6):1607-15.
571. Thompson K, Maltby J, Fallowfield J, McAulay M, Millward-Sadler H, Sheron N. Interleukin-10 expression and function in experimental murine liver inflammation and fibrosis. *Hepatology*. 1998;28(6):1597-606.
572. Chiamonte MG, Mentink-Kane M, Jacobson BA, Cheever AW, Whitters MJ, Goad ME, et al. Regulation and function of the interleukin 13 receptor alpha 2 during a T helper cell type 2-dominant immune response. *J Exp Med*. 2003;197(6):687-701.
573. Chiamonte MG, Schopf LR, Neben TY, Cheever AW, Donaldson DD, Wynn TA. IL-13 is a key regulatory cytokine for Th2 cell-mediated pulmonary granuloma formation and IgE responses induced by *Schistosoma mansoni* eggs. *J Immunol*. 1999;162(2):920-30.
574. Fallon PG, Richardson EJ, McKenzie GJ, McKenzie AN. Schistosome infection of transgenic mice defines distinct and contrasting pathogenic roles for IL-4 and IL-13: IL-13 is a profibrotic agent. *J Immunol*. 2000;164(5):2585-91.
575. Holden WE, Kishiyama SS, Dong SP, Osborne ML. Endothelium-dependent effects of cigarette smoke components on tone of porcine intrapulmonary arteries in vitro. *Toxicol Appl Pharmacol*. 1990;104(2):191-9.
576. Liu Y, Meyer C, Müller A, Herweck F, Li Q, Müllenbach R, et al. IL-13 induces connective tissue growth factor in rat hepatic stellate cells via TGF- $\beta$ -independent Smad signaling. *J Immunol*. 2011;187(5):2814-23.

577. Sugimoto R, Enjoji M, Nakamuta M, Ohta S, Kohjima M, Fukushima M, et al. Effect of IL-4 and IL-13 on collagen production in cultured LI90 human hepatic stellate cells. *Liver Int.* 2005;25(2):420-8.
578. Seki E, de Minicis S, Inokuchi S, Taura K, Miyai K, van Rooijen N, et al. CCR2 promotes hepatic fibrosis in mice. *Hepatology.* 2009;50(1):185-97.
579. Wynn TA. Cellular and molecular mechanisms of fibrosis. *J Pathol.* 2008;214(2):199-210.
580. Bronte V, Zanovello P. Regulation of immune responses by L-arginine metabolism. *Nat Rev Immunol.* 2005;5(8):641-54.
581. Gordon S. Alternative activation of macrophages. *Nat Rev Immunol.* 2003;3(1):23-35.
582. Sass G, Koerber K, Bang R, Guehring H, Tiegs G. Inducible nitric oxide synthase is critical for immune-mediated liver injury in mice. *J Clin Invest.* 2001;107(4):439-47.
583. Arribas-López E, Zand N, Ojo O, Snowden MJ, Kochhar T. The Effect of Amino Acids on Wound Healing: A Systematic Review and Meta-Analysis on Arginine and Glutamine. *Nutrients.* 2021;13(8).
584. Doeing DC, Borowicz JL, Crockett ET. Gender dimorphism in differential peripheral blood leukocyte counts in mice using cardiac, tail, foot, and saphenous vein puncture methods. *BMC Clin Pathol.* 2003;3(1):3.
585. Mestas J, Hughes CC. Of mice and not men: differences between mouse and human immunology. *J Immunol.* 2004 ;172(5) :2731-8.
586. Casanova-Acebes M, Nicolás-Ávila JA, Li JL, García-Silva S, Balachander A, Rubio-Ponce A, et al. Neutrophils instruct homeostatic and pathological states in naive tissues. *J Exp Med.* 2018;215(11):2778-95.
587. Liew PX, Kubes P. The Neutrophil's Role During Health and Disease. *Physiol Rev.* 2019;99(2):1223-48.
588. Liu K, Wang FS, Xu R. Neutrophils in liver diseases: pathogenesis and therapeutic targets. *Cell Mol Immunol.* 2021;18(1):38-44.
589. Ramaiah SK, Jaeschke H. Role of neutrophils in the pathogenesis of acute inflammatory liver injury. *Toxicol Pathol.* 2007;35(6):757-66.
590. Phillipson M, Kubes P. The Healing Power of Neutrophils. *Trends Immunol.* 2019 ;40(7) :635-47.



591. Devalaraja RM, Nanney LB, Du J, Qian Q, Yu Y, Devalaraja MN, et al. Delayed wound healing in CXCR2 knockout mice. *J Invest Dermatol.* 2000;115(2):234-44.
592. Hossain M, Kubes P. Innate immune cells orchestrate the repair of sterile injury in the liver and beyond. *Eur J Immunol.* 2019;49(6):831-41.
593. Ariel A, Serhan CN. New Lives Given by Cell Death: Macrophage Differentiation Following Their Encounter with Apoptotic Leukocytes during the Resolution of Inflammation. *Front Immunol.* 2012;3:4.
594. Elliott MR, Koster KM, Murphy PS. Efferocytosis Signaling in the Regulation of Macrophage Inflammatory Responses. *J Immunol.* 2017;198(4):1387-94.
595. Silvestre-Roig C, Hidalgo A, Soehnlein O. Neutrophil heterogeneity: implications for homeostasis and pathogenesis. *Blood.* 2016;127(18):2173-81.
596. Cassatella MA, Scapini P. On the Improper Use of the Term High-Density Neutrophils. *Trends Immunol.* 2020;41(12):1059-61.
597. Millrud CR, Bergenfelz C, Leandersson K. On the origin of myeloid-derived suppressor cells. *Oncotarget.* 2017;8(2):3649-65.
598. Schultze JL, Mass E, Schlitzer A. Emerging Principles in Myelopoiesis at Homeostasis and during Infection and Inflammation. *Immunity.* 2019;50(2):288-301.
599. Sengupta S, Caldwell CC, Nomellini V. Distinct Neutrophil Populations in the Spleen During PICS. *Front Immunol.* 2020;11:804.
600. Yvan-Charvet L, Ng LG. Granulopoiesis and Neutrophil Homeostasis: A Metabolic, Daily Balancing Act. *Trends Immunol.* 2019;40(7):598-612.
601. Ning X, Wang WM, Jin HZ. Low-Density Granulocytes in Immune-Mediated Inflammatory Diseases. *J Immunol Res.* 2022;2022:1622160.
602. Veglia F, Sanseviero E, Gabrilovich DI. Myeloid-derived suppressor cells in the era of increasing myeloid cell diversity. *Nat Rev Immunol.* 2021;21(8):485-98.
603. Jung S, Aliberti J, Graemmel P, Sunshine MJ, Kreutzberg GW, Sher A, et al. Analysis of fractalkine receptor CX(3)CR1 function by targeted deletion and green fluorescent protein reporter gene insertion. *Mol Cell Biol.* 2000;20(11):4106-14.

604. Martin-Murphy BV, Holt MP, Ju C. The role of damage associated molecular pattern molecules in acetaminophen-induced liver injury in mice. *Toxicol Lett.* 2010;192(3):387-94.
605. Palma E, Doornebal EJ, Chokshi S. Precision-cut liver slices: a versatile tool to advance liver research. *Hepato Int.* 2019;13(1):51-7.
606. van de Bovenkamp M, Groothuis GM, Draaisma AL, Merema MT, Bezuijen JI, van Gils MJ, et al. Precision-cut liver slices as a new model to study toxicity-induced hepatic stellate cell activation in a physiologic milieu. *Toxicol Sci.* 2005 ;85(1) :632-8.

## **Annexe 1 : Manuel Flores Curriculum Vitae**

**MANUEL FLORES MOLINA**

Email: manuel.flores@umontreal.ca

### **EDUCATION**

**Ph.D. Candidate, Virology, and Immunology**

**Sept 2016- Current**

Université de Montréal, Montréal, QC

Thesis: The spatial and temporal characterization of hepatic macrophages during acute liver injury.

Supervisor: Dr. Naglaa Shoukry

**M.Sc. Immunology**

**Jan 2015- May 2016**

Université de Montréal, Montréal, QC.

The role of IL-17 and IL-22 in liver fibrosis and hepatocellular carcinoma

All but degree because of direct transfer to Ph.D.

Supervisor: Dr. Naglaa Shoukry

**B.Sc., Biochemistry**

**Sept 1992- June 1997**

Havana University, Havana, Cuba.

Thesis: Assessment of the genotoxic activity of *P. orbicularis*, a medicinal plant with antiviral properties.

Supervisor: Dr. Angel Sánchez Lamar

## PEER-REVIEWED PUBLICATIONS

1. **Flores Molina M**, Abdelnabi MN, Mazouz S, Villafranca-Baughman D, Trinh VQ, Muhammad S, et al. Distinct spatial distribution and roles of Kupffer cells and monocyte-derived macrophages in mouse acute liver injury. *Front Immunol.* 2022;13:994480.
2. Abdelnabi MN, **Flores Molina M**, Soucy G, Quoc-Huy Trinh V, Bédard N, Mazouz S, et al. Sex-Dependent Hepatoprotective Role of IL-22 Receptor Signaling in Non-Alcoholic Fatty Liver Disease-Related Fibrosis. *Cell Mol Gastroenterol Hepatol.* 2022;14(6):1269-94.
3. **Flores Molina M**, Fabre T, Cleret-Buhot A, Soucy G, Meunier L, Abdelnabi MN, et al. Visualization, Quantification, and Mapping of Immune Cell Populations in the Tumor Microenvironment. *J Vis Exp.* 2020(157).
4. **Molina MF**, Abdelnabi MN, Fabre T, Shoukry NH. Type 3 cytokines in liver fibrosis and liver cancer. *Cytokine.* 2019; 124:154497.
5. Fabre T, **Molina MF**, Soucy G, Goulet JP, Willems B, Villeneuve JP, et al. Type 3 cytokines IL-17A and IL-22 drive TGF- $\beta$ -dependent liver fibrosis. *Sci Immunol.* 2018 ;3(28).
6. Fodil N, Moradin N, Leung V, Olivier JF, Radovanovic I, Jeyakumar T, **Flores Molina M**, et al. CCDC88B is required for pathogenesis of inflammatory bowel disease. *Nat Commun.* 2017;8(1):932.
7. Bolt AM, Grant MP, Wu TH, **Flores Molina M**, Plourde D, Kelly AD, et al. Tungsten Promotes Sex-Specific Adipogenesis in the Bone by Altering Differentiation of Bone Marrow-Resident Mesenchymal Stromal Cells. *Toxicol Sci.* 2016;150(2):333-46.
8. Bolt AM, Sabourin V, **Molina MF**, Police AM, Negro Silva LF, Plourde D, et al. Tungsten targets the tumor microenvironment to enhance breast cancer metastasis. *Toxicol Sci.* 2015;143(1):165-77
9. Lemaire M, Negro Silva LF, Lemarié CA, Bolt AM, **Flores Molina M**, Krohn RM, et al. Arsenic Exposure Increases Monocyte Adhesion to the Vascular Endothelium, a Pro-Atherogenic Mechanism. *PLoS One.* 2015;10(9): e0136592.

10. Lemaire M, Lemarié CA, **Flores Molina M**, Guilbert C, Lehoux S, Mann KK. Genetic deletion of LXR $\alpha$  prevents arsenic-enhanced atherosclerosis, but not arsenic-altered plaque composition. *Toxicol Sci.* 2014 ;142(2) :477-88.
11. Garnier N, Petruccelli LA, **Molina MF**, Kourelis M, Kwan S, Diaz Z, et al. The novel arsenical Darinaparsin circumvents BRG1-dependent, HO-1-mediated cytoprotection in leukemic cells. *Leukemia.* 2013;27(11):2220-8.
12. Kelly AD, Lemaire M, Young YK, Eustache JH, Guilbert C, **Molina MF**, et al. In vivo tungsten exposure alters B-cell development and increases DNA damage in murine bone marrow. *Toxicol Sci.* 2013 ;131(2) :434-46.
13. Lemaire M, Lemarié CA, **Molina MF**, Schiffrin EL, Lehoux S, Mann KK. Exposure to moderate arsenic concentrations increases atherosclerosis in ApoE $^{-/-}$  mouse model. *Toxicol Sci.* 2011;122(1):211-21.
14. Padovani AM, **Molina MF**, Mann KK. Inhibition of liver x receptor/retinoid X receptor-mediated transcription contributes to the proatherogenic effects of arsenic in macrophages in vitro. *Arterioscler Thromb Vasc Biol.* 2010;30(6):1228-36.

## RECOGNITIONS

### **Trainee Travel Award for 2018 AASLD**

**Sep 2019**

Single Topic Conference: Hepatic Fibrosis:  
New Concepts and Controversies. AASLD.  
Texas, United States of America

**Best Poster Presentation** in Light Microscopy,  
Canadian Microscopy and Cytometry Symposium,  
Montreal, QC, Canada.

**May 2017**

**Fellowship Award,**  
Canadian Microscopy and Cytometry Symposium,  
Montreal, QC, Canada.

**May 2017**

**Bourse de fin d'études doctorales-** 11,000 (Canadian dollar). **Sep 2019 – Aug 2020**

**Doctoral Fellowship** - 60,000 (Canadian dollar). **Sep 2016 – Sep 2019**  
Fonds de recherche du Québec - Santé (FRQS).

**Graduate Studentship Award (Declined)** **July/2016 – July/2018**  
40,000 (Canadian dollar)  
Canadian Liver Foundation (CLF).

**Bourse d'excellence Gabriel-Marquis 2015-2016** - 9,500 **Sep 2015 – Sep 2016**  
(Canadian dollar) Université de Montréal.

**Bourse de recrutement de la faculté de médecine** **Jan 2015 – Dec 2015**  
Concours Hiver 2015 - 8,000 (Canadian dollar).  
Université de Montréal.

## **RESEARCH-RELATED SKILLS**

Mouse work-related skills (simple surgical procedures, genotyping, cardiac bleeding puncture, dissection), tissue processing for histology and isolation of leukocytes (liver, spleen, blood, bone marrow, intestines), flow cytometry (panel design, FlowJo, t-SNE FlowSOM), ELISA, imaging techniques (IHC, IF, ICC), histological stains (sirius red, toluidine blue, oil red o, H&E, reticulin), image analysis (VIS, ImageJ), bright field and immunofluorescence microscopy, western blotting, cell culturing, qPCR, PCR, DNA/RNA/Protein gel electrophoresis, CHIP assay, patient recruitment and obtention of informed consent.

## **ORAL PRESENTATIONS**

**Webinar: Strategy for Visualizing, Quantifying and Mapping Immune Cells in the Tumor Microenvironment** **March 2021**  
Presented at XTalks webinar

**CIACCO 2018** **May 2018**  
7th Annual symposium on Cytokines in Inflammation, Ageing, CanCer and Obesity  
Ste- Camille, Quebec, Canada,  
Neutrophils and mast cells are major producers of IL-17 in hepatocellular carcinoma

## **POSTER PRESENTATIONS**

**Canadian Liver Meeting 2021** **May 2021**  
Virtual Meeting  
Poster: Spatio-Temporal Characterization Of the Immune Landscape During Acute Liver Injury Uncovers A Pathogenic Role For Il-17A

**The AASLD Liver Meeting Digital Experience** **Nov 2020**  
Virtual Meeting  
Poster: Spatio-temporal characterization of the immune landscape during acute liver injury

**AASLD Single Topic Conference** **Sep 2019**  
Hepatic Fibrosis: New Concepts and Controversies  
Texas, United States of America  
Poster: Neutrophils and mast cells are major producers of IL-17 in hepatocellular carcinoma

**Keystone Symposia: Lymphocytes and their role in cancer** **Feb 2018**

Keystone, United States of America

Poster: Opposite compartmentalization of Tregs and IL17 + cells in hepatocellular carcinoma.

**CCMA and ACCM Symposium**

**May 2017**

The Canadian Microscopy and Cytometry Association

Montreal, QC, Canada

Poster: The role of IL-17 and IL-22 in liver fibrosis and progression to hepatocellular carcinoma

**7e Journée scientifique du CRCHUM,**

**Oct 2016**

Montreal, Canada,

Poster: The role of IL-17 and IL-22 in liver fibrosis and hepatocellular carcinoma

**18e congrès des étudiants, stagiaires et résidents,**

**May 2016**

CRCHUM, Montréal, Canada,

Poster: The role of IL-17 and IL-22 in liver fibrosis and hepatocellular carcinoma

**4e Journée de la Recherche du Département,**

**Mar 2016**

Département de microbiologie, infectiologie et immunologie 2016

Montreal, Canada

Poster: The role of IL-17 and IL-22 in liver fibrosis and hepatocellular carcinoma

**ACADEMIC-RELATED WORK EXPERIENCE**

**Clinical Research Coordinator,**

**Sept 2021 – Current**

Clinical Research Unit (CRU). Jewish General Hospital

Supervisor: Dr. Wilson Miller and Dr. Marie Hudson

**Research Assistant, Dr. Koren Mann Lab.**

**Nov 2008 – Oct 2014**

Lady Davis Institute for Medical Research



**Research Assistant**, Department of Autoimmunity  
Havana School of Medicine, Havana, Cuba

**Sep 1997- Dec 1999**

## **TEACHING EXPERIENCE**

**Teaching Assistant**, Université de Montréal,  
Faculty of Medicine, MCB 2985

**Aug 2019- Dec 2019**

Travaux pratiques en immunologie.

**Teaching Assistant**, Université de Montréal,  
Faculty of Medicine, MCB1979

**Jan 2019- April 2019**

Travaux pratiques en microbiologie.

**Teaching Assistant**, Université de Montréal,  
Faculty of Medicine, MCB 2985

**Aug 2018- Dec 2018**

Travaux pratiques en immunologie.